Complexation of Cationic Polymers with Nucleic Acids for Gene Delivery

A thesis submitted to the University of Manchester for the degree of Doctor of Philosophy in the Faculty of Engineering and Physical Sciences

2014

Amy Freund

School of Physics and Astronomy

Abstract

The prospect of gene delivery for therapeutic purposes has created much hope for the treatment and prevention of diverse illnesses, both inherited and environmental. One major challenge for the realisation of this potential is the availability of a suitable vector for trafficking foreign DNA into a cell. Many viruses are effective but carry unacceptable risks of dangerous host immune response or infection. Cationic polymers have been identified as promising candidates to neutralise the DNA's negative charge and gain entry to the cell. In this work a structural study was conducted on a range of established and novel cationic polymer vectors in complexation with nucleic acid molecules for gene delivery. The high neutron flux of the recently available SANS2D instrument on the second target station at the ISIS pulsed neutron source was used in conjunction with a stopped-flow apparatus to study the static and kinetic structure of aggregates of complexes formed between different architectures and molecular weights of polyethylenimine, a commonly used, highly cationic polyelectrolyte, and nucleic acids. Findings indicated the stability of high molecular weight branched polyethylenimine was superior to any other architecture studied. Subsequently, the zeta potential of these polymers complexed with biologically relevant siRNA molecules was studied, which suggested was established that aggregation still proceeds, even with the most apparently stable of the complexes. Finally, structural studies of the complexation between a family of synthetic, biocompatible cationic block copolymer vectors which incorporate a stabilising, hydrophilic conjugate block, designed to mitigate aggregation of the extent encountered by PEI complexes upon binding are described. The variation of neutron scattering with charge ratio of polymer to DNA was elucidated for this family of systems.

"Wir müssen uns daran erinnern, daß das, was wir beobachten, nicht die Natur selbst ist, sondern Natur, die unserer Art der Fragestellung ausgesetzt ist."
W. Heisenberg, "Physik und Philosophie"

I gratefully acknowledge significant help and guidance from Prof. Jian Lu, Dr XiuBo Zhao, Dr Fang Pan and Dr Mohammed Yaseen. I also thank Dr Henggui Zhang, Dr Tom Waigh, Dr Salman Rogers, Dr Steven Magennis, David Pearce, Dr Paul Coffey, Faheem Padia, Jamie Fearnley and other members of the Biological Physics Group and others at the University of Manchester for helpful discussions. Additionally, my thanks to Eric Brunner, Dr Stuart Fisher, Dr Liam O'Ryan, Dr Natasha Fox, Elliot Woods and Roger Goldsbrough for their considerable advice, support and assistance.
I am grateful to the EPSRC DTA and John and Stephanie Forrest for their financial support.
The help of Dr. Sarah Rogers and Dr Richard Heenan for technological work, support, guidance and assistance with preliminary data analysis on SANS data was invaluable, and without whom the SANS work would not have been possible, as well as Dr Ann Terry and Dr Stephen King.
Importantly, and not exclusive of those mentioned above, I am extraordinarily grateful to my friends and family for their ongoing support.

Table of Contents

Word count: 77,274

Chapter 1

Introduction to Gene Delivery and Study Motivation

The field of gene delivery is gaining growing interest as an area of potential and, increasingly, realised therapeutic relevance. Many medical applications of this principle currently under development are starting to show real success in animal and clinical trials for diseases as diverse and significant as Leber's Congenital Amaurosis[132], tumour treatments [206], chronic lymphocytic leukemia(CLL)[146] and Parkinson's disease[90] and work is continuing towards genetic therapies for Duchenne's Muscular Dystrophy[128], which has the additional challenge of requiring uniform genetic delivery throughout the body for successful skeletal muscle therapy, genetic vaccination[19], and a large-scale cystic fibrosis trial was scheduled to commence this year[107]. Additionally, and no less importantly, transfection techniques are already indispensable in numerous areas of fundamental biomedical research to enable the study of the function of particular genes[29] and enable investigation of other cellular processes[50].

This chapter will outline the principle barriers to successful transfection of human cells and present some of the currently available vector solutions. Viral vectors leading to stable expression have been among the most commonly used vectors developed and are frequently selected for used for in vivo applications, for reasons of their high efficacy and stability of expression over the long term[74][90], due to integration into the cell's genome [92]. However, certain applications require non-viral particles, such as treatments which

are required to cross the blood-brain barrier. Traditionally used viral envelopes are unable to do this[139], as the barrier is formed of tight junctions and, in the case of the relatively few virus types which are known to traverse the barrier, barrier disruption due to immune response is thought to frequently facilitate entry. [166]. This is, however, an undesirable and potentially dangerous effect in therapeutic processes. Liposomes and other non-viral vectors have, however, proven successful.

However, significant bio-safety hazards associated with their use prevent viral vectors from achieving approval for widespread use in humans. The application of synthetic vectors with greater transfection efficiency is widely regarded as being among the most promising routes to success in therapeutic applications of transfection.

The aim of this work is a fundamental study of the complexation process of the well studied cationic vector, PEI, and of the physical characteristics and mechanisms of action of a family of synthetic, diblock copolymers, based on the biocompatible, zwitterionic phosphorylcholine polymer and the cationic diethylamine, which demonstrate high transfection efficiency in vitro[202]. By examining the physical processes involved in polymer complexation, and the resulting complex structures formed, it is hoped to gain insight into relevant factors to contribute to enabling optimisation of transfection efficacy, which may guide the design of improved, biocompatible synthetic vectors.

1.1 Motivation for Complexation

DNA molecules are negatively charged, semi-flexible polymers[162], although in practice, double-stranded DNA molecules have among the highest rigidity of biological polymers[144]. DNA molecules consist of phosphates, sugars and nitrogenous bases. Their charge comes from the phosphate groups which alternate with deoxyribose sugars to form the molecules' backbones. In cells, DNA molecules exist in helical pairs, held together by a combination of hydrogen bonds between complementary bases which, together with the sugar and phosphate molecules, make up the nucleotide, as well as hydrophobic effects which also play a role in providing a binding force for the double helical molecule. The sequence of four types of base, A, T, C and G, make up the code which is translated within the cell to synthesise proteins. Each kind of base will bind specifically only to its complementary pair, hence a sequence of single stranded sense DNA will bind exclusively

to a molecule with its complementary antisense sequence of bases. The asymmetry between these two strands running in opposite directions results in the familiar twisted or helical, double strand structure.

In eukaryotic cells, chromosomal DNA exists in compacted coils, condensed by the histone proteins which form part of the chromatin in approximately equal mass to DNA. This condensation is able to compact the DNA into a chromosome of length 10^6 times less than that of the extended molecule.[5] That packing of this magnitude occurs naturally, in cell nuclei as well as in viral capsids, is an encouraging fact providing a precedent in the search for transfection vectors. To introduce a double-stranded DNA plasmid such as the Luciferase plasmid, which consists of approximately 5,000 nucleotide pairs, into a cell would be extremely difficult in its extended form. Molecular size is, therefore, one of the key barriers to transfection which we seek to overcome through condensation with a vector.

The other most significant hurdles to cellular internalisation of DNA are outlined briefly here.

1.1.1 Charge Neutralisation

DNA molecules carry a large negative charge due to the phosphate groups which form part of each nucleotide. As an individual phosphate group in a DNA molecule is likely to be fully protonated, carrying one negative charge unit per nucleotide at physiological pH[21], the overall molecular weight of DNA per charge unit is approximately 308 amu (the mass of a single nucleotide) although the precise, appropriate value for calculation of charge mass density varies fractionally between different bases due to slight variation in the masses of different bases. Hence, different short oligonucleotides in particular may have significant variations in the proportion of each type of base and hence variations in their average mass per charge. The contribution of associated salt to the molecule may also affect the mass per unit charge and will be discussed where relevant in the context of individual experiments.

Given the fact that the cellular membrane is also negatively charged, fluid phase diffusive and non-specific adsorptive endocytosis of naked DNA are unlikely to occur due to fundamental electrostatic repulsion.[186] Through complexation with a cationic polymer such as Polyethylenimine (PEI) or Diethylamine (DEA) investigated in this work, the nucleic

acids negative charge can be neutralised, or even inverted, depending on the mixed charge ratio of available cationic polymer to DNA, enabling cellular uptake by these non-specific pathways. This is in addition to the potential for specific, receptor-mediated endocytosis where the relevant ligands are present, although even in this case the chances of specific binding would also be enhanced by eliminating electrostatic repulsion.

The charge neutralisation of DNA results in increased flexibility and an ability to compactly fold or pack the molecules due to removal of electrostatic intra-molecular repulsion, as discussed in Section 2.1.2.

1.1.2 Cellular Targeting, Extracellular Obstacles and Cellular Entry

As with the delivery of any drug, the first challenge in the pathway is to target the complex to the required cells or tissues. Certain structures, such as tumours, are characterised by a difference in pH in the surrounding tissue, so pH-mediated targeting or cargo release by external transport vectors is one mechanism which has attracted much interest for drug delivery in general[179]. Of the established polymer genetic vectors, some such as PEI, are postulated to exploit a pH dependent process for intracellular endosomal escape. In this case, if pH-dependent extracellular targeting was desired in addition to pH-dependent intracellular unpacking, development of a complex which incorporated two different pH-dependent structural changes for these two different goals without interference would be required. A 'double-targeting' technique working on similar principles, consisting of a coated micelle, with different pH responses to the extracellular and endo/lysosomal environment is described by Lee et al, who investigate such a system for potential applicationt to solid tumour targeting[**?**]. This is analagous to the technique employed by viruses, as is discussed in Section 1.3.2.

There are multiple non-specific routes to cellular entry, which typically involve encapsulation of the particle in a fold of the cellular membrane, which then detaches as an endocytic vesicle. The precise method of cellular entry depends largely on the size of the particle. This will be discussed further in the context of the study of PEI-DNA aggregation in Chapter 4.

A potentially complementary method for instigating specific cellular uptake is the conjugation of targeting ligands to the complexing polymer, which have a strong binding affinity

for specific endocytic receptors on surfaces of particular kinds of cells. Such ligands commonly include monoclonal antibodies or peptides[136], and may particularly be used for complex targeting to certain cell types, such as tumour cells. This is also likely to effect more efficient uptake through receptor-mediated endocytosis than non-specific cellular entry pathways, but requires additional tailoring of polymers or other synthetic nanoparticles to the particular application and the addition of ligands which may be costlier and more demanding to produce in comparison to commercially available polymers, such as PEI. No ligand-conjugated particles were used in this work.

It is also necessary that the complex and its DNA cargo reach their cellular target without enzymal degradation or aspecific binding of bloodstream proteins, where these may block their membrane adsorption and uptake into cells. Exposure to proteins has been found to have various, in many cases, negative, protein-specific effects on DNA-vector complexes[194] and transfection. Serum proteins, for instance, may bind to complexes causing structural rearrangement, aggregation or blocking binding, and thereby hindering cellular membrane binding and uptake, according to Xu et al[194]. Non-specific membrane binding occurs through electrostatic interaction between the cationic surface charge of polyplexes and anionic proteoglycans on the cell surface [176][101]. These proteoglycans are then observed to diffuse laterally through the membrane to cluster around the complex, forming a raft, and actin filaments may subsequently drive invagination of the particle initiating endocytosis or phagocytosis[101]. However, some proteins, such as fibrinogen, have been found to enhance the transfection efficiency of DNA complexes, by the postulated mechanism of promoting cellular uptake through facilitating binding to certain membrane receptors. The net effect of exposure to complete serum on transfection rates for some lipid-based vectors has been shown to be negative[173], however, this is likely to depend on the specific vector used. For instance, in their previous work on transfection with MPC-DEA copolymer vectors, Zhao et al [202] found little difference in transfection efficiency of oligonucleotides (ODN) at high charge ratios in the presence or absence of serum, suggesting sufficient colloidal stabilisation of the complexes may protect them from the effects of exposure to serum proteins.

1.1.3 Endosomal Escape

Cellular uptake of DNA complexes by endocytosis is followed by their intracellular transport in endosomes. A principle purpose of cells capturing cargo within endosomes is the sorting of the contents into structural or receptor proteins, destined to be recycled back into the membrane, and other functional proteins for use within the cell, to be transported via endosomal fusion with lysosomes, along the microtubule network to their specified destination.

Acidification of the late endosomes to pH 5-6[89] may induce dissociation of membrane receptors from bound ligands, enabling the two to be transported separately and the receptor recycled to the membrane. It is thought that enzymes may have a role in this process, althought the precise molecular process and participating molecules may be unclear[37]. In order to effectively induce expression in cells, it is likely that DNA must escape these compartments before the pH drops too far and nuclease activity rises. Indeed, studies of non-viral gene vectors have shown that complexation results in the slowing of trafficking to lysosomes, such that DNA when complexed to non-viral vectors is not found to be present in lysosomes on the timescales when naked DNA is observed there[186], and enhanced rates of endosomal escape at a relatively early stage are key for delivery of intact nucleic acids to the nucleus[**?**].

Two principal mechanisms of endosomal escape have been postulated. Amine-rich polymers such as polyethyleneimine (PEI) consist of primary, secondary and tertiary amine groups. These have different acid dissociation constants and can consequently efficiently absorb protons at different pHs, having the effect of buffering changes in pH strongly across a wide range of pH, enabling such polymers to effectively buffer the decrease in endosomal pH[10]. One commonly held theory is that this may result in a destabilising stream of protons entering the endosome and the electroneutralising chloride ions which accompany them are thought to cause an imbalance of osmotic pressure, leading to swelling and rupture of the endosome.[2] [183] It should be noted, however, that this postulated approach is debated and in particular a notable study by Funhoff et al[53], using a novel synthesised polymer, suggests that endosomal escape is not always enhanced by buffering of low pH by polymers.

An alternative method, employed by many viruses, is the fusion of the complex with the endosomal membrane, which facilitates escape of its genetic contents into the cell. The

capacity of viruses to shed parts of their complex in this way is an adaptive mechanism which may inspire future generations of synthetic vectors.[185] It is believed that many cationic lipid or polymer vectors also exploit this membranolytic mechanism of fusing with and rupturing the membrane, as they have been shown to be membrane disruptive in vitro, and may potentially dissociate from their cargo in the process.[186] The MPC-DEA copolymers studied here are not known to be membranolytic but establishing the predominant mechanism contributing to endosomal escape in the case of the DEA-based polymers being studied here would nonetheless be of interest for future intelligent vector design.

1.1.4 Intracellular Trafficking

It is known that endosomal vesicles associate with the microtubule motors dynein and kinesin and are actively transported[51], displaying directional transport modes through the cytoplasm. Several studies have shown motion of fluorescently-tagged DNA complexes along similar trajectories, or noted that transfection is reduced following microtubule disruption with nocodazole[25], implying that they are also associated with the microtubule network, at least while contained within endosomes. However, whether this active transport persists following the complexs escape from the endosome is uncertain. PEI/DNA complexes are found to associate strongly with extracted microtubules in vitro, so continued active transport after endosomal escape is plausible.[170] However, this association with microtubules could potentially also be detrimental for nuclear entry once complexes are in the peri-nuclear region.

1.1.5 Protection from Enzymatic Degradation

Nuclease exposure goes hand in hand with acidification in the late endosomes or lysosomes. Common endonucleases break up the DNA molecule at points along the length of its chain. Research by Wattiaux et al[186] has shown that the presence of cationic vectors reduces DNA degradation by DNAses when compared to naked DNA, with the extent of resistance depending on the type of cationic vector. This is thought to be due to compaction and surrounding of the DNA by cationic polymers[56] or liposomes[42], creating a physical or electrostatic barrier to enzyme penetration, according to Godbey et al[56].

1.1.6 Dissociation and Transcription

A fine balance must be struck to achieve the optimum strength of complexation to overcome the various hurdles in transfection. If binding is too weak and the complex dissociates too early, then the DNA is likely to be rapidly trafficked to lysosomes and degraded before it reaches the nucleus. However, if binding is too strong and persists into and within the nucleus, it may reduce the ability of the transcription machinery in the cell to initiate expression of the protein encoded by the transgene.

Studies of PEI and its variants as gene delivery vehicles have indicated that a complex with higher binding strength can sometimes have lower transfection efficiency, suggesting that a reluctance to dissociate is impairing expression.[2] This apparently causal link has not, however been proven conclusively and further investigation may offer insight into the severity of these effects and the mechanism by which polymer condensation may interfere with transcription, in view of the fact that chromosomal DNA is also condensed around histones in nucleosomes without adversely affecting access of transcription factors to the DNAs bases. Should the vector be able to remain attached until transcription without hindering expression, this knowledge could elucidate useful opportunities to exploit advanced nuclear targeting mechanisms.

1.1.7 Nuclear Localisation and Entry

Molecules are able to enter the nucleus through nuclear pore complexes. These have a diameter of approximately 50nm at their narrowest opening, although only particles of a size considerably smaller than this are able to pass through by simple diffusion.[49] Any particle larger than this must be actively transported into the nucleus by binding to receptors such as importin proteins, which utilise energy from the RAN-GTP process to transport cargo[182]. Nuclear localisation signals (NLS) such as those found on viruses ensure rapid uptake by the nuclear transport machinery. The potential for targeting ligands such as NLS to be conjugated to the vector-DNA complexes exists. It seems likely, however, that achieving nuclear entry by this mechanism, could be at the expense of some degree of expression of the transgene, as discussed above, as the necessity for the vector to remain tightly bound to the DNA for nuclear entry could reduce transcription of the plasmid. However, the nuclear entry point is only an obstacle to large DNA molecules, such as plasmids, which must be expressed by nuclear transcription machinery, as oligonu-

cleotides and siRNA intended for downregulation may bind to their target mRNA in the cytoplasm.

1.1.8 Stability of Expression

Stability refers to gene expression which persists over several cell generations and consequently is normally ascribed to integration of the transgene into one of the hosts chromosomes. During the prophase of mitosis, chromatin assembles into ordered chromosomes for replication. It is unlikely that extra-chromosomal transgenes within the nucleus would be processed and duplicated in a similar way. Therefore it is generally thought that chromosomal integration is necessary for semi-permanently stable and persistent expression; however this has not been conclusively shown. Viral gene delivery vectors are commonly used in clinical trials, due in part to their superior ability to integrate DNA into the host chromosome[115], thus providing stable expression of the transgene. However, some authors express concern at the potential for integration in an unfavourable chromosomal location, which has the potential to cause mutagenic effects [8]. It would be of interest, therefore, to understand better the relationship between inserted DNA and interphase chromatin for non-viral vectors, to determine whether it may be included into the chromosomes and how the DNA replication functions determine the transience or stability of gene expression. Depending on the foreseen therapeutic application, transience of expression could be advantageous (eg. in a short duration, single-episode cancer treatment), or permanence could be desirable, (eg. in treating inherited genetic abnormalities).

1.2 Gene Delivery Applications

Many potential medical applications of gene therapy have begun to show real potential, with successful treatment of significant, serious conditions from blindness to leukaemia and work progressing rapidly into other areas, such as cystic fibrosis and HIV. Recent years have seen many treatments progress to the clinical testing stage, while many are continuing in vitro or in animal models, and the European Medicines Association have approved the licence for the first gene therapy product for mainstream, commercial medical treatment approved in the European Union[45] to target the rare inherited deficiency, Lipoprotein Lipase Deficiency (LPLD). The wide range of potential applications brings

a correspondingly broad variety of demands for gene delivery vectors. The necessity for transfection to be stable or transient, for instance, depends strongly on the application. The combination of stable plasmid transfection with regulatory promoter regions which regulate the expression may be optimal in many cases,[59] but in certain circumstances, such as for curable, short-term diseases, transience of expression may suffice or even be preferred.

1.2.1 Plasmid DNA and Underexpression

Only 2 % of genomic DNA in humans encodes a physiologically functional protein[172]. Some disorders, such as, for example, thalassemia [150], are due to a failure to produce enough or any of the protein in question, leading to a deficiency or complete absence of the protein in the body, which in turn leads to pathological symptoms. Conventional medicinal approaches to treating disease focus on replacing or substituting for the missing protein, or masking the symptoms through other means of mitigation. In gene therapy, however, the principle of reintegration of the missing genetic sequence into the host nucleus, whether stably into the chromosome, or transiently, serves to enable the cell to produce the protein as it would in a healthy individual, solving the problem at source.

Mechanism of Plasmid Expression

Chromosomal DNA is first transcribed by nuclear enzymes known as RNA polymerases, mediated by proteins known as transcription factors, producing a complementary strand of RNA to generate molecules of messenger RNA (mRNA). These leave the nucleus and are translated by ribosomes to produce proteins built up from amino acids in a sequence determined by the sequence of bases.[91] Plasmid DNA which has entered the nucleus is transcribed and translated in a similar way to chromosomal DNA.

Applications of Plasmid Delivery

Plasmid DNA is a versatile nucleic acid format which can encode many kinds of therapeutic proteins. Plasmids have been shown to enable relatively stable transfection for up to 270 days, when integrating into the host genome,[134] and the expression of the functional gene can be regulated by the control of promoter regions incorporated in the plasmid[59]. A plasmid expressing tumour necrosis factor-alpha delivered via intramus-

cular transfection mediated by electroporation in skeletal muscle has been shown to be effective in treating mice with collagen-induced arthritis [59]. DNA vaccines are also being developed, which employ plasmids encoding specific antigens to viruses such as HIV-1. Particularly promising initial results have been obtained by Brave et al.[19] through the combination of genes from several different subtypes of HIV, encoding for antigens to different viral components. As a significant problem with HIV vaccines appears to be the variety of subtypes and mechanisms required to target the virus, the authors believe that by incorporating several different components into the vaccine, which promote both cellular and humoral responses, the chances of successfully inducing immunity are raised.[19] The genes are delivered in separate plasmids to different sites to avoid competition between antigens, which may impair the efficacy of delivery.

The question of how transfection efficiency is impacted when vectors are used to perform simultaneous transfection of multiple plasmids is of great relevance to this application.

In both these cases, the search for non-viral vectors is particularly relevant as the therapy is envisaged for either entirely healthy patients or those with a non-life-threatening condition. Safety of the vector is therefore paramount and the relative security of a synthetic polymer when contrasted to a viral vector is a significant advantage.

Typically, however, viral vectors are superior at producing stable integration of the gene sequence into the genome[115], so progress in the design of improved synthetic vectors is key where this outcome is desired.

1.2.2 Overexpression and Downregulation by ODN or siRNA

In analogy to the scenario described regarding plasmid DNA transfection to replace a missing DNA sequence and restore production of a protein of interest to the cell, some pathologies result from the over production of a particular protein due to the overexpression of the relevant gene. This type of fault plays a role in many types of cancer, including some lung [117], prostate[106], breast and ovarian cancers[129]. In this case, genetic intervention can offer solutions through blocking of translation of the transcribed RNA into the protein of interest, resulting in greatly reduced levels of protein expression.

Mechanism of Downregulation

Oligodeoxynucleotides (ODNs) are short, synthetic, single strands of DNA, engineered to have a specific base sequence, which is complementary or antisense to a target sequence of mRNA.

They are being studied for application in blocking or down-regulating the production of proteins from mutated or over-expressed genes. Expression of a gene occurs by preliminary transcription of the DNA in the nucleus to produce mRNA, a single-stranded nucleic acid which contains the same base sequence as its source DNA. This is then exported to the cytoplasm, where ribosomes mediate translation of the messenger RNA (mRNA) to produce the protein it encodes. In order for this process to occur, transfer RNA (tRNA) which imports the amino acids necessary to construct the proteins, needs to bind to and move along the base sequence sites to translate the sequence into protein. The goal of antisense therapy with ODNs is to bind the complementary sequence to the target mRNA strands, thus blocking their translation in cases where regulation of an over-expressed gene is required.[4] Short RNA strands known as short interfering RNA (siRNA) are also commonly used for applications such as these and operate in a similar way. The ODN investigated in this work in complexation with diblock cationic copolymers has the antisense code for the proto-oncogene C-Myc, while the siRNA used in the study of complexation with PEI is complementary to the sequence for glyceraldehyde 3-phosphate dehydrogenase (GAPDH), a housekeeping gene ubiquitous in mammalian cells.

Applications of Downregulation

The protein, C-Myc, produced by this gene is a transcription factor with a role in cell signalling and cell-cycle regulation and is able to trigger a halt in the cell cycle if mutations or abnormalities are detected during prophase, or may induce apoptosis. Approximately 15% of cellular DNA is regulated by C-Myc.[159] However, many tumours and patients with Leukaemia are found to have elevated levels of the protein and the down-regulation of this oncogene has been demonstrated to reduce the level of the protein present in cells, with positive effects on susceptibility of certain tumours to chemotherapy. In one study in mice administered with a combination of antisense medication targeted at C-Myc and a second protein, bcl-2, and conventional chemotherapeutic agent cis-diamine dichloroplatinum (DDP),[206] the drop in cellular levels of C-Myc correlated positively

with reduction in tumour mass and growth rate in two kinds of metastatic melanoma which do not respond significantly to traditional chemotherapeutic treatments. Although removal of C-Myc alone was not found to be sufficient in over 50% of C-Myc initiated mammary tumours to induce tumour regression in one study,[61] it has been demonstrated in several cases to cause susceptibility to other chemotherapeutic agents by reinstating the apoptotic cell-signalling pathways.[206] Another study in 2007 on human patients with advanced melanoma recorded a similar drop in tumour resistance to the chemotherapeutic drug Doxorubicin (DXR) when treated with C-Myc ODN, finding, among other effects, that the tumour blood vessel density was reduced.[140] This is just one example of the type of treatment which can be produced through down regulation of expression with oligonucleotides, which may be DNA molecules (ODNs) or short interfering RNA (siRNA).

1.2.3 In Vivo Gene Delivery - Additional Complications

Much of the research utilising or examining transfection, and indeed some therapies [146], involve transfection of cells in vitro. However, there are many cases where DNA complexed with vectors are required to be directly administered in vivo, which presents many additional obstacles.

For the treatment of neuro-degenerative disorders, such as Parkinson's, which has seen some success in gene therapy trials [90] , complexes must cross the blood-brain barrier, which is notoriously difficult to traverse. Designing vectors with long circulation times, which do not suffer from protein adsorption or degradation, and small, compact lipoplexes increase the chances of successful delivery, compared with earlier attempts using large, viral vectors. While typical vasculature passage is limited by a tightly packed endothelial cell layer with gaps $\leq$2 nm, with a base membrane underneath which would be expected to limit particle size to 13-15 nm[55] in typical vasculature, and the endothelial junctions are thought to be even tighter in the blood-brain barrier, channels enabling passage of larger particles are thought to exist, although the precise size limit is unclear. One study in particular reports transfection with liposome complexes of around 85 nm[139].

Other applications require pulmonary delivery by inhalation or uniform delivery to skeletal muscles throughout the body, which each pose their own difficulties. Viral vectors in particular run the risk of provoking potentially hazardous immune responses, and this must be mitigated and the risks balanced with the requirements for stable transfection

against the transient transfection more commonly achieved with synthetic or non-viral vectors.

1.3 Existing Transfection Methods

1.3.1 Physical Techniques

Some early methods for transporting foreign DNA into cells in vitro were based on fairly aggressive, physical techniques. A gene gun involves conjugating the target segment of DNA to a sphere of gold or similar nanoparticle and firing it at a target cell with sufficient momentum to overcome the resistive forces of the cellular membrane. [**?**]

Another physical method which has met with some success and has proven effective in vivo is electroporation. The application of pulses of electric field permeabilises cell membranes, enabling intramuscular administration of plasmid DNA. As mentioned earlier, in Section 1.2.1, expression following naked plasmid transfection was shown to be stable for a period of 270 days when introduced into skeletal muscle with electroporation.[134]

1.3.2 Viral Vectors

Viruses are natural gene delivery vectors. Their life cycle revolves around transduction of their DNA into cellular nuclei, where they utilise the cells replication machinery to reproduce their DNA and manufacture the proteins necessary to build new viral capsids. They may then escape through lysis of the cell, or through fusing with the cell membrane to form the viral envelope. The mechanisms utilised by viruses to deliver their DNA cargo to the nucleus of the target cell, as described by Wagner,[185] are more dynamic than the synthetic vector approach typified by complexation to polymer or lipid vectors such as PEI. Mimicking of this approach would involve multi-component complexes, specifically designed to target different barriers in the transfection pathway. This approach would be among the most versatile of the synthetic vector methods, having the advantage that one polymer is not required to simultaneously overcome all the diverse barriers to transfection described above. It is possible to employ certain aspects of viral design within the framework of existing vector models by binding ligands, for instance nuclear localisation signals, to the polymer vector in order to enhance nuclear targeting and uptake, applying

coatings to complexes as well as designing particles capable of pH-responsive unpacking.

Safety concerns over viral vectors

Many concerns, fuelled by serious incidents in early clinical trials,[43] surround the use of disabled recombinant viral vectors for gene transfer in patients. A key concern is associated with recognition of viral surface proteins by the hosts immune system, which may stimulate the immune cascade of responses, leaving the patient in danger of experiencing serious symptoms. Nonetheless, it is becoming clear that gene therapy offers hope for treatment of many conditions currently lacking powerful, viable alternatives[43] and the high efficiency of gene transfer offered by viruses, together with progress in improving viral safety frequently justifies the use of viral vectors. Encouraging results have been obtained from recent, small-scale clinical trials, such as using adeno-associated virus-mediated gene therapy to treat an inherited retinal dystrophy, Leber congenital amaurosis (LCA) which causes low levels of sight at birth, degenerating to complete blindness by the time the patient is in their 40s. There is currently no traditional treatment for LCA, but the recent gene therapy trials targeting one of seven genes known to be associated with the condition showed encouraging improvements in several of the patients vision and little or no immune response to the viral vector.[132] Although the eye is a special case, being less susceptible to immune reactions than other tissues, this is an exciting step towards proving the concept of safe gene therapy.

1.3.3 Non-viral Vectors

A range of vector types have application in gene delivery, each with their respective advantages and limitations or side-effects[**?**]. Due in no small part to concerns about the safety of viral vectors for use in human patients, development of synthetic complexes mimicking the viruss capacity for transfection has been the focus of much research. Synthetic, chemical vectors also have the advantage of being tailorable in various respects to facilitate targeting to particular cell types or intracellular locations or manifest environmentally-responsive unpacking.

Lipids

As cationic molecules with a hydrophilic head group and hydrophobic chain, which are able to surround and encapsulate DNA within spherical lipid bilayers known as liposomes, which can self-assemble from mixtures of cationic lipids with DNA. The lipids form a protective barrier around the DNA and, with the high biocompatibility of membrane-derived phospholipids, are able to fuse with the cell membrane to facilitate endocytosis and are widely studied gene-delivery vehicles due to their efficacy and biocompatibility[9]. Endosomal escape of liposomes can be facilitated through incorporation of fusogenic lipids, which fuse with and disrupt the endosome membrane, enabling escape of the complex. This is akin to the viral disruption mechanisms of fusogenic peptides from virus coatings, which may also be conjugated to complexes for use in gene delivery.[54] Conjugation of lipids to hydrophilic moieties such as polyethylene-glycol, also helps to maintain complex colloidal stability in solution and certain complexes have been shown to reduce the toxicity associated with pure liposomal transfection.[109] Cationic liposomes are thought to dissociate within the cytoplasm or on escape from endosomes, as microinjection of lipoplexes into the nucleus has excluded the possibility of transfection with intact complexes.[89]

Polymers

Cationic polymers have been used for some time as transfection agents for plasmid DNA and oligonucleotides. A wide variety of suitable polymers are available, albeit with varying degrees of toxicity and efficacy. Until recently, the transfection efficiency of polymer vectors was far behind that of viral vectors, although advances in recent years have improved the situation such that levels of transfection are comparable.[60] One of the great advantages of synthetic polymers is their high tailorability. A multiplicity of functional ligands may be conjugated to them, such as nuclear localisation signals, which improve the efficiency of transfection by promoting nuclear uptake. PEGylation is a term coined to describe conjugation of poly-ethylene-glycol (PEG) to a molecule. PEG is used in a variety of drug delivery applications, including DNA delivery, to increase the colloidal stability and solubility of drugs in suspension.[27]

Polyethyleneimine (PEI) is one of the most widely used cationic vectors, due to its high positive charge density and resulting strong ability to bind DNA and high number of protonable amine groups,[78] which give it a particular capability for buffering decreasing

pH, potentially contributing to facilitating endosomal escape by rupture of the endosome through increased osmotic pressure, as discussed above. Its structural evolution during the process of aggregation following complexation with short DNA fragments, comparable in size and structure to the commonly used siRNA, is studied in Chapter 4 of this work.

Novel Synthetic Vector Design

Highly branched cationic dendrimers with high charge density have an advanced ability to condense DNA and many available sites for ligand conjugation[24], diblock copolymers can incorporate targeting moieties or stabilising, hydrophilic blocks to increase colloidal stability and, potentially, circulation time of complexes[111], while other vectors include pH-responsive or membranolytic polymers[11], each designed to overcome a specific obstacle to efficient gene delivery.

1.4 Aim of Research

In this research, we seek to improve understanding of the physical structure and structural evolution of complexes formed between a range of different cationic polymers and nucleic acids, in order to contribute to the overall understanding of gene delivery complexation and how factors such as charge ratio, pH, copolymer block ratio and other solution conditions affect complex structure and colloidal stability. Greater understanding of the physical structure and processes is desirable precursor to support improvements in future vector design.

Chapter 2 gives some theoretical background to the process of polyelectrolyte binding and DNA complexation and compaction, as well as the process of gene delivery and the most significant hurdles we have identified. Chapter 3 describes the principal techniques utilised in this study and outlines the common methodologies applied. Chapters 4, 6 and 5 focus on addressing key research questions, outlined below, while Chapter 7 examines the overall findings of the work and explores potentially fruitful future directions for extension of the work.

1.4.1 Structural Evolution of Cationic Polymer Complexes with DNA

PEI is a commonly used vector for gene delivery, but its association and binding pathway is not fully characterised. PEI and its complexes with DNA have been well characterised, but there has been relatively less focus on the structural evolutionary studies immediately following mixing. ITC work has been undertaken, notably by Choosakoonkriang et al [28], however this does not enable direct structural analysis of the complexes. PEI complexes are notoriously difficult to stabilise in the size regime required for SANS. Therefore, as far as we are aware, previous structural neutron-scattering work, to the extent that it has been carried out, has been static and focused on the particular formulations of complexes which can be produced to be stable after 24 hours [130]. However, this is not likely to resemble strongly the formulations and complexation procedure typically used in transfection work. Therefore, we sought to contribute to the understanding of the formation of complexes over a relevant time frame for transfection work as it is commonly carried out, employing the ability of SANS to probe detailed structural features, by combining stopped-flow mixing apparatus to enable precise identification of the age of the PEI-DNA mixture, with the structurally sensitive SANS technique to enable further understanding of the aggregation process in this important, commonly used transfection agent, and sought to relate it to what is known from the literature about its transfection efficacy in vitro.

Selection of the System and structural expectations

In this study, two types of PEI architecture, linear and branched, of two different molecular weights approximately an order of magnitude apart, were investigated in the formation of complexes with a DNA fragment of a similar size to siRNA, in order to examine their different structural geometries and evolutions in the time following mixing, with a particular emphasis on colloidal stability.

PEI was selected based on its common use and success as a gene delivery agent. PEI of a relatively low molecular weight ($\lesssim$ 25 kDa), as used in this investigation, has been found to have superior transfection ability using siRNA as well as other types of DNA.

DNA of this size and structure was selected for study due to the relevance of transfection, both therapeutic and research-based, of short, double-stranded nucleic acid fragments. Commonly used siRNA consists usually of double-stranded fragments, while short, double-

stranded segments of DNA may include Dbait, a stabilised short DNA segment (short interfering DNA) with potential applications in cancer treatment, through its inhibiting action on repair of DNA breakage caused by conventional cancer therapy[30]. Larger DNA molecules were initially tested for comparison, but preliminary mixing trials showed large scale, visible flocculation and apparently high viscosity, which it was thought could make it unsuitable for stopped-flow mixing and it was decided to focus on one type of DNA system.

Although the DNA samples used were just fragments with a given physical size range, rather than functional sequences, the size ranges chosen corresponded to relevant functional nucleic acids which have applications in gene delivery. The fragments thought to be 15-50 bp (approximately 51 - 170 Å) in length, are of a similar order of magnitude to siRNA sequences, which are commonly used for gene knockdown. Importantly, although siRNA and DNA-based oligonucleotides differ in some of their chemical makeup, both our chosen DNA system and siRNA molecules have a similar charge density, as all nucleic acids contain one phosphate group per nucleotide, a similar mass per nucleotide of 330 Da for DNA and 340 Da for RNA[102], and, importantly for their solution conformation and interaction with polymers, the fragment lengths lie within the persistence lengths of their respective types of nucleic acid, the herring sperm DNA fragments of 15-50 bp being well below the 150 bp persistence length of ds DNA, while typical siRNA have a length between 18 and 26 nucleotides[7] with a persistence length of 62 +- 2 nm [1] for double stranded RNA. These factors contribute to the relevance of comparisons, from a biophysical perspective, of these structural findings with transfection efficiencies of siRNAs, as well as short, double-stranded DNA fragments, described in the literature, with a considerable degree of confidence.

The relative sizes of the molecules studied are presented in Table 1.1. As the DNA is thought to be double-stranded, based on previous published studies[31][**?**], the manufacturer's description and electrophoretic size estimation, the length is smaller than the persistence length, indicating the molecule will be stiff on this length scale. However, it is expected to be shorter than or of a similar length scale to the lower molecular weight PEIs, particularly the linear ones. This stiffness may hinder efficient complexation, although the branched PEI may be more flexible and therefore better able to bind the DNA charges more fully.

The high molecular weight polymers are expected to be an order of magnitude longer than

the DNA, and may have greater flexibility, depending on solution conditions and charge neutralisation by the DNA molecules.

Some authors suggest the DNA and PEI bind into a mixed, globular structure, while others emphasise the importance of a surrounding polymer structure, which may consist only of radial branches, in blocking nuclease degradation. The precise structure may depend on the vector and nucleic acid size and types and solution conditions. Utsuno et al[180] highlight two binding modes for PEI and DNA, one which takes place directly to the DNA bases, even when unprotonated, and the other to the backbone, which they postulate results in tighter binding when pH falls.

Polymer Type	LPEI		BPEI		DNA
	Low Molecular Weight	High Molecular Weight	Low Molecular Weight	High Molecular Weight	
Polymer Molecular Mass (kDa)	2.5	25	1.8	25	$\lesssim 31.6$
Approximate polymer contour length (Å)	265	2650	87	1205	$\lesssim 170$

Table 1.1: Molecular mass and length paramaters structures of large and small, branched and linear PEI and DNA fragments investigated in this study

1.4.2 The Impact of Cationic Polymer Structure and Molecular Weight on Zeta Potential

The PEI complexes whose formation was studied with SANS were further investigated using zeta potential studies to examine some of the forces involved in complexation and aggregation. High and low MW branched and linear PEI molecules were complexed with a commonly used type of nucleic acid, siRNA, which has great structural similarity to the DNA fragments utilised in the SANS study, to investigate the associated zeta potential of the complexes which also gives indications as to their colloidal stability.

1.4.3 The Structure of Complexes of Cationic Diblock Copolymers with ODNs and Plasmid DNA

The sections above describe studies of one of the most fundamentally important and commonly used cationic polymers for transfection. Our study also focused on a type of cationic diblock copolymer, part of a family of copolymers studied previously by Zhao et

al [202]. Complexes formed with pure cationic polymers, such as PEI, tend to aggregate under certain conditions, at times to such an extent that they may effect their transfection ability and colloidal stability in solution, either positively or negatively.

A family of diblock copolymers, introduced as a novel system in previous work by Zhao et al[202], aims to address this by sterically stabilising the complexes in solution by means of their amphipilic block, while binding DNA with the cationic block. Previous work has focused on one particular polymer of this family, and in the present study it was aimed to extend understanding of these polymers' behaviour in delivery of oligonucleotides, an important potential therapeutic agent, by examining other members of the copolymer family with varying block degrees of polymerisation ratios to identify the relative differences in structure as examined by small angle neutron scattering.

Chapter 2

Relevant Polyelectrolyte Theory and Focus of Study

2.1 Fundamental Polymer Theory

The problem of DNA complexation incorporates questions of polyelectrolyte structures and binding models, solubility and solvent conditions and colloidal stability.

2.1.1 Polymers

Polymers are chemically bonded chains of repeated chemical units or monomers. They may have branched or linear structures and may consist of only one type of monomer, or may take the form of random or block copolymers, where monomer units of several different kinds are grafted together, commonly in a defined ratio. Polyelectrolytes are polymers which possess an electrostatic charge. In this work, both the nucleic acid and complexing polymers used are polyelectrolytes of opposite charge. The specific polymer types used in this work are discussed in further detail below.

Cationic Polymers

The cationic polymers used in this work are linear and branched polyethylenimine (PEI) polymers of molecular weights ranging from 1.8 kDa to 25 kDa, which corresponds to a

degree of polymerisation ranging from approximately 41 to 580 repeats of the fundamental chemical formula unit, aziridine (C_2H_5N) although for branched polymers, the structurally repeated unit typically contains between 3 and 11 of the fundamental chemical units. Each chemical monomer unit contains one protonatable amine group, which can carry up to a maximum of one positive charge unit, depending on the pH which, in conjunction with the apparent pKa, determines its state of protonation. At neutral pH, there is some uncertainty about the theoretical proportion of amine groups which are protonated in PEI, as described by Ziebarth et al[204], although titrations suggest at least 50 % of amines are protonated around physiological or neutral pH.

As can be seen from the range of polymers used, PEI can be synthesised at various molecular weights in either a branched (BPEI) or linear (LPEI) configuration. BPEI is synthesised by polymerisation of aziridine in the bulk in a reaction whose rate and extent are determined by the temperature and available quantity of necessary initiators. LPEI, conversely, is produced by ring-opening polymerisation of aziridine derivatives, such as 2-ethyl-2-oxazoline [133], followed by hydrolosis. [193] The typical structures of PEI in its linear and branched forms are shown in Figure 2.1.

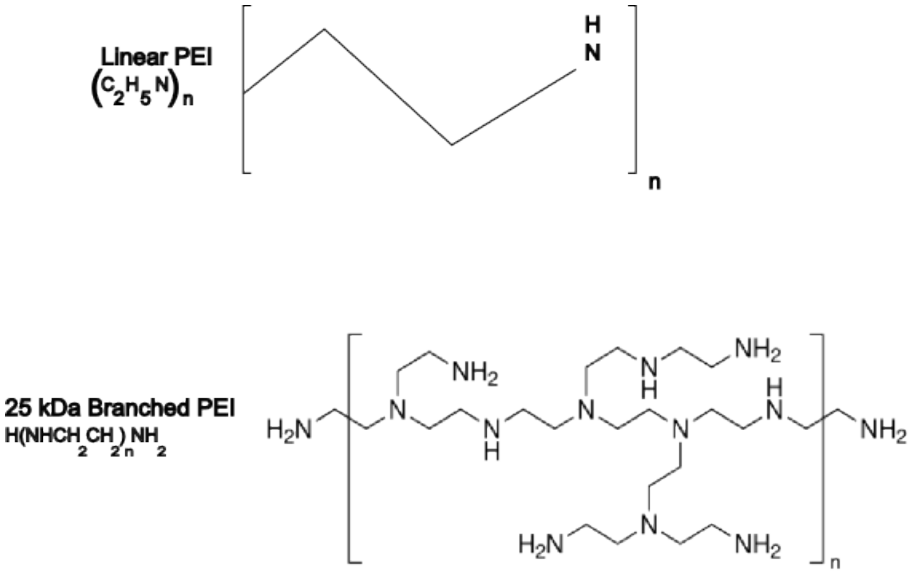

Figure 2.1: Linear and Branched PEI structures; Linear structure adapted from Polysciences.com; Branched schematic incorporated directly from the manufacturers' online description of the 25kDa BPEI used in this study (www.sigmaaldrich.com)

The MPC-DEA copolymer studied in Chapter 6 consists of one linearly polymerised block of phosphocholine monomers grafted to a linear block of diethylamine in varying, specified proportions. In the family of copolymers examined here, the MPC block always had a

degree of polymerisation of 30, while for the DEA block, this varied between 30 and 100. The structural schematic is shown in Figure 2.2.

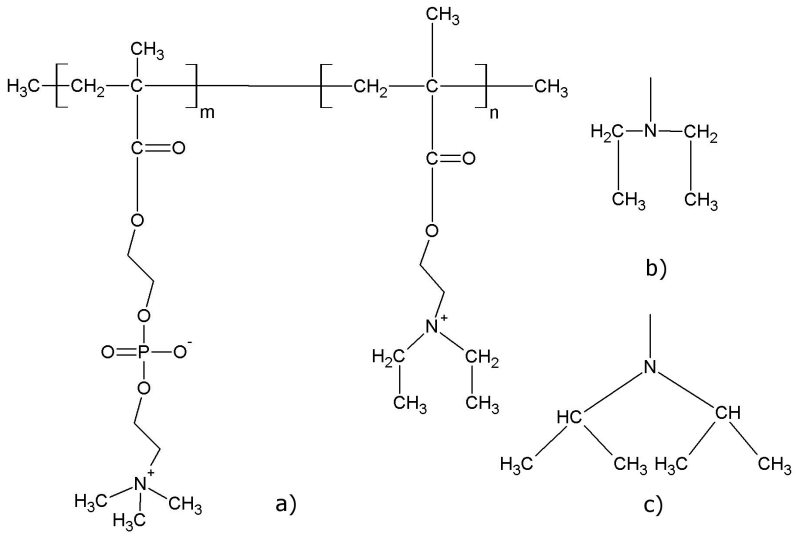

Figure 2.2: a) Chemical Structure of MPC_m-DEA_n diblock copolymer; m and n refer to mean degrees of polymerisation of MPC and DEA respectively and may take the values m = 30, n = 30, 70, 100. (Adapted from Zhao et al [203]); In other variations on this family, b)Methyl groups of MPC-DMA copolymer; or c) Isopropyl groups of MPC-DPA copolymer may be substituted for the ethyl groups of DEA (Only DEA polymers are used in this work)

Sub-figures b) and c) of Figure 2.2 depict the other potential cationic blocks in this polymer family, not examined in this work, where the ethyl groups of DEA are replaced with methyl and isopropyl groups in DMA and DPA blocks, respectively.

Synthesis of the copolymers, described by Zhao et al [202] with reference to original descriptions by Ma et al[118], prepares copolymers by initial polymerisation of the MPC monomer, with subsequent additional polymerisation of the DEA block. Polymerisation progressed by sequential monomer addition through atom transfer radical polymerization (ATRP) at 20^{o}C. The MPC block is zwitterionic while the DEA block is cationically charged, possessing one protonatable amine group per monomer unit.

The MPC block is hydrophilic, designed such that its polarity facilitates solubility in water, and hence serves to stabilise the polymer as a whole in solution, which is particularly important when the DEA block becomes engaged in complexation with anionic DNA, which may lead to overall charge neutralisation of the complex and increase tendency towards aggregation, as is observed in the case of PEI, which lacks this stabilising component. The question of solubility and stabilisation is discussed in greater depth below.

Nucleic Acids

There are various forms of nucleic acids which are suitable candidates for gene delivery with important medical or biological applications, yet their structures may vary considerably and each presents different challenges for complexation. The main types of nucleic acids for which complexation is required are described below:

Plasmid DNA

Plasmid DNA is a long, double-stranded, circular DNA molecule, which may have a wide range of sizes. In this work, plasmids of approximately 5 kBP, such as Luciferase plasmid (5.1 kBP [202]) were used for physical studies. This corresponds, with an average length per base of 3.4 $\mathring{A}$[202] to a total chain length of around 17,340 $\mathring{A}$. Double-stranded (ds)DNA has a persistence length of $\approx$ 50 nm [199], so it can be seen that in comparison to its overall length, the large DNA molecules are able to coil relatively tightly, despite its high stiffness and significant persistence length, which is advantageous for condensation in gene delivery, or indeed the native histone-coiled form in nuclear chromatin, aided of course by neutralisation of its charges through binding, reducing the intra-molecular repulsion which contributes to its high inherent stiffness.

Oligo-deoxynucleotides

Oligo-deoxynucleotides (ODNs) are single-stranded (ss), short, DNA fragments, which are typically synthesised to have a particular sequence, which may be complementary to a mRNA sequence of interest for down-regulation. The ODN molecules used in this work are 15-base antisense sequences to the C-Myc proto-oncogene, with the sequence 5'-AAC-GTT-GAG-GGG-CAT-3' and were obtained from Eurogentec or provided by a colleague, Dr XiuBo Zhao. As single stranded DNA chains have greater contour lengths per base than double stranded DNA in its helically folded conformation [198][125], these have a length of 7 $\mathring{A}$ per base of ssDNA, corresponding to a total chain length of 105 $\mathring{A}$. SsDNA is significantly more flexible than dsDNA with a persistence length around the same as the length of one base, around 7$\mathring{A}$. [197]

Short interfering RNA

Short interfering RNA (siRNA) consists of short RNA fragments in a similar size range to ODN, typically between 18 and 26 nucleotides[7], but is commonly double-stranded. Double stranded siRNA has been found to be more effective at knock-downs than single-stranded siRNA[196], and siRNA commonly has this form, hence comparisons are drawn in this work with double stranded rather than single-stranded siRNA. RNA differs from DNA in one component base, with Uracil instead of Thymine, but otherwise has a similar mass per nucleotide, with 330 Da for DNA and 340 Da for RNA[102]. In a similar manner to ODN, siRNA is used to bind and down-regulate specific sequences of DNA, hence is also synthesised in complementary sequences. Double-stranded RNA has a persistence length of 62 +- 2 nm [1] which is, again, slightly higher than dsDNA but broadly similar, enabling structural comparisons to be made between the behaviour of dsDNA and dsRNA. The molecules' varying persistence lengths have implications for the nucleic acids' behaviour when binding to other polyelectrolytes, particularly contributing to determining whether they are more likely to behave in a rod-like manner, as with dsDNA, or adopt a more flexible, potentially even coiled conformation, as with the highly flexible ssDNA.

2.1.2 Polyelectrolyte Binding Models and Complexation Kinetics

Nucleic acid condensation and compaction

DNA condensation occurs when 89-90% of DNA charges are neutralised through binding with a condensing polymer[33][181][99] and can result in a significant decrease in molecular volume. The resulting DNA structures may resemble toroids or rods, depending on the form of the initial nucleation, the solvent and the condensing agent. [33] Efficient condensation of DNA in eukaryotic cells by histone proteins makes the existence of chromosomes and a nucleus possible - without condensation on this scale all the genetic material required for life could not be contained within a cell. Similarly, the survival and replication of viruses based on importing their DNA into host cells requires the DNA package to be as small as possible to enable cellular and nuclear entry. This depends on the action of proteins like spermine to condense the DNA into toroidal structures. [141] Thus, models of the desired DNA compaction system exist in nature.

Ion-bridging model and salt concentration

Compaction of negatively charged, free DNA is made possible through binding of bridging counterions in solution. These act to shield the negative charges from each other when they come into close proximity and thus reduce the electrostatic repulsion which the molecule must overcome for condensation. Hence, a minimum ionic strength of the solvent solution is thought to be necessary for condensation to take place. [99].

Counterions in solution play several roles in condensation of DNA. Manning counterion condensation onto the surface of highly charged polyelectrolytes affects their charge in solution and the release of these ions upon complexation acts to reduces the entropic penalty of condensation of free polymers into an ordered complex, as discussed further in Section 2.1.2.

DeRouchey et al [36] studied the electrostatic self-assembly of polyplexes of DNA with cationic polymers at varying salt concentrations with small angle X-ray scattering (SAXS) and found that above a critical, polymer-dependent salt concentration, the compact, ordered complexes dissociated into loose bundles and then to systems with little long range order. This suggests that too high a presence of salt ions in the solution will shield electrostatic interaction so effectively that the DNA no longer feels the attraction of the cationic polymer and condensation ceases.

It would be interesting to determine this critical salt level at which MPC polymer complexes dissociate in relation to physiological ionic strength. The same authors[36] additionally proposed a method for complex formation at high salt concentration, which is then gradually reduced to the desired ionic strength (eg through dialysis). The mixing of polymer and DNA solutions under conditions where most interactions are electrostatically screened by high salt concentration[176], before slowly reducing the screening such as through dialysis with a lower salt solution to reintroduce electrostatic attraction is likely to enable diffusion into an evenly distributed mixture before significant binding takes place and, thereby, may reduce the size and charge polydispersity of resulting complexes. This theory is substantiated by work by Bloomfield et al.[16] who suggest that slow complexation kinetics may be required for rod-like condensation of large DNA molecules to allow time for DNA conformation to adjust, removing kinks and bends, before equilibrium is reached.

Theoretical models - Free energy and entropic gains

The binding of charged polymers in solution has been frequently simulated using various models such as non-linear Poisson-Boltzmann models, Monte Carlo simulations and free energy vs. entropy considerations. [33] The kinetics of DNA condensation with a cationic polymer depend on the balance between between the principle competitive forces of free energy of condensation and conflicting entropic changes. [152] [36] Free energy is gained upon condensation of the electrostatically opposed polymers. Additionally, the release of counterions bound to the two highly charged molecules contributes positively to the entropy of the system, which is thought to be involved in the phenomenon of overcharging. Conversely, the condensation of the two macromolecules into the highly-ordered, dense hexagonal close-packed structure results in significant entropic losses in the system.

The applied models have relevance for describing polymers' complexation and may facilitate predictions of the binding and dissociation parameters.[36] Particularly, Monte Carlo simulations have predicted and explained the charge inversion observed at high polymer-DNA ratios in similar polyelectrolytes to those used in this work. Fundamentally, overcharging effects are thought to arise due to correlations in the polyelectrolyte's adsorbed charges, caused by the initiation of binding, particularly for multivalent counterions, or by excluded volume effects [86].

Another contributing factor in the case of DNA is the release of condensed counterions predicted by the Manning counterion condensation theory[149], mentioned above, which predicts condensation of a neutralising counterion layer to reduce the overall linear charge density of a linear polyelectrolyte, such as DNA, to a critical, maximum value. Upon binding of another polyelectrolyte, therefore, counterions are released, resulting in an entropy gain, which has been related to the phenomenon of overcharging.[149] A deeper understanding of the effects of this cooperativity of binding could enable optimisation of the complexation procedure to more effectively counteract the DNA's inherent negative charge. [26]

The forces driving complexation, discussed above, can be elucidated experimentally through measurement of the heat of binding by isothermal titration calorimetry, which has been extensively studied for systems of PEI complexation with nucleic acids [28].

Complexation Kinetics

Initial complexation proceeds via electrostatic attraction of anionic DNA with the cationic polymer on a short timescale. Subsequent rearrangement has been shown to occur under some conditions, but is likely to depend on factors such as concentration and uniformity of mixing methods.

For stabilised diblock copolymers, the complexes are expected to have stability conferred by the hydrophilic MPC block, although the dependence of SANS fitted dimensions on the block size ratio does suggest some dependence on block size of stability, as discussed in Chapter 6. PEI-based complexes, on the other hand, are widely known to aggregate under certain solution conditions and the study of complexation of PEI with DNA fragments aimed to elucidate the process of this aggregation and factors affecting it.

2.1.3 Complex Structure and Charge Ratio

Prevailing structural models of DNA complexes with cationic polymers vary significantly with the type of DNA involved, depending crucially on the relative persistence lengths of the two components. Related copolymer molecules have been modelled as flexible polymer chains with a persistence length of approximately 1nm[**?**], although some differences may exist. Double-stranded plasmid DNA, in contrast to this, while still described by a semi-flexible chain model, has a persistence length of 50nm[36]. In their SAXS study of cationic DNA-polymer complex structures, Derouchey et al therefore represent the DNA as a stiff rod with the long, relatively flexible polymer chains binding electrostatically around them, linking DNA molecules. However, for charged polymers generally, the molecular stiffness will vary depending on the solution conditions, particularly salt concentration, which may have the effect of screening electrostatic repulsion from a like charged polymer and thus reducing its persistence length.

Much of the DNA molecules' stiffness is attributed to the double-strand bonding. For single-stranded polynucleotides such as synthetic ODNs, a persistence length of approximately 1nm has been established. [175] Previous SANS studies by Zhao et al.[192] of the structure of MPC-DEA-ODN complexes therefore presented a model where the single stranded ODNs coil around rod-like polymers. When the ODN is in excess, the polymers are bound end-to-end and, at higher charge ratios, several cylindrical structures are clustered adjacent to each other by the surplus ODNs.[192] Further to this, the work by

DeRouchey et al. investigated the structure of plasmid complexes with several cationic polymers including PLL and linear and branched PEI.[36] Their work concluded that the cylindrical components were bound in a hexagonally packed structure, the densest possible packing arrangement for parallel cylinders. [168]

2.1.4 Solvents, Solubility and Colloidal Stability

Solubility and aggregation is also to a great extent determined by properties of the solvent. The chain conformation of a polymer is dependent on solvent conditions such as polarity, ionic strength, pH and temperature. A polymer will exist in a random walk conformation under so-called theta conditions in a good solvent, while in poor solvents, the polymer may experience intra-molecular attraction, causing collapse into globular conformations[38]. Ultimately, in the extreme case, precipitation occurs or the polymer is found to be insoluble in the selected solvent conditions.

The Flory-Huggins theory of polymer solutions describes the solubility of a polymer in a particular solvent in terms of contributions from interactions of each particle with itself, other particles and the solvent, to calculate the energy of mixing. A contribution due to the entropy of mixing is also incorporated.

The solubility of individual, pure polymer molecules in water depends on the presence of polar groups, such as in the MPC block of the copolymer. Nonetheless, addition of a small quantity of concentrated HCl is sometimes required for complete dissolution of the cationic polymer.

Similarly, linear PEI is insoluble in water at neutral pH at room temperature, hence to dissolve a stock solution, the pH must first be adjusted to a low level using concentrated HCl, and subsequently back-titrated to the desired experimental pH.

These phenomena are probably related to the electrostatic double layer, characterised by the Debye length, surrounding the molecules. In pure water or low ionic strength media, there will not be sufficient available Hydrogen ions to fully protonate the polymer, hence intra-molecular electrostatic repulsion, which would prevent self-association of the polymer, is limited.

Aggregation of complexes is expected to occur at an increased rate when the net surface charge of the complex is close to neutrality, as they are driven by hydrophobic forces and the Van der Waals force, but counteracted by electrostatic repulsion between the like-

charged complexes, which increases the distance between them due to the electric double layer. This is discussed in more detail in the context of the study of aggregation of PEI-DNA complexes in Chapter 4. The addition of salt to the medium, which screens the electrostatic interaction, or the reduction of net charge of the complexes should lead to weakening of the electrostatic repulsive force, and an increased tendency for aggregation. Steric stabilisation can be achieved through grafting of extended, solubilised polymer chains to a polymer involved in complexation, as is the case with the MPC-DEA diblock copolymers, or modifications of PEI which conjugate a hydrophobic polyethyleneglycol (PEG) chain to improve solution stability of complexes.

2.2 Areas of Interest

The key areas of interest for study in terms of structural parameters which are thought likely to influence the cellular uptake efficiency and specific mechanisms, which in turn influence transfection efficiency, are the net surface charge, complex size and structure and solubility or stability against aggregation in solution. As discussed in Chapter 1, these questions were selected as the main areas of focus of the biophysical studies of cationic diblock copolymers and PEI complexation with nucleic acids presented in this work.

Chapter 3

Relevant Experimental Techniques and Associated Theory

3.1 Sample Preparation and Characterisation

3.1.1 Glassware

Glassware, including optical quartz cuvettes, was typically cleaned with 5% Decon90 solution and rinsed with copious tap water, followed by distilled water and then by UHQ water (Millipore), then dried in an oven or with a nitrogen stream. Periodically, or if glassware appeared to be extremely dirty, or did not manifest a hydrophilic surface following cleaning, it was cleaned using piranha solution, followed by thorough rinsing, as above. The exact composition of the piranha solution was not precisely controlled, as SANS is not a surface technique and was often prepared in conjunction with other lab members who were conducting surface work with a prescribed composition. Piranha is an exothermically heated mixture of H_2SO_4 and H_2O_2 and a typical composition used in the lab was of the order of 2:1 or 3:1, although higher proportions of H_2SO_4 were used on occasion.

Additionally, if solvents other than water were to be used, glassware was rinsed with the

relevant solvent before sample preparation and large-volume, disposable plastic-ware was similarly rinsed with the relevant solvent before use. For particular samples, such as the highly cationically charged polyethylenimine complexes, cleaning with highly concentrated (3 M) NaCl solution was found to be the most effective at dissociating complexes from the anionic surface of quartz cuvettes, used in either dynamic light scattering(DLS) or small angle neutron scattering (SANS), while rinsing with ethanol was avoided until preliminary, thorough cleaning had been undertaken, in case it induced precipitation.

3.1.2 Nucleic Acids Preparation

The protocol for preparation of nucleic acids differed depending on the experimental technique to be used and the type and state of the nucleic acid samples. Typical protocols for preparation of nucleic acid samples are outlined below:

Oligodeoxynucleotides

Oligonucleotides (ODN) were obtained from Dr. XiuBo Zhao at relevant stock concentrations, typically dissolved in D_2O for SANS experiments. For SANS studies, ODN was typically used at a mixing concentration of 1 mg/ml, mixed in equal volumes with copolymer solutions at the necessary concentrations to generate complexes at the required charge ratios with a final DNA concentration of 0.5 mg/ml.

Short Interfering RNA for Glyceraldehyde 3-Phosphate Dehydrogenase

Short interfering RNA (siRNA) with the binding sequence for the glyceraldehyde 3-phosphate dehydrogenase (GAPDH) gene (Silencer, Ambion) was purchased from Invitrogen and diluted to the required concentration with UHQ water, based on the quantity determined by the manufacturer quoted in the accompanying, batch-specific information. The stock solution was diluted to required concentration for experiments and a small quantity of concentrated NaCl solution was added to bring the final solution composition to 10 mM NaCl for zeta potential studies, for comparison with SANS studies of PEI-DNA complexes. Although the siRNA was supplied in the manufacturer's buffer (20 mM potassium acetate, 6 mM HEPES-KOH pH 7.4, 0.4 mM magnesium acetate) for storage, it was diluted approximately 150 times to attain the experimental working concentration, and was thus judged to make minimal contribution to the final solution composition.

DNA Fragments

'Crude oligos' of partially-degraded of herring sperm DNA fragments (D3159, Sigma) were selected as they were of a size comparable to commonly used siRNA molecules to enable physiologically relevant conclusions to be drawn and were purchased in the quantities required for kinetic SANS studies following purification (several grams) from Sigma-Aldrich.

The fragments were claimed to be of a size range $\leq$50 bp, and purity was unknown, so fragments were purified extensively with chloroform, followed by ethanol precipitation and resuspension and finally, filtration before use. The purification protocol is described in detail in the relevant method Section of Chapter 4, Section 4.2.1

DNA Quantitation and purity determination

Subsequently, the concentration and resulting purity of the purified sample were estimated using UV absorption. Small quantities of purified stock of unknown concentration (typically 1 - 10 μl) were added serially to a known quantity of water (typically 600 μl) and the difference in absorption at a wavelength of 260 nm measured to calculate the concentration of DNA contained within that sample. It was determined that the stock concentration of herring sperm DNA fragments solution was 7.7 mg/ml. DNA sample purity was determined by simultaneous measurement of the absorption at 280 nm and calculation of the A260/A280 ratio, and was found to be acceptable with a value of 1.62.

The stock concentration was subsequently validated independently by Michal Smiga of the Genomic Technologies Core Facility, Michael Smith Building, University of Manchester from a sample provided for DNA fragment size analysis and was found to be 8.2 mg/ml - similar, given the differences in the techniques used and the sample concentration supplied, to the value determined by manual dilution of multiple aliquots and UV absorption measurements in a high-volume cuvette. Nanodrop is an alternative, automated spectrophotometer for nucleic acid concentration determination which can determine the UV absorption by addition of a single drop of sample solution. However, the stock concentration was outside the manufacturer's recommended range of operation and no repetition was conducted, due to the single drop nature of the technique and it was hence decided to accept the originally determined concentration as accurate within tolerable uncertainty.

Electrophoretic DNA Fragment Sizing with Bioanalyser

The 'crude oligo' DNA fragments purchased from Sigma for neutron studies had an approximate size range, as quoted by the manufacturer, of $\leq$ 50 bp and were considered to be double-stranded fragments, based on the manufacturer's quoting of the fragment sizes in base pairs, and work by Cristofolini et al[31][**?**], who were able to fit models to layers of the same sample using parameters for double-stranded DNA, although there is a possibility that mechanical effects in the purification processes used here could have had an impact on this. It was therefore desirable to characterise the DNA sample prior to use, to verify its exact size range and polydispersity.

Stock samples were provided to Michal Smiga of the Genomic Technologies Facility who included them in running a Bioanalyser (Agilent) electrophoretic chip for fragment size determination. The Bioanalyser technology enables electrophoretic sizing of up to 12 samples in individual wells to be conducted on a single proprietary chip[138], with calibration by a standard set of DNA size markers run in an adjacent lane and the addition of two reference markers to the sample well for alignment. The Bioanalyser applies an electric field across a gel matrix deposited on the chip and by measuring the electrophoretic mobility of the sample through the gel, can deduce the size of DNA molecules through comparison with known size standard markers. DNA is visualised by inclusion of a fluorescent, nucleic acid intercalating dye[138], and the proprietary software generates a sizing profile, displayed for these fragments in Chapter 4.

Plasmid DNA

Plasmid DNA for small angle neutron scattering studies was cultivated in transducted Escherichia Coli (E. Coli) bacterial hosts which were cultured and the plasmids extracted using the Endofree Plasmid Mega Kit (Qiagen).

Plasmid DNA can be produced in relatively large quantities (mg) and extracted from cultures of bacteria, which has been genetically modified to include the plasmid of interest, in this case, Luciferase (Luc), co-transfected with genetic material which gives the bacteria specific antibiotic resistance. E. Coli incorporating the Luciferase plasmid are engineered for resistance to Ampicillin, enabling specificity of culture to the bacteria of interest containing the plasmid. Bacteria were cultured and plasmids extracted following the protocol described by Zhao et al [**?**] and the manufacturer's protocol was followed for

plasmid extraction (Qiagen plasmid mega kit).

Typically, Luria Bertani medium (LB Broth, Difco, 244620, pH 7) is prepared by diluting LB Broth powder to a concentration of 25g/l in UHQ water. The medium is autoclaved in covered conical flasks and allowed to cool before the appropriate selective antibiotic (1000x) is added at a concentration of 1ml/l.

A 1ml vial of bacteria starter culture is removed from the liquid nitrogen storage and defrosted rapidly (in under 1 minute) in a water bath at 37^o. Care is taken to avoid contact of the vial lid with the water to prevent possible contamination. The defrosted cells are seeded in two 50ml conical flasks of LB and incubated at 35^oc overnight with vigorous shaking (typically 300 rpm).

1ml of the seeded culture is added to each of six flasks containing approximately 150 ml of LB medium, covered and incubated for between 12 and 16 hours under the same conditions.

An endotoxin free Plasmid Extraction Kit Endofree Plasmid Mega Kit, Qiagen is used to extract the plasmid DNA from the harvested cells, following the manufacturer's protocol. Briefly, the E. Coli are harvested by centrifugation of the culture at approximately 4,000 rpm. The cell pellets are resuspended and lysed to break the cell membranes and release proteins and genomic DNA, which are then precipitated and filtered under vacuum. The precipitate is chilled and the solution containing the plasmids is passed through a treated filter which binds the plasmids and is then washed and the DNA subsequently eluted. The plasmid DNA is precipitated with isopropanol and centrifuged at high speed to obtain a pellet. This is then washed with ethanol to remove additional salt and centrifugation repeated, followed by resuspension in a small volume (typically up to 2-3ml) H_2O or D_2O.

The plasmid concentration is established by diluting a small volume of the suspension to an estimated concentration of approximately 1mg/ml by adding approximately 0.5 μl of DNA suspension to 1 ml of water. The concentration of DNA in the solution is measured by UV absorption at 260nm and an indication of the purity of the solution gathered by comparing this with the absorption at 280nm, the peak wavelength of protein absorption. Surplus culture medium and all non-disposable glassware are disinfected, typically overnight, in Virkon solution (Antec International) after use.

3.1.3 Cationic Polymer Preparation

3.1.4 MPC-DEA Copolymers

Stock solutions of cationic diblock copolymer solutions for SANS were either obtained from Dr. XiuBo Zhao, or prepared freshly from dried polymer sample. Solutions were typically dissolved in low ionic strength media, such as 10 mM PBS and solutions for SANS were prepared in D_2O-based solvents. D_2O is a more suitable medium for the samples in question as it provides strong scattering length density contrast, as discussed below, and minimises incoherent background scattering, due to the low incoherent scattering cross-section of deuterium in comparison to hydrogen, thus improving the signal-to-noise ratio.

Stock solutions in the relevant solvent were typically dissolved overnight with gentle stirring, and pH was reduced using concentrated HCl, if required, to aid dissolution, and subsequently returned, using NaOH dissolved in the relevant solvent, to the relevant value required for experiment.

3.1.5 Polyethylenimine

Branched and linear polyethylenimine samples of different molecular weights (MW) were purchased from Polysciences (linear PEI 2.5 kDa and 25 kDa and branched PEI 1.8 kDa) and Sigma (branched PEI 25 kDa).

Stock solutions of all four polymers were prepared, typically at concentrations of 5 - 10 mg/ml for LPEI, which is minimally soluble in water, and 10 - 100 mg/ml for BPEI solutions.

Branched PEIs are easily soluble in water, hence the required amount was weighed and dissolved at room temperature on a rocker for up to several hours to overnight. Linear PEIs, on the other hand, as described in further detail in Chapter 4, are not soluble in water at room temperature or neutral pH, so they required the addition of concentrated HCl to lower the pH until no remaining polymer was visible in the solution. While the precise volume was not recorded for all samples, the pH was typically required to reach very low levels (of the order of $\approx$ pH 1), but the added quantity was roughly estimated for some samples for considerations of likely levels of added salt, which were not thought to be significant. Typically, solutions were incubated with rocking at room temperature

for several hours at this stage to ensure stable dissolution, before back-titration of the pH to the required value with concentrated NaOH in the relevant solvent (D_2O for SANS experiments, H_2O for zeta potential studies) with the addition of NaCl or glucose as required for experiments.

Where possible, PEI solutions were prepared in advance and the pH checked and adjusted several times before use, as PEI is able to strongly buffer changes in pH and drift was found to occur on occasion. However, pH was always checked and finally adjusted shortly prior to experiments, which in some cases did require a relatively large adjustment. Where potential pH drift was suspected, as in some stopped-flow SANS experiments, the effect of some degree of pH variation on scattering outcomes was investigated, as discussed in Section 4.4.4. Minimal effect on structure was found to result from pH variation in the range examined.

3.1.6 pH Measurement in H_2O and D_2O

pH was measured with a glass electrode calibrated against at least 2 or, more usually, 3 standard buffers of pH 4, 7 and 10. The pH probe was rinsed with UHQ water and dried with lint-free tissue, before gently stirring the solution to be measured until the reading stabilised to within approximately $\pm$ 0.1 pH units.

As Beynon describes [14], the pH reading for samples in D_2O should actually be converted to a pD reading which is easily performed for a pH meter which has been calibrated in protonated as opposed to deuterated buffers, by the addition of an offset of 0.4 to the pH reading, giving the true pD value. Hence, for SANS samples with pH readings of 7, an actual equivalent value of pH 7.4 was quoted and, where comparison with experiments performed on samples in protonated solvents was required, a pH reading of 7.4 was used for those samples for equivalence.

3.2 Physical Techniques

3.2.1 Size and Structure

Dynamic Light Scattering

Dynamic light scattering was used predominantly for supporting measurements and screening of sample conditions in preparation for small angle scattering studies. Some sample curves have been included for reference. Samples were diluted in an appropriate buffer or solvent and measured added to a quartz cuvette.

Theory

Dynamic light scattering (DLS) or photon correlation spectroscopy (PCS) is a technique for determining the hydrodynamic radius of particles in solution. Suspended particles will undergo Brownian motion due to their thermal energy and collisions with other particles in solution will cause a random-walk type motion. Laser light scatters from a solution in all directions. For particles much smaller than the wavelength of the scattered light, the Rayleigh approximation is valid, giving the relations for the scattered intensity, $I \propto d^6$ and $I \propto \frac{1}{\lambda^4}$. For particles above this threshold, Mie theory gives a more detailed relationship between scattered intensity and particle size, which is used to derive information about the volume of particles in the sample from the intensity data. Scattering patterns separated by a short time interval will not be identical, as the particles' positions will have changed and the scattering profile will be altered correspondingly. The correlation between these profiles after a time interval, τ, is given by the auto-correlation function of the sample, observable through the speckle pattern of scattering, which depends on the position and intervening velocity of the scattering particles, and is related to their diffusion coefficient, D. This function will approach 1 at short times and decay exponentially to zero after the decay time, which is, intuitively, proportional to the particles' size, falling off steeply as a single exponential for a monodisperse sample. A broader slope indicates polydispersity of particle sizes, having a correlation function described by a sum of exponentials. The decay constant Γ is the inverse of the decay time and is related to the diffusion coefficient of the particles' thermal motion, D, by

$$\Gamma = Dq^2 \tag{3.1}$$

where q is the scattering wave vector given by

$$q = \frac{4\pi n_o}{\lambda} \sin \frac{\theta}{2} \tag{3.2}$$

with n_o the refractive index of the dispersive medium, λ the wavelength of the laser light and θ the scattering angle. The hydrodynamic diameter of the particles, the equivalent diameter of a perfect sphere with the same diffusion coefficient, can be deduced using the Stokes-Einstein equation

$$d_H = \frac{kT}{3\pi\eta D} \tag{3.3}$$

where k is the Boltzmann constant, T the temperature and η the viscosity of the medium. In the instrumental configuration of the Zetasizer Nano (Malvern) used in this work, light is measured at a backscattered angle of 173^o to reduce the path of scattered light through the sample and, consequently, the incidence of multiple scatterings, in addition to reducing noise from dust and other very large particles, whose scatter peak lies around zero degrees, ie. predominantly forward scatter. [124] Data is analysed and interpreted using the accompanying software DTS Nano (Malvern Instruments).

Data Analysis

For a sample with a narrow decay function, the autocorrelation function can be analysed employing the cumulants method. The logarithm of the autocorrelation function is of an identical form to the mathematical function for generating the cumulants of a probabilistic distribution. The first, second and third cumulants of a function are related to, respectively, the mean decay rate, variance (both positive) and a measure of the skew or asymmetry of the function, which may be positive or negative. Correspondingly, the correlation function can be expanded in terms of its cumulants to obtain this information about the mean value of the decay constant, Γ. [52] Systems with greater polydispersity and longer data collection times may be interpreted using distribution analysis. More advanced analyses include the CONTIN algorithm which performs an inverse Laplace transform of the correlation function to identify peaks corresponding to the separate exponential components of the function, which can be attributed to different decay functions of particles in polydisperse systems. [76]

Experimental Method

A minimum of 200-300 μl of the sample were typically inserted in a rectangular, optical glass cuvette in the Zeta Nanosizer-S (Malvern Instruments). Measurements were carried out at a temperature of 25^{o}c and samples were typically left for approximately 3 minutes to equilibrate. Laser light is scattered from the particles and the scattering pattern is recorded over a typical period of 10 seconds and repeated on average between 10 and 15 times. Data analysis is carried out by the accompanying DTS Nano software (Malvern Instruments) to deduce the particle size in question. [112]

Zeta Potential

Zeta potential is a measure related to the surface charge of a particle in solution. The existence of a surface charge on a particle will cause adsorption of condensed counterions onto the surface, forming an electric double layer. The inner, Stern region of the double layer contains counterions which are strongly bound to and move with the particle and the mobility of the more diffuse outer layer up to a critical boundary determines the zeta potential of the particle. The zeta potential is, therefore, the potential at the boundary of hydrodynamic shear, ie. at the boundary between the region of the double layer which is strongly bound to and moves with the particle, and that which is more diffuse and remains independent of the particle's motion. [123]

Movement of a particle with its double layer under an applied electric field provides information about its electrophoretic mobility, which is related to the zeta potential of the particles or colloids by the Henry equation,

$$U_E = \frac{2\epsilon z f(\kappa a)}{3\eta} \tag{3.4}$$

, where U_E is the electrophoretic mobility, z is the zeta potential, ϵ isi the dielectric constant, η is the viscosity and $f(\kappa a)$ is Henry's function.

Using the Zetasizer Nano-ZS (Malvern Instruments), electrophoretic mobility, related to zeta-potential as shown above, is determined by the application of an oscillating electric field and exposure to a scattering laser, with a reference laser for comparison. The electrophoretic mobility of the particles produces a Doppler effect in the scattered light, shifting its phase relative to the reference beam, and hence providing information about

the speed of motion of the particles, while the frequency of motion can be related to the frequency of the applied field to give information about the particles' size. The Henry Equation is approximated for practical interpretation using the Smoluchowski approximation for polar solvents and relatively large particles, which was thought to be the most appropriate model for the PEI-siRNA complexes studied in water, using the approximation $f(\kappa a)$=1.5. This approximation is valid where moderate electrolye concentrations are present in the dispersant and particles are relatively small (according to the manufacturer's guidance, electrolyte concentrations greater than approximately 1 mM and size above approximately 200 nm. As these studies were used for aggregation, but the dispersant used was 10 mM NaCl, it is likely that the approximation is close to the validity regime, but may be borderline due to the particle size. It should be noted, then, that the zeta potential is estimated under these conditions and may not be a precise calculation from the electrophoretic mobility, but nonetheless provides a useful indication, particularly between different systems under similar conditions. [80]

The zeta potential is strongly affected by medium, dielectric constant, ionic strength, and pH. Knowledge of the zeta potential is useful for understanding colloidal stability of particles, as explained by the DVLO theory, which states that a particle's colloidal stability is predicted by its total potential energy function, V_T, which is given by

$$V_T = V_A + V_R + V_S \tag{3.5}$$

where V_A, ,V_R and V_S are the attractive and repulsive potential energy contributions and the contributions due to solvent interaction, respectively, and where the repulsive potential energy, V_R is given by

$$V_R = 2\pi\epsilon a\zeta^2 e^{-\kappa D} \tag{3.6}$$

with a, the particle's radius, κ is related to the ionic composition, ϵ is the dielectric constant, D is the particle separation and ζ the zeta potential. Hence, the extension of the double layer and the zeta potential at the boundary point is an important consideration when evaluating the likely stability of a colloidal system.

Measurements were conducted in a disposible folded capillary cell purchased from Malvern. The cells were rinsed with ethanol to promote wetting, as recommended by the manufac-

turer, and subsequently flushed several times back and forth with syringes containing the buffer to be used, before sample addition and measurement. Due to the limited quantity of siRNA available, and the slight variations which would inevitably occur due to manual mixing and addition to the cuvette and initiation of the measurement routine, independently repeated measurements were not conducted. However, each measurement run was performed multiple times, typically approximately $\geqq 10$ times. Due to the time-dependent nature of the system studied, no temperature equilibration time was included before measurements commenced.

Small Angle Neutron Scattering

Neutron Source

Small angle neutron scattering (SANS) is used to determine the size and structural composition of the complexes in solution with nanometre resolution. SANS was carried out on the LOQ and SANSD diffractometer instruments at the ISIS Spallation Neutron Source, Rutherford Appleton Laboratory (RAL), Oxfordshire. A broad energy range 'white' neutron beam is generated by firing a 200 μA beam of protons generated in a synchrotron in 50Hz pulses at a tungsten target protectively coated with tantalum[158], which results in the emission of, typically, 2×10^6 neutrons per second, equivalent to around 15 - 20 neutrons per incident proton[81]. As relatively low energy, thermal neutrons with typical energies on the order of 0.05 eV[155] are used for SANS, in order to have wavelengths on the order of the interatomic distances to be probed, cold moderators, such as He or He/Methane, are used to initially slow the neutrons down. These are followed by rotating disk choppers which select neutrons in the specific required energy range using a time-of-flight method. The rotational velocities and aperture sizes in the counter-rotating discs determine the pulse structures and neutron energy, and hence frequency, based on the flight time for a neutron to traverse the opening in both rotating discs (see Figure 3.1. The apertures at the source and at the sample typically provide collimation of the beam to the desired size and an area detector records the 2D scattering intensity. [65] The specific SANS setups in use at ISIS for the two instruments used in this work, LOQ and SANS2D, are depicted in Figure 3.1.

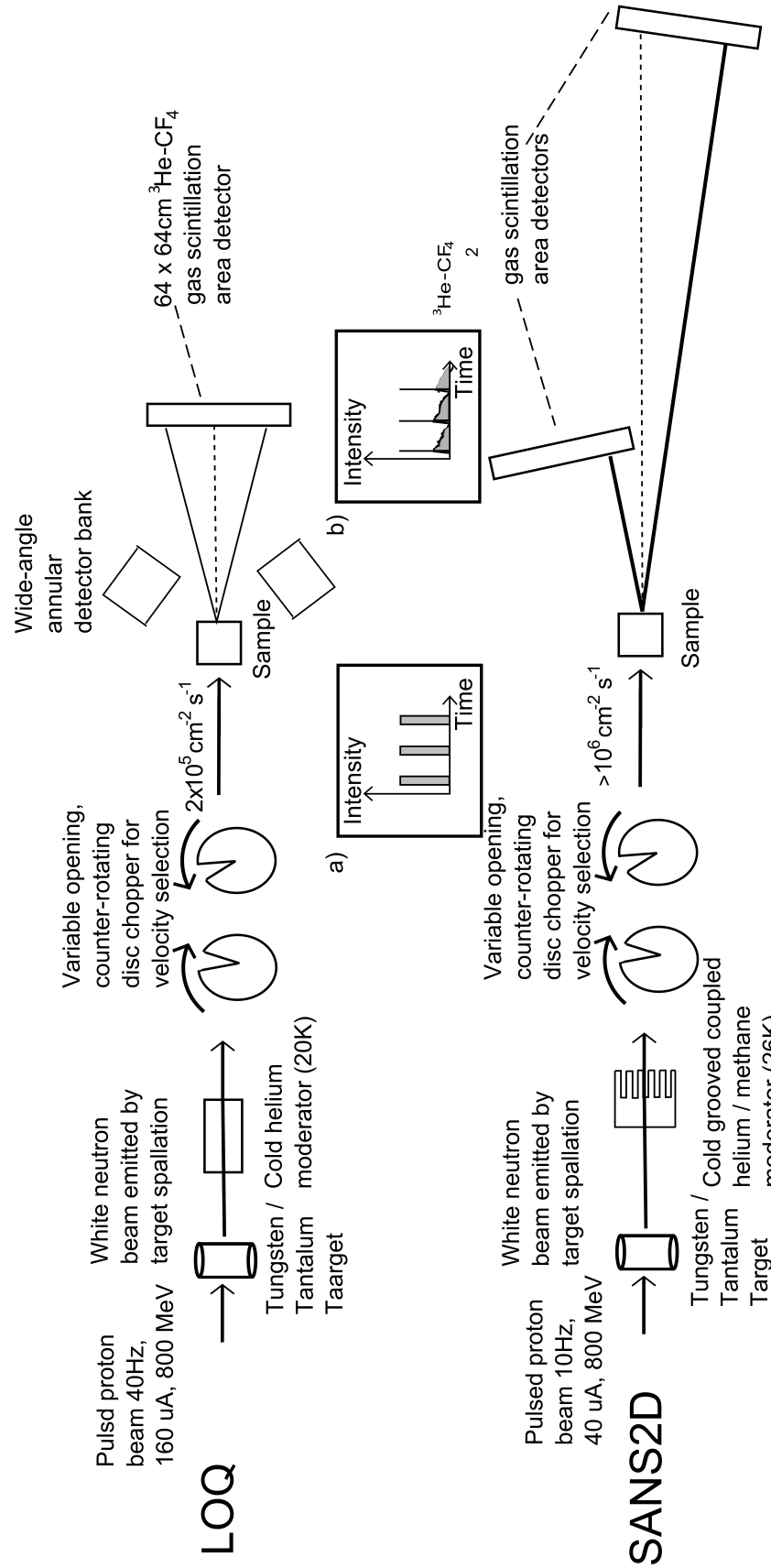

Figure 3.1: Schematic showing beamline configurations for LOQ and SANS2D SANS beamlines at ISIS spallation neutron source, based on information and schematics by Hammouda [65] and Heenan et al [73] [72], as well as the ISIS Facility's own technical webpages [83] . [82]. Sketched graphs a) and b) are adapted from Hammouda [65]

Properties of Neutrons

Neutrons are uncharged particles which possess a magnetic moment. Consequently, they scatter through interaction with atomic nuclei, rather than from the atomic electron cloud, as is the case with X-ray scattering.

Neutron diffraction techniques can thus differentiate strongly between isotopes, enabling enhancement of the scattering signal by careful selection of the dispersive medium to obtain the greatest scattering contrast to the sample particles. D_2O, with a scattering length density (SLD) of 6.38, in contrast to that of ordinary water with an SLD of -0.56,[95] is a frequently used solvent for hydrogenated sample particles and, additionally, produces less incoherent scattering than H_2O. The fact that H_2O and D_2O have SLDs of opposite sign with considerable separation enables them to be combined in various proportions to make a solvent with a range of different SLDs, and samples may be selectively deuterated to enable scattering data to be obtained from one particular structural aspect with the technique of contrast matching.

For SANS, thermal neutrons are typically selected to have wavelengths on the order of 0.01 - 3 nm, on a similar size scale to molecular bonds and polymer radii. Due to their finite mass, neutrons allow probing of the sample system on these length scales at relatively lower energies than would be possible with X-rays of the same wavelength. This is advantageous for fragile biological samples in particular.[95]

SANS Scattering Geometry

A schematic of SANS scattering geometry is shown in Figure 3.2.

The scattering vector or momentum transfer, $\mathbf{Q}$, depicted in Figure 3.3, is found by the difference of the incident and scattered wavevectors, $\mathbf{k}_0$ and k_1, respectively, as described by Equation 3.7:

$$\mathbf{Q} = \mathbf{k}_1 - \mathbf{k}_0 \tag{3.7}$$

For elastic scattering, the magnitudes of the incident and scattered wavevectors are the same, ie. no energy is transferred to or from the nucleus. In practice, this is mostly true due to the large mass of the nucleus in comparison to the scattered neutron, however inelastic scattering can arise from interactions with vibrational modes, for example, as discussed in Section 3.2.1, "Types of Scattering".

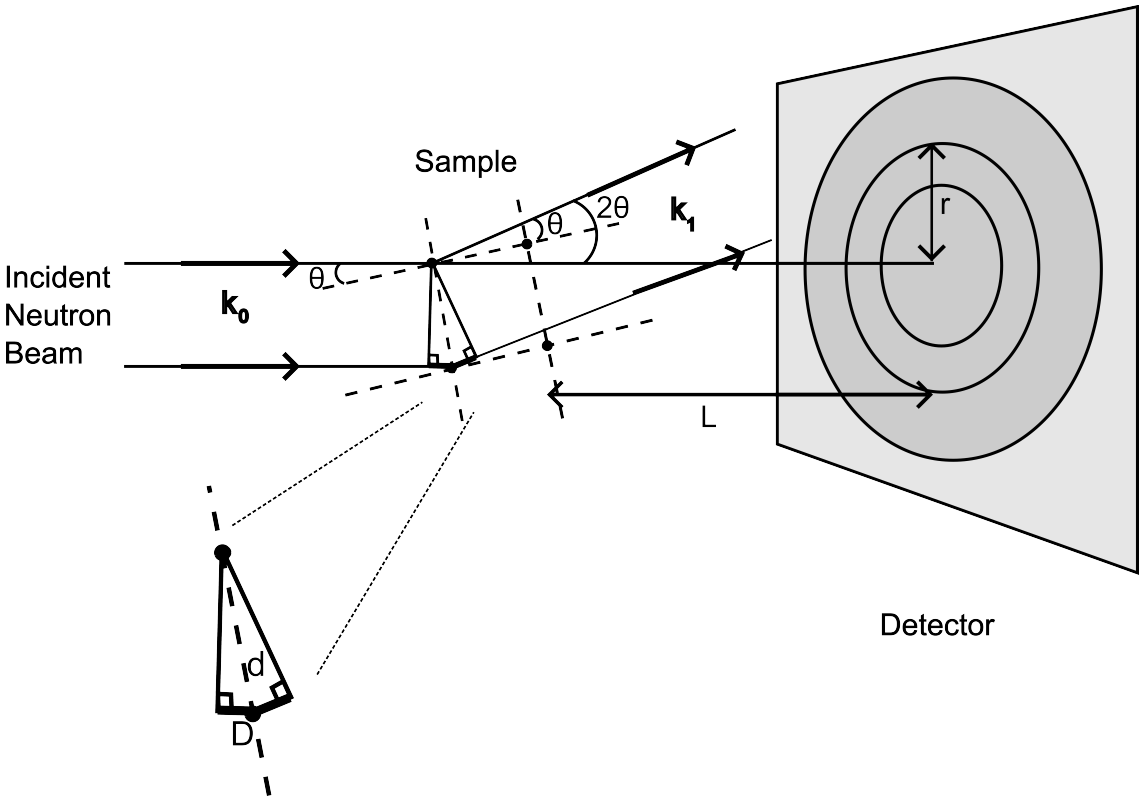

Figure 3.2: Schematic of neutron small angle scattering geometry, adapted from The Neutron Data Booklet, by Dianoux [105]

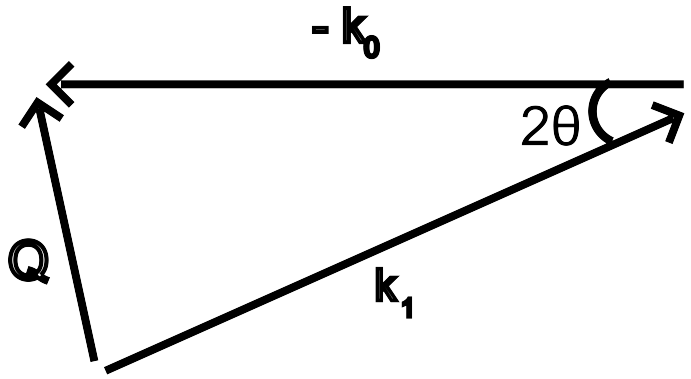

Figure 3.3: Schematic of neutron small angle scattering geometry, adapted from The Neutron Data Booklet by Dianoux [105]

The wavevector, $\mathbf{k}$, has magnitude $\frac{2\pi}{\lambda}$, where λ is the wavelength of the incident neutron beam.

Hence,

$$Q = 2k \sin\theta = \frac{4\pi}{\lambda} \sin\theta \tag{3.8}$$

where θ is the beam incident angle with respect to the sample. The neutrons are thus scattered through an angle 2θ as is shown in Figure 3.2, where the sample lattice shown

represents the array of atomic scattering centres in a particle, with d the interatomic or lattice spacing. Hence, the path difference, D, between scattered neutrons from adjacent scattering centres is given by Bragg's Law as follows:

$$D = 2d\sin\theta \tag{3.9}$$

. Therefore, interference maxima occur where the following condition is fulfilled:

$$n\lambda = 2d\sin\theta \tag{3.10}$$

or, for first order peaks,

$$\lambda = 2d\sin\theta \tag{3.11}$$

and scattering peaks occur at

$$Q = \frac{2\pi}{d} \tag{3.12}$$

for a given point scatterer spacing, d. In the small angle limit,

$$Q = \frac{4\pi}{\lambda}\sin\theta \text{can be approximated as} Q = \frac{4\pi r}{\lambda L} \tag{3.13}$$

as

$$\lim_{\theta\to 0}\sin\theta \approx \theta, \lim_{\theta\to 0}\cos\theta \approx 1 \tag{3.14}$$

Hence

$$\lim_{\theta\to 0}\sin\theta \approx \tan\theta = \frac{r}{L} \tag{3.15}$$

Therefore, the interference maxima will be observed as radially symmetric rings on the 2D area detector at a radial distance r from the direct beam, given by

$$r = \frac{Q\lambda L}{4\pi} \tag{3.16}$$

Types of Scattering - Coherent and Incoherent Scattering, Elastic and Inelastic

Neutrons interact with and hence scatter primarily from atomic nuclei through an elastic, short-range nuclear interaction and with unpaired electrons due to magnetic dipole interactions. [148]

Coherent scattering is the principle focus of SANS as it arises from interference between neutrons scattered from adjacent scattering centres in the sample molecules, as described by the static pair correlation function [148], and thus contains information about the interparticle distances and positional correlations, which provide insight into the form factor of the scattering body through known expressions derived for various geometric structures. The scattering observed on the 2D area detector is radially isotropic and is visible as a series of concentric rings, as the samples generally used in SANS are disordered in solution, hence only the magnitude of the scattering vector, Q, not its direction, contains information about the momentum transfer of the scattering[105]. The scattered intensity is therefore radially averaged to obtain a 1D scattering intensity, following correction and normalisation to standard samples, measured sample transmission and incident, direct beam intensity, to give an absolute scattering intensity as a function of Q.

While elastic, coherent scattering, where no energy is lost or gained by the neutron, results from correlations between positions of neighbouring atoms, inelastic coherent scattering depends on the self-correlation function of atoms and would be dependent on correlated positional fluctuations between neighbouring nuclei[148] , ie. elastic and inelastic scattering arise from interactions with the stationary nucleus and vibrational modes of the scattering atom, respectively.

Inelastic coherent scattering can give information about correlated motion of the scattering centres in techniques such as neutron spectroscopy. In SANS, inelastic scattering contributes to the background in the same way as elastic incoherent scattering[148].

Incoherent scattering also takes place, which has contributions from spin incoherence and disorder incoherence [65] and is dependent on correlations of an individual particle at different points in time, and hence contains no information about interparticle distances or structure as it does not relate to interference between the scattering from neighbouring particles. The main component of incoherent scattering arises from the interaction of neutrons, which have spin $\frac{1}{2}$, with other particles with spin. Composition incoherence arises from isotopic incoherence and disorder incoherence within a molecule, although this contribution is usually secondary to the spin incoherence. Overall, as incoherent scattering relates to auto-correlation of the scattering centre, it depends on the motion of the particle. Thus, different modes of motion and levels of excitement, determined by rotational, torsional or vibrational modes due to binding to other particles or thermal energy of the sample, respectively, may change the incoherent scattering and may be probed by

techniques which focus on incoherent scattering. In SANS, however, it contributes only to an isotropic background, which must be subtracted from the total scattering signal, hence, the scattering cross-sections referred to in scattering equations typically relate to coherent elastic scattering, while inelastic and multiple scattering contribute to the measured background[41].

As hydrogen has a much higher incoherent scattering cross-section than deuterium, D_2O is used as the solvent for SANS experiments in this work, with an incoherent cross-section of 4.17 barn, in comparison to 168.12 barn for H_2O. [65] [148]

Scattered Intensity

The intensity of the scattered beam at a given detector angular position ,θ,is given by [95]

$$I(\lambda, Q) = I_0(\lambda)\,\Delta\Omega\eta(\lambda)\,TV\left(\frac{\delta\sigma}{\delta\Omega}\right)_{tot}(Q) \tag{3.17}$$

where I_o is the intensity of the neutron flux incident on the sample,$\Delta\Omega$ is the active solid angle element of the detector, η is the detector efficiency as a function of λ, T is the transmission coefficient of the sample, V the illuminated sample volume and $\left(\frac{\delta\sigma}{\delta\Omega}\right)_{tot}(Q)$ the total differential scattering cross-section equal to the sum of the Q-dependent, coherent scattering cross-section, $\left(\frac{\delta\sigma}{\delta\Omega}\right)_{coh}(Q)$,and the isotropic, incoherent scattering cross-section, $\left(\frac{\delta\sigma}{\delta\Omega}\right)_{inc}$, as follows [65]:

$$\left(\frac{\delta\sigma}{\delta\Omega}\right)_{tot} = \left(\frac{\delta\sigma}{\delta\Omega}\right)_{coh}(Q) + \left(\frac{\delta\sigma}{\delta\Omega}\right)_{inc} \tag{3.18}$$

The coherent particle cross-section is a measure of the scattering power of the particles and is formulated, in the limit of dilute, non-interacting particles, as an integral over the particle volume of the density correlation function, modulated by the scattering length density contrast between the particles and their solvent, $\Delta\delta$, as follows:

$$\left(\frac{\delta\sigma}{\delta\Omega}\right)_{coh}(Q) = N_p\Delta\delta^2 \mid \int e^{i\underline{q}\cdot\underline{r}}dV \mid^2 \tag{3.19}$$

where N_p is the number density of the scattering bodies, $\Delta\delta$ the scattering length contrast, r and q the positional vector and scattering vector, respectively, of scattering centres in a particle, with volume V, determined by integration over dV. where the particle form

factor P(Q) is given by[108]

$$P(Q) =\mid \frac{1}{V}\int dV e^{-i\underline{Q}.\underline{r}} \mid^2 \tag{3.20}$$

which is the density correlation function within the particle, integrated over the particle volume.

The expression may be generalised through multiplication by the particles' structure factor, where applicable, which accounts for particle-particle interaction potentials, and tends to 1 for non-interacting systems, as:

$$\frac{\delta\sigma}{\delta\Omega} = N_p V_p^2 \Delta\delta^2 P(Q) S(Q) + B_{inc} \tag{3.21}$$

where N_p and V_p are the number density and volume respectively of the scattering bodies and $\Delta\delta$ is the contrast or difference in scattering length densities between the scattering particles and the dispersant, as follows:

$$\Delta\delta = (\delta_p - \delta_d) \tag{3.22}$$

. The scattering length density for a scattering particle is calculated by

$$\delta = \Sigma_i b_i \frac{DN_A}{M_W} \tag{3.23}$$

with b_i the scattering length of an individual atom, i, and D and M_W, the bulk density and molecular weight of the particle, respectively. $P(Q)$ is the particle form factor and $S(Q)$ the interparticle structure factor, Q is the magnitude of the scattering vector and B_{inc} the incoherent background signal. It can readily be seen, therefore, that a substantial amount of structural information about the sample is contained in the scattering cross-section.[95]

Form Factor

The form factor, which is the integral of the density correlation function over the whole particle, normalised by the volume, is an expression which is hence defined by the distribution of mass in particular geometric forms of the scattering particle. The form factors for some particle structures frequently used in this work are described in the context of kinetic SANS data fitting in Section 4.3.1.

Structure Factor

While the form factor represents the scattering bodies' structural conformation, the structure factor describes interaction potentials between scattering bodies, and tends to 1 where there is no interaction.

Measurement Method

Samples are measured in cuvettes, made of quartz, which has a high transparency to neutrons. Circular cuvettes are loaded into a motorised sample rack which can be controlled remotely. SANS measurements on each sample on the LOQ beamline at ISIS Neutron Source, Rutherford Appleton Lab, Harwell Oxford, last approximately one hour. However, because of the changeable nature of the beam current from a synchrotron spallation source, for non-time-sensitive samples, the data acquisition system can be programmed to count until a total flux is reached, rather than for a specified time, to ensure that sufficient data is collected to enable confident analysis and fitting, minimising statistical uncertainty. Sample transmission measurements are also carried out, as well as scattering and transmission on a relevant background solvent to provide the first, crude, incoherent background subtraction, which is subsequently refined during data fitting, by extrapolating from the baseline at high Q, where SANS is absent, and an empty beam measurement for normalisation. Standard samples of known scattering intensity and polydispersity are also run for calibration of the instrument and scattered intensity to absolute values. Data reduction is carried out using the program Mantid Plot.

Model-free data interpretation can be carried out by studying the broad features of the scattering curve and independently analysing different Q regimes to determine structural features, such as the radius of gyration at low Q (corresponding to the largest particle length scales), and Porod anaylses, typically at higher Q values, which thus give information about the scattering structures on smaller length scales, and can be used to infer the polymer conformation, whether rod-like, expanded, coiled or collapsed [64], which can also aid form factor identification to inform model selection for model based data fitting. Model-based data fitting is undertaken with the custom Fish software[71] written by R.K. Heenan at the ISIS facility. Standard geometric models such as rod-like cylinders, spheres or ellipsoids, or semi-flexible, wormlike chains, or limited combinations of these, consistent with understanding of the sample's physical structure are implemented for data fitting

following a least squares fitting method implemented by a Levenburg-Marquardt algorithm [71]. Finally, for time-resolved scattering, as conducted on SANS2D using PEI and DNA samples, (see Chapter 4), singular value decomposition (SVD) may be applied to identify the principal structural components constituting a mixture of aggregates or other particles and the proportions of the mixture which they account for at a given time. However, for the present systems, it was decided that the data quality was not sufficient and the component systems were not appropriately well characterised to allow reliable analysis through principal components.

Guinier Analysis

The scattering intensity can be simplified in the limit of Q $\longrightarrow$0 for a dilute system of non-interacting, ideally monodisperse particles, using the well-known Guinier approximation, which leads to the fact that the plot of ln(I) against Q^2 at low Q gives a straight line region, the gradient of which corresponds to the square of the radius of gyration of the molecule divided by 3, when $QR_G \leq$ a certain limit, commonly taken to be 1.3.

For anisotropic particles, such as cylinders or disks, which are characterised by two significant dimensions, cross-sectional radius and cylinder length, it may be that two straight-line sections are visible at low Q. In this case, an additional relevant plot may be a modified Guinier (or Kratky-Porod) plot, of ln(QI(Q)) against Q^2, which enables determination of the cross-sectional radius of gyration, which may be used to derive an estimated cross-sectional radius for the elongated particle.

Porod Analysis

Another useful model-free tool, more commonly applicable at high Q, is the Porod plot of ln(I) against ln(Q). Here, the gradient of a plot of ln(I) vs. ln(Q) will give rise to the so-called Porod exponent, a value ranging from 1 to 4 which indicates, at the upper end of the scale, the surface roughness of a particle with 4 corresponding to a smooth and 3 to a rough interface, while values between 2 and 3 may indicate a mass fractal, polymer chain structure and exponents close to 1 the presence of rigid rods. [64].

The Porod model is particularly sensitive to accurate background subtraction. The power-law fit functions in programs such as the NCNR Igor Proper SANS Analysis program[97],

written for Igor Pro, performs simultaneous background fitting. The fitted background was subtracted for further processing.

Singular Value Decomposition and Analysis of Mixtures

As the most likely suitable structural form factors have been identified, a more in-depth analysis of the kinetic data was considered using Singular Value Decomposition (SVD). This consists of expressing the set of time-resolved scattering data as a matrix which can be reformulated in such a way as to identify the rank of the resulting matrix, yielding the total number of significant component species of particle [178] present in the time series at any measured point, including those which may be generated and then altered as intermediate components, and thus are not present in the initial or final states of the mixture. This enables separation of significant species present from noise, in a model-independent manner, and their respective changing proportions of the mixture with time, in a time-resolved study as in this case, or, equally, concentration,where this is varied. However, although this method of analysis was attempted, it was not considered to be appropriate for the molecular system in question, being insufficiently well characterised, as ideally the component parts would have clear, relatively well-known and defined structures, and hence results of this analysis are not presented here.

Model Fitting

Informed by the radius of gyration, or multiple radii, where applicable, identified by Guinier analysis and the initial indication from the Porod exponent of the most likely structural form of the particles, fitting to a structural model, or combination of models, is undertaken using the FISH program by R.K. Heenan[71]. The program allows the user to specify initial conditions and select a physical model and, subsequently, iterations towards a best fit are made using a Levenberg-Marquardt least squares fitting algorithm. The program author advises users to initially allow only certain parameters to float, fixing the other parameters, and subsequently to release those for fitting, to ensure a physically meaningful fit in the appropriate region of values is achieved, as other possible mathematical but unphysical solutions may exist. [156] Typically, DNA-cationic polymer systems could be fit by a single or a combination of two cylinders, a globular ellipsoidal model or a worm-like chain.

Stopped-flow SANS

For kinetic studies of the structural evolution of complexes between DNA fragments and PEI, a stopped-flow apparatus (Biologic), described in further detail in Chapter 4, was coupled with SANS instrumentation on the SANS2D beamline, ISIS Neutron Source, Rutherford Appleton Lab, Harwell, Oxford, to collect time-resolved SANS data from a mixture of polymer and DNA solutions at known ages after mixing. Separate polymer and DNA samples and cleaning solutions were loaded into syringes and programmed using the proprietary software to flow together in a turbulent mixing cell and, subsequently, into a quartz SANS measurement cuvette. The end of mixing was set to trigger the start of SANS data collection from the sample, which was collected over a period of 30 minutes and subsequently time-sliced into defined age ranges after mixing, using an analytical program written in Python for the Mantid Plot software by R.K. Heenan and S. Rogers of the SANS2D beamline, ISIS. The cell and flow lines were cleaned with concentrated (3M) NaCl solution and rinsed with the appropriate dispserant solution in D_2O, commonly 10 mM NaCl, and the measurement was repeated with a fresh mixture, typically 5 times in total, in order to collect sufficient data for summing of time-slices and subsequent statistical validity for model-free and model-based data fitting. Data was reduced with background subtraction obtained from pure solvent scattering and normalised with known standard samples and the incident and transmitted beam intensities for calibration to an absolute scattering intensity scale, and repeated samples' scattering were summed before data analysis was conducted using the range of analytical techniques discussed above, and described in further detail in Chapter 4.

Chapter 4

Static and Kinetic SANS Study of Polyethylenimine-DNA Complexes

4.1 Introduction

4.1.1 Background and Relevance

DNA condensation with cationic polymers is an area of great relevance for biological research in vitro and in vivo, with ultimate application to medical science and therapeutic techniques.

A great deal of research effort relies on the application of gene delivery and focuses on the development of new and improved gene delivery vectors. However, much remains unknown about the process and mechanism of interaction, binding and aggregation leading to the final complex structure and the ways in which various conditions affect complex structure and its evolution.

One of the most established, commonly used and well-characterised cationic polymers which has found application as a gene delivery vector is polyethylenimine (PEI), a polymer of aziridine with a high positive charge density around physiological pH, which can be synthesised at various lengths in either a branched (BPEI) or linear (LPEI) form, by bulk polymerisation of aziridine in a reaction controlled by temperature and initiator quantity, or ring-opening polymerisation of aziridine derivatives, followed by hydrolosis, respectively.

[193]

Detailed studies of the structural evolution of complexes in the time immediately following mixing have been limited, particularly in the SANS regime, with many studies focusing on indirect studies of interactions through fluorescent dye binding or binding energies.

PEI in its various forms and its derivatives has been found to be an extremely effective transfection agent for a variety of applications, from condensation and compaction of large DNA molecules, such as plasmids[77][200][135], to small nucleic acid molecules, such as siRNAs [187][75], and has high efficacy in a variety of cell lines in vitro[18][200], and animal models in vivo[58]. It is known to enter cells through both clathrin-dependent and independent endocytic pathways[154], although the authors present evidence which suggests the clathrin-independent pathway is the only one which leads to biologically effective transfection. The internalisation route is thought to depend, among other factors, on the size of the complexes formed[127], as particularly large cationic complexes may exceed the size limit for clathrin-mediated uptake and are believed to be taken up by a method analagous to phagocytosis[101]. In some instances in vitro, perhaps counter-intuitively, larger complex formations have been found to be more effective transfection agents, postulated to be due to sedimentation onto the cell surface, although they are expected to face hindrances to extracellular mobility in vivo, resulting in lower transfection efficiency. [110]

There is an established belief that PEI owes its high gene delivery efficiency to its high charge density and ability to bind and condense DNA, in addition to its strong buffering capacity. This is supposed to provide the advantage of buffering endosomal pH change[176] leading to osmotic swelling and rupture through the so-called proton sponge effect, which it is suggested, affords it superior capacity for endosomal escape[18], a significant hurdle in gene delivery.

For instance, relatively little has been studied regarding the structural evolution of complexes of different types and sizes of PEI with DNA following complex formation under biologically relevant conditions in solution[165]. This question has great relevance for the application of PEI as a transfection agent.

From a literature review of the extensive body of research utilising or studying PEI in transfection applications, it appears that a range of complexation times, charge ratios and solvent conditions are commonly used, frequently without explicit consideration of their impacts and sometimes not even specifying incubation time[164]Yet, several authors

report a difference in transfection efficacy after different periods of complex incubation after mixing, although without consistency from system to system. [75][35][69] Hence, an understanding of the evolution of the complexes and their aggregation or rearrangement with time will provide valuable insight which may contribute to enabling optimisation of the incubation conditions.

Techniques such as isothermal titration calorimetry (ITC) and circular dichroism have been utilised to probe the binding and DNA conformation in complexes[28], as well as fluorescent dye displacement and exclusion measurements [3][205]as an indicator of the DNA binding process, however these give relatively little insight into the physical form of the structure of complexes and how this changes during and following initial complexation and aggregation. AFM has been used in this respect[165]. However, its conclusions and the extent to which quantitative parameters can be extracted are affected by the interaction with the substrate, frequently charged, which can alter the native solution conformation, although manipulation of experimental conditions can theoretically enable trapping of the molecule in a 3D molecular conformation.

SANS is very well suited for this purpose of structural characterisation in solution and has been used extensively in previous work by Zhao et al[192] to characterise the physical structure of biomolecules and DNA-polymer complexes.

4.1.2 Choice of Technique

Small angle neutron scattering (SANS) is a valuable technique in the study of biomolecular structures as it can provide detailed structural information in native solution conditions, which can be selected for physiological relevance, or the study of other specific conditions, rather than requiring crystallisation or surface adsorption, which can markedly alter the structure compared to the hydrated form, and allows evaluation of the response of the molecules to variation of solution conditions such as ionic strength and pH. Additionally, it can give form and structure factor information by fundamental model-free methods or model-based data fitting, in contrast to other solution techniques, such as dynamic light scattering (DLS), which typically only provide a hydrodynamic radius, under the assumption of a spherical form factor. The relatively low energy of the thermal neutrons used mean even delicate biological samples are relatively protected from radiation damage, which can significantly constrains maximum exposure times with analagous small angle

scattering techniques using x-rays.

The sample to be studied was believed, from preliminary dynamic light scattering screening (data not shown), to lie near the maximum size range accessible with SANS, and DLS, in combination with information from the literature, was used to probe a selection of buffer conditions to enable complexes at the lower end of the size range to be obtained, but for which it was expected the evolution would be observable on the desired timescale. However, as DLS measures particles' hydrodynamic radius, it was thought likely that elongated molecules' radii or overall shape of globular particles, could be examined in greater detail with SANS, as these dimensions would be of the same or smaller size as the hydrodynamic radius indicated by DLS.

The second target station at ISIS offers high flux and large, extremely sensitive area detectors (setup shown in Figure 3.1), which considerably reduce the required time for a measurement, among other factors, which allow short time-scales, on the order of seconds, to be probed with acceptably high signal-to-noise ratio, even for samples which have a relatively low scattering intensity, such as these. Additionally, the SANS2D instrument configuration offers accessible Q ranges significantly lower than the previous SANS setups available at ISIS, the LOQ beamline at ISIS's Target Station One. Access to very low Q regimes is particularly important in this study, given the large size of aggregates concerned, as mentioned above.

In this work, small angle neutron scattering was combined with a stopped-flow mixing device (Biologic) to enable characterisation of the structural evolution of a family of widely used cationic polymers for gene delivery, polyethylenimines, over the 30 minutes immediately following mixing. Despite the large size of the aggregates and the process of aggregation which occurred, with careful optimisation of the solution conditions and choice of model DNA type studied, time-resolved SANS data from PEI/DNA complexes was aquired and the widely reported[163] colloidal instability due to aggregation was studied using the kinetic, stopped-flow technique, in an attempt to further elucidate the structural changes which take place following mixing.

Some of the main factors affecting polyethylenimine's use as a transfection agent and the structure and efficacy of the complexes it forms, as well as the main areas addressed by this study are outlined below:

4.1.3 Polyethylenimine as Transfection Agent

PEI is widely known as an effective condensing agent for DNA, with reports by various authors, as described by Ziebarth et al[204], indicating a range of possible pKas of pure PEI, depending on structure and chain length, with the overall consensus that PEI is likely to be mostly protonated at neutral pH, although Ziebarth et al highlight the uncertainty around its level of protonation [204], and hence, with its high charge density at physiological pH, an efficient condenser of DNA, which is thought to require neutralisation of 90% of its charges to be condensed[16]. PEI is also hypothesised to exploit its high buffering capacity to create the proton sponge effect, facilitating endosomal rupture and escape[18], a notorious hurdle on the path to nuclear entry, although this mechanism has been disputed by some authors in recent years[53][10], and is debated in the literature[183].

While it is known that the presence of an excess of largely free PEI in addition to complexes enhances the efficiency of gene delivery[17], to the extent that some authors[93] found it necessary for significant transfection, Ziebarth et al [204] also found that unprotonated amines remained following titration in the presence of a polycation, such as DNA, in their simulations, suggesting that linear PEI could retain some buffering capacity even when bound to DNA, so the debated proton sponge effect may not wholly rely on the presence of free polymer particles.

Different molecular weights and branched and linear structures of PEI have been synthesised and are used with varying success in a wide variety of conditions. Branched PEI contains a mixture of primary, secondary and tertiary amine groups. Many primary groups are highly sterically accessible, and are thought to promote efficient DNA binding, while the secondary and tertiary amines also contribute to the wide pH range of buffering capacity.[116] However, linear PEI is a more effective gene delivery vector in many circumstances[137]. Paradoxically, it appears this may be due to its lower steric stability, as larger aggregates show greater transfection success, at least in vitro, than smaller particles in some cases. It is postulated that they may be more likely to sediment onto the cell monolayer surface in vitro. However, regardless of the test environment, if particles are above the size limit for clathrin-mediated uptake, they may avoid lysosomal degradation to a greater degree than small complexes, as Rejman et al[154] have shown the clathrin-dependent pathway to lead to a higher instance of lysosomal degradation. Thus, longer incubation times, if correlated with particle aggregation and size increase, might

be expected to improve transfection efficiency.

Linear PEIs contain purely secondary amines, while branched PEIs have a mixture of primary, secondary and tertiary amines. BPEI-1.8 contains primary, secondary and tertiary amine groups in the proportions 1:2:1 according to the manufacturers information (Polysciences, Germany), while for the higher molecular weight BPEI-25, this ratio is 4/3/4 according to the suppliers structural information.

Despite this, however, according to Von Harpe et al[184] there is little difference in buffering capacity between linear and branched PEIs or those of different molecular weights in the physiological pH range from cytosolic pH 7.4 through early- to late-endosomal pH, thought to be approximately pH 5[104]. This implies that any difference in transfection efficiency between the linear and branched specimens are due more to the strength of binding or the size and structure of complexes formed, as well as colloidal stability, than to the advantageous endosomal escape mechanism of the, admittedly disputed, proton sponge effect.

Charge density and accessibility are also potentially influential factors, as branching shown in hyperbranched PEI may lead primary amine groups to be more sterically accessible for DNA binding, as noted by Gad et al[116]. Additionally, Brissault et al [20] note that polycations which contained tertiary amines showed poorer transfection, but the authors suggest flexibility or solubility of the polymers are other important, potentially significant factors.

BPEI is known to have greater solubility and stability in solution than LPEI, a tendency which appears to be confirmed in this study, at high N\P ratios. This may be due to the many charged branches being less efficiently neutralised by DNA binding molecules due to their limited flexibility and consequent steric inaccessibility, leaving more charged branched groups free to contribute to solution solubility and uniform electrostatic repulsion from aggregation with other complexes.

The size of polymer is also important, and may be associated with binding strength, as Ogris et al [137] state that small PEI molecules are more effective transfection agents for small nucleic acid molecules than high molecular weight (MW) PEIs, due to the relatively weaker binding which enables dissociation of the small, siRNA from the complex once internalised in the cell, as failure to dissociate hinders the nucleic acid from producing biological effect.

On the other hand, the colloidal stability of low MW PEI complexes appears in the

present study to be lower than for larger PEI complexes, perhaps due, in a similar way to LPEI in general, to the reduced excess availability of charges per complex. Petersen et al[145] describe low MW PEI-DNA complexes which are loosely formed and aggregate to very large particle sizes. It seems likely that each low MW PEI molecule involved in complexation could be more completely neutralised by DNA than with large BPEI, leaving a lower remainder of charged amine groups to contribute to solubility, and a greater proportion of almost completely free polymer molecules with limited involvement in complexation.

PEI protonation, pKa and pH

As the charge density of the cationic polymer is such a key factor, the protonation state of PEI and its pKa are important to understand. Utsuno et al [180] performed titrations with HCl of a small, branched PEI (600 Da), which they supposed to be representative of a range of other molecular sizes and structures, and calculated, using the model from Suh et al [169], its pKa in the vicinity of pH 6, 7 and 8, as well as the fraction of protonated nitrogens at each of these pHs. The small, branched PEI was found to be 47%, 33% and 21% around pH 6, 7 and 8, respectively.

Ziebarth et al[204] describe the conflicting results obtained surrounding PEI protonation, which hinders calculation of actual charge ratios, possibly due to the changing pKas of its different amine groups which can change their protonation state and complex interactions between neighbouring charged sites on a polymer chain. They also found that no free DNA remained in solution after N/P = 2 at pH 6, 7 or 8 (or lower for pH 6 and 7), a value approximately confirmed by Bertshchinger et al, who found no DNA remained in solution above N/P = 2.3 [13] Although this does not necessarily mean all the DNA has been condensed or compacted (as they state 80-90% charge neutralisation is required for condensation to occur), the result does imply that all DNA is bound to PEI by that point.

It can hence be seen that a wide array of factors and their interplay contribute to the structural features and transfection efficacy of a particular formulation of PEI/DNA complex, and the importance of deepening understanding of both the initial binding and structure, and the subsequent evolutionary process of the complexes is clear. Identification of relationships between complexation conditions such as PEI type and size, charge ratio and solution conditions and the complexes' stability and structure are of great importance for

informing the practical approach to transfection in order to equip researchers to make improvements in transfection efficiency.

4.1.4 Principal Questions

A broad survey of existing literature studies was conducted in order to explore the principle contributing factors in the application of PEI as a non-viral gene delivery vector, from biophysical, structural studies to in vivo gene delivery using animal models. Across the studies examined, a range of N/P ratios, complexation times and solutions conditions were used with different success rates, compounded by the different sizes and forms (linear or branched) of PEI and types of DNA, cells for transfection and techniques, some overall observations were made, if few generalised absolute conclusions could be drawn:

A wide range of charge ratios were found to be used, with authors exploring N\P ratios from 0.5[77] to 100[187] across the works surveyed, with greatest transfection success commonly achieved where excess cationic polymer was present, with several authors finding optimal ratios in the range of N\P $\approx$ 6[35] to 13[18], which is reasonable, as the point of neutralisation is thought to occur at a N\P ratio of approximately 2:1, although with some uncertainty.

Commonly, complexes were formed in 150 mM NaCl[35][18][153][191][200], close to physiological ionic strength[143], or 5% glucose[35][200], although other solvents, such as pure water or cell culture medium are also common. These two conditions are both recommended by some commercial suppliers of PEI for gene delivery[46], raising questions as to the equivalence of their effects, and how this can be reconciled with differences in the effect of these solution conditions on polyplex structure.

A wide range of complex incubation times prior to addition to cell cultures, 30 seconds[69] to 2 hours[75] or more, were used across the works surveyed, while at least one study in vivo[164] did not report the incubation time, leading to the important question of whether incubation time has an effect on complex structure and, consequently, on transfection efficiency. Most common were incubation times of 10 - 30 minutes[200][103][34][28], while Derouazi et al[35] found transfection efficiency decreased beyond 10 minutes of incubation.

Some of the most pertinent factors are discussed in further detail below, which this study will attempt to examine from the perspective of complex structure and structural evolution with time following mixing of the two components.

Aggregation

The degree of stability against aggregation in solution is the outcome of competing attractive and repulsive potentials. PEI complexes are similarly charged and, hence, experience mutual electrostatic repulsion which counteracts hydrophobic aggregation tendencies. However, having no means of hydrophilic stabilisation in their pure form, unlike the diblock MPC-DEA copolymers examined in Chapter 6, which possess a zwitterionic, and hence, hydrophilic block for stabilisation in solution, long range Van der Waals forces and hydrophobic attraction driving aggregation means this is a commonly-experienced phenomenon in the condensation of DNA with PEI[163], and is known to vary under many solution conditions. Increasing the ionic strength of the medium reduces the Debye length, and hence increases the degree of salt screening of electrostatic repulsive potential between particles, increasing the net attractive force between particles and the likelihood they will experience a net attraction to the point of aggregation. The ability to control aggregation through understanding and manipulation of the complexation conditions seems likely to have implications for transfection success. The impact of this tendency to aggregate is such that many studies focus on modification of PEIs to increase their hydrophilicity and colloidal stability, commonly based around grafting a hydrophilic, if neutral, moiety such as PEG[171] to the cationic polymer, which may be particularly important in vivo[176], even if it does not necessarily increase in vitro delivery, as LPEI complexes, which show greater tendencies to aggregate than high MW BPEI-based complexes as discussed above are, in some circumstances, more effective transfection agents[189].

The driving forces behind aggregation following binding are therefore relatively well understood in principle, as outlined above, and in some circumstances aggregation may be beneficial for transfection. Additionally, attempts at structural characterisation of PEI/DNA complexes with small angle neutron scattering have been hampered by aggregation. The challenges of ensuring a high enough proportion of the sample remains solubilised for a sufficient length of time to collect scattering data with an acceptable signal/noise ratio with typical neutron source fluxes and optimising the solution conditions to ensure complexes form in the limited, small size regimes of conventional neutron sources, has limited work in this area.

One study [130] noted the difficulty in obtaining appropriate complexes for SANS investigation, and elected to study complexes formed one day before experimentation. With

this exception, no other significant study of PEI complexes with DNA using small angle neutron scattering had been identified to our knowledge at the time of this work, plausibly due at least in part to the extent of this difficulty of obtaining stable particles in the appropriate size range for SANS. Given the importance of understanding and being able to tune the process of aggregation, the expanded Q-range and high flux of the new SANS2D beamline at ISIS, described in Section 4.2.9,was used in this work, in conjunction with stopped-flow apparatus in an effort to characterise the aggregation process in terms of structural evolution of PEI complexes with DNA.

PEI Structure and Size

As mentioned briefly above, branched and linear PEIs differ not only in their structure, depicted in Figure 2.1, BPEI encompassing primary, secondary and tertiary amines in approximately 25:50:25 proportions[116], while LPEI contains only secondary amines, but also in their effectiveness for different applications of gene delivery.

BPEI is more readily soluble than LPEI, which is insoluble in water at room temperature near neutral pH in its pure form. The molecular weight of the polymer also has an impact on solubility, stability and, according to some reports, strength of binding, Ogris et al noting that small nucleic acids are advantageously able to dissociate more easily from low MW PEI-based complexes than from high MW PEIs, resulting in increased transfection activity. [137]

In this study, two types of PEI architecture, linear and branched, of two different molecular weights approximately an order of magnitude apart, were investigated in the formation of complexes with a DNA fragment of a similar size to siRNA, in order to examine their different structural geometries and evolutions in the time following mixing, with a particular emphasis on colloidal stability and complex size and shape transitions with time.

Charge Ratio

The mixing charge ratio of nitrogens to phosphate (N\P) is an important parameter in DNA complexation. Authors have reported that approximately 90% of DNA's negative charges need to be neutralised in order for it to be condensed[122][190] and the excess positively charged polymer may not only influence the resultant net charge of the complexes, but the amount of free polymer available, both of which have been shown [122][17]

to play an important role in transfection success.

Ziebarth et al[204] describe the conflicting results obtained surrounding levels of PEI protonation, which hinders calculation of actual ratios of positive to negative charges under given solution conditions, possibly due to the changing pKas of its amine groups which can change their protonation state depending on complex interactions between neighbouring charged sites on a polymer chain, and potentially again on binding to DNA. The ratio of PEI's Nitrogens to DNA's phosphates (N/P), each containing one protonatable site, is used as a measure for potential charge ratio.

They also found that no free DNA remained in solution after N/P = 2 at pH 8, or lower at pH 6 or 7, a value approximately confirmed by Bertshchinger et al, who found no DNA remained in solution above N/P = 2.3 [13] Although this does not necessarily mean all the DNA has been condensed or compacted, which has been shown to require around 90% charge neutralisation, the result does imply that all DNA is bound to PEI by that point. Based on this, an N/P ratio of approximately 2 or above should see all DNA bound at pH 7.4, so this indicated a good choice of lower limit for study in this work. Zeta potential results from Jorge et al [87] reinforced this view with a neutralisation of surface charge around N/P = 2 at various pH values.

Initially, an N/P ratio of 10/1 was therefore chosen for the study of all polymer types, as it was in the range generally reported in the literature, described above, to give good transfection efficiency with a range of PEI and nucleic acid types, and additionally, it was anticipated that aggregation would be slowed sufficiently by the presence of a significant positive charge excess to be observable on the timescale of experimental observation, up to 30 minutes.

Complexes at this charge ratio were investigated with stopped-flow SANS in an attempt to observe any existing difference in the early-time complex formation and initial structural rearrangement, and to identify whether any difference in aggregation kinetics over the longer time frame of 30 minutes existed between PEIs of different structures and molecular weights under different solution conditions.

Additionally, higher ratios of N/P = 20 were also used for some samples, and the kinetic data was complemented with static SANS studies of 25 kDa (high MW) BPEI complexes at N\P ratios of 2:1, 5:1, 10:1 and 20:1 on LOQ, all selected to fall within a range where full DNA neutralisation should be possible and within charge ratios commonly found in transfection studies in the literature.

Solvent Media

Many studies use glucose or 150mM NaCl for complex formation for in vivo or in vitro work and some manufacturers [46] recommend either formulation for optimum transfection. However, preliminary DLS screening and SANS trials (data not shown) reinforced the consensus in the literature, suggesting significant differences in size between the particles formed in these two media, which leads to interesting questions about their equivalence for use in vitro and their mechanisms of action.

A large proportion of publications referenced had used either 5% glucose or approximately 150mM NaCl (ranging from 100 mM to 165 mM) in formation of the complexes, or studied both, often alongside other formulations. It has been reported that complexes formed in 5% glucose are compact, small particles[79] and significant aggregation was only observed at charge ratios near neutrality. High ionic strength media, such as 150 mM NaCl, lead PEI-DNA complexes to aggregate significantly[96] to large sizes, to the extent that preliminary SANS studies produced very little scattering signal in comparison to complexes formed in glucose solutions under these conditions (data not shown). The effect of some degree of added salt, at 10 mM NaCl, was chosen to compare to pure D_2O or 5% Glucose to investigate effect of solution conditions on the process of aggregation over the first 30 minutes.

Effect of pH - Reason for Investigation

The range of host pHs encountered by the complexes during internalisation and intracellular trafficking is likely to extend from around pH 5 in late endosomes to pH 7.4 in the extracellular media. In fact the degree of protonation reported for PEI is reported to change dramatically over the pH range from 7 to 5, going from 20 to 45% protonation over this range[137] (although the uncertainties described elswhere[204] should be borne in mind), which makes the question of structural change over this range interesting, in addition to the fact that this is the range over which pH is likely to change during endosomal acidification, and hence physiologically very relevant.

PEI's renowned buffering capacity, however, is likely to mean that the pH experienced by a complex which ultimately leads to successful transfection may not reach the lowest extent of this range, due to buffering by the polymer. The static structures of high MW BPEI and LPEI complexes (25 kDa) at a N\P ratio of 10:1 and pH values of 5.4, 6.4 and

7.4 were therefore selected for static SANS investigation on the LOQ beamline.

Additionally, as PEI is notoriously able to buffer changes in pH, some degree of pH drift (± less than 1 pH unit) was suspected in the stock solutions over the course of the kinetic experiments as final pH adjustments were conducted shortly prior to the experiment, so SANS on complexes at these pH values was carried out to verify or eliminate any effect which may have arisen due to pH drift. Slight changes, considered to be of little significance, were observed between repeats of stopped-flow scattering, and as this potential source of uncertainty had been identified, the possibility of this effect was explored. This is discussed further in Section 4.4.1, however no significant structural difference was found due to pH variation in the Q range accessed across the range of pH 5.4 to 7.4.

4.1.5 A Notable Study

Although in general very little work has been done on PEI complexes using SANS, one notable 2011 study by Mengarelli et al[130] did undertake SANS study of complexes of PEI with, among other things, a DNA fragment. However, their experimental conditions are sufficiently different from those presented here that only limited comparisons may be made. Additionally, the selection of DNA fragment size of 150 bp has limited direct physiological relevance for transfection systems, and the process of obtaining stabilised complexes after 24 hours is not representative of typical transfection protocols.

The DNA fragments used in the present study are of a similar size to double-stranded siRNA molecules, enabling comparison to be drawn between this model system, which, albeit somewhat more polydisperse than the single enzymatically generated fragments studied by Mengarelli et al are likely to be, still had an acceptably narrow fragment size range, and the sample was available in the large quantities required to obtain the short timescale snapshots for kinetic SANS, necessitating as it did many repeats per sample at high concentrations and volumes compared to many other techniques. Additionally, findings could be closely related to the widely used siRNA complexes, which have direct physiological relevance.

Fundamentally, the use of different DNA fragments and different ionic strength conditions, as well as the focus on the stable complexes which persist beyond 24 hours, in comparison to our focus on the early stages of complexation, distinguish these two works and limit the direct comparisons which can be made, as well as reinforcing the gap in the current

literature which this work aims to complete, concerning the process of complexation of PEI molecules, both linear and branched, with nucleic acids and the structural evolution and timescales involved. However, despite the differences between the studies, some broad features such as the lack of stability of many forms of complexes in solution and the large, sharp $Q^{-}4$ Porod gradient indicating large bundles of complexes were confirmed in our study.

The aproach of preparing stable polyplexes in advance and studying only the most stable is in contrast to our intention to use dynamic SANS to probe the changing structural features of newly formed complexes, as relevant to applied gene delivery protocols.

4.1.6 Selection of the System and Expected model

Some discussion was given previously in Section 1.4.1 of the choice of these samples to study and the relative molecular sizes and expected mode of binding were discussed previously.

Kwok et al[103] report that complexes formed with 25 kDa BPEI and DNA or siRNA exhibit higher transfection efficiency and are more stable than complexes formed with 22 kDa LPEI, which the authors say highlights the importance of stability for transfection. In this study we seek to understand in more detail the aggregation process and structural stability of various types of PEI complexes under different conditions.

Generally speaking, large BPEI forms complexes which give stronger gene delivery than small ones.[137] However, Ogris also reports that LPEI gives stronger transfection than BPEI, through suspected aggregation once on the cellular surface, hence both of these polymers are of interest for study. However, this will be influenced by net surface charge of the complexes and composition of the complexation media. Some reports indicate that large complexes are disadvantageous for cellular entry, as 150nm is the reported size threshold for clathrin-coated-vesicle-mediated uptake.[127] Paradoxically, Han et al[68] found that small complexes show lower transfection efficiency than larger particles, and Ogris et al describe the sedimentation of large aggregates onto cells (in vitro) as a potential driving force of high entry rates. Additionally, for small nucleic acids, increased internal binding stability of the complexes can be a disadvantage for dissociation and expression, hence Ogris[137] reports that only low molecular weight PEI is effective in producing the intended biological impact of the transfected DNA [137], with large LPEI found to be

superior to large BPEI for siRNA transfection. [127] Kwok et al emphasise the importance of cationic vector flexibility for complexing siRNAs, highlighting branched PEI as superior in this application, in contrast to linear PEI which is thought to be superior for long, linear, plasmid DNA[103]. They also find, through heparin assays, that BPEI provides superior stability against dissociation from bound siRNA than LPEI.

4.2 Materials and Methods

4.2.1 DNA Preparation

Well-characterised DNA fragments were sought to study the complexation of DNA with PEI. Relatively high mixing concentrations (1.5 - 3 mg/ml DNA) were necessary to produce sufficiently strong SANS scattering intensity, while large sample volumes were required for the stopped-flow technique, due to a combination of dead volume in the stopped-flow system, excess sample solutions to flush the system through and ensure previous sample and cleaning solutions were completely replaced in the experimental range of the apparatus and in order to carry out cycling repetitions to enable access to the shortest time frames required with high signal-to-noise ratio. It was therefore decided that fragmentation via enzymatic cleavage (eg. of chromatin), as used in the work of Mengarelli et al [130], discussed above, although producing monodisperse fragments, would not be feasible in the quantities required (up to the order of grams were prepared to ensure sufficient availability). Additionally, the size of fragments prepared by nucleosome cleavage of the nucleosome length, 147 bp, bears little similarity to those used for physiological gene delivery applications, which tend to fall into very large, plasmid DNA molecules, or short, single- or double-stranded fragments or oligonucleotides and siRNA, which are generally much shorter, commonly approximately 20-25 bp or less. It was therefore desirable to study DNA molecules within one of these core regimes of biological relevance. Physical methods of fragmentation, such as extrusion or sonication, were deemed to produce too unpredictable and polydisperse fragment sizes, as well as running the risk of shearing the DNA and producing an unknown mixture of single- and double-stranded molecules.

A commercial sample of partially-degraded DNA fragments, described by the manufacturer as being less than 50 bp in size (D3159, Sigma), was selected for its relatively narrow anticipated size distribution, availability in bulk and physiologically relevant size regime.

Fragment sizing was verified by electrophoresis (see Section 4.2.2) and previous work by Cristofolini et al[31] based analysis and interpretation on the premise that fragments were double-stranded, and we worked on the basis of this assumption also, that the sample was predominantly double-stranded.

Fragment sizing post-purification assumed double-stranded DNA and fell broadly in the size regime quoted by the manufacturers, which would not have been the case had the fragments been single-stranded, where their electrophoretic mobility would probably have been much higher, which would give the appearance of a smaller range of fragment sizes. As it was, our obtained sizing estimate was at the very upper end of the manufacturer's estimated range. The possibility should be acknowledged, however, that a proportion of the DNA could have separated to become single-stranded, although this was not considered likely to be significant.

The purity of the sample was unknown and expected to be relatively low, so purification with chloroform and filtration with a 0.45 μ m syringe filter was undertaken before use. Briefly, a solution of DNA at the manufacturer's recommended concentration of 5 mg/ml was made by dissolving with gentle shaking in a Tris-HCl buffer (Trizma-HCl, Trizma-Base, Sigma, T6666, T6791, respectively) of 10 mM , adjusted to pH 8, in a 50 ml centrifuge tube with vigorous shaking and incubated at 4^oC overnight for complete dissolution. An alkaline pH is important to prevent the DNA from partitioning into the organic phase when mixed during the purification procedure.

Once fully dissolved, a half volume of chloroform, found in one study to be as effective as the more commonly used 1:1 volume in DNA extraction from plant tissues[23]), was added and the tube vigorously shaken until the phases were emulsified. This was allowed to rest for several minutes and subsequently repeated, typically up to around 10 times. Multiple tubes were prepared at once, due to the large quantities of sample required. The tubes were balanced to within $\pm$ 0.1 g and centrifuged at 3,000 rpm for approximately 15 mins, until the organic and aqueous phases had separated.

A precipitate of proteins, lipids or other impurities was visible at the interface of the chloroform and water, with the DNA sample dissolved in the water. The aqueous phase, containing the partitioned DNA, was removed, and the process repeated up to approximately 10 times, until minimal remaining precipitate was visible at the interface.

Subsequently, the DNA was precipitated by addition of a concentrated NaCl solution to bring the solution composition to 0.2M NaCl and 2 volumes of ice-cold ethanol. The DNA

was precipitated overnight at -20^oC before centrifugation at 4,000 rpm for approximately 60 mins to pellet the precipitated DNA in several tubes as the quantity of DNA was large. The supernatant was discarded and the pellet was washed 3 times in 70% ethanol with vortexing to detach the pellet from the tube wall for thorough washing, to remove remaining salt from the sample, followed after each wash by repeated centrifugation (typically approximately 10 mins at 4,000 rpm) to recover the pellet. The ethanol concentration is sufficient to prevent the DNA from redissolving, while the water is able to dissolve salts present in the pellet. A slight coloured tint to the sample was noticed, so during each wash stage, the pellet was incubated in 70% ethanol on an orbital incubator (S150, Stuart)for approximately 30 mins to ensure thorough removal of impurities.

After the final wash and centrifugation, the pellet was allowed to air dry for at least 30 mins to an hour.

Finally, the sample was resuspended in D_2O and filtered through 0.45 μ m filters, before final concentration and purity estimation by UV absorption spectroscopy.

The purified DNA solution in D_2O was stored at -20^{o}C when not in use, and wherever possible at 4^oC between experiments, although for some periods of time it was not possible to return sample to the fridge as stability of temperature and pH was desirable. However, as the solution was in D_2O and the DNA had been extensively purified and filtered, bacterial growth and enzyme activity was expected to be minimal. Additionally, room temperature would be too low for DNA melting and the fragments were already partially degraded when purchased, so any limited further cleavage which did occur would not fundamentally alter the nature of the sample fragments.

4.2.2 DNA Characterisation

The stock concentration was determined to be 7.7 mg/ml by UV absorption at 260 nm and with a purity of 1.62 based on the ratio of absorption at 260 nm to 280 nm, the so-called A260/A280 ratio. A rectangular quartz cuvette of 0.6 ml volume and 1 cm path length was used in conjunction with a UV spectrophotometer to determine the concentration and purity of DNA samples by UV absorption spectroscopy. The peak absorbance of DNA lies in the UV range at 260 nm, while that of proteins at 280 nm. Thus, the ratio of a samples absorbance at these two wavelengths (known as the A260 / A280 ratio) can be used to gauge the level of contamination of a DNA sample with protein

When stock concentration was later checked by another method, Nanodrop, in the context of fragment sizing preparations, it was found to be 8.2 mg/ml, approximately 6.5 % higher than the originally determined value. As the stock solution is very concentrated, leading to potential inaccuracies in a method based on absorption, and is in any case outside of the recommended range of operation of the Nanodrop, which can lead to $1-2\%$ inaccuracies according to the manufacturersome overestimation is not surprising. Hence, readings were found to have an acceptable level of agreement, despite the difference in technique, and the originally determined value was used for all experiments.

DNA fragment size determination was performed on an Agilent Bioanalyzer Chip with High Sensitivity DNA Kit. The concentrated, stock solution in D_2O was delivered to Michal Smiga of the Genomic Technologies Facility, Michael Smith Building, University of Manchester, who performed the measurement and provided the second estimate of concentration using Nanodrop.

The chip-based size analysis relies on a gel matrix and DNA-binding fluorescent dye mixture for detection of DNA migration times through the gel matrix, calibrated with the marker ladder for size vs. electrophoretic migration time. The larger fragments migration through the gel matrix is hindered by their size, typically relying on a process of reptation[40], while the smaller fragments migrate relatively quickly and freely under an applied current.

A 15-point DNA marker ladder was run alongside the sample in a separate well of the chip to calibrate the fragment sizes, covering a range from 35 bp to 10,380 bp, and small quantities of these smallest and largest fragments were included in each sample well to scale the sample fragment positions to the sizing ladder. The sample was diluted to 100 μg/ml for measurement and pipetted onto the chip with the manufacturer-supplied gel matrix and dye mixture (as noted, size measurement performed by the facility operator, Michal Smiga).

Agilents proprietary software was used to analyse the data and derive the relative abundance of different DNA fragment sizes and the results are shown in Figure 4.1. Two main peaks were discovered, in very close proximity, at 56 and 65 bp, with a steep tail dropping off to baseline by approximately 200 bp. The lower size marker peak, at 35 bp, was superimposed on the left-hand tail of the sample peak, and appeared to show a very narrow peak with height of approximately 400 Fluorescence Units (FU), while the same concentration of marker run in the ladder well without sample produced a peak height of

approximately 150 FU. This suggests the marker DNA at 35 bp also concealed another significant sample peak around 35 bp, with the tail extending below this lower marker into the uncalibrated region of smaller fragments. This conforms to the manufacturer's description of the sample as partially degraded DNA fragments, less than 50 bp in length, although the predominant peak lies just above this range at 56-65 bps. The DNA sample was assumed to be double-stranded, based on the manufacturer's description and other authors' analyses[31], as discussed above.

(a) DNA fragment size distribution

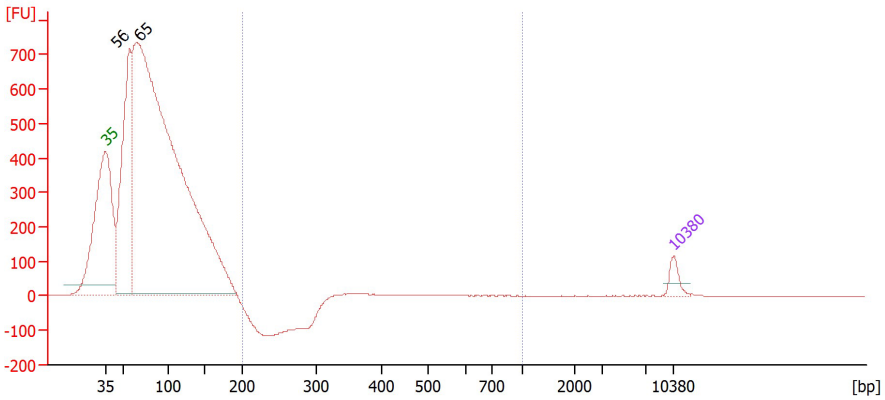

(b) Electrophoretic gel-like representation of DNA fragment size distribution, generated by Agilent Bioanalyzer software

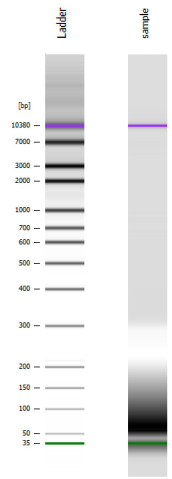

Figure 4.1: DNA fragment size distribution as measured by Agilent Bioanalyzer Chip with High Sensitivity DNA Kit, at a concentration of 0.1 mg/ml, scale in fluorescence units. Peaks at 35 bp and 10380 bp correspond to size markers, included for calibration to a separately run DNA sizing ladder.

4.2.3 PEI Preparation

Anhydrous linear PEIs (M.W. 2,500 and 25,000 Da, Polysciences, Germany) are solid at room temperature, while branched PEIs (M.W. 1,800, Polysciences, Germany, and 25,000, $\leq 1\%$ H_2O, Sigma-Aldrich) are liquids, independent of molecular weight. Samples'

molecular weights were selected to enable investigation of behaviours over approximately an order of magnitude's range in size. Typical structures of branched and linear PEIs are shown in Figure 2.1, and repeated below in Figure 4.2, for reference.

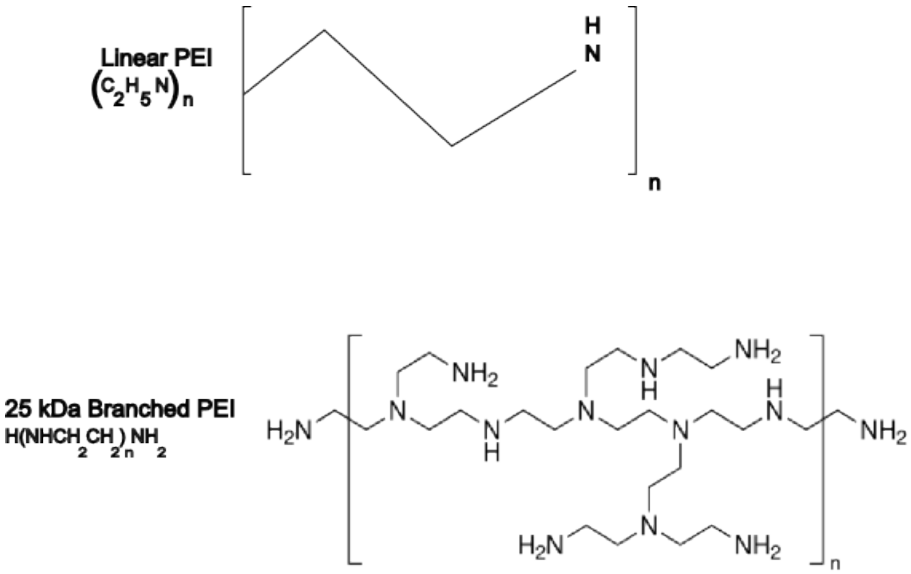

Figure 4.2: Linear and Branched PEI structures; Linear structure adapted from Polysciences.com; Branched schematic incorporated directly from the manufacturer www.sigmaaldrich.com, the manufacturers' online description of the 25kDa BPEI used in this study

Branched PEIs are soluble in water at room temperature, and were dissolved in the required volume of D_2O with gentle rocking for up to several hours, after which the pH was checked and adjusted to the required level with concentrated HCl or NaOH in D_2O.

Linear PEIs are not soluble in cold water at neutral pH, so the pH was reduced with conc (37%) HCl until all polymer was dissolved. Subsequently, the solution was incubated with gentle rocking for several hours to ensure the solution was stable, then the pH was gradually returned to just below neutral, with concentrated NaOH solution (in D_2O). It was further incubated at room temperature for several hours to overnight, before the pH was finally adjusted to the desired value. Due to anticipated pH drift due to the buffering capacity of PEI, pH was rechecked shortly prior to experimental use. PEI solutions in D_2O were kept at 4^oC for long term storage when not in use, except for periods between experiments where it was considered necessary to maintain stability of temperature and pH, when they were kept at room temperature.

Molecular dynamics simulation work on the protonation of linear PEIs in solution by Ziebarth et al[204] finds that, under physiological conditions , 55% of amine groups are protonated, in a nearly alternating pattern of protonated and non-protonated amines,

with a separation corresponding to the Bjerrum length in water. This is, however, likely to change when bound to DNA. A fundamental study on the solubility of linear PEI by Goethals et al[188] found that significant crystallisation of the solubilised polymer on back-titration to higher pH was initiated by a sequence of 10 amine groups becoming deprotonated, something which is unlikely to occur at the physiological pH range we are studying, based on the molecular dynamics work, and indeed which is confirmed by Goethals et al as occurring somewhat above neutral pH. Goethals et al[188] found that above a specific pH recrystallisation started to occur at a significant rate, such that the solution pH dropped on addition of further base. This is higher than the typical range investigated in this work so LPEI solutions were expected, and indeed found, to be stable once dissolved.

Due to the crystallisation process described above, linear polyethylenimines are insoluble in water of neutral pH at room temperature. Solubilisation is therefore effected by gradual addition of excess HCl until dissolution is complete as determined by observation of the point of disappearance of remaining visible particles. Although the molecular dynamics simulation study's authors themselves comment that their model does not show good agreement with experiment involving variation of salt, this provided reassurance that the method of solution preparation of LPEI, which requires the pH to be lowered with an excess of HCl and subsequent back-titration towards the desired pH, would be acceptable and not cause crystallisation at the physiological pHs used in this study.

Gentle rocking at room temperature for several hours ensures thorough and stable solubilisation at low pH, before gradual back-titration to the desired pH with concentrated, aqueous NaOH solution in the relevant protonated or deuterated solvent. The quantity of concentrated HCl required to enable full dissolution of the polymer at a stock concentration of 5 mg/ml even if it were to be fully neutralised with NaOH, would only correspond to the addition of an estimated 0.1 mM NaCL in the stock solution, which can be taken to be negligible.

4.2.4 pH Calculation in D_2O and H_2O

The pH of a D_2O-based solution, as measured by a pH meter calibrated against buffers in H_2O, will be 0.4 units lower than the actual pD. [14] Therefore, pHs for SANS solutions in D_2O were taken to be 0.4 units lower than their actual values for comparison with

techniques requiring solutions in H_2O, such as cell culture. Hence the pHs quoted in this chapter, pH 7.4, 6.4, 5.4, were actually measured as pH 7, 6, 5.

4.2.5 Solvent Media Selection

Informed by the literature, as discussed in Section 4.1.4 above, it was found that complexes for transfection are frequently formed in either 5% glucose or 150 mM NaCl. However, the size of these complexes is significantly different[58] from complexes formed in high ionic strength media forming much larger particles, leading to questions surrounding their respective mechanisms of action.

Preliminary attempts to conduct SANS on samples in 150 mM NaCl produced a negligibly low scattering signal and preliminary DLS screening (data not shown), supported by understanding from the literature[58], appeared to reinforce that the size range of these complexes were greater than that accessible with SANS, limited by the inverse of the lowest Q value, in the case of SANS2D, around 300 nm[83], while complexes formed in a glucose solution appeared to be relatively small and were within the accessible range for SANS.

Following preliminary screening of broad hydrodynamic sizes with DLS, it was decided that a low ionic strength medium of 10 mM NaCl would be used as the main solution condition, with investigations conducted into the effect of other types of media, conducive to formation of complexes sized within the accessible regime of SANS.

In this case, the static scattering over the entire 30 minutes post-mixing from complexes in 10 mM NaCl as opposed to glucose or D_2O appeared broadly similar, for both linear and branched PEI of high MW, which accounted for stronger scattering in both cases than low MW PEI complexes. High MW BPEI complexes formed in D_2O showed weaker scattering at low Q than the samples prepared in 10 mM NaCl or 5% glucose, although an upturn at very low Q was still present, which might suggest lower stability and increased aggregation in pure D_2O in comparison to solutions with a slightly higher ionic strength (10 mM NaCl) or in the presence of glucose . This is likely to be due to the effect of slightly increased levels of monovalent ions promoting cationic overcharging more effectively by counterion correlations and increasing the flexibility of the polymer due to the degree of charge screening provided by the added salt, as described in the review of Ankerfors [6], enabling more stable, positively charged complexes to be produced, providing a greater

degree of electrostatic repulsion between complexes which are, according to Lu et al, driven to aggregate together by hydrophobic effects [113].

High MW BPEI in glucose exhibited slightly stronger scattering in the mid Q range and marginally weaker low-Q scattering than in 10 mM NaCl, also suggesting less severe aggregation. These differences are explored further in the analyses detailed in the following sections.

4.2.6 Complex Formation

Stock solutions of DNA and PEI in D_2O were diluted to the required concentrations and solvent compositions, typically 10 mM NaCl, pH 7.4, unless otherwise indicated. Mixing always took place at equal volumes, the concentrations having been adjusted accordingly. For static experiments not undertaken in the stopped-flow cell, DNA solution was pipetted into an equal volume of PEI solution and immediately mixed by gentle inversion approximately 10 times in an eppendorfer tube. The resulting mixture was subsequently loaded into experimental cuvette and these, in turn, into the experimental rack as quickly as possible, and measurement typically commenced within 5 minutes of mixing. The flux on LOQ is significantly lower than SANS2D, meaning longer counting times are required for good scattering statistics, and hence samples were measured for up to 60 mins. If longer than this was required due to low neutron flux for a particular period, the sample was repeated with a freshly mixed sample to avoid any long-time changes far beyond our regime of study, and the data files averaged using the program Primus[100].

For studies on SANS2D, mixing took place through injection into a turbulent mixing cell integrated within stopped-flow apparatus (Biologic). Again, equal volumes of DNA and PEI solutions at the appropriate concentrations were mixed together. However, in this case, both were injected simultaneously at 3 ml/s into a mixer cell within the stopped-flow configuration, described below, designed to ensure turbulent flow and, hence, thorough mixing. Mixed sample then flowed immediately into the experimental cell, and data collection was triggered once the defined volume had been mixed and flow had stopped. Scattering data was initially analysed on a 30-minute averaged, static basis and, subsequently, time-sliced into desired intervals over the same period to evaluate the structural kinetics following initial mixing.

For samples where kinetic study as well as static was intended, fresh samples were mixed

and SANS data collection was repeated 5 times with the fresh mixtures, which enabled both static and time-sliced data files to be summed, which was necessary to improve the signal-to-noise ratio for short collection intervals. Samples in pure D_2O were exceptionally not repeated 5 times, as they were principally intended to serve as a static reference structure for comparison with other solvents, and hence the additional signal was not needed, but whose kinetics were nonetheless examined for any kinetic changes which could be observed despite the poorer accumulated statistics.

4.2.7 Stopped-flow Configuration

The structural evolution during complexation and subsequent aggregation of branched and linear polyethylenimines of different molecular weights with double-stranded DNA fragments was studied using time-resolved SANS. Time-frames up to a maximum of 30 minutes post-mixing were studied in order to investigate structural evolution over the range of complexation times commonly used in transfection work, based on a range of studies examined in the literature (See Section 4.1.4). Incubation is commonly carried out at room temperature and is allowed to proceed for between 10 and 30 minutes after mixing[103][189], but often longer, sometimes with vortexing[187]. Several authors found significant differences between complexes which had been allowed to form for different time periods [75][70], although studies differed in their findings of optimum times for transfection, depending on the precise conditions and types of PEI and cell models, with some finding transfection efficiency decreased the longer some types of complexes were incubated[70], and others finding the peak of efficiency after just 5 - 10 minutes[35]. It was therefore decided to study structural evolution over the first 30 minutes after mixing, with shorter timeframes used in the initial periods, when dynamic changes were expected to be greatest, and intervals gradually extended up to mixture ages of 30 minutes.

Stopped-flow kinetic studies were performed using a Bio-Logic SFM-400 fitted with a 1 mm path length, rectangular, quartz Hellma cuvette and a high density mixer. 10 ml disposable syringes were used to fill the reservoir at the recommended speed setting of 3 ml/s and reservoirs were filled and mixing and flow established consistent with the manufacturer's instructions. Briefly, reservoirs were filled and emptied in reverse numerical order (beginning with the syringes closest to the final mixing site and cuvette). Gentle downwards pressure was applied to the syringe manually during automated filling and,

once filled, the solution was expelled back into the external, filling syringe once or twice to allow any bubbles in the reservoir to escape. Finally, a small quantity of solution was flowed from the reservoir into the cuvette to remove any remaining air bubbles from the system. Samples to be mixed were loaded into the two syringes closest to the experimental cell, while a 3M NaCl solution and the appropriate solvent for cleaning were loaded into the remaining two. A schematic of the principal features of stopped-flow apparatus is shown in Figure 4.3 In this work, four syringes were used, although only two were involved in sample mixing, the others being used for cleaning solutions and buffer, and remained filled at all times during the experiments. Equal volumes of PEI and DNA solutions at appropriate concentrations to result in the desired charge ratio, with a constant DNA concentration of 1.5 mg/ml were mixed at a flow rate of 3 ml/s and flowed into the quartz experimental cell. 1.5 times the required volume was flowed into the cell to ensure complete flushing of the previous sample and cleaning solutions.

Data collection was triggered to begin once the desired sample volume had flowed through the cuvette. The total system, inclusive of lines between the mixing point and the valve after the cuvette had a volume of 0.6 ml. Typically, approximately 1.5 volumes of 3M NaCl in H_2O were flowed through and allowed to remain briefly in the cell following each sample run, to remove previous complexes and clean the cuvette, as concentrated NaCl solution was found to be effective in detaching highly cationic PEI-DNA aggregates from the anionic quartz cuvette surface, through screening of the electrostatic attraction, which appeared to be supported by preliminary dynamic light scattering testing. This was allowed to remain in the cuvette for approximately one minute, before 1.5 volumes of the relevant experimental buffer in D_2O were flowed through the cell, followed by 1.5 volumes of the sample for the following run, to ensure that all previous suspensions had been flushed out of the experimental system. Sample mixing took place at the closest mixing point to the cuvette, to reduce delay time and the potential for sample dilution with additional solutions in the lines, and flow following mixing took place at a constant rate of 3 ml/s, which was intended to be low enough to avoid significant turbulence with this narrow, 1 mm path length Hellma quartz cuvette, but fast enough to ensure thorough mixing, falling within the manufacturer's stated range[15]. At this flow rate, the age range of samples in the cuvette volume at any point during the experiment is very narrow, but the limiting factor in the minimum age resolution of the experiment is the signal-to-noise ratio of scattering rather than the dead volume or age span of the mixing system.

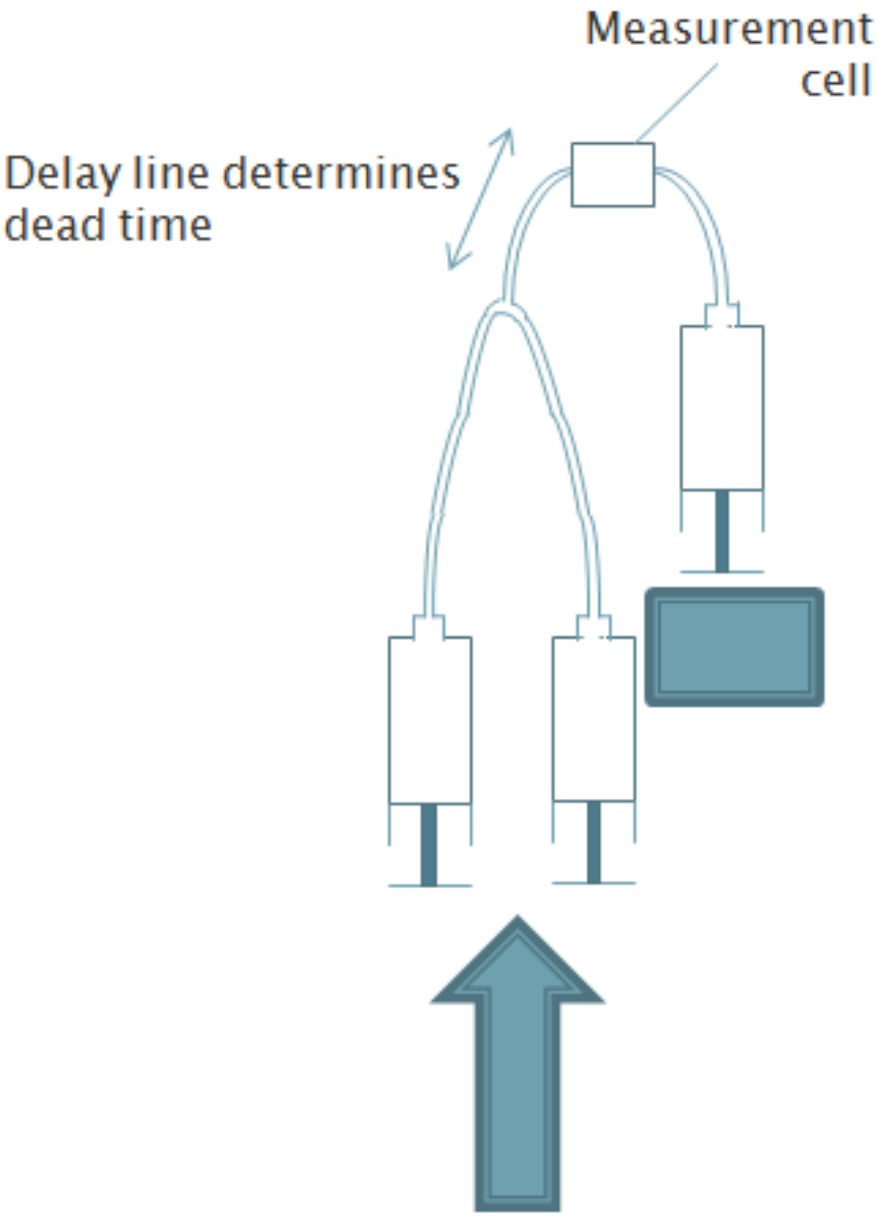

Figure 4.3: Schematic showing the fundamental mode of operation of a stopped-flow apparatus, where samples contained in syringes flow into a mixing cell and through a minimal length of tube to a measurement cell, until a defined volume is reached and a stop is reached, which triggers the start of time-calibrated measurements)

Following a set of experiments, all reservoirs, lines and the cuvette were cleaned by flushing through with at least 2 volumes of 3 M NaCl solution, followed by 2 volumes of pure water, pure ethanol to expedite drying and, finally, several volumes of air to dry out the system before storage. All reservoirs were filled and the system flushed through with one volume of relevant buffer prior to use, the equipment having previously been cleaned as described.

4.2.8 Time Resolution and Complex Age Span

The time-stamped scattering data from the SANS2D stopped-flow mixing experiments were averaged to provide static scattering data for the 30 minute period and were separately time-sliced into specific time periods of interest relative to the start of data collection at the point of mixing, to enable any structural evolution to be detected. Time-slicing into periods was conducted using a proprietary script written for MantidPlot, provided by R.K. Heenan and Sarah Rogers from the SANS2D beamline at the ISIS Neutron Facility, Rutherford Appleton Laboratory, Harwell Oxford. The time-periods selected for slicing of all kinetic data were 0 - 50, 50 - 100, 100 - 200, 200 - 300, 300 - 600, 600 - 900, 900 - 1200, 1200 - 1500 and 1500 - 1800 seconds, while some samples were selected for additional examination at short time-scale resolutions, due to the appearance of features of interest at early times, in which case, 10 data slicing periods of length 5 seconds from 0 to 50 seconds age after mixing were generated.

While the theoretical dead time of the stopped-flow apparatus is on the order of ms, the actual lower limit of time resolution of the system is determined by a combination of the acquisition and readout time of the detector as well as the scattering intensity of the sample and number of times that the snapshot can be repeated to ensure sufficiently good signal to noise ratio for reliable fitting of the scattering data. In theory, this means a time-frame of 100 ms is the minimum possible although, realistically, for the samples concerned here, several seconds was the minimum achievable, where necessary, albeit with high noise levels, even with the addition of up to 5 repeated time-slices. Where a particular phenomenon of interest was suspected, as described, shorter time-slices of 5 seconds were taken over the initial 50 seconds. Although a high level of noise is clearly present, as indicated by the size of statistical error bars, these short time-slices are included where relevant, as they are still useful for an indication of the broad trend under consideration. All complex ages are time-averages of freshly mixed complexes, meaning a range of complex

ages is present in the observational cell at any one time. This is also insignificant in comparison to the length of the time-sliced periods. It should be noted, however, that if, as anticipated, aggregation proceeds with time to larger sized particles, the resulting scattering over a time-averaged period will effectively be weighted more towards the longer time contributions due to the stronger small angle scattering intensity from larger particles.

4.2.9 SANS Conditions

LOQ

SANS data collected using the stopped-flow device on the SANS2D beamline for static and kinetic analysis was very time intensive, due to the need for repetition to access short time-scales, so was supplemented with static scattering data collected on the LOQ beamline.

Due to the relatively weak scattering and large size of the complexes and LOQ's reduced accessible range at low Q, where the most intense scattering was frequently recorded, samples conducted on the LOQ beamline were conducted at twice the concentration of those on SANS2D, with a DNA mixing concentration of 3 mg/ml rather than 1.5 mg/ml. This enabled the effect of concentration on sample scattering to be studied, albeit over a limited Q- and concentration-range. It was anticipated that this increased concentration would likely contribute to more extreme aggregation, although the restricted accessible regime at low Q means Guinier treatment is curtailed, so less information can be gleaned regarding the size of the large aggregated particles than on SANS2D. The intensities shown are absolute intensities, due to prior normalisation of the scattering with beamline standards and all data fitting and analysis was carried out on absolute intensity data.

SANS samples conducted on LOQ did, in some circumstances, require repetition and averaging in order to keep the complexes' age within a reasonably short time-frame (less than 1 hour), to avoid the possibility of further structural changes which may occur at times outside the regime of interest contributing to the scattering data. In this case, averaging of the data files to improve the statistical uncertainty on data points for improved interpretation and data fitting was conducted using the Average function in Primus[100].

SANS2D

Small angle neutron scattering was carried out on the SANS2D instrument at the ISIS spallation neutron facility at the Rutherford Appleton Laboratory, Didcot and analysed on both a static and time-resolved basis. Beamline configuration is shown in Section 3.2.1. Standard samples were run and the direct beam determined using a sample changer setup prior to stopped-flow experiments, whereupon the sample changer was replaced by the stopped-flow mixing apparatus (Biologic). Scattering and transmission were measured for each relevant buffer solution and used for data reduction of the sample scattering to provide an accurate estimate of the background and transmission of the solvent. SANS data was collected continuously over the period of interest, in this case, 30 minutes, with a transmission reading also taken of a representative sample following scattering, and initially analysed on a static, time-averaged, basis. Complexes were formed at charge ratios of 10:1 and 20:1, with a final DNA concentration of 0.75 mg/ml, as mixing took place between polymer solutions of varying concentrations with DNA solutions of 1.5 mg/ml at a 1:1 volume ratio. Pure polymer solutions were conducted on LOQ at a concentration of 5 mg/ml, but showed relatively weak scattering in static SANS experiments. Pure polymer or pure DNA solutions were not studied on SANS2D.

SANS2D operates on the second Target Station at ISIS, which benefits from increased intensity of neutron flux, due in large part to the significant change in moderator design to a grooved methane/helium geometry, resulting in more than 4 times the intensity on LOQ, despite receiving only 1 in 4 of the frequency of proton pulses of beamlines on Target Station 1[72]. Schematics and further details on both beamline setups can be seen in Figure 3.1, Section 3.2.1. Static scattering data resulting from SANS2D studies was conducted over 30 minutes and the sum of 5 repeats was typically calculated for both static and time-sliced data during the data reduction process in the standard program, Mantid Plot [174], using the SANS - ISIS Macro.

4.3 Analysis

The approaches of Porod and Guinier analyses with the Debye-Bueche model and Kratky-Porod models, as appropriate, have been combined with form-factor-based model fitting and applied to time-resolved small angle neutron scattering from complexes of different

forms of cationic polymer, PEI, and double-stranded DNA fragments to elucidate the structure of the different polymers' complexes formed under varying conditions of charge ratio and solvent, despite their large size, on the edge of the accessible size regime, and the evolving structure of complexes during the aggregation process in a time frame of practical relevance to applied complexation for transfection in gene delivery research.

These models allow estimates of certain parameters, however errors in the fitted parameters were not determined for these basic models, which served as a guide. Only in the case of FISH model fits were uncertainties in parameters obtained.

Static scattering data averaged over the 30 minutes (in the case of SANS2D) or 1 hour (for LOQ) experimental time, which was, in some cases, repeated and summed to improve measurement statistics, as described in Section 4.2.9 above, was first analysed with model-independent techniques, using Guinier and Porod plots to provide an estimate of the size and broad conformation(rod-like, mass fractal, surface fractal, globular) of the complexes, which could be used to inform further, model-based analysis, which was undertaken with the FISH program from R.K. Heenan of ISIS Neutron Facility, Rutherford Appleton Lab. [71]. For the study of aggregation in this work, following static analysis, the stopped-flow data were time-sliced into intervals of interest, using a routine developed by R. K. Heenan and S. Rogers of the ISIS Neutron Facility, Harwell Oxford. Singular value decomposition is an analytical technique which can provide insight into the main sample structural components and their changing proportions across a series of time-resolved or concentration varying data. Informed by the static analysis conducted, SVD was applied using the Matlab program (Mathworks, USA), to identify the minimum number of components required to reconstruct the scattering function at any measured time point. However, it was felt that the interpretation of the analysis was not sufficiently reliable as the constituent elements of the mixture were not sufficiently well characterised to provide confidence in the suggested components, so these are not presented here. These analytical methods are described in further detail in the following sections.

4.3.1 Static Analysis

To inform the choice of model structure for dimensional model fitting, there is a great deal of information which may be obtained by analysing the scattering data through model-free techniques. As Khayat et al describe[94], it is first necessary to subtract the incoherent

background scattering, before the use of model-free techniques, which are sensitive to this absolute base intensity, in particular, when performing Porod analyses. Khayat et al undertake this through subtraction of the linear fit of the data points at high Q. The various Q-ranges correspond to the Fourier transform of different size-regimes, so by looking at the scattering form at the different Q-ranges, inferences can be made about the physical structure of the scattering body on different length-scales. However, the main contribution of the background at low Q is to the intercept, which is only used for Guinier analyses which aim to estimate the molecular weights of samples, which is not the aim of this analysis, as it requires accurate estimation of the SLD of the complexes, so only the gradient was considered in this work, which is less sensitive to absolute accuracy of background subtraction.

Commonly, as depicted for sample scattering from a cylinder by Hammouda et al[66], the low Q regime, down to Q $\approx$0.001, which may only be accessible with the extended Q range offered by the SANS2D at ISIS TS2, is considered the Guinier regime, giving insight into the overall radius of gyration of a molecule, while for LOQ (minimum Q $\approx$ 0.006), the intermediate Guinier regime, which can probe the dimensional parameters of rod-like structures, is likely to be the lowest attainable Q range, possibly bordering on the low Q Guinier region, but with limited reliability of fitting in this region due to the limited extent of the data. High Q scattering, from 0.1$\lesssim$ Q $\lesssim$1, commonly corresponds to the Porod regime, which can provide information on interfacial roughness or mass fractal structure at small length scales.

However, the appropriate interpretation of features in a given Q-range in fact depends on the relative size of the scattering particles' structural features, hence, information about the surface roughness of a particle interface may be obtained at low Q values for a particle which is very large with large features, as in the Debye-Bueche model applied in this work (see Section 4.3.1), while further structural information, beyond the broadly identified shapes such as globular or elongated particles, may then be hard to obtain as they lie beyond the lowest accessible Q-value, while for smaller particles such as stable proteins or vesicle structures, the Porod region may indeed, as is commonly assumed, lie at high Q and correspond to very small scale features on a small overall structure.

The Guinier-Porod model ([63]) is a unified model enabling simultaneous fitting of Guinier factors and Porod exponents for multiple levels, which correspond to different dimensions of particles, where applicable, in the relevant size regime, or alternatively, to the relevant

dimension of multiple particles or aggregates, which must be interpreted as appropriate for the system in question.

In this case, however, we are frequently dealing with particles which are on the edge of the accessible size regime with SANS, even with the extended Q-range available on SANS2D, and, furthermore, with aggregating systems, which must be interpreted with caution when attempting any Guinier analysis. Hence, models for large particles and two-phase aggregates were thought to be potentially appropriate for many samples and hence the greater versatility desired was obtained with separated, individual model fitting, rather than a combined analysis with the unified model. The stages in the data reduction and analysis process and relevant alternative models are outlined below.

Data Reduction and Background Subtraction

Data reduction was carried out on all SANS data following the procedure described in Section 3.2.1. Briefly, SANS scattering profiles were converted to absolute intensity by calibration of the beam and instrumentation with known standard samples. Direct beam intensity, sample and dispersant media scattering and transmission measurements are used to generate background-corrected SANS data on an absolute intensity scale.

Following careful subtraction of the measured solvent background scattering, with high-Q background fitting and correction by further subtraction, if necessary (with the exception of samples prepared in 5% glucose, described in Section 4.4.4), a Porod plot of log(I) against log (Q) can show the Porod exponent as its gradient. Many authors use the fit of the Porod law to adjust background subtraction at high Q[201], however this method is only applicable if there is certainty that the particles being studied have the Porod exponent of 4 for a smooth interface. If the sample obeys Porod's law and yields a Porod exponent of 4, this can enable the Porod volume of the complexes to be deduced. Where there is uncertainty about the precise morphology and conformation of the particles, however, the Porod exponent is to be experimentally determined to provide information about the conformation and flexibility of polymer complexes. In this case, background fitting was incorporated within the power-law fit to ensure background was accurately treated, particularly when determining low Porod gradients at high Q which are particularly sensitive to inaccurate background subtraction.

Accurate background subtraction is thought to be critical for correct Porod fitting and

exponent estimation as it depends on high-Q scattering, where the incoherent background is proportionally more significant, and the gradient of a double-logarithmic plot in the Porod region which gives the Porod exponent is subject to a multiplicative factor due to any background unaccounted for, directly altering the value obtained.

The combined Guinier-Porod fit proposed by Hammouda et al[62] fits an area up to approximately Q=0.1, ignoring data above this point which is assumed to correspond to the incoherent background, but does incorporate a background term into the model for high-Q Porod exponent fitting. Other authors found a similar treatment advisable, limiting useful fitting to a maximum Q of around 0.1 to 0.2, where, according to Zhang et al[201], the level of I(Q) became of the order of the uncertainty in the incoherent background, which was found to be around 0.01. [98] [201]

However, work by Lugo et al [114] highlights the minimal difference a variation in the level of background subtracted can make to this gradient in practice, particularly when the fitting region is limited to $Q \lesssim 0.1$, as advised above, which gives confidence in this method. Additionally, the power-law fitting (using NIST's NCNR program in IgorPro)[97]model used to obtain Porod constants contains an explicit background term at high-Q.

As many samples exhibited two Porod regimes at lower and higher Q, the background was fit simultaneously with the higher Q Porod exponent, as this resulted in a more accurate outcome, and the background was subsequently held fixed at this value while the fit was repeated in the relevant low Q Porod regime, selected with cursors in the NCNR program. The combination of these measures gives confidence that any effects due to uncertainty of background incoherent scattering will be minimised.

Guinier Analysis

Guinier plots of ln(I) against Q^2 manifest a linear section in the Guinier regime, whose gradient is related to the radius of gyration of particles. The region of validity for Guinier analysis is typically thought to be QR_g ¡1. However, some authors[126] have shown that an extended regime can be used to model Guinier parameters, depending on the particle structure, but that the commonly cited limit of QR_g¡1 may be the most conservative extreme, and in some cases values up to 2[44] or even 3 [126] may be valid, depending on the particle form factor model deduced, which should be used to inform selection of an appropriate limit for quantitative conclusions, rather than 1 as commonly used.

Initial examination of the static scattering data using Guinier plots showed either an upturn superimposed on a relatively linear region or a uniformly curved region rather than a pure linear plot. This indicates the presence of aggregation in the samples, which was observed visually through sample turbidity, as anticipated and was, in part, the intended focus of the kinetic, stopped-flow study.

Many small angle scattering texts caution against attempting analysis on severely aggregating particles, suggesting that the significant presence of aggregates may affect the entire scattering profile in ways which are hard to isolate in the absence of simultaneous fitting of scaled concentration series. In this work, however, we are concerned with treatment of the different sizes of PEI complexes and their temporal evolution. Hence, the majority of particles of interest are aggregates of sorts, rather than aggregation being solely a nuisance, interfering mass obscuring the monomer particles, which may be of interest, in, for example, systems such as protein studies, which are often the focus of macromolecular studies and which are a predominant field of application of soft matter techniques such as small angle scattering.

Some authors [147] claim that data from aggregated samples is unprocessable. Indeed, the selection of a relatively linear region with the presence of aggregation-derived curvature makes the selection of valid linear Guinier regimes somewhat subjective and the gradient and derived R_g sensitive to precise choice of points. However, in any case, visual comparison of Guinier plots from different samples can be informative, as can some indicative fitting of broad regions. Given the presence of aggregation, the Guinier plots must, at a minimum, be divided into two linear regions characterising the R_g of the upturn and the main scattering function, and in the presence of aggregation be interpreted with care, allowing for the fact that they may overestimate the size of the complexes, as scattering is weighted heavily by larger particles, due to the dependence of the scattered intensity on the 6^{th} power of the particle radius. [22] Guinier fitting is conducted on background subtracted data, based on Porod fits and Guinier plots are shown as insets in Porod plots of the scattering data.

Aggregation, therefore, limits the extent to which Guinier analysis may be utilised in this work, at least without some caution in interpretation. Hence, Guinier parameters are presented only as approximate indicators and a guide for the behaviour of the scattering at low Q and, most importantly, the extent of the presence of aggregation, as well as giving an measure for comparison of approximate R_g values. The Guinier regime is curtailed

in LOQ data, however comparison with the value of QR_g can still indicate whether any recognised regime of validity is accessible.

The observation of the presence of aggregation in the primary Guinier analysis can inform the choice of appropriate models for further analysis, such as the Debye-Bueche model for two phase systems, described below, which may lead to a better understanding of the complex structures.

Porod Analysis

As aggregation was found to be present in the majority of samples, the scattering was first examined to identify broad structural features. As described by Ramzi et al [151] for similarly aggregated samples forming large scattering particles, the second model-free technique to turn to is to establish the Porod exponent or exponents of a sample, derived from the gradient of a Porod (double-logarithmic) plot, which gives an indication of the form of the particle, frequently a mass fractal when applied to polymer chains, or the surface roughness of a globular particle, or potentially a combination of the two, indicating both the surface structure or packing density of the aggregate, and the structure of any component parts.

The Porod exponent, m, is related to the Flory excluded volume parameter, ν as

$$m = \frac{1}{\nu} \tag{4.1}$$

,[67] where a Porod exponent around 1 indicates a rigid rod conformation, values between approximately 5/3 and 3 indicate gradation from swollen chains to gaussian coils and finally tangled networks of chains as mass fractals, and exponents from 3 to 4 characterise the surface roughness of a globular particle as surface fractals, with 3 indicating surface roughness and 4 corresponding to a smooth surface.

The scattering observed in many of these samples follow a broadly similar shape to those presented by Ramzi et al and a similar analytical approach was taken here. Firstly, the gradient at Q values below the 'heel' of the Porod plot was looked at to characterise the scattering of the surface or mass fractal conformation of the overall aggregates based on Porod's law. Additionally, the gradient above this critical value was evaluated to indicate the shape of the sub-particles which make up the aggregates, where present, or a relevant characteristic length, eg the statistical kuhn segment length of component rods.

In a similar manner to Ramzi's study, the observation of a Q^{-3} - Q^{-4} Porod gradient at low Q indicating large, globular aggregates led to analysis with a Debye-Bueche model, which was then used to generate a correlation function, producing estimated characteristic length scale parameters for the aggregates, where applicable. As this method is dealing with aggregates on the fringes of sensitivity of the technique, it should be treated as an approximate estimate. Fits were conducted using a simple curve fit based on pure background-subtracted data points without error weighting to give an approximate indication of the gradient and intercept. As discussed previously, however, there was a high sensitivity to the choice of points for inclusion in the linear region and also whether the fit was conducted with errors or without. There may also be high sensitivity to accurate background subtraction.

While the precise values derived from the fit are uncertain, meaning the resulting characteristic aggregate size is not in itself a reliable absolute value, (whether or not errors are taken into account during the fitting, results in a very slight difference in observable fit and makes the difference between a positive and a negative outcome),the method still enables useful comparison between curves of different complexes. The fit without the use of SANS errors, given uncertainties from background subtraction and the very slight difference between these fits, is presented in the relevant section, below, as an indicative comparison. As described elsewhere, the intercept used to define the characteristic aggregate size is in all cases very close to zero and so is likely to have high uncertainty and therefore unlikely to be a reliable value, but may facilitate comparison between samples so the characterisation may nonetheless have some value in building a picture of the complexes.

Where high Q Porod gradients indicated rod-like structures, a modified Guinier or Kratky-Porod analysis of these particles was carried out, following background subtraction. This resulted in the rod lengths being given by

$$l = \frac{12}{\pi Q^*} \tag{4.2}$$

, where Q^* marks the start of the Kratky-Porod region, the 'heel' between the Debye-Bueche -4 exponent region and the -1, rod-like regime, and the cross-sectional radius of gyration is found from the gradient of the Kratky-Porod plot of ln(Q I(Q) vs. Q^2 as

$$gradient = -\frac{r_g cs^2}{2} \tag{4.3}$$

, where the cylinder radius, r, can be derived as

$$r = \sqrt{2} r_{gcs} \tag{4.4}$$

[167], with r_{gcs} denotes the cross-sectional radius of gyration for an elongated particle. As it is QR which is limited by the small angle assumptions in the Guinier analysis, it is possible to extend to larger Q, provided R is small, according to some authors [177], based on studies of alloy precipitates, up to the range of $0.8 \leq QR_g \leq 2$ or up to the range $1.46 \leq QR_g \leq 2.21$[167], on aggregated peptide fibrils, which the authors accept as an approximately accurate result in this extended range. Additionally, the Kratky-Porod or modified Guinier analysis for rods is valid once the Q^{-4} term has died off in the intermediate Q regime, enabling deduction of the rod lengths and cross-sectional radii. The rod-like structures visible at this length scale are related to the persistence length of a polymer, or, where small particles, identified as rods binding to form larger aggregates, they may be interpreted as the length scale of the individual complexes. Hence, a Kratky-Porod (or modified Guinier) analysis may be applied where rods are detected, to give the length and cross-sectional radius, or where this is very small, the length only, the flat gradient of the Kratky-Porod plot in this region confirming the rods are negligibly thin. [151] The Porod gradient of $Q^{-\alpha}$, with α typically 4 for sharp interfaces, while commonly thought to be valid at large Q values, can be observed at low Q for large particles with a sharp interface. [177] Intuitively, as these regimes are typically defined in relation to the magnitude of the product of QR, all the regimes are shifted to lower Q for large particles, hence it may not be within the measurable Q range to access the Guinier regime for large particles, so the Porod regime of the large aggregates may potentially occur first, at lower Q than the Guinier regime of the small constituent particles.

Exponent Interpretation

One of the main advantages of the SANS technique is its ability to decipher geometric forms of structures randomly oriented in solution, rather than only hydrodynamic sizes, as with the simple DLS setup provided by the Malvern Zetasizer Nano. Sophisticated standard and combined models are available [71] for fitting of data, but the variety of models available means a sound understanding of the overall form of the structure is key to choosing the most appropriate model for physically meaningful parameters.

An initial evaluation of the Porod exponents of a system can inform the choice of models by indicating properties of surface or mass fractals and polymers, as introduced above. The Q-region in which an exponent is located on a Porod plot corresponds to the size range of particles meeting that criteria. For instance, the 'Porod regime' is commonly considered to lie at high Q values, to give an indication of surface roughness on a very small scale. However, as Ramzi et al[151] described in their work on recombinant gelatin aggregates, the Debye-Bueche model is based on the principle that large aggregates on the edge of the Q regime accessible with SANS manifest a -4 gradient on the logarithmic, Porod plot at low Q, corresponding to very large, smooth aggregates, while porod gradients of -1 at higher Q indicate the presence of rods on a smaller length scale, hence suggesting the conformation of large aggregates composed of rod-like particles, which can then be further analysed by a Kratky-Porod model, both of which are described in further detail below.
This analytical approach is followed in this work, as it is frequently concerned with similar combinations of structures. However, many other Porod exponents may be encountered, and these indicate various degrees of flexiblity in a mass fractal or chain, with 1 indicating rods, 5/3 indicating swollen chains, 2, Gaussian chains, 3 a network or, in terms of surface fractals, a rough surface, and 4 a smooth surface. This initial approach offers a powerful method to gauge the likely overall structure of particles under investigation, and forms the basis for further, more detailed analysis, such as model-based data fitting in this work.

Resulting Models

Debye-Bueche Model and Plot One approach which may succeed in delivering more detailed size information in systems where large aggregates are observed is the Debye-Bueche model for a two-phase system[151].
For large, phase-separated particles, which may exceed the limits of size range typically probed, such as large PEI-DNA aggregates, the Debye-Bueche model offers a means of identifying a characteristic aggregate size, Ξ, by examination of the decay of the correlation function, γ, over the typical length, as follows:

$$\gamma(r) = \exp \frac{-r}{\Xi} \tag{4.5}$$

[151]
The Fourier transform of the correlation function corresponding to aggregates of this

characteristic size gives the scattering intensity as follows:

$$I_D B(Q) = \frac{I(0)}{(1 + Q^2\Xi^2)^2} \tag{4.6}$$

, where I(0) is the scattered intensity at Q = 0, and Ξ, again, is the typical size of the aggregates. [151] The Debye-Bueche plot of $I^{-\frac{1}{2}}(Q)$ against Q^2 can thus give the characteristic size from the gradient divided by the intercept, I(0).

Kratky-Porod Model and Plot The Debye-Bueche approach can be combined with the Kratky-Porod model for elongated, rod-like particles, if suggested to be appropriate by the Porod exponent around -1 at intermediate to high Q, indicative of rigid rods. A modified Guinier or Kratky-Porod plot, ln(QI(Q)) against Q^2, in the intermediate Q regions, can be used to find the cross-sectional radius of gyration for an elongated particle as

$$gradient = -\frac{r_{gcs}^2}{2} \tag{4.7}$$

, which in turn gives the cross-sectional radius of a rod as

$$r = \sqrt{2} r_g cs \tag{4.8}$$

[167] The Q value, Q*, where the Kratky-Porod region begins, at the heel between the Debye-Bueche -4 exponent region and the -1, rod-like regime is related to the length, l, of the component cylindrical rods as follows:

$$l = \frac{12}{\pi Q^*} \tag{4.9}$$

.

Model Fitting

As the sample particle form and structure factors, which partially determine the coherent scattering cross-section, are functions of scattering vector or angle, Q, the scattered intensity at different (small) angles resulting from diffraction from scattering bodies in the sample can be related to particular structural features through determination of the form and structure factors.

The form factor describes the structural geometry of an individual scattering body as it depends on correlations between neighbouring scattering centres or scattering density correlations in a particle. Hence, form factors specific to spheres, cylinders, flexible or semi-flexible rods or chains may be distinguished by their Q-dependent contribution to the scattering cross section as the fourier transform of the interparticle positions. [142] Thus, studying the scattered intensity as a function of the scattering vector, which represents reciprocal space (see Section 3.2.1), enables different form factors to be identified. Broadly speaking, features in the scattering curve at high Q provide information about structures on small length scales, as related by Bragg's Equation, while low Q features correspond to the large length scales of a structure or aggregate. The coherent scattering cross-section additionally depends on the structure factor, which is determined by the interaction potential between scattering bodies. [142] For spheres, this is a relatively standard model of 'sticky-spheres' interaction, however, for more complex form factors, such as those typical of polymers, a more complex model, such as a PRISM (Polymer Reference Interaction Site Model)[161] model may be necessary to fully account for any interaction present. [142]

Model Selection

Following these preliminary analyses, form-factor model-based fitting of the data to known structures was used to identify likely structural parameters for the complexes.

Porod exponents and resulting models were used as a guide, where appropriate, for form-factor model selection for fitting with the FISH program [71], but in some cases the most appropriate system fell between two available models, as with worm-like chains in the presence of large, smooth aggregates, as only mixtures of similar form factors could be explicitly modeled. Similarly, the distinction between rods and ellipsoids can be uncertain and, for aspect ratios $X \gtrsim 7$, the equation for ellipsoids is approximately equivalent to that of rods [32]. An alternative method, according to Weber et al is to compare the calculated scale factors with those fitted by the respective models in the FISH software [160], however, in this case, as the precise composition of aggregates as well as their volumes were not precisely known, consisting as they do of mixtures of polymer and DNA in unknown final bound proportions, with an unknown quantity of free excess polymer, and an unknown quantity of incorporated water, which contributes to the particle scattering [202], this method was not relied upon. Rather, decisions were based on indications from the Porod

exponents found for the complexes, and subsequent goodness of fit of the most likely physical models.

Additionally, the Kholodenko worm-like chain model and two cylinders models may appear to lead to equivalently good representations, consisting each as they do of two length scales of, in several of these cases, relatively large aggregates and smaller rod-like particles. In some cases, the fact that cylinders are detected in the Kratky-Porod region of the Porod plot may seem to imply the presence of rod-like particles, but the overall Porod exponent may indicate a gaussian chain, in which case, ultimately, FISH model-based data may produce a good fit to a combination of two cylinders, if the chain is also in the presence of large aggregates. However, these should not necessarily be taken to be an indication of the presence of rod-like particles, as they may equally be equivalent to the Kuhn length of what is in fact a worm-like chain lying between rods and flexible, Gaussian coils.

Careful examination of the parameters and particle dimensions is, hence, key to distinguishing a true difference in structure from a different expression of the model and the two cylinders in the two core/shell cylinders model may in any case represent the same structural features as the two length scales of a worm-like chain model, given by the statistical segment length and overall length as determined from the product of the number of segments and segment length, and not necessarily distinct particles.

Form factor models are calculated as the integral of the correlation function of scattering density over the particle volume, averaged over all possible orientations for a randomly oriented, elongated structure.[65] The available models used for fitting of SANS data from the complexes are outlined below:

Cylindrical Rods

Either a single cylindrical rod-like form factor, or a combination of two sizes and aspect ratios of rods in varying proportions, as denoted by their individual scale factors, can be modelled. This gives a high degree of versatility and is frequently an appropriate choice of model for this work, as the combination of large aggregates and smaller, rod-like components are well fit by a two rod model, where the aspect ratio of the larger rod may tend to a more globular rather than elongated shape. It is therefore a useful tool for fitting both sample components simultaneously.

Ellipsoid

Fits to an ellipsoid model were attempted where a single, smooth, large aggregate was suspected based on the Porod exponent. Form factors were fit without any structure factor, as the often already complex combination of model parameters combined with the observed uncertainty of some parameters meant increasing the available variables in a fit would not be likely to give a more realistic result, and in almost every case a good fit was achieved to the data with available form factor models without an interaction potential. As the process of aggregation was expected to be due to hydrophobic attraction, the most likely identified potential would be a 'sticky' hard sphere which is a hard sphere potential combined with an attractive square well potential. However, for the fits undertaken here, the hard sphere volume was set equal to 0, meaning no interaction potential was included in the fit. A greater range of concentration series would constitute an interesting extension of the study to investigate quantitatively the impact of the interaction potential, as well as extending the charge ratio to yet higher values in order to slow the aggregation and observe the process in greater detail.

The ellipsoidal form factor is given by a modification to the spherical form factor,

$$F(Q,\mu) = \frac{3j_1(QR_e)}{QR_e} \tag{4.10}$$

, where j_1 is the first order spherical Bessel function and the effective radius, R_e, is defined for an ellipsoid as

$$R_e^2 = a^2\cos^2(\alpha) + b^2\cos^2(\beta) + c^2\cos^2(\theta) \tag{4.11}$$

, where α, β, and θ denote the angles of the axes to the Q direction. The distinction between rods and ellipsoids can be uncertain and, in fact, for aspect ratios X $\gtrsim$ 7, the equation for ellipsoids approximates to that of rods. [65]

In this work, an ellipsoid of revolution is used, whereby a = b $\neq$ c and, hence, the effective radius becomes

$$R_e^2 = a^2(\cos^2(\alpha) + \cos^2(\beta)) + c^2\cos^2(\theta) \tag{4.12}$$

As for the cylindrical form factor, where the sample is randomly oriented, the form factor is an average over all possible orientations, as given in the Equation above [65].

Kholodenko Worm-like Chain

For elongated particles possessing some degree of flexibility, as indicated by a Porod exponent between 1 and 3, the Kholodenko worm-like chain model option in FISH can fit the structure as a number of short rods which correspond approximately to the local persistence length of the particle, indicating the length scale over which no flexibility is observed. Hence, the model can fit a range of structures from stiff rods to Gaussian chains. In this model, the scattered intensity is proportional to a product of the worm-like form factor and the axial radius form factor, as[71]

$$I(Q) \propto P_{Worm}(Q)P_{Axial}(Q) \tag{4.13}$$

Fitting Parameters Uncertainty The resolution of the SANS technique is limited to the size regime corresponding to the minimum accessible Q value, hence, where models fit values to dimensions of the order 1000 $\mathring{A}$ or greater, or frequently, in practice, several hundred $\mathring{A}$ or above, changes in this value tend to make little difference to the model fit. Hence, these values are given as fit as a guide, but in practice may be larger, but cannot be absolutely determined.

An example is given in Table 4.6, where it can be seen that the fitted parameter errors for high MW LPEI complexes at 10:1 N/P ratio have high uncertainty in the length which approaches 1000 $\mathring{A}$.

When this uncertain size regime is encountered it may be that it has an impact on other parameters, most notably the scale factor, where an increased apparent size of the particles may correlate with a reduction in scale factor. In these cases, it is important to compare the whole picture given by each model, rather than solely one parameter in isolation. Where there was uncertainty, and a range of well fitting parameters, particularly in the case of time-slicing, it was generally assumed that the most likely of a family of possible solutions corresponded to a smooth variation in the parameter values with time.

Uncertainties in the fitted model parameters using the FISH program were derived from fitting, however these were typically small and hence likely to be underestimates of the actual uncerainty in the parameters, as noted by the program developer himself. Additionally, he advises resetting certain parameters to zero for the final fit to obtain a more accurate error estimate. However, this was not done here, and rather the obtained error treated as a conservative estimate. One author estimated the actual errors in SANS

structural parameters fit using another modelling program as ±5% [167]

The exception is, as discussed above, for extremely large sizes, where estimates possess high uncertainty due to loss of sensitivity of the SANS technique at low Q. Previous work by Zhao et al [202] did not claim to be able to resolve length scales in the region $\gtrapprox 1000\mathring{A}$ for work on LOQ for dimensions greater than $1000\mathring{A}$, and any such apparent model output should be cautiously interpreted. However, for SANS2D, this range is likely to be extended. Parameters are included with the values fit, however those greater than $\approx 1000\mathring{A}$ on LOQ particularly may therefore be taken to be indicative of a very large length scale, approaching or exceeding the SANS size range, rather than the precise value generated by the model.

Errors estimated from the different plot types are typically included in data tables below, including for Guinier radius of gyration, Kratky-Porod radius of gyration and cross-sectional radius. Fitted uncertainties in parameters were not available for Debye-Bueche parameters or rod length estimates in Kratky-Porod plots, as these are indicative approximations, relying on visual estimates of a 'heel' in the curve, for instance, and were estimated principally to inform or attempt to validate more rigorous model fitting, such as that undertaken with FISH.

FISH Model Data Fits Several examples of the key static SANS data for complexes between the different types and molecular weights of polyethylenimine and DNA with fitting to models in the FISH program are shown in Figure 4.4.

As the other plot types are used largely as approximations to suggest likely structures and inform the choice of FISH model to be fit and give an approximate indication, where possible, of likely length scales, it was not thought necessary to include these approximate fits to the data for all samples, but fits for some key datasets are included in the sections which follow.

4.3.2 Kinetic Analysis

Time-resolved SANS involves slicing the neutron scattering intensity distribution into time segments to enable the study of dynamic evolution of the scattering pattern. When combined with a stopped-flow apparatus, set up to trigger counting synched with the end of mixing, the time resolution may be determined in absolute terms of the age of the

(a) 25 kDa BPEI 10:1 Complex in 10 mM NaCl with Kholodenko wormlike chain fit shown

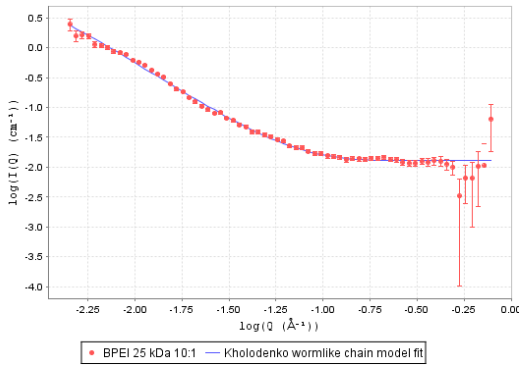

(b) 1.8 kDa BPEI 10:1 Complex in 10 mM NaCl with single cylindrical rod fit shown

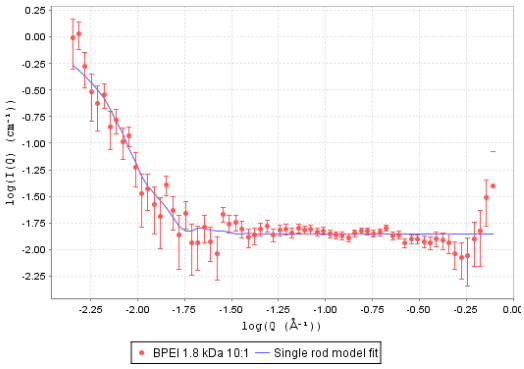

(c) 25 kDa LPEI 10:1 Complex in 10 mM NaCl with two cylindrical rods fit shown

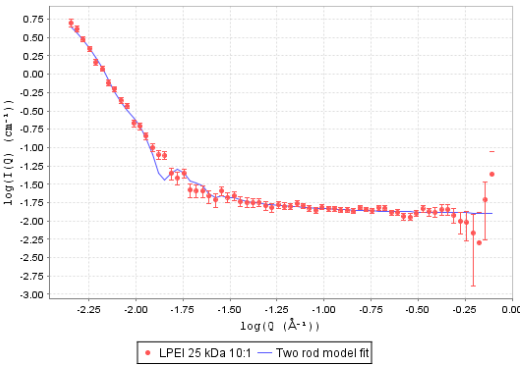

(d) 2.5 kDa LPEI 10:1 Complex in 10 mM NaCl with two cylindrical rod fits shown

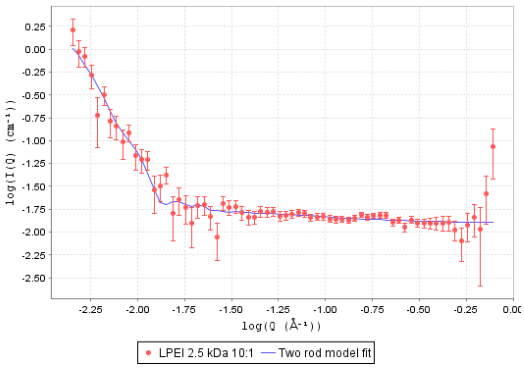

Figure 4.4: Examples of FISH Model fitting to static SANS data for 25 kDa and 1.8 kDa BPEI and 25 kDa and 2.5 kDa LPEI complexes with DNA at a N/P ratio of 10:1, pH 7.4 in 10 mM NaCl in D_2O with DNA concentration of 1.5 mg/ml; Captions indicate polymer type.

mixture. In this SANS2D kinetic study, time-slicing was carried out using a proprietary program written by R.K. Heenan, ISIS, in the Mantid Plot software package. Following slicing of the data, the scattering files were reduced using standard procedures, and the data analysed and fit as described above. Further to standard model-free and model-based data fitting, a series such as this of time-resolved data may, in the same way as a series of concentration data, be analysed using singular value decomposition (SVD) to separate the scattering intensity matrices for a series of concentrations or times, for kinetic work, into the principal form factor components, followed by model fitting using FISH to identify the number of main components and their changing proportions for different times or concentrations. However, it was not thought to have sufficient resolution in this application.

Complex Age and Time-Slicing

Plots are shown with times indicated at the midpoint of the slicing period,indicating the average age of the complexes after mixing, while legends describe the time range of the data presented, in seconds, following mixing, unless otherwise indicated.

Porod Analysis of Time-sliced Data

In a similar manner to static data, time-sliced data can be interpreted by plotting on a log-log plot. These are shown for the first and last time slice for each sample, with intervening time periods omitted from graphs for clarity.

Model Fitting

Time-sliced data were fit using form-factor models in FISH[71] to evaluate the model-based view of structural evolution with time. The parameters for various samples and their evolutions with time are also plot to enable visualisation of parameter trends with time.

Several example model fits are shown for static data in Figure 4.4. Generally, the signal to noise ratio is slightly worse for time-sliced data, due to the shorter data collection time, which may result in poorer fits on particularly short timescales. On the other hand, for complex structures which evolve significantly over the relevant time period, the signal for static datasets will be a product of this mixture, leading to different but potentially still significant impacts on resolution. In any case, trends and changes are the key points of interest in evaluating differences in the time evolution of the complexes, based on structural differences between the different polymer types and mixing conditions.

4.4 Results

A variety of analytical methods, described above, have been conducted on samples of a range of types of PEI complexes with DNA under varying conditions of charge ratio, solution, pH and concentration. The results with fit parameters, where applicable, are presented below and the key observations and differences discussed. The fitted functions for Porod plots are included for key datasets. It should be noted that in some cases the lines corresponding to the fitted equation are extrapolated beyond the precise region

fitted, where only a limited region of the data curve was fit. Guinier plots of data are given as insets without fitted background subtraction. Separate fits are shown for some key datasets on background-subtracted data, indicating the Guinier regimes used for the fitting.

Kratky-Porod analysis is relevant for particular datasets, such as notably 10:1 complexes of 25 kDa LPEI and DNA. However, the gradient is approximately zero in this instance, which does not allow the cross-sectional radius of gyration to be determined, but rather suggests negligibly thin rods - fits are not shown. The Q* is derived from analysis of the Porod plot, and estimated visually, hence is also not shown. A key example of a Debye-Bueche fit, particularly relevant for 10:1 complexes of 25 kDa LPEI and 1.8 kDa BPEI, being those complexes suited to the analysis of large, globular, phase-separated aggregates, is shown below. 25 kDa BPEI complexes, conversely, exhibited apparently greater stability or a chain-like structure, as will be discussed further in Section 4.4.1 below.

4.4.1 Static Data

Pure Polymers

Examining the pure polymer scattering in detail for high MW LPEI and BPEI, as shown in Figures 4.5 and 4.6 and detailed in Tables 4.1, 4.2 and 4.3, it can be seen that the BPEI scatters more strongly, showing a defined structure with Porod exponent indicative of a mass fractal structure of Gaussian chains, as might be expected from a branched polymer. A Kratky-Porod analysis of the BPEI rods, which are thought to represent the Kuhn length of a Gaussian chain, given in the table of 96 $\mathring{A}$, is approximately one third shorter than the length fitted to the LPEIs of similar width, which were in fact modelled by cylindrical rods. This is expected, firstly as the branched nature of the polymer for an equal molecular weight will naturally lead to a shorter end-to-end length, while the nature of a semi-flexible chain is that its characteristic rod-like length will be less than the total polymer length. Due presumably to the side-chains and flexible structure, the best-fitting model in FISH was found to be an ellipsoid, with a radius of gyration of 27 $\mathring{A}$ and an aspect ratio around 2.1. This may represent the structure of one persistence length of the polymer‘, rather than the complete molecule.

Pure BPEI showed a marked drop in intensity towards low Q, which, according to Putnam

et al[147], can indicate repulsion between particles, which is likely in this highly cationically charged system. The same is seen to a lesser extent with LPEI, which plateaus and falls slightly at low Q, although in this case, the slight fall in intensity at low Q cannot be unequivocally distinguished from error.

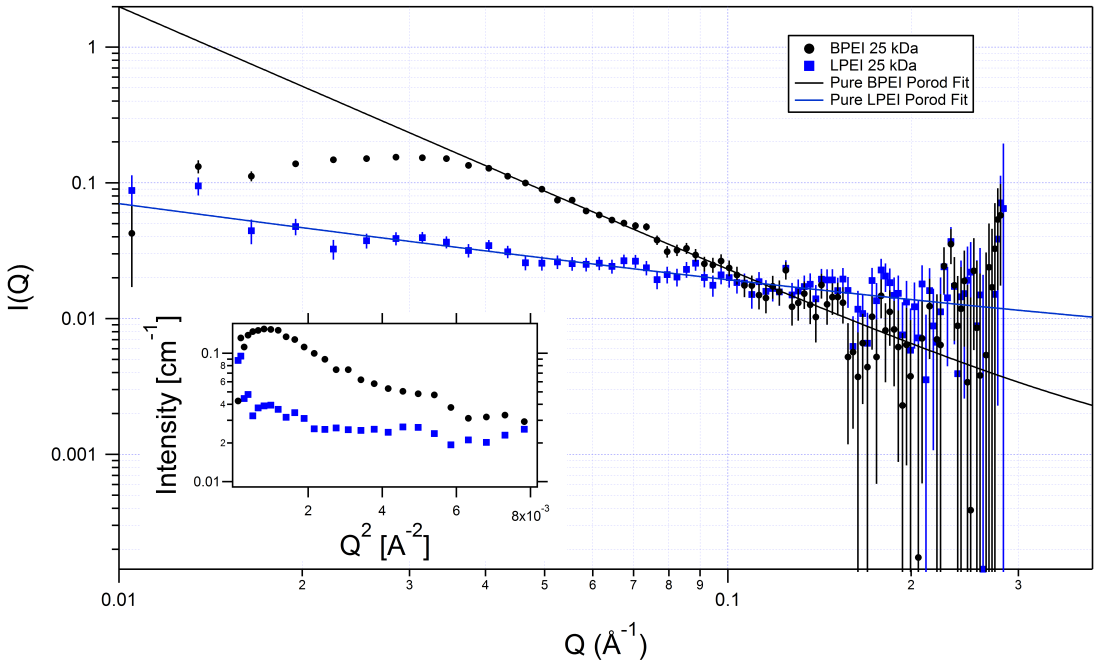

Figure 4.5: Porod plot of log(I) vs. log (Q) for pure 25 kDa linear and branched polymers at a concentration of 5 mg/ml conducted on LOQ; Inset shows Guinier plot of log(I) vs. Q^2 for the same samples; Legend indicates polymer type

Polymer Type	Porod Analysis				Guinier Analysis*		
	Low-Q Porod Exponent	Low-Q Model	High-Q Porod Exponent	High-Q Model	Estimated R_{g_1}: Lowest-Q (Upturn)	Estimated R_{g_2}: Low-Q	Estimated R_{g_3}: Intermediate-Q
BPEI 25kDa	n/a	No Large Aggregates	1.95± 0.12	Mass Fractal: Gaussian Chains	n/a	n/a	33.6± 0.6
LPEI 25kDa	n/a	No Large Aggregates	0.63± 0.17	Rod-like particles: Limited Fitting Range	n/a	14.9± 0.6	n/a

Table 4.1: Parameters from Porod and Guinier fits to SANS scattering data from pure 25 kDa branched and linear PEI at a concentration of 5 mg/ml ratio

Linear PEI of 25 kDa MW showed lower intensity scattering overall than the equivalent branched PEI, with the exception of an upturn towards the lowest Q values accessible

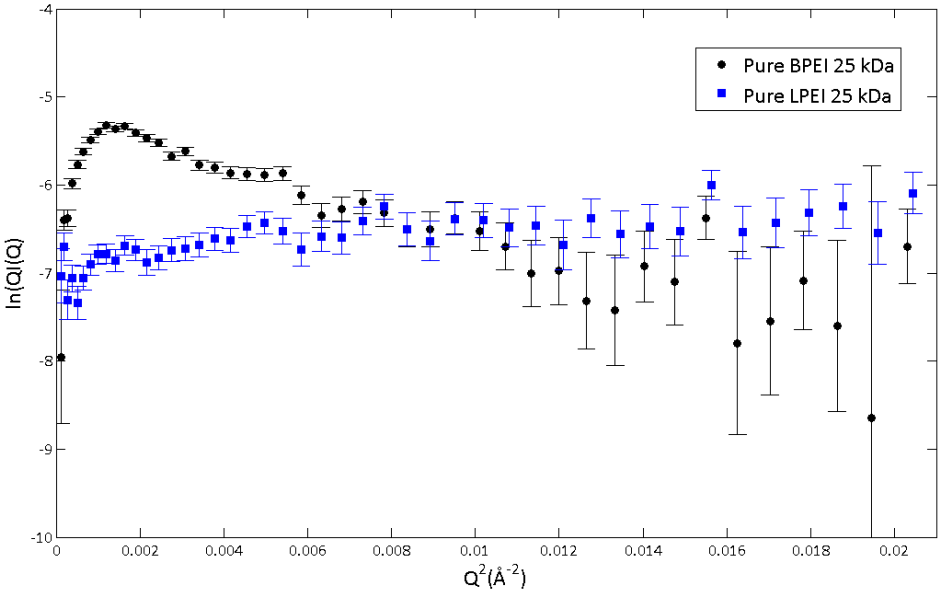

Figure 4.6: Kratky-Porod plot of log(QI) vs. Q^2 for pure 25 kDa BPEI and LPEI at a concentration of 5 mg/ml; Legend indicates polymer type

Polymer Type	Debye-Bueche Model			Kratky-Porod Model				
	Debye-Bueche Intercept	Debye-Bueche gradient	Debye-Bueche Characteristic Aggregate Size	Q* - Start of Linear K-P regime	Rod Length (Å)	Kratky-Porod Plot Gradient	Kratky-Porod Plot R_g (Å)	Kratky-Porod Cross-Sectional Radius (Å)
Pure BPEI 25k	n/a	n/a	n/a	0.04	96	Negative	14.7± 0.4	20.8±0.5
Pure LPEI 25k	n/a	n/a	n/a	n/a	n/a	Inverted	n/a	n/a

Table 4.2: Parameters from Kratky-Porod fits to SANS scattering data from pure 25 kDa branched and linear PEI at a concentration of 5 mg/ml ratio in D_2O

PEI Type	Porod-predicted Model	FISH Model	Cylinder 1			Cylinder 2			Ellipsoid		
			$Scale_1$	$Radius_1$ (Å)	$Length_1$ (Å)	$Scale_2$	$Radius_2$ (Å)	$Length_2$ (Å)	$Scale_E$	R_E (Å)	X
BPEI 25 kDa	Gaussian chain	Ellipsoid	—	—	—	—	—	—	0.175	27.3	2.13
LPEI 25 kDa	Rods	Cylinders	9.48 E-07	9.63	164	—	—	—	—	—	—

Table 4.3: Parameters from model fitting to SANS scattering data from pure branched and linear PEIs at a concentration of 5 mg/ml; Fitting was carried out with FISH[71]

with LOQ, and a study with SANS2D could thus have provided greater information on the structure. A Porod analysis indicated rod-like particles, with an exponent of 0.6 taken to be approximately 1. Although the fitting range for Guinier analysis was limited, due to the larger size of the polymers, the cylindrical-rod model in FISH provided a good fit to the data with a rod of length approximately 164 $\AA$ and 9.6 $\AA$ width. As the calculated theoretical length for a linear PEI molecule is around 2600 $\AA$ and Kakuda et al[88] find LPEI to adopt a zig-zag conformation in water at room temperature, this rod length is likely to represent the Kuhn segment length of this extended chain, equal to twice the persistence length of the polymers, with the overall linear molecule not visible as a single linear rod in its free, expanded state. For the large BPEI, again, the fitted ellipsoid size is likely to represent a distinct portion of the overall polymer chain, while the very lowest Q value looks to be turning upward again, ossibly suggesting a larger structure out of range of LOQ.

As discussed further in the following sections, the size fit to pure linear polymers corresponds well to the intermediate-Q structures observed for some high MW LPEI complexes.

PEI Type

Complexes of four types of PEI with a sample of double-stranded DNA fragments were studied, as shown in Figure 4.7. The Porod and Guinier curves of the data are shown in Figure 4.7 and the Debye-Bueche and Kratky-Porod plots, where applicable, are shown in Figure 4.9, while the resulting parameters are reported in Tables 4.4 and 4.5, respectively. It can be seen that the smaller PEI, whether linear or branched, formed complexes which scattered relatively weakly with relatively little scattering detail at high and, to some degree, intermediate Q, and a strong, steep upturn at low Q, suggesting the presence of very large particles or aggregates. By contrast, the large branched and linear PEI samples, which were approximately a factor of 10 larger in molecular weight gave stronger scattering and more structure at high Q, particularly in the case of large BPEI complexes. The Guinier plots inset in the same figure demonstrate this effect more emphatically, with the small PEI complexes, both linear and branched, exhibiting a relatively shallow gradient, indicating either very small particles or, more likely, lack of detectable structure, and then a strongly curved, steep upturn, with the upturn present in the large LPEI and, particular, BPEI complexes being much more restricted in its Q range, and the subsequent

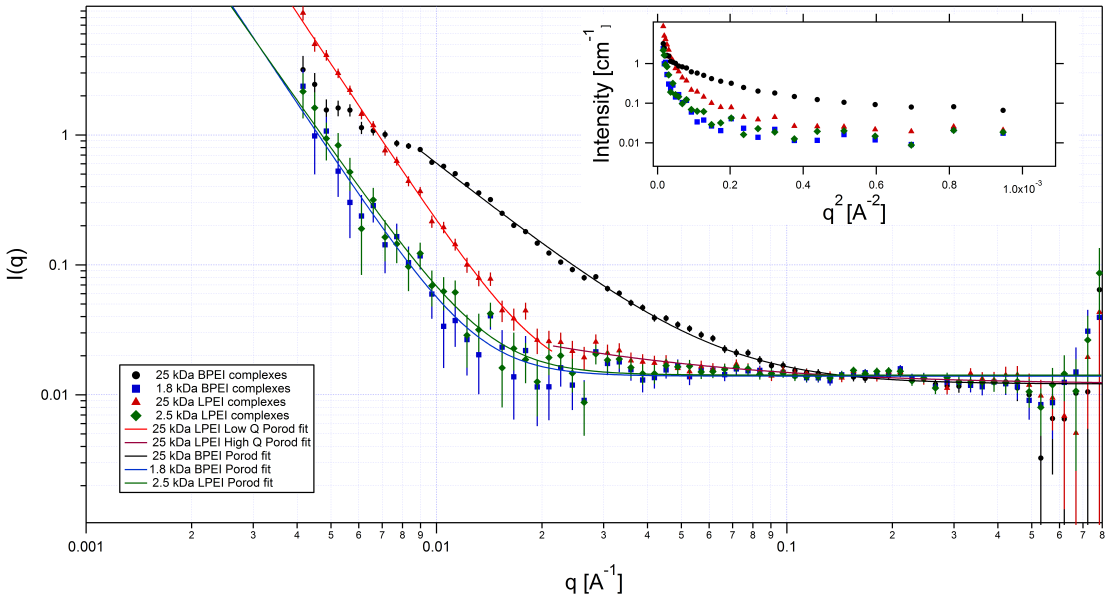

Figure 4.7: Porod plot of log(I) vs. log (Q) for large and small, branched and linear PEI complexes with DNA fragments at pH 7.4 at a charge ratio of N\P = 10:1 in 10mM NaCl in D_2O; Inset shows Guinier plot of log(I) vs. Q^2 for the same samples; Legend indicates PEI type (branched or linear) and size (kDa)

Polymer Type	Porod Analysis				Guinier Analysis*		
	Low-Q Porod Exponent	Low-Q model	High-Q Porod Exponent	High-Q Model	Estimated $R_{g_1}(\AA)$: Lowest-Q (Upturn)	Estimated $R_{g_2}(\AA)$: Low-Q	Estimated $R_{g_3}(\AA)$: Intermediate-Q
25 kDa BPEI	n/a	n/a	2.13 ± 0.02	Mass Fractal: Gaussian chains	308 ± 30	144 ± 2	n/a
1.8 kDa BPEI	4.1± 0.3	Debye-Bueche: Large, smooth aggregates	0	No high Q features	601 ± 64	288 ± 25	n/a
25 kDa LPEI	4.1 ±0.1	Debye-Bueche: Large, smooth aggregates	0.92 ± 0.11	Rod-like	445 ±11	251 ± 6	n/a
2.5 kDa LPEI	3.84±0.24	Debye-Bueche: Large, smooth aggregates	0	No high Q features	560 ± 65	209 ± 13	n/a

Table 4.4: Parameters from Porod and Guinier fits to SANS scattering data from complexes of large and small, linear and branched PEI with DNA fragments in 10mM NaCl in D_2O at pH 7.4

(a) Lowest Q Guinier regime - Guinier fit of 25 kDa LPEI 10:1 Complex in 10 mM NaCl

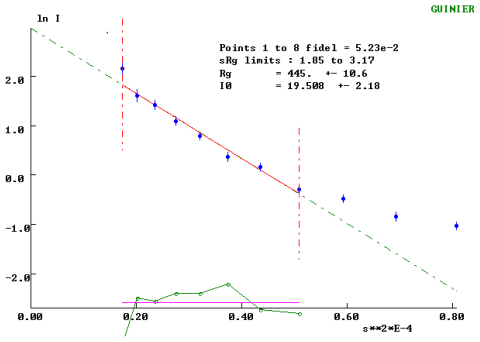

(b) Low / intermediate Q Guinier regime - Guinier fit of 25 kDa LPEI 10:1 Complex in 10 mM NaCl

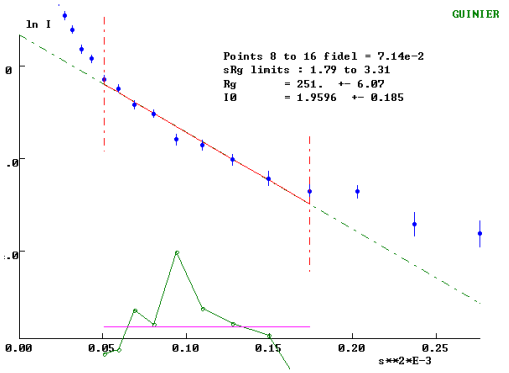

(c) Lowest Q Guinier regime - Guinier fit of 25 kDa BPEI 10:1 Complex in 10 mM NaCl

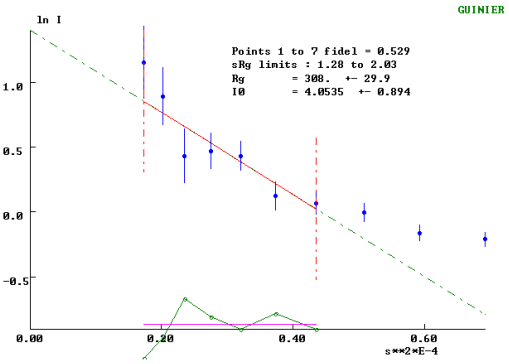

(d) Low / Intermediate Q Guinier regime - Guinier fit of 25 kDa BPEI 10:1 Complex in 10 mM NaCl

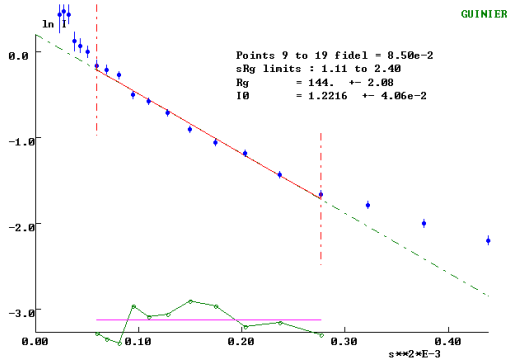

Figure 4.8: Guinier fits to background-subtracted SANS data for the samples presented in Figure 4.7 at low and intermediate q guinier regimes, where the notation 's' is used to indicate 'q' in these figures. The green lines are residuals to the fit. Fitting was carried out in the IGOR programme; Continued below.

Polymer Type	Debye-Bueche Model			Kratky-Porod Model				
	Debye-Bueche Intercept	D-B gradient	Resulting characteristic D-B aggregate size (Å)	Q* - start of linear K-P regime	Rod length (Å)	Kratky-Porod Plot Gradient	Kratky-Porod Plot R_g (Å)	Kratky-Porod Cross-Sectional Radius (Å)
25 kDa BPEI	n/a	n/a	n/a	n/a	n/a	n/a	n/a	n/a
1.8 kDa BPEI	0.0326	4.80E+04	1214.4	n/a	n/a	n/a	n/a	n/a
25 kDa LPEI	0.05	2.08E+04	645.60	0.0219	177.7	0 within error	negligible	negligible
2.5 kDa LPEI	0.0566	4.45E+04	887.25	n/a	n/a	n/a	n/a	n/a

Table 4.5: Parameters from Kratky-Porod and Debye-Bueche fits to SANS scattering data from complexes of large and small, branched and linear PEI with DNA fragments in 10mM NaCl in D_2O at pH 7.4

(e) Lowest Q Guinier regime - Guinier fit of 2.5 kDa LPEI 10:1 Complex in 10 mM NaCl

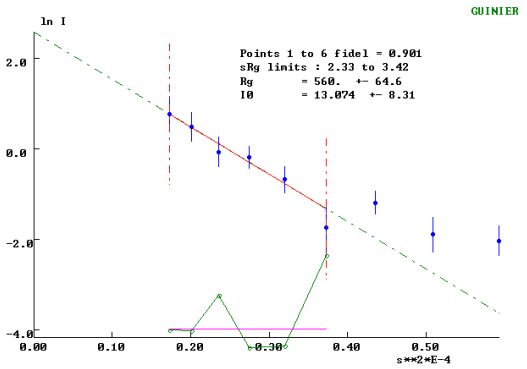

(f) Low / Intermediate Q Guinier regime - Guinier fit of 2.5 kDa LPEI 10:1 Complex in 10 mM NaCl

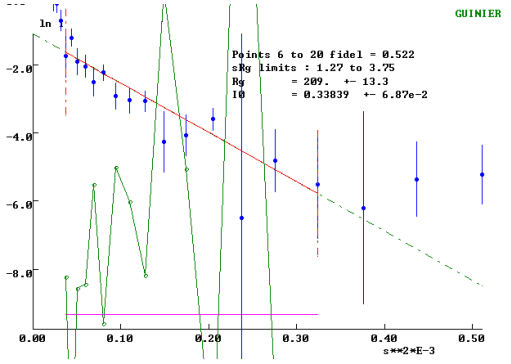

(g) Lowest Q Guinier regime - Guinier fit of 1.8 kDa BPEI 10:1 Complex in 10 mM NaCl

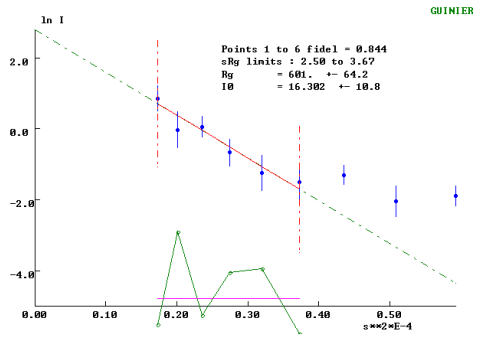

(h) Low / Intermediate Q Guinier regime - Guinier fit of 1.8 kDa BPEI 10:1 Complex in 10 mM NaCl

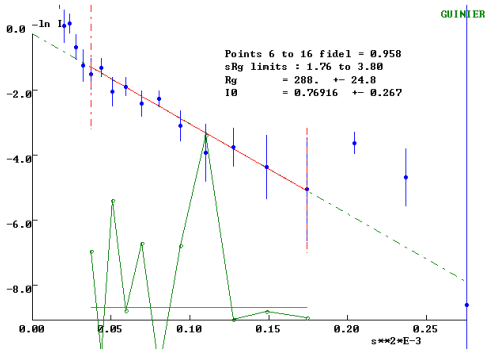

Figure 4.8: Continued: Guinier fits to background-subtracted SANS data for the samples presented in Figure 4.7 at low and intermediate q guinier regimes, where the notation 's' is used to indicate 'q' in these figures. The green lines are residuals to the fit. Fitting was carried out in the IGOR programme;

Q regime also displaying a gradient indicative of a measurable, more stable component particle, distinct from the aggregate, which is in any case less prominent than for small PEIs. The fitted gradients for the different sections of the Guinier regime for the lowest Q upturn and subsequent, flatter region, for all four polymer types suggested similarly that the size of small BPEI and LPEI complexes formed the largest aggregates, followed by high MW LPEI complexes and, lastly, the high MW BPEI complexes. Interestingly, the Guinier fits to the linear section at higher Q than the lowest upturn are similar for both high and low LPEI molecular weight complexes and low MW BPEI complexes, with high MW BPEI smaller again.

This suggests initially that the complexes formed with small PEI, regardless of their molecular weight, were inherently less stable as small, separate particles, but rather aggregated in solution. This could reasonably be expected as aggregation of PEI-nucleic

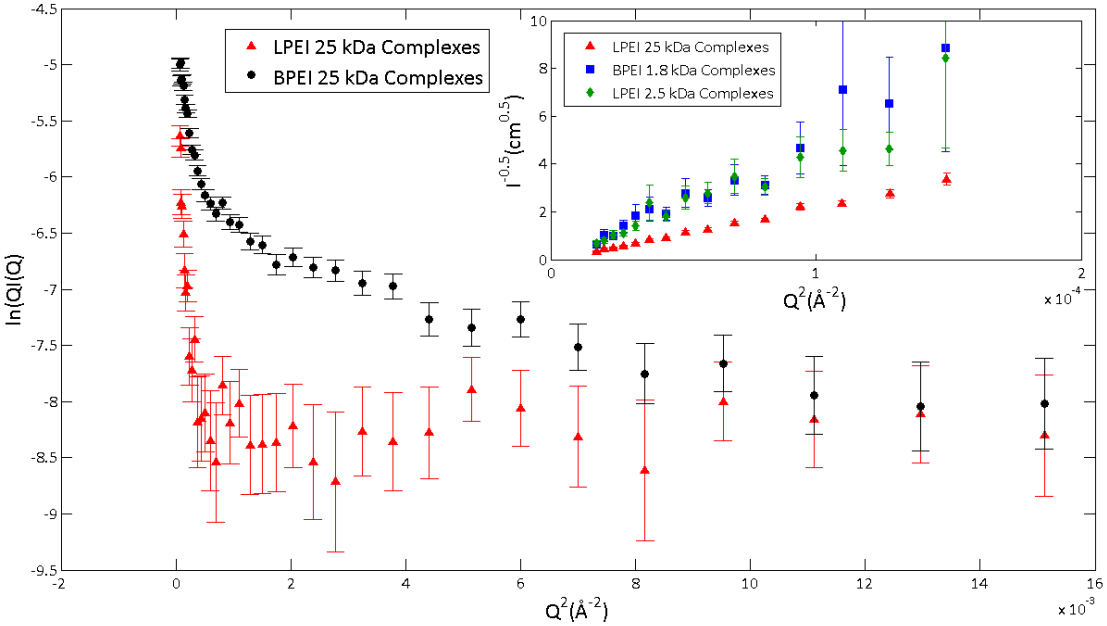

Figure 4.9: Kratky-Porod plot of log(QI) vs. Q^2 for large and small, branched and linear PEI with DNA fragments at pH 7.4 at a charge ratio of N\P = 10:1 in 10mM NaCl in D_2O; Inset shows Debye-Bueche plot of $I^{-\frac{1}{2}}$ vs. Q^2 for the same samples; Legend indicates polymer type (branched or linear) and size (kDa)

acid complexes is thought to be at least partially hydrophobically driven, with a repulsive electrostatic effect due to like charge of the complexes. However, a large polymer molecule may be more likely to be incompletely charged with DNA for a given charge ratio, and hence it would be expected that large polymers may tend to produce more stable, mid-sized aggregates, while small particles would collapse.

Mady et al[119] study PEI/DNA complex aggregation at 150 mM NaCl by turbidity and their findings that the larger PEI (25 kDa) showed the slowest aggregation, with complex turbidity increasing as the molecular weight decreased. They describe differences in the pKa of branched PEI of different sizes determined by potentiometric titration with HCl, decreasing from around 8.6 for 2 kDa PEI to 7.1 for 25 kDa PEI, although they do not relate this explicitly to the differences in coagulation.

Additionally, we can infer that the linear PEI, even when of a high molecular weight, is also relatively unstable against aggregation, with little scattering at high Q, corresponding to smaller particle sizes or length scales, in comparison to complexes formed with large BPEI, which show an upturn at low Q, followed by an extended peak tail to higher Q values. This may indicate that the stability of BPEI is superior to LPEI. As it has been shown that high

positive charge contributes to stronger transfection [122], it is likely that, in a situation where an excess of cationic polymer charges are available, a greater number of sterically inaccessible positive charges on a polymer binding to DNA, which are free to contribute to the net positive charge of the complex, will contribute to increased transfection efficiency, but also very likely to the stability of the complex in solution, where the polymer is purely cationic, as is the case with PEI, unlike the diblock copolymers studied in chapters 5 and 6, which contain a hydrophilic, zwitterionic block in addition to a cationic block as a means of hydrophilic stabilisation in solution. Hence, it is reasonable that complexes formed with large, BPEI, have a greater available positive charge per complex than linear PEI, which may account for their apparent greater stability.

The observation that even large LPEI appears to aggregate to a greater degree than large BPEI may reinforce the idea that LPEI is a stronger transfection agent than large BPEI[137] in certin circumstances following the theory that strong aggregation to form large complexes enhances cellular association and avoids the clathrin-dependent uptake mechanism, which has been shown to result in low biological efficacy of transfected nucleic acids, thus increasing the chance of successful uptake. The question of this apparently greater stability will be studied further with the analysis of the time-sliced scattering data.

As the large (25kDa) BPEI samples gave the strongest scattering and allowed observation of scattering structures on the broadest range of length scales (shows structural features over a wider Q-range), as well as being among the most relevant forms for effective transfection, as described in Section 4.1.6 this sample was selected for further studies into the effects of charge ratio, solution type, pH and concentration, with comparison to the large LPEI complexes, which also showed stronger scattering than either of the complexes resulting from small PEIs and isknown to be a strong transfection agent, which it is concluded had a higher incidence of precipitation beyond the accessible size range of SANS, resulting in relatively weak scattering intensity.

Two main characteristic forms were found for large linear and branched PEI complexes at a charge ratio of 10:1.

High MW, linear PEI shows a low Q^{-4} gradient Porod region, which indicates the particles can be analysed with a Debye-Bueche model for a two-phase random system. The high Q Porod gradient of approximately -1 means the data can be interpreted in terms of aggregates of cylindrical rods, which can be analysed using the Kratky-Porod plot.

The question arises of whether indeed these rod-like structures are free component com-

plexes or separate polymers, or segments within a large aggregated chain, indicative of persistence length. It can be seen from the porod slope at lower Q, corresponding to larger size, that the overall shape of the aggregate appears predominantly globular, however we cannot say for sure to what extent the bound, aggregated segments are contributing or free polymer segments - it is likely that they are virtually indistinguishable in this technique, and predominantly changes in the degree of aggregation may be observed by changes in the large aggregate size. It is likely that the form factors of minimally complexed and completely unbound polymers are very similar when a low degree of DNA binding to the free polymers occurs, and the resulting high net charge is responsible for their non- or slow aggregation.

The characteristic size of the aggregates themselves resulting from a Debye-Bueche plot indicates a length of approximately 646 $\mathring{A}$. However, as described above, there is considerable uncertainty in this characterisation, given that the intercept value is so close to zero and the use of errors in fitting or the selection of values to include in the linear fitting range can have a significant impact on the result, determining whether it is negative or positive and therefore whether it could produce a physically meaningful size.

The fits of pure data points, without using an error component, are presented and give the indicative, potential sizes which are quoted in the tables in this work. However, it should be noted that the inclusion of errors in the fit, or indeed the selection of a different range of points, lead at least some of these to become negative, meaning it is not possible to derive a physical parameter with certainty for characteristic aggregate size.

However, a comparison of the gradient of the sample curves, as shown above, is also informative, as it is suggestive of a more compact aggregate (more positive intercept) for the high molecular weight PEI than for either of the lower molecular weight PEI complexes. As discussed above, therefore, while the Debye-Bueche model may contribute to the picture supporting this analysis, it is insufficient on its own to draw conclusions. Both possible fits using errors and without are given as an indication of the sensitivity of this approach to slight variations in conditions in Figure 4.10. The values for Debye-Bueche, where given, should therefore be taken only as possible indications of the relative sizes of different particles.

The high MW, branched PEI, in contrast, lacks this -4 Porod gradient at low Q, suggesting it either does not form these large aggregates. However, the Porod gradient at intermediate to low Q of approximately -2 indicates a structure of Gaussian chains, less compact and

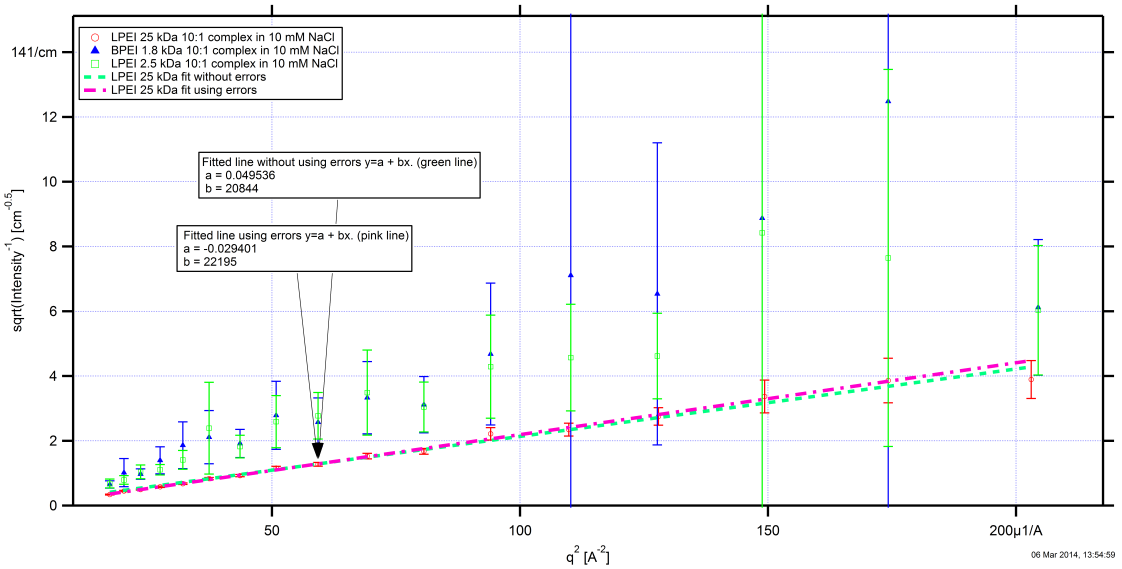

Figure 4.10: Example fitting of Debye-Bueche plot for 25 kDa LPEI complexes with DNA in 10 mM NaCl in D_2O. Fits with and without the use of errors, conducted in IgorPro, are shown with fit parameters given in the legend. Low molecular weight PEI complexes, which appear to be more prone to aggregation than those of high molecular weight LPEI, are shown for comparison.

with apparently greater colloidal stability than LPEI complexes.

Geometrical Shapes of different PEI types from Porod and Model-based fitting

The complexes formed with high molecular weight BPEI were therefore the only ones to show a chain or network like structure, with significant observable structure at smaller length-scales, indicating Gaussian-like chains. Low molecular weight (MW) PEIs of both linear and branched type and high MW LPEI complexes all formed aggregates, although the Porod exponents fit to the SANS data suggested the presence of rod-like components at intermediate Q. Despite the limitations of this method due to proximity of intercepts to zero, making accurate determination difficult in some cases, the Debye-Bueche aggregate models suggest larger aggregates for small PEIs of both types than for large LPEI (See Table 4.5, while this model was not appropriate for the chain-like conformation of high MW BPEI complexes. Generally, the Debye-Bueche intercept was very close to zero, and in some cases was found to be negative, and was in some instances sensitive to the choice of included points in the linear range. Where this is the case, there is a great deal of uncertainty in the resulting correlation lengths and these are indicated in the results table. However, the proximity of all intercepts to zero means the characteristic sizes are approximate, estimated values, as discussed above.

LPEI shows negligibly thin component rods, as indicated by the level gradient of the Kratky-Porod plot,which is again broadly consistent with the FISH model fitting. Additionally, low MW LPEI complexes could be fit by a similar combination of negligibly thin component rods, which appeared to be, however, at least an order of magnitude shorter than for large LPEI (this cannot be specified with greater precision due to the limits of the available Q range on size range accessible), while both types of polymer showed a significant component of large aggregates, which, based on the aspect ratio of the fitted cylinder in the model, could equally be described as elongated but globular, ellipsoidal, as it is cylindrical.

FISH Model Fitting FISH model types and fit parameters for high and low MW branched and linear PEI complexes at a charge ratio of 10:1 with DNA fragments at pH 7.4 are shown in Table 4.6. Parameters are included exactly as the fitting produced, however it should be considered, as discussed previously, that large sizes have high uncertainty, particularly above 700-1000 Angstroms, due to the size resolution limits of the technique.

As expected from the Porod plots, large aggregates, modelled as cylinders, are present for large and small LPEI and small BPEI. In the case of low MW BPEI, however, only one cylinder is needed for a good fit to the data, as confirmed by the Porod plot, which did not show a Porod gradient at high Q to indicate any detectable structure on smaller scales. High MW BPEI complexes could be well fit by a Kholodenko worm-like chain model, consistent with the expected Gaussian chain indicated by the Porod exponent.

The uncertainty in parameters is significantly higher for some components of the low molecular weight LPEI complexes, which can be seen from the FISH fitted data and is indicated by the relatively high noise level of the complex scattering, and lack of observable structure at higher Q, particularly for the rod-like component of the two-rod model, where one is more globular, representing the larger scale aggregate, the other, short rod component, likely representing short, rod-like components of a larger aggregate, has very high uncertainty in its fitted dimensional parameters. This is to be expected, given the lack of structure at high Q, and although a two-rod model fit well, it could be that a single-rod model, as was used for low molecular weight BPEI complexes, which show a similar scattering profile, would be well suited to this system.

PEI Type	Porod-predicted Model	FISH Model	Cylinder 1			Cylinder 2			Kholodenko Worm-like Chain			
			$Scale_1$	$Radius_1$ (Å)	$Length_1$ (Å)	$Scale_2$	$Radius_2$ (Å)	$Length_2$ (Å)	$Scale_K$	n	L (Å)	R_ax (Å)
BPEI 25 kDa	Gaussian chains	Kholodenko Chain	—	—	—	—	—	—	1.36E-07 ± 6E-12	2308.6 ± 2.7	28.2 ± 1.4E-3	12.5 ± 2.7E-4
BPEI 1.8 kDa	Large Aggregates - Component Structure Not Detected	Cylinders	5.38E-09 ± 5.5E-11	400 ± 4	364 ± 4	—	—	—	—	—	—	—
LPEI 25 kDa	Aggregated Rods	Cylinders	1.98E-06 ± 2E-7	3.19 ± 0.16	2153 ± 1135	3.11E-08 ± 7E-10	527 ± 8	482 ± 9	—	—	—	—
LPEI 2.5 kDa	Large Aggregates - Component Structure Not Detected	Cylinders	7.47E-07 ± 6.5E-7	5.4 ± 3	54 ± 32	7.57E-09 ± 7.2E-10	549 ± 36	450 ± 36	—	—	—	—

Table 4.6: Parameters from model fitting to SANS scattering data from complexes of large and small, branched and linear PEI with DNA fragments in 10mM NaCl in D_2O at pH 7.4; Fitting was carried out with FISH[71]

Charge Ratio and Pure Polymers

The scattering from complexes formed at different charge ratios was compared for high MW branched and linear PEI in 10 mM NaCl complexes in two ways: On SANS2D, High MW BPEI and LPEI complexes at charge ratios of 10:1 and 20:1 were studied, while on LOQ, high MW BPEI complexes were investigated at charge ratios of 20:1, 10:1, 5:1 and 2:1, shown in Figures 4.11b and 4.11a, respectively.

SANS2D - High MW BPEI and LPEI complexes at 10:1 and 20:1

It can clearly be seen that increasing the charge ratio from 10:1 to 20:1 with the large LPEI complexes increases the logarithmically transformed scattered intensity uniformly over almost the entire measured Q range. The scattering from pure polymer, shown in Figure 4.5, shows a slightly raised peak around Q = 0.03-0.04 $\AA^{-1}$, which can also be seen in the complexes' scattering. However, the most significant feature remains the strong -4 gradient observed at low Q scattering.

The fact that doubling the charge ratio (ie. doubling the polymer concentration while keeping the DNA concentration constant) increases the scattering so smoothly across the log plot, indicating an overall increase, which is greater at lower Q values due to the weighted logarithmic appearance, suggests that the size or number of scattering bodies is increased, but not necessarily that any significant structural features have changed as a result. It is also interesting to note that there appears not to be a particularly strong

(a) Porod plot of log(I) vs. log (Q) for complexes of 25 kDa branched PEI with DNA fragments at pH 7.4 at charge ratios between N\P = 20:1 and 2:1 in 10mM NaCl in D_2O conducted on LOQ; Inset shows Guinier plot of log(I) vs. Q^2 for the same samples; Legend indicates charge ratio

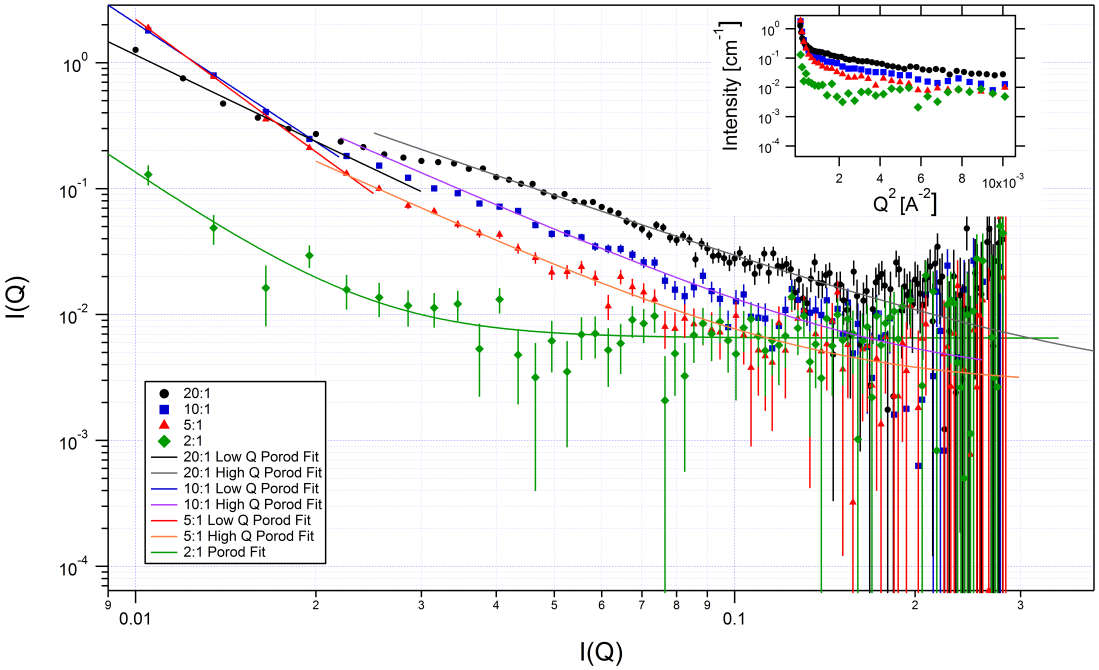

(b) Porod plot of log(I) vs. log (Q) for complexes of 25 kDa linear and branched PEI with DNA fragments at pH 7.4 at charge ratios of N\P = 20:1 and 10:1 in 10mM NaCl in D_2O conducted on SANS2D; Inset shows Guinier plot of log(I) vs. Q^2 for the same samples; Legend indicates charge ratio and PEI type

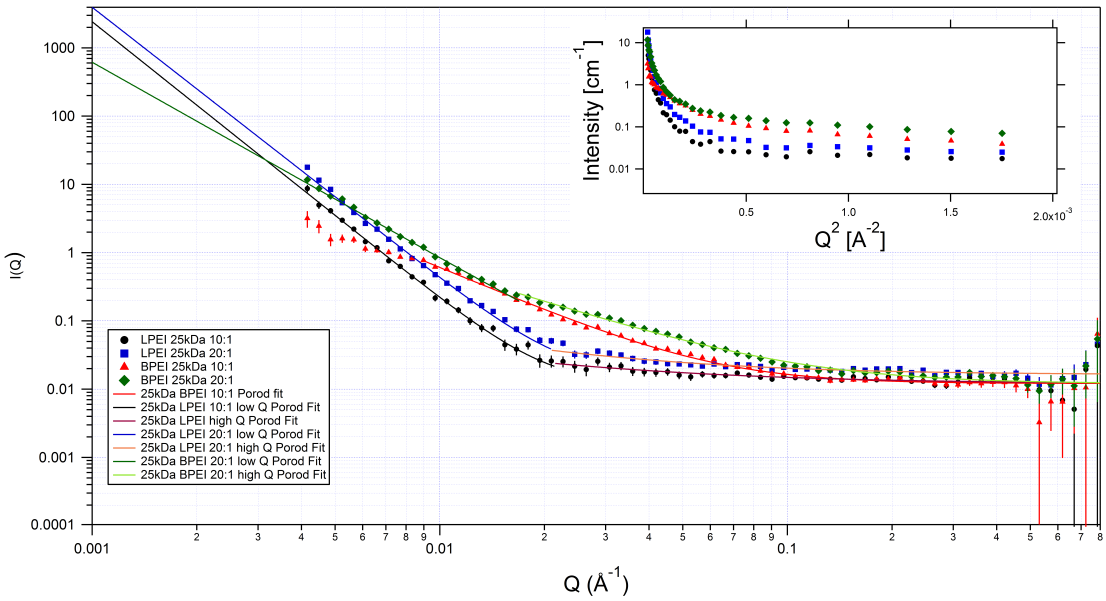

Figure 4.11: Porod plots of log(I) vs. log (Q) for complexes of high MW, 25 kDa, linear and branched PEI with DNA fragments at pH 7.4 at charge ratios of N\P = 20:1 and 10:1 in 10mM NaCl in D_2O; Insets shows Guinier plot of log(I) vs. Q^2 for the same samples; Legend indicates charge ratio and PEI type (branched or linear)

increase in scattering corresponding to scattering from free polymer in the mid-Q range, although this is itself only weak, with a slight peak at low Q values, which may not be noticeable on top of the already strong low-Q complex scattering. This uniformity of the intensity increase with doubling of charge ratio could suggest the excess scattering may largely be due to the increase in free polymer contributions. The Porod exponent profile of 25 kDa LPEI complexes does not change considerably, implying the overall composition of complexes as large, aggregated rods is unchanged, although they may be tighter or looser. However, the Guinier plot for 10:1 complexes has steeper gradients in the region surrounding and including the low Q upturn, and although this effect is somewhat masked in the deduced radii of gyration, as the curvature of this low Q region required fitting of shorter linear segments, the steepness of the gradient broadly indicates slightly larger aggregates overall for N/P = 10:1 than 20:1. The Porod plot appears to fit with this interpretation, with a shallower Debye-Bueche gradient obtained for particles at 20:1 than 10:1, although the translation of this plot into actual aggregate size is limited by the fact that the 20:1 intercept is very close to zero, and in fact slightly negative, as the gradient is very sensitive to small deviations in fitting points, meaning the gradient fit should be interpreted with caution. However, the intercept of both 20:1 and 10:1 LPEI aggregates is approximately zero, and, insofar as the features of this gradient alone can contribute to the overall picture, they appear to point to the fact that 10:1 aggregates are slightly larger than those at 20:1, which could be expexted due to the lower positive charge available, which may lead to lower overall compaction of DNA, due to reduced strength of binding, mediated by counterions and small nucleic acids, , and the diminished tendency towards aggregation of complexes formed at N/P = 20:1, due to higher positive charge of complexes[137]. This size trend, of decreasing size with increasing charge ratio is additionally consistent with the condensation effect of charge neutralisation and condensation.

A Kratky-Porod analysis at intermediate Q shows very little difference in the dimensions of the component rods which are thought to make up the aggregates and these rods are, with a length of approximately $170\mathring{A}$, as determined from the heel Q between the two Porod exponent regions, very similar to the free, large linear PEI molecules as fit to a cylindrical model using FISH, which gave a length of $164\mathring{A}$ and a small fitted radius of $9.6\mathring{A}$, consistent with the neglible Kratky-Porod gradient, which led to the conclusion of very thin rods. FISH fitting was followed to get a different, model-based interpretation, but informed very much by the model-free analyses and, in fact, FISH models fit very well

to both 10:1 and 20:1 LPEI data with only a change in the scale factors, but otherwise identical dimensions. When allowed to float freely, the dimensional parameters did adjust slightly, but they were largely very similar.

The change in scale factors indicates an increased number density of smaller, component rod-like particles in 20:1 high MW LPEI complexes with a slight increase in scale factor and size of the larger aggregates compared to 10:1, albeit by a relatively small amount, which potentially conflicts with the earlier suggestion that 20:1 aggregates may be smaller than 10:1 In practice, therefore, a significant difference in size could not be identified with certainty from both methods.

The large, branched PEI complexes, on the other hand, have a different underlying scattering form, and do show a peak in a similar regime to that of the pure polymer solution. When the charge ratio is doubled here from 10:1 to 20:1, an increase in intensity is not observed across the Q spectrum, but rather concentrated in pronounced increases in the mid- to high-Q range, particularly in the region where the pure polymer's scattering peak was found to be, and at very low Q, indicating an increased number of the largest measurable aggregates, although it is possible that the increase in polymer excess led to a reduction in size of the largest aggregates from unmeasurable to just measurable on this scale, rather than an increase in the largest overall particles. However, between these two regions, there is an area where no relative increase in intensity is observed.

A Debye-Bueche aggregate size to high MW BPEI complexes at N/P = 10:1 did not easily fit an aggregate size to the data as intercept is $\approx$0. The appearance of the start of another upturn at very low Q could suggest the aggregate size is very large, and the slight peak at higher Q could actually correspond to the component size rather than the aggregate size. Complexes formed at N/P = 20:1, on the other hand, appear to have a smooth porod exponent of $\approx$ 3, with another peak at higher q, in a similar Q-range to free polymer, although this does not necessarily indicate that the excess polymer is completely free, as it could also be minimally bound to DNA.

Comparing the LPEI complexes at the two charge ratios, in the presence of additional excess polymer at the higher charge ratio, the form factor indicated by the Porod exponent in the mid-Q region is shifted more towards a loose or Gaussian chain from a rod, which is unlikely to be attributable to free polymer, while at the lower charge ratio, the appearance was more like a rod. Again, at lower charge ratio, the scattering bodies are expected to be less positively charged overall, and therefore expected to be more compact. It therefore

seems likely that the greater excess of polymer at the higher charge ratio contributes to greater repulsion leading to smaller, looser aggregates, as observed in the low Q regime.

Charge Ratio	Porod Analysis				Guinier Analysis*		
	Low-Q Porod Exponent	Low-Q Model	High-Q Porod Exponent	High-Q Model	Estimated R_{g_1} (Å): Lowest-Q (Upturn)	Estimated R_{g_2} (Å): Low-Q	Estimated R_{g_3} (Å): Intermediate-Q
20:1	2.30± 0.06	Mass Fractal: Gaussian chain to dense network	1.7± 0.1	Swollen Chains	n/a	31.7± 0.43	n/a
10:1	3.15± 0.04	Dense network although uncertainty due to limited range for fitting	2.0± 0.2	Gaussian Chain	n/a	34.5± 0.5	n/a
5:1	3.52± 0.04	Aggregate with slightly rough surface, or dense mass fractal network	2.2± 0.1	Gaussian Chain	n/a	43.9± 1.5	26.2± 2.1
2:1	n/a	n/a	3.3± 0.4	Dense Network	n/a	95.7± 11.8	n/a

Table 4.7: Parameters from Porod and Guinier fits to SANS scattering data from complexes of 25 kDa BPEI with DNA fragments at charge ratios from 20:1 to 2:1 in 10mM NaCl in D_2O at pH 7.4 collected on LOQ

Polymer Type	Charge Ratio	Porod Analysis				Guinier Analysis*		
		Low-Q Porod Exponent	Low-Q Model	High-Q Porod Exponent	High-Q Model	Estimated R_{g_1} (Å): Lowest-Q (Upturn)	Estimated R_{g_2} (Å): Low-Q	Estimated R_{g_3} (Å): Intermediate-Q
BPEI 25kDa	20:01	2.9± 0.03	Mass fractal: Dense network	1.6± 0.03	Swollen Chains	393± 11	222± 3	50± 1
BPEI 25kDa	10:01	n/a	n/a	2.1	Mass Fractal: Gaussian Chains	308± 30	144± 2	n/a
LPEI 25kDa	20:01	3.97± 0.04	Debye-Bueche: Large, smooth aggregates	1.1±0.2	Rod-like	522± 11	308± 5	159± 4
LPEI 25kDa	10:01	4.06±0.08	Debye-Bueche: Large, smooth aggregates	0.9± 0.1	Rod-like	445± 11	251± 6	n/a

Table 4.8: Parameters from Porod and Guinier fits to SANS scattering data from complexes of 25 kDa LPEI and BPEI with DNA fragments at charge ratios of 20:1 and 10:1 in 10mM NaCl in D_2O at pH 7.4 collected on SANS2D

LOQ Charge Ratio

Although the Q-range observable with LOQ data is limited at low Q to a higher cutoff value, it can be seen that the low-Q upturn corresponding to aggregates appears to start

at a lower threshold Q value, Q*, as charge ratio decreases (See Figure 4.11a), indicating the corresponding constituent particles of the aggregates are longer, as may be expected due to the reduction in electrostatic repulsion, leading to larger aggregate particles.

Additionally, it is only the lowest charge ratios (2:1 and 5:1) which show evidence of the -4 Porod gradient at low Q, corresponding to smooth aggregates, while higher charge ratios have a gradient at low Q closer to 3, which indicates a tangled network of chains, for mass fractals, or equivalently can be interpreted as a rough surface on the aggregates, and a higher Q Porod exponent between 1 and 2, indicating the constituent parts are chains with a conformation between rod-like and gaussian. The 20:1 charge ratio exhibits a flattening at very low Q, which indicates a reduction in large aggregate formation, as expected due to the predicted increase in electrostatic repulsion caused by the presence of excess cationic polymer and associated predicted increased net surface charge of the complexes.

At very low charge ratios of 2:1, thought to be around the point of complex neutrality, for reasons described in Section 4.1.4, the scattering is very much weaker than at higher charge ratios, due to increased flocculation, clearly visible to the naked eye, with a large proportion of the scattering particles thus leaving the size regime accessible with SANS. The scattered intensity at a N/P ratio of 2:1 was correspondingly much lower than for complexes with a greater mixing excess of cationic polymer.

Porod plots of the LOQ data from 25 kDa BPEI complexes where charge ratio varied from 20:1 to 2:1 showed that, as charge ratio decreased, the overall conformation of the complexes shifted from loose, swollen chains or Gaussian chains at 20:1, to a dense network at 10:1 and as it decreased still further towards the point of overall charge neutrality, expected at 2:1 in the vicinity of pH 7, a more compact, rough aggregate or dense mass fractal network of Gaussian chains formed at N/P = 5:1, and by 2:1 only a dense network of chains was detected. The overall scattering intensity also decreased over this range of charge ratios, especially at mid-Q,indicating both the presence of less total scattering material, particularly the free or minimally bound polymers, which scatter predominantly in the mid-Q regime, as can be seen from Figure 4.5.

In particular, the slight flattening off of the steep gradient at low Q into a slight bump for N/P = 20:1, disappears to a flat continuation for 10:1, and then drops again for 5:1 by a similar proportion. By 2:1, however, the scattering is extremely weak at anything but very low Q, and the Guinier plot, shown in the inset of Figure 4.11a, shows a similar

trend, with the low to intermediate Q scattering dropping off steadily between 20:1 and 5:1, and the steep upturn appearing to begin at increasingly large Q values as the charge ratio falls and the degree of curvature of the otherwise linear low-intermediate Q region also increases with falling charge ratio, indicating the presence of a greater degree of aggregation. However, the complexes at 2:1 show an essentially flat background in the Guinier regime, superimposed on which is a very steep upturn, divided into two clear linear sections, indicating the presence of very large aggregates, but perhaps little other observable fine structure. The overall weakness of scattering of the 2:1 complexes indicates their great instability and precipitation out of the SANS size regime and, to an extent, out of solution, as evidenced by the extreme turbidity which can be observed.

Meaning of Mid-Q Plateau and Excess Polymer Contributions

It is unclear from the data to what extent excess polymer is involved in complexation and binds partially to DNA, cooperatively with other polymers molecules, or whether it remains completely free once the total DNA charge has been neutralised or a moderate charge excess has been created by overcharging due to charge correlations in the condensed counterions predicted by the Manning condensation theory, combined with entropic effects for curved rods. [131]

This is elucidated somewhat by work by Ogris et al, who found that, at N/P ratios over 2:1, there is free polymer in solution [137] As the polymer excess increases, it can clearly be seen that, while the intensity of the very low Q peak remains approximately unchanged, the scattering in the mid to high Q regime increases with charge ratio, up to a maximum studied of 20:1. In this case, the low Q peak even falls slightly, in comparison to charge ratios of 5:1 and 10:1, suggesting greater stability of complexes.

In this case, it is likely that this mid-Q scattering is contributed by free polymers, although pure polymer scattering was weak, but exhibited a peak at mid- to low- Q, particularly pronounced for high MW BPEI.

An alternative explanation is that a greater excess of polymer increasingly stabilises the complexes against aggregation, and this peak is at least partially representative of free, unaggregated complexes. The extent to which this effect could contribute to the observed feature, and the question of whether non-aggregated polymers are bound to DNA or completely free, may be determined by the method of mixing. In the lab, during complexation for transfection, mixing in the bulk typically takes place gradually using pipettes in an

(a) Kratky-Porod plot of log(QI) vs. Q^2 for 25 kDa BPEI with DNA fragments at pH 7.4 at charge ratios from N\P = 20:1 to 5:1 in 10mM NaCl in D_2O; Inset shows Debye-Bueche plot of $I^{-\frac{1}{2}}$ vs. Q^2 for the same samples; Legend indicates charge ratio

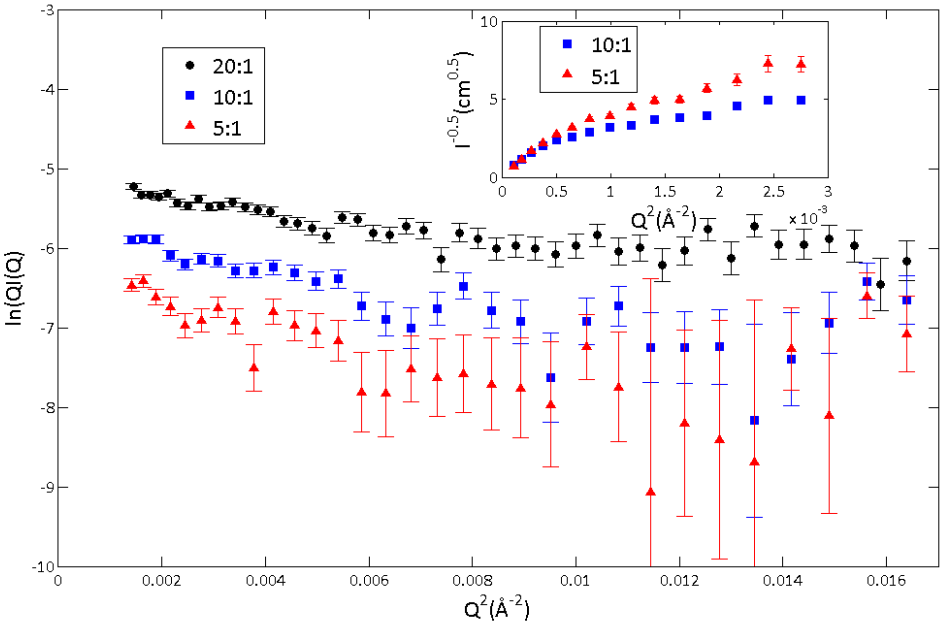

(b) Kratky-Porod plot of log(QI) vs. Q^2 for 25 kDa linear and branched PEI with DNA fragments at pH 7.4 at charge ratios N\P = 20:1 and 10:1 in 10mM NaCl in D_2O; Inset shows Debye-Bueche plot of $I^{-\frac{1}{2}}$ vs. Q^2 for the same samples; Legend indicates charge ratio and PEI type (branched or linear)

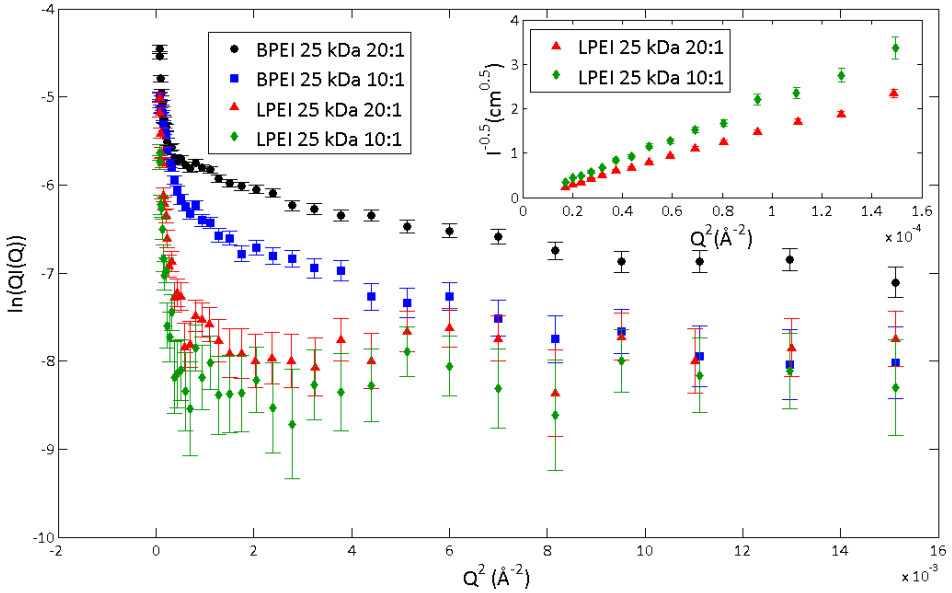

Figure 4.12: Kratky-Porod plot of log(QI) vs. Q^2 for large branched and linear PEI complexes with DNA fragments at pH 7.4 at charge ratios ranging from N\P = 20:1 to 2:1 in 10mM NaCl in D_2O; Insets show Debye-Bueche plot of $I^{-\frac{1}{2}}$ vs. Q^2 for the same samples; Legend indicates polymer type (branched or linear) and size (kDa)

Eppendorfer tube and with mass addition of one component into another. It is expected that iniital binding takes place rapidly, dominated by first contact electrostatic attraction and saturation of initially exposed molecules, hence an excess of polymer will not have a chance to participate significantly in binding, as the majority of DNA will be bound by the relatively few molecules it initially has contact with.

Han et al find reversibility of DNA compaction near N/P = 1[68], and Maltsev et al [121] describe in their model of reversible DNA-polymer binding that the amount of charge neutralisation when binding is reversible decreases, as a longer timescale is available for rearrangement of DNA charges, suggesting that excess polymers would be unlikely to be totally free from complexation. However, the application at much higher charge ratios is uncertain, although the overall higher net charge of complexes described by Mehrotra [127] et al also suggests excess polymers do participate in DNA charge neutralisation and complexation and that not all excess polymer molecules remain free, as reported by Ogris [137] who describes reported ranges of 50% to 86% free PEI above N/P = 2. The same author, writing with Boeckle et al [17] found the role of free PEI in transfection was important, however this does not necessarily preclude the possibility that 'free' excess PEI participates partially in complexation given the time opportunity, or that particularly following uniform mixing, such as in stopped-flow turbulent injection, the excess PEI would not also participate, resulting in the higher net surface charge complexes observed in the study mentioned above.[127]

However, in the stopped-flow configuration, where equal volumes of polymer and DNA solution are mixed rapidly by injection into a turbulent mixer cell at equal rates, a much more even process of mixing takes place and may lead to a greater proportion of PEI participating in binding when there is a large excess of polymer, increasing the likelihood still further that the free polymers are not completely free of DNA binding. Although some studies look at the quantity of DNA remaining outside of large complexes, separated by centrifugation from the more massive complexes, such as through ethidium bromide binding, the tight binding of PEI complexes with DNA suggests that complete dissociation and rebinding to other, free polymer molecules is unlikely to take place to a great extent, hence with manual mixing, it could be that the stoichiometric excess of polymer charges to DNA added last has no opportunity for electrostatic binding to DNA, while the stopped-flow injection mixing in equal proportions could enable greater dispersion and the formation of more uniform complexes, pre-aggregation, at binding charge ratios

closer to the mixing charge ratio than with manual mixing, which may result in more saturated complexes and a separate population of the excess of free polymers. This may lead to greater electrostatic stabilisation of complexes as charge ratio increases, leading to a larger proportion of individual, non-aggregated (or low-aggregation number) particles for higher charge ratios. However, although scattering is seen for the 25 kDa complexes of BPEI carried out at charge ratios of 20:1 and 10:1 on SANS2D with stopped-flow mixing, in the Porod plot of Figure 4.11a for LOQ at charge ratios between 2:1 and 20:1, we cannot confirm the impact on overall aggregation as the low Q range is restricted on LOQ compared to SANS2D. Additionally, it cannot be detemined from observation of the mid-Q peak whether it is comprised of pure polymer or individual complexes, as the peaks appear very similar and any differences are only attributable to the difference in polymer or complex concentration.

Charge Ratio	Debye-Bueche Model			Kratky-Porod Model				
	Debye-Bueche Intercept	D-B gradient	Resulting characteristic D-B aggregate size	Q* - start of linear K-P regime	Rod length (Å)	Kratky-Porod Plot Gradient	Kratky-Porod Plot R_g (Å)	Kratky-Porod Cross-Sectional Radius (Å)
20:1	n/a	n/a	n/a	0.03	127	Negative	13.6±0.4	19.2±0.5
10:1	0.25	4727	138	0.025	153	Negative	19.7± 0.5	28±0.8
5:1	0.144	5469	195	0.032	196	Negative	21.4± 1.1	30.3±1.6
2:1	n/a	n/a	n/a	n/a	n/a	n/a	n/a	n/a

Table 4.9: Parameters from Kratky-Porod and Debye-Bueche fits to SANS scattering data from complexes of 25 kDa BPEI with DNA fragments in 10mM NaCl in D_2O at pH 7.4 at charge ratios from N\P = 20:1 to 2:1, collected on LOQ

Polymer Type	Charge Ratio	Debye-Bueche Model			Kratky-Porod Model				
		Debye-Bueche Intercept	Debye-Bueche gradient	Debye-Bueche Characteristic Aggregate Size	Q* - Start of Linear K-P regime	Rod Length (Å)	Kratky-Porod Plot Gradient	Kratky-Porod Plot R_g (Å)	Kratky-Porod Cross-Sectional Radius (Å)
BPEI 25kDa	20:1**	(0.125)	(10730)	(292)	0.0169	226	Negative	18.4 ± 0.4	26.0 ± 0.63
BPEI 25kDa	10:1	n/a	n/a	n/a	n/a	n/a	n/a	n/a	n/a
LPEI 25kDa	20:1	Negative ≈ 0	16680	Undetermined, Large: Steep negative gradient but negative intercept, ≈ 0	0.021	182	0	Negligible	Negligible
LPEI 25kDa	10:1	0.05	20840	645.601	0.022	178	0	Negligible	Negligible

Table 4.10: Parameters from Kratky-Porod and Debye-Bueche fits to SANS scattering data from complexes of 25 kDa branched and linear PEI with DNA fragments in 10mM NaCl in D_2O at pH 7.4 at charge ratios of N\P = 20:1 and 10:1, collected on SANS2D

Solvent Media

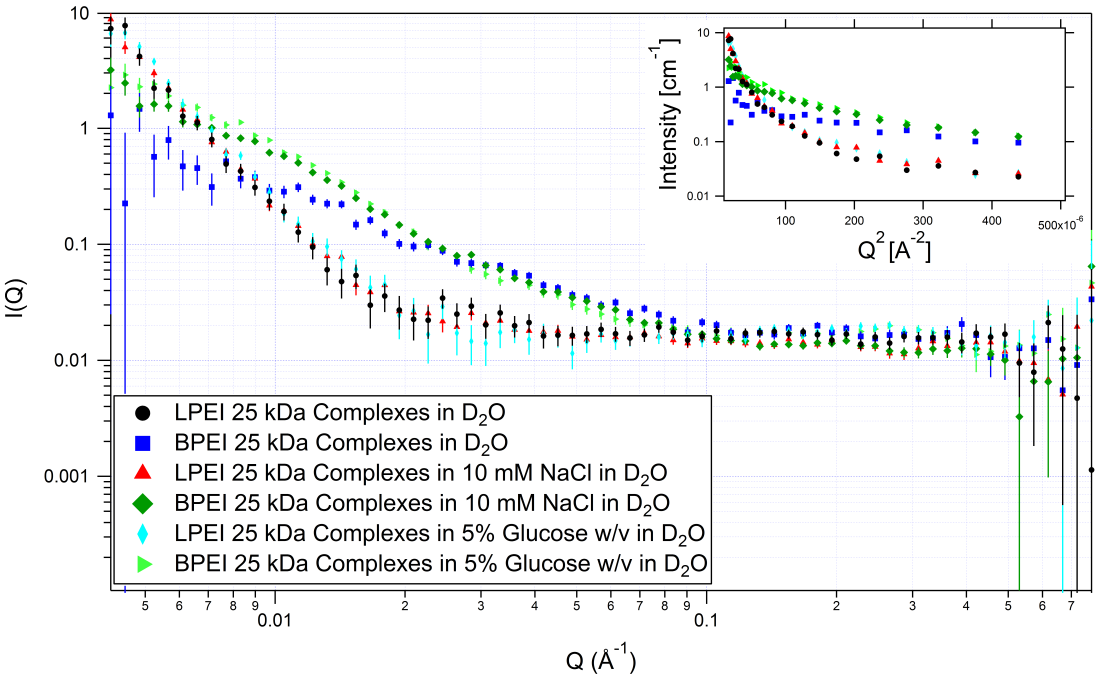

Figure 4.13: Porod plot of log(I) vs. log (Q) for complexes of 25 kDa branched and linear PEI with DNA fragments at pH 7.4 at a charge ratio of N\P = 10:1 in various solvents; Inset shows Guinier plot of log(I) vs. Q^2 for the same samples; Legend indicates solvent and polymer type

The effect of solvent media on complex structure and stability is of great relevance for transfection studies, due to the variety of media which are used for complex preparation, and the range of conditions experienced by the complexes during transfection. PEI complexes in high NaCl, over 50 mM [137] are reported to form large aggregates compared to

Charge Ratio	PEI Type	Concentration (mg/ml DNA)	Porod-predicted Model	FISH Model	Cylinder 1			Cylinder 2			Kholodenko Worm-like Chain			
					$Scale_1$	$Radius_1$ (Å)	$Length_1$ (Å)	$Scale_2$	$Radius_2$ (Å)	$Length_2$ (Å)	$Scale_K$	n	L (Å)	$R_g x$ (Å)
10:1	BPEI 25 kDa	1.5	Gaussian Chains	Kholodenko Chain	—	—	—	—	—	—	1.29 E-07	2441	25	17
20:1	BPEI 25 kDa	1.5	Dense Network or Rough Aggregate of Gaussian Chains	Cylinders	4.43 E-07	28	360	6.72 E-08	636	371	—	—	—	—
10:1	LPEI 25 kDa	1.5	Aggregated Rods	Cylinders	4.99 E-07	7	381	3.16 E-08	525	479	—	—	—	—
20:1	LPEI 25 kDa	1.5	Large, Smooth Aggregates of Rods	Cylinders	4.97 E-06	3	373	6.04 E-08	529	473	—	—	—	—
20:1	BPEI 25 kDa	3	Swollen to Gaussian Chains	Kholodenko Chain	—	—	—	—	—	—	1.23 E-06	3825	66	12
10:1	BPEI 25 kDa	3	Dense Network or Rough Aggregate of Gaussian Chains	Kholodenko Chain	—	—	—	—	—	—	2.94 E-07	12154	16	13
5:1	BPEI 25 kDa	3	Large, Slightly Rough Aggregate of Gaussian Chains	Cylinders	1.75 E-07	33	1502	1.44 E-07	247	240	—	—	—	—
2:1	BPEI 25 kDa	3	Dense Network or Rough Aggregate	Cylinders	1.30 E-08	268	121	—	—	—	—	—	—	—

Table 4.11: Parameters from model fitting to SANS scattering data from complexes of large, branched and linear PEI with DNA fragments at charge ratios from N\P=20:1 to 2:1 in 10mM NaCl in D_2O at pH 7.4; Fitting was carried out with FISH[71]; Complexes at a DNA concentration of 3 mg/ml were studied on LOQ and those at 1.5 mg/ml were studied on SANS2D.

low salt conditions, which reduces the hydrated double layer around the complexes and increases their hydrophobic instability.[137] However, based on a survey of the literature, 150mM NaCl is a frequently used solvent condition and, as has been discussed above, a highly aggregated complex is not necessarily a barrier to cellular entry, although has been shown to have lower transfection efficiency in some conditions, when compared to those formed in glucose solution[79][57]. As any amount of increased NaCl will increase the tendency to aggregate, a low level of 10 mM was selected for the majority of samples to enable the study of aggregation. It may be expected that increasing the NaCl concentration could create an exaggerated or accelerated version of the behaviour observed in our model system at 10 mM NaCl, enabling these findings to be related to the higher salt

Polymer Type	Solvent Type	Porod Analysis				Guinier Analysis*		
		Low-Q Porod Exponent	Low-Q Model	High-Q Porod Exponent	High-Q Model	Estimated R_{g1}: Lowest-Q (Upturn)	Estimated R_{g2}: Low-Q	Estimated R_{g3}: Intermediate-Q
LPEI 25 kDa	D_2O	4.17 ±0.18	Debye-Bueche: Large, smooth aggregates	1.68 ±0.52	Swollen chains	449 ± 18	229 ± 10	n/a
BPEI 25 kDa	D_2O	n/a	n/a	1.62 ±0.04	Swollen chains	120 ±4.5	40.1 ± 1.8	n/a
LPEI 25 kDa	10 mM NaCl in D_2O	4.1 ±0.1	Debye-Bueche: Large, smooth aggregates	0.92 ±0.11	Rod-like	445 ± 11	251 ± 6	n/a
BPEI 25 kDa	10 mM NaCl in D_2O	n/a	n/a	2.13 ±0.023	Mass Fractal: Gaussian Chains	308 ±30	144 ± 2	n/a
LPEI 25 kDa	5% w/v Glucose in D_2O	4.15 ±0.09	Debye-Bueche: Large, smooth aggregates	≈ 0	No rods or distinguishable high Q structure	493 ± 24	303 ± 9	163 ± 11
BPEI 25 kDa	5% w/v Glucose in D_2O	1.83 ±0.07	Swollen Chains	2.44 ±0.04	Mass Fractal: Gaussian Chains	268 ± 17	152 ± 2	76.5 ± 3.1

Table 4.12: Parameters from Porod and Guinier fits to SANS scattering data from complexes of 25 kDa branched and linear PEI with DNA fragments at a charge ratio of N\P = 10:1 in a range of solvent media at pH 7.4

Polymer Type	Solvent Type	Porod-predicted Model ~~Ellipsoid~~	FISH Model	Cylinder 1			Cylinder 2			Kholodenko Worm-like Chain			
				$Scale_1$	$Radius_1$ (Å)	$Length_1$ (Å)	$Scale_2$	$Radius_2$ (Å)	$Length_2$ (Å)	$Scale_K$	n	L (Å)	$R_a x$ (Å)
	$Scale_e$	R_1	X										
BPEI 25 kDa	D_2O	Swollen chains	Kholodenko Chain	—	—	—	—	—	—	2.13 E-07	855	190	26
	—	—	—										
LPEI 25 kDa	D_2O	Aggregated Rods	Cylinders	7.23 E-07	5	380	2.84 E-08	530	455	—	—	—	—
	—	—	—										
BPEI 25 kDa	10 mM NaCl in D_2O	Gaussian chains	Kholodenko Chain	—	—	—	—	—	—	1.29 E-07	2441	25	17
	—	—	—										
LPEI 25 kDa	10 mM NaCl in D_2O	Aggregated Rods	Cylinders	1.84 E-06	3	91249	3.11 E-08	523	479	—	—	—	—
	—	—	—										
BPEI 25 kDa	5%w/v glucose in D_2O	Gaussian chains	Kholodenko Chain	—	—	—	—	—	—	5.14 E-08	1153	64	48
	—	—	—										
LPEI 25 kDa	5%w/v glucose in D_2O	Large aggregates	Ellipsoid	—	—	—	—	—	—	—	—	—	—
	2.46E+04	1.81E+03	3.63E+00										

Table 4.13: Parameters from model fitting to SANS scattering data from complexes of large, branched and linear PEI with DNA fragments at a charge ratio of N\P=10:1 in a range of solvent media at pH 7.4; Fitting was carried out with FISH[71].

concentrations commonly used in transfection.

The results for statically averaged high MW linear PEI complexes show little difference in structure for the range of complexes studied, implying that the addition of small amounts of NaCl or glucose are not sufficient to have an impact on the overall structure. The only noticeable distinction was that, for complexes formed in glucose solution, no high-Q structure could be distinguished, and ellipsoidal aggregates were fit to the data, possibly due to binding of glucose molecules to the complexes, while for both other solvents, large aggregates and component cylinders, with very similar dimensions (with the exception of the fitted length, which is large but has a great degree of variation due to error), could be fit for both. However, examination of the dynamics of complexation and aggregation is necessary to highlight any difference in stability over this time range. (See Section 4.4.2)

For high MW BPEI complexes, 10 mM NaCl and 5% glucose media show no difference in scattering pattern, however, complexes formed in pure D_2O showed a noticeably decreased intensity in the low Q, Guinier, regime. This loss of structure at low Q is reminiscent of the pure BPEI scattering pattern and could be due to reduced binding and complexation, which utilises some degree of counterions to mediate attraction. In the absence of any salt, it could be that complexation is hindered. With the shallower Porod gradient of approximately 5/3 the complexes in pure D_2O resemble swollen chains rather than the gaussian coils found in glucose or NaCl solutions, and the Kholodenko worm-like chain model fit to the data in FISH, which incorporates the number and length of statistical rod-like segments, suggested that the segment lengths for complexes in D_2O were much longer but fewer, (see n and L values in Table 4.13), indicating stiffer, swollen chains, rather than truly flexible particles. Additionally, the fitted axial radius of the chain is noticeably larger in complexes formed in glucose solution, which could again be indicative of glucose participating in the complexation.

Concentration

The effect of sample concentration on scattering can be informative in aggregation studies [147] as a series of concentrations to dilute levels can highlight changes in upturns at low Q suggestive of aggregation. In this case, two concentrations were carried out for several types of PEI complexes with DNA. However, the accessible Q-range was not the same for both samples, as one was conducted on LOQ and one on SANS2D beamline, hence it is not

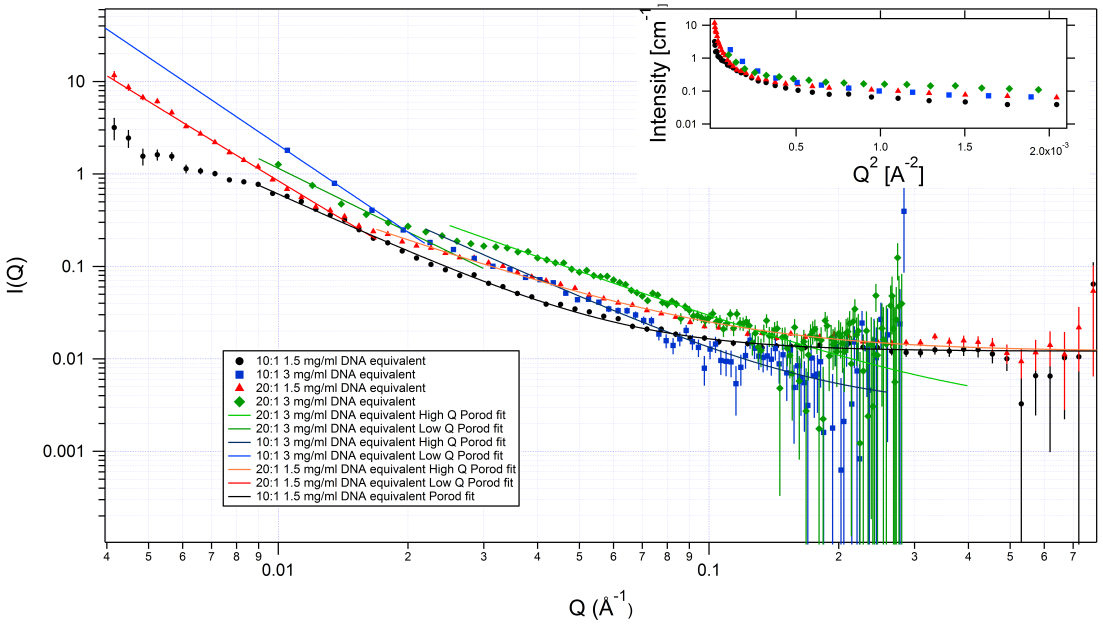

Figure 4.14: Porod plot of log(I) vs. log (Q) for complexes of 25 kDa branched PEI with DNA fragments at pH 7.4 at charge ratios of N\P = 10:1 and 20:1 in 10 mM NaCl in D_2O; Inset shows Guinier plots for the same samples; Legend indicates polymer type, concentration and charge ratio

possible to observe the effect of concentration on the very low Q scattering from aggregates, where any difference due to interaction potentials of complexes would be emphasised by deviations in scattering pattern with curvature in the Guinier plot. Additionally, there were inevitable differences in the method of mixing, as discussed above, SANS2D using turbulent mixing by injection in a stopped-flow cell, with complex mixing on LOQ being performed by manual addition and inversion.

However, in the available Q-range from LOQ, which may still follow Guinier behaviour at its lowest extreme, there appeared to be a slight deviation in the overall shape of the scattering curve between complexes formed at different concentrations, with the appearance of an exaggerated deviation at low Q for large BPEI complexes at a charge ratio of 10:1with its lower aggregation experienced a noticeably increased aggregation pressure with the increased concentration on LOQ. At the higher charge ratio of 20:1, BPEI complexes did not show this deviation, indicating that the increased net positive charge excess was sufficient to combat the increased tendency to aggregation due to the concentration increase. The hypothesis of increased aggregation is explored further with Guinier analysis below.

Additionally, for 10:1 N/P ratios at both concentrations, the upturn indicative of large aggregates at the lowest Q ranges was steeper and more pronounced than for 20:1, suggesting the additional excess of polymer does afford complexes some additional stability

against aggregation.

Only a slightly increased intensity was observed for those complexes at higher concentration overall, however, as would be expected due to the increased amount of scattering material present. That the scattering intensity does not increase proportionally to the concentrations of scattering components as they double is not surprising, as a certain amount of scattering aggregates will be out of the accessible size range, possibly a proportionally higher percentage of that present, as aggregation may be favoured at higher concentrations due to increased proximity of the particles, increasing the likelihood of overlap of their double layers.

An effect which should also be considered for its potential contribution to structural differences is the method of mixing, which was done via turbulent injection in stopped-flow data collection on SANS2D, while samples were mixed by hand for static experiments on LOQ. This difference in mixing could potentially impact binding heterogeneities within the samples and may be an additional source of structural variation, as discussed above (Section 4.4.1), although was not expected to impact the overall particle stability.

pH Variation

The degree of protonation reported for PEI is reported to change dramatically over the pH range from 7 to 5, going from 20 to 45% protonation over this range[137], which makes the question of structural change over this range interesting, in addition to the fact that this is the range over which pH is likely to change during endosomal acidification, and hence physiologically very relevant.

pH	Porod Analysis				Guinier Analysis*		
	Low-Q Porod Exponent	Low-Q Model	High-Q Porod Exponent	High-Q Model	Estimated R_{g_1}: Lowest-Q (Upturn)	Estimated R_{g_2}: Low-Q	Estimated R_{g_3}: Intermediate-Q
5.4	3.02± 0.05	Mass Fractal: Dense network	2.30± 0.24	Mass Fractal: Gaussian chains	n/a	81.4±2.3	35.7± 0.8
6.4	2.93± 0.05	Mass Fractal: Dense network	2.1± 0.3	Mass Fractal: Gaussian chains	n/a	86.1±2.2	33.9± 0.7
7.4	2.91± 0.08	Mass Fractal: Dense network	2.0 ± 0.4	Mass Fractal: Gaussian chains	n/a	84.1±3.7	29.4± 1.2

Table 4.14: Parameters from Porod and Guinier fits to SANS scattering data from complexes of 25 kDa BPEI with DNA fragments in 10mM NaCl in D_2O at pH 5.4, 6.4 and 7.4

The scattering of high MW BPEI complexes at a charge ratio of 10:1 in 10 mM NaCl were compared under variation of pH levels in order to attempt to control for effects

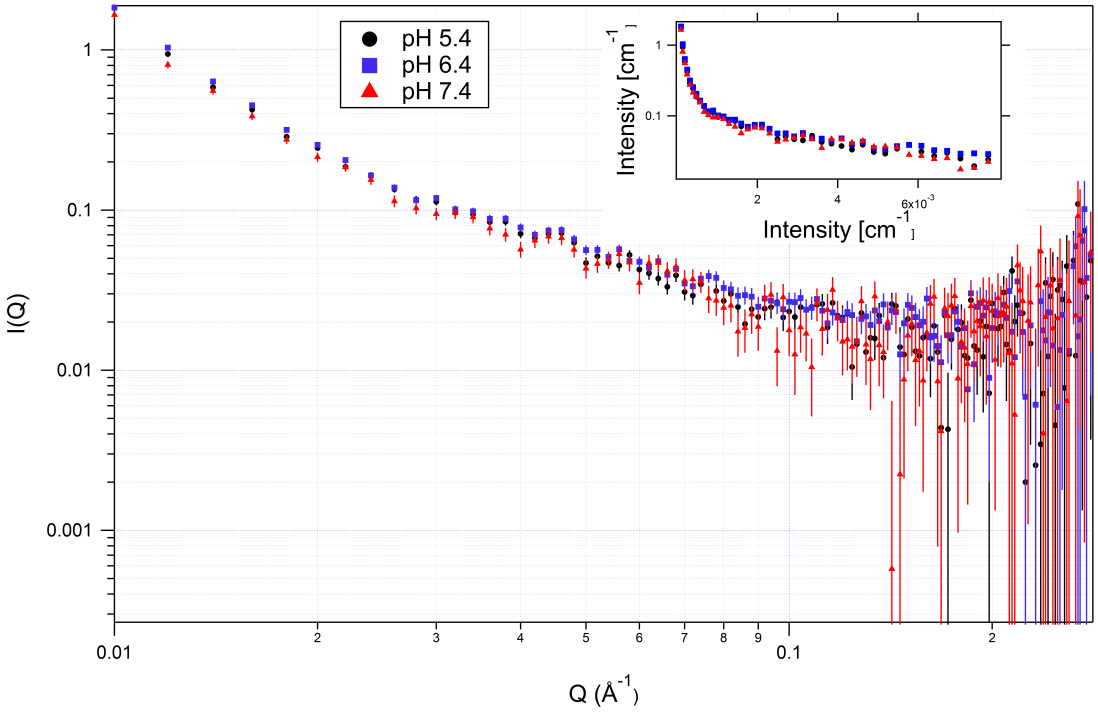

Figure 4.15: Porod plot of log(I) vs. log (Q) for 25 kDa BPEI with DNA fragments at pH 5.4, 6.4 and 7.4 at a charge ratio of N\P = 10:1 in 10mM NaCl in D_2O; Inset shows Guinier plot of log(I) vs. Q^2 for the same samples; Legend indicates sample pH

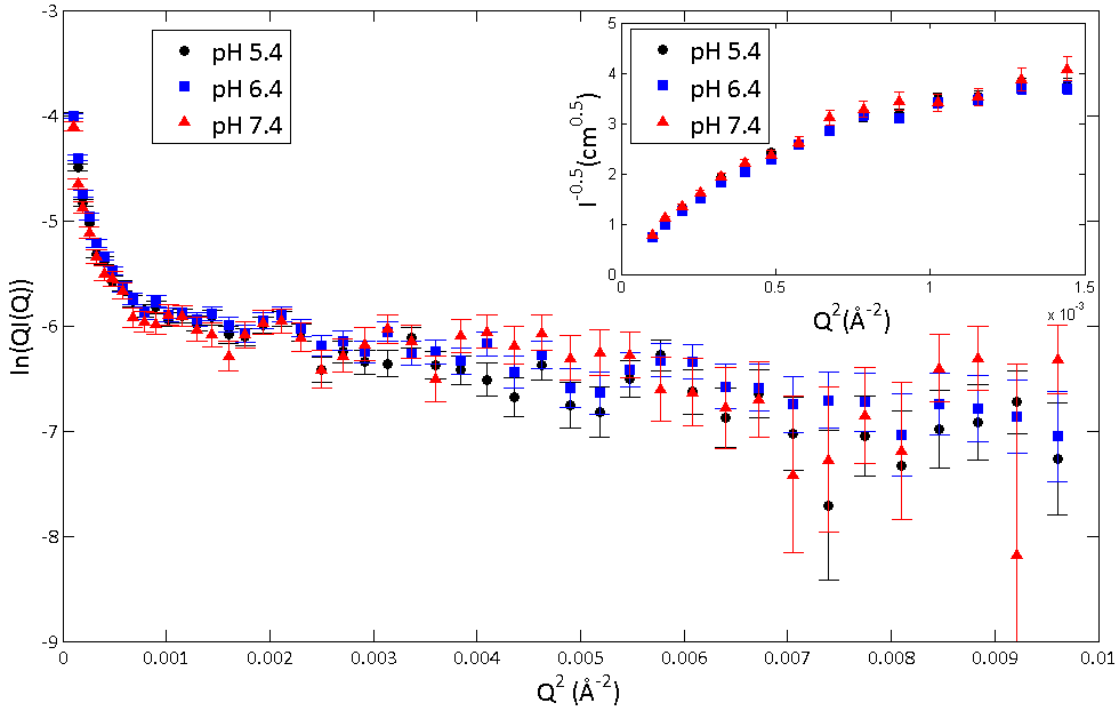

Figure 4.16: Kratky-Porod plot of log(QI) vs. Q^2 for 25 kDa BPEI withDNA fragments at pH 5.4, 6.4 and 7.4 at a charge ratio of N\P = 10:1 in 10mM NaCl in D_2O; Inset shows Debye-Bueche plot of $I^{-\frac{1}{2}}$ vs. Q^2 for the same samples; Legend indicates sample pH

pH	Debye-Bueche Model			Kratky-Porod Model				
	Debye-Bueche Intercept	Debye-Bueche gradient	Debye-Bueche Characteristic Aggregate Size	Q* - Start of Linear Kratky-Porod regime	Rod Length (Å)	Kratky-Porod Plot Gradient	Kratky-Porod Plot R_g (Å)	Kratky-Porod Cross-Sectional Radius (Å)
5.4	(0.376)	(4512)	(110)	0.026	460	Negative	18.1 ± 0.7	26±1
6.4	(0.365)	(4355)	(109)	0.032	335	Negative	15.9 ± 0.7	23±1
7.4	(0.400)	(4678)	(108)	0.024	318	Negative	14.9±1.1	21±1.6

Table 4.15: Parameters from Kratky-Porod and Debye-Bueche fits to SANS scattering data from complexes of 25 kDa BPEI with DNA fragments in 10mM NaCl in D_2O at pH 5.4, 6.4 and 7.4

of potential pH drift following solution pH adjustment shortly prior to experiments, as PEI is a notoriously strong buffer, and to identify structural changes under relevance to cellular pH levels, thought to range typically from around 5 to 7.4 , corresponding to late endosomes or lysosomes to the cytosol, but hypothesised to be buffered with PEI, as described by the proton sponge theory, so studied at a slightly higher level here. However, negligible structural variation was observed over the pH range examined, as might be expected due to the very high isoelectric point of the polymers. pH buffering over a wide range is particularly strong in PEI. With BPEI, the presence of primary, secondary and tertiary amine groups contributes to the buffering ability, with pKas ranging from pH 6-7 for tertiary amines to pH 9 for primary [120]. However, multiple pKas are reported for PEIs, with Jiang[85] et al reporting a pKa of pH 10.2, and other authors [68] determining values near pH 7.

This lack of apparent structural dependence on pH in the range studied is significant as no significant structural changes are therefore thought to occur due to the pH typically experienced by the polymer within intracellular compartments. It may be, however, that some loosening of binding could occur which is not significantly discernable with this technique. It could be possible that a structural change could occur if the pH changes following complexation, rather than complexation of components at the pH in question, as occurred here, but this would seem to be unlikely given the strong similarity between the scattering curves from samples prepared at different pHs. Both Guinier parameters and all fits showed strong agreement between the curves at different pHs, with slight differences seeming to be due solely to background variations, which may be related to the adjustment of pH with small amounts of concentrated HCl or NaOH contributing protons to the incoherent background scattering. Otherwise, however, no significant structural variation was observed over the range of pHs examined.

4.4.2 Kinetic Data

Stopped-flow SANS data was sliced into 9 time sections. The Porod plots of the earliest and longest time sliced SANS data, from 0 - 50 seconds and 1500 - 1800 seconds are presented and discussed in the following sections, as an indicator of the structural stability or aggregation of complexes of various types under different conditions. For clarity, the intermediate time sections are not presented, however these are used in the model-based data fitting, except where examination of the early and late scattering indicates little significant change, such as in the case of high MW BPEI complexes at N\P = 10:1.

A preliminary singular value decomposition (SVD) analysis was undertaken but is not presented, as it is uncertain whether the systems being studied consist of sufficiently well-defined components to produce a reliable analysis. All datasets showed predominant contributions to the total variance from the first basis vector which typically varied the most smoothly and had a contribution to variance in excess of 97% in all cases. However, this parameter alone may not take sufficient account of the potential contributions of smaller particles which scatter at higher Q values and hence lower intensities, as scattering intensity is proportional to particle size.

Finally, the time-sliced data are fitted with appropriate form factor models using the FISH program[71], and the evolution of the relevant parameters with time are shown in the plots below.

PEI Type

Figure 4.17 shows the earliest and longest time slices for each of the four PEI types and sizes studied. For complexes of high MW BPEI complexes, it can clearly be seen that very little change in scattering occurs over the time period studied, with only a slight drop in intensity at low Q over the 30 minutes. This confirms the indication from the static SANS data of an absence of large, smooth aggregates for high MW BPEI complexes and their relatively greater stability in low ionic strength solution.

The slight change in Kholodenko statistical rod length observed over the time period for these complexes suggests the chain becomes more tightly curved and compacted over the time period, which also correlates with the slight fall in intensity at the lowest to intermediate Q range, and very slightly higher scattering at intermediate to high Q at the longest time, although the uncertainty surrounding short time scales is relatively high.

Further investigation of intermediate time scales was considered unlikely to elucidate this further, as the most rapid change is expected shortly after the point of mixing.

Porod plots of low MW PEI complexes, both branched and linear, and high MW LPEI complexes show much greater change in scattering over the observed time period. From the Porod plots, it can be seen that the difference is particularly great for low MW PEI complexes at low Q, where a substantial fall in scattering intensity is observed. For large LPEI, this is observed over the entire -4 Porod region, while over the higher Q range the scattering is very similar. Low MW BPEI complexes show a similar Porod gradient over the low to mid Q range, but at a slightly lower intensity at later times than immediately following mixing, while at the very low Q regime, the deviation of the slopes is amplified. These observations appear to be supported by the model-fitting data of a single cylindrical rod. The predominant scattering structure then appears to grow in radius over the course of observation, with the scale factor, proportional to particle number density, falling, indicating some scattering material has been lost from visibility, and the observable aggregate size is increasing over the course of the 30 minute observation period. From the time-course evolution of parameters shown in Figure 4.22 and Table 4.16, it appears that the fall in scale factor occurs rapidly in the early times and continues to fall off gradually over the course of the 30 minutes, until a slight peak is observed at the end, while the radius falls gradually and then begins to climb towards later times, with the fitted length remaining relatively constant.

LPEI, both large and small, show similar behaviour, as mentioned above. High MW LPEI complexes are well modelled by a combination of two cylinders, with the larger, representing aggregates, remaining relatively constant in size, but with significant loss of scale factor of both structures, although predominantly of the smaller rod, which is thought to represent individual component complex structures as they are gradually compacted into larger aggregates.

Low MW LPEI complexes were well modelled by a single cylindrical structure, although their low scattering intensity and associated diminished signal-to-noise ratio hindered fitting with high feature resolution. This was characterised, much as for high MW LPEI, by the reduction of scale factor of large aggregates, indicating the loss of scattering material from the accessible size range, accompanied by a slight growth in the radius of particles, and a loss of length, tending more toward globular-like aggregates. The drop in scale factor over the time-course is more gradual for low MW LPEI complexes than for others,

which manifest a sharper fall at the very earliest times, perhaps indicating a somewhat greater stability leading to slower kinetics of aggregation and precipitation.

Indicative SVD analysis led overall to the conclusion that, for the majority of particles, one predominant component contributed to most of the variance, while one or two other basis vectors with a significant non-noise component were observed. Overall, preliminary SVD analysis therefore broadly supported the extent to which aggregates dominated the scattering, however a detailed analysis using this technique was not thought to be reliable.

Table 4.16: Variation of model parameters fit to time-sliced SANS data with time for complexes of large and small, linear and branched PEI with DNA fragments in pH 7.4 10 mM NaCl in D_2O with DNA concentration of 1.5 mg/ml.

		Cylinder 1			Cylinder 2			Kholodenko Worm-like Chain			
Polymer Type	Time After Mixing (Seconds)	$Scale_1$	$Radius_1$ (Å)	$Length_1$ (Å)	$Scale_2$	$Radius_2$ (Å)	$Length_2$ (Å)	$Scale_K$	n*	L (Å)	$R_g x$ (Å)
BPEI 25 kDa	0 - 50	—	—	—	—	—	—	6.96E-08	3556	66	40
	1500 - 1800	—	—	—	—	—	—	6.49E-08	5250	32	26
BPEI 1.8 kDa	0 - 50	5.09E-08	325	359	—	—	—	—	—	—	—
	1500 - 1800	2.50E-08	838	336	—	—	—	—	—	—	—
LPEI 25 kDa	0 - 50	7.00E-08	468	372	—	—	—	—	—	—	—
	1500 - 1800	3.79E-08	659	781	—	—	—	—	—	—	—
LPEI 2.5 kDa	0 - 50	3.30E-08	497	529	—	—	—	—	—	—	—
	1500 - 1800	3.43E-09	553	312	—	—	—	—	—	—	—

Charge Ratio

Complexes of high MW LPEI and BPEI formed at N/P charge ratios of 20:1 and 10:1 in 10 mM NaCl in D_2O at pH 7.4 were also compared in kinetic studies.

The most immediately noticeable difference when higher charge ratios are examined is the difference in scattering pattern in the intermediate to high Q regime and background level for both high MW LPEI and BPEI complexes between the charge ratios of 10:1 and 20:1 as can be seen in Figure 4.19. At 10:1, as already discussed, High MW BPEI shows little structural change, while LPEI complexes lose some intensity at low Q, thought to be due to progression of aggregation beyond the size regime accessible with SANS, which was verified by the reduction in scale factors for the relevant modelled particle in SANS data fitting with FISH. At 20:1, however, a marked change is observed between the intermediate to high Q background level at the earliest and latest times.

(a) 25 kDa BPEI 10:1 Complex in 10 mM NaCl

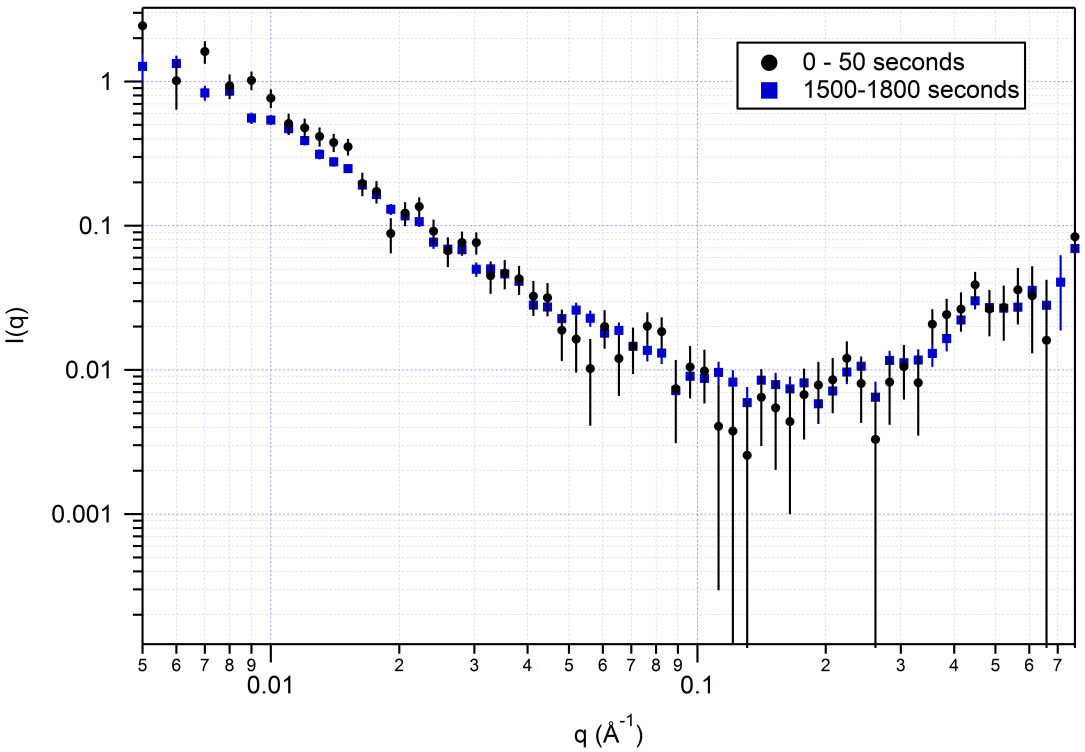

(b) 1.8 kDa BPEI 10:1 Complex in 10 mM NaCl

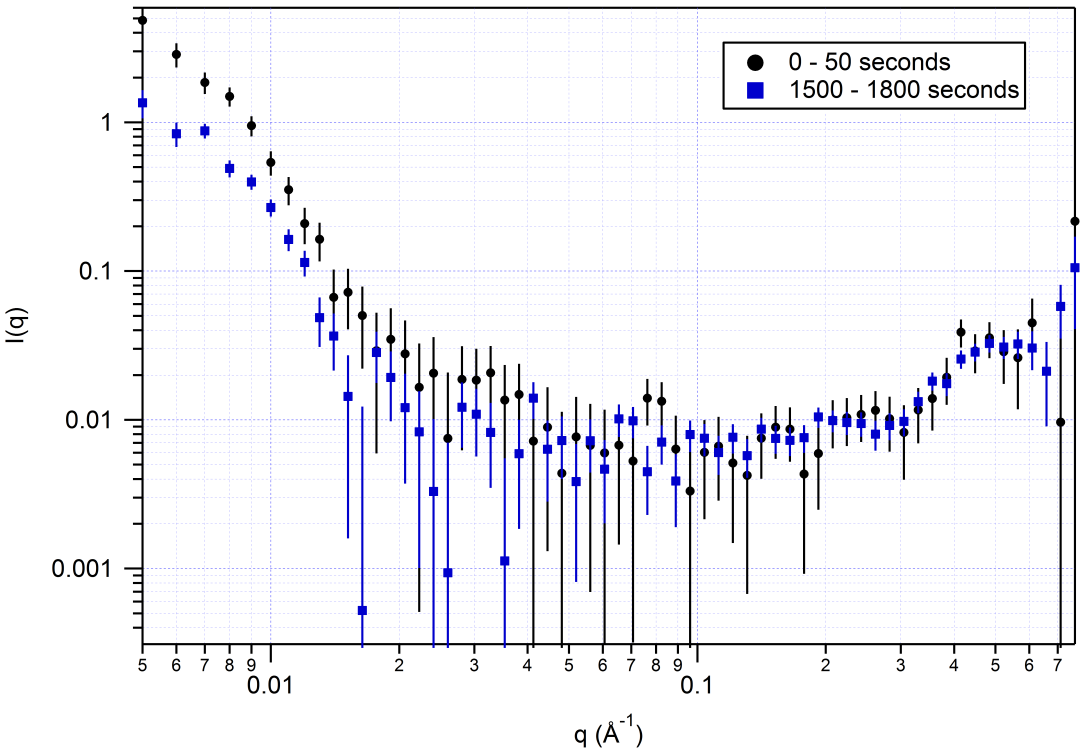

Figure 4.17: Porod plots of log(I) vs. log (Q) of time-sliced SANS data from complexes of large and small, linear and branched PEI with DNA fragments in pH 7.4 10 mM NaCl in D_2O with DNA concentration of 1.5 mg/ml; Legends indicate time period.Continued below.

(c) 25 kDa LPEI 10:1 Complex in 10 mM NaCl

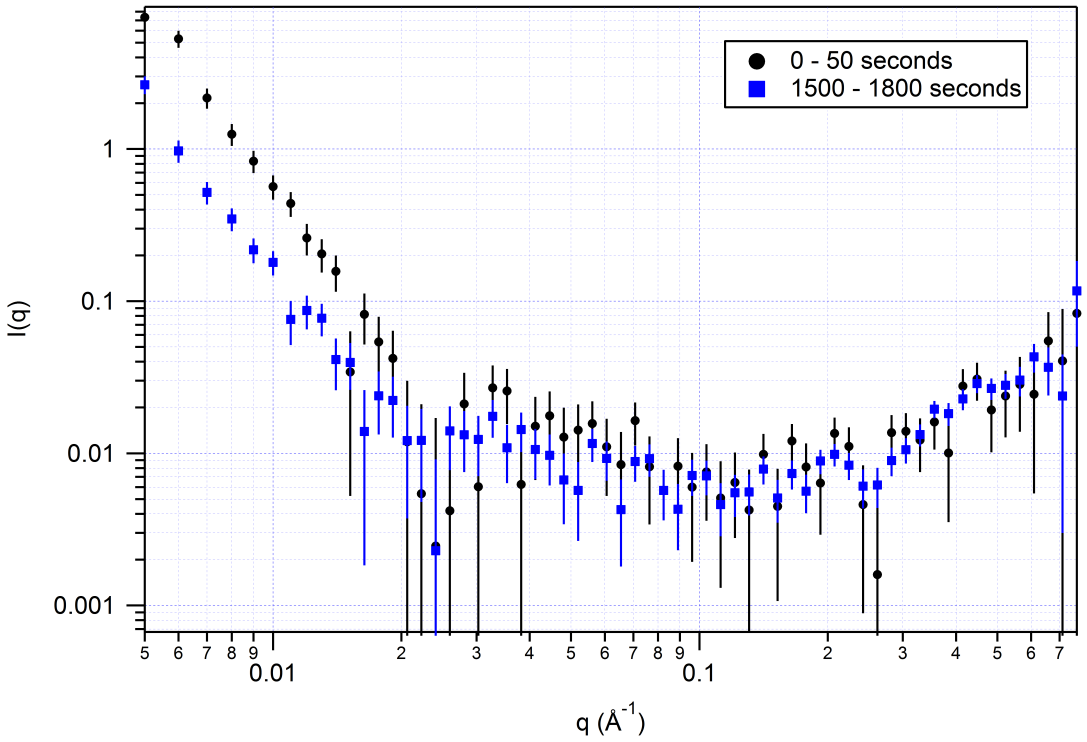

(d) 2.5 kDa LPEI 10:1 Complex in 10 mM NaCl

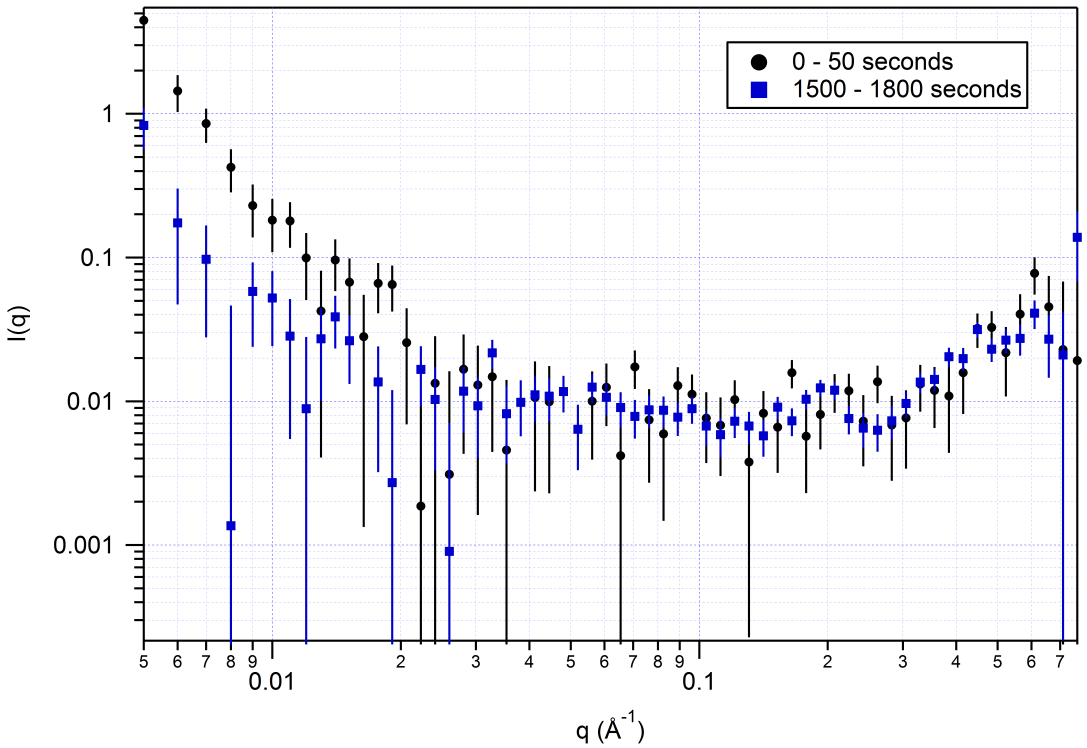

Figure 4.17: Continued:Porod plots of log(I) vs. log (Q) of time-sliced SANS data from complexes of large and small, linear and branched PEI with DNA fragments in pH 7.4 10 mM NaCl in D_2O with DNA concentration of 1.5 mg/ml; Legends indicate time period.

(a) Model parameters for the cylindrical structures fit to time-resolved SANS data from complexes of 1.8 kDa BPEI with DNA fragments at a charge ratio of 10:1 in 10 mM NaCl

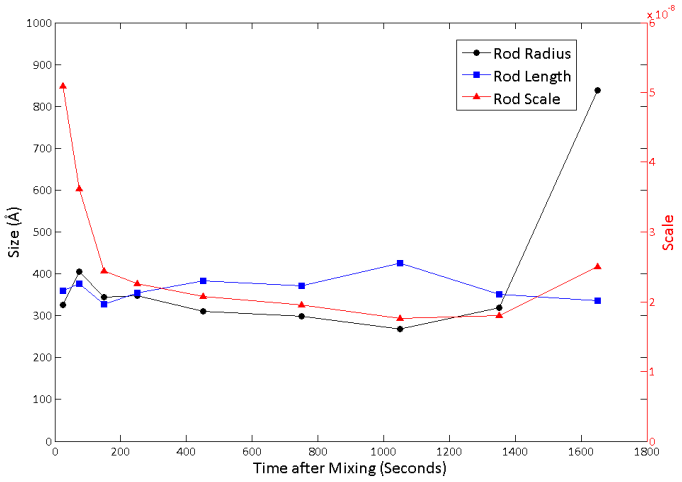

(b) Model parameters for the cylindrical structures fit to time-resolved SANS data from complexes of 25 kDa LPEI with DNA fragments at a charge ratio of 10:1 in 10 mM NaCl

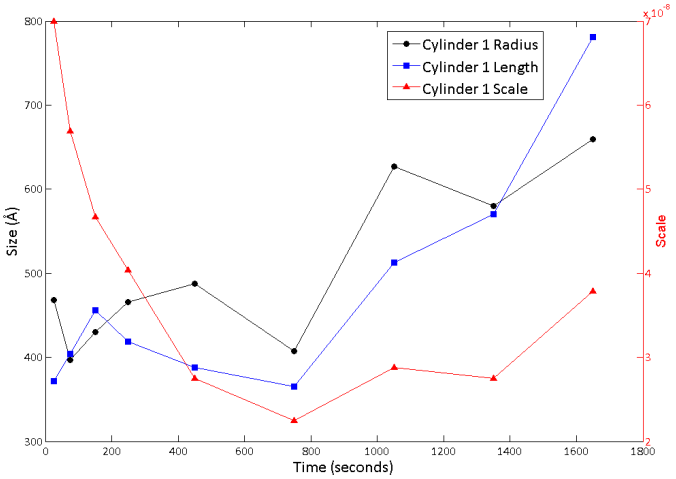

(c) Model parameters for the cylindrical structures fit to time-resolved SANS data from complexes of 2.5 kDa LPEI with DNA fragments at a charge ratio of 10:1 in 10 mM NaCl

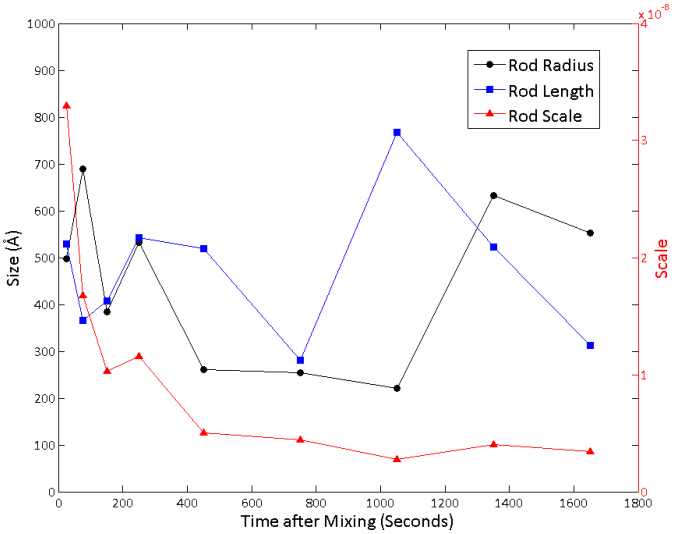

Figure 4.18: Variation of model parameters fit to time-sliced SANS data with time for complexes of large and small, linear and branched PEI with DNA fragments in pH 7.4 10 mM NaCl in D_2O with DNA concentration of 1.5 mg/ml; Legends indicate model fit parameter.

(a) 25 kDa BPEI 10:1 Complex in 10 mM NaCl

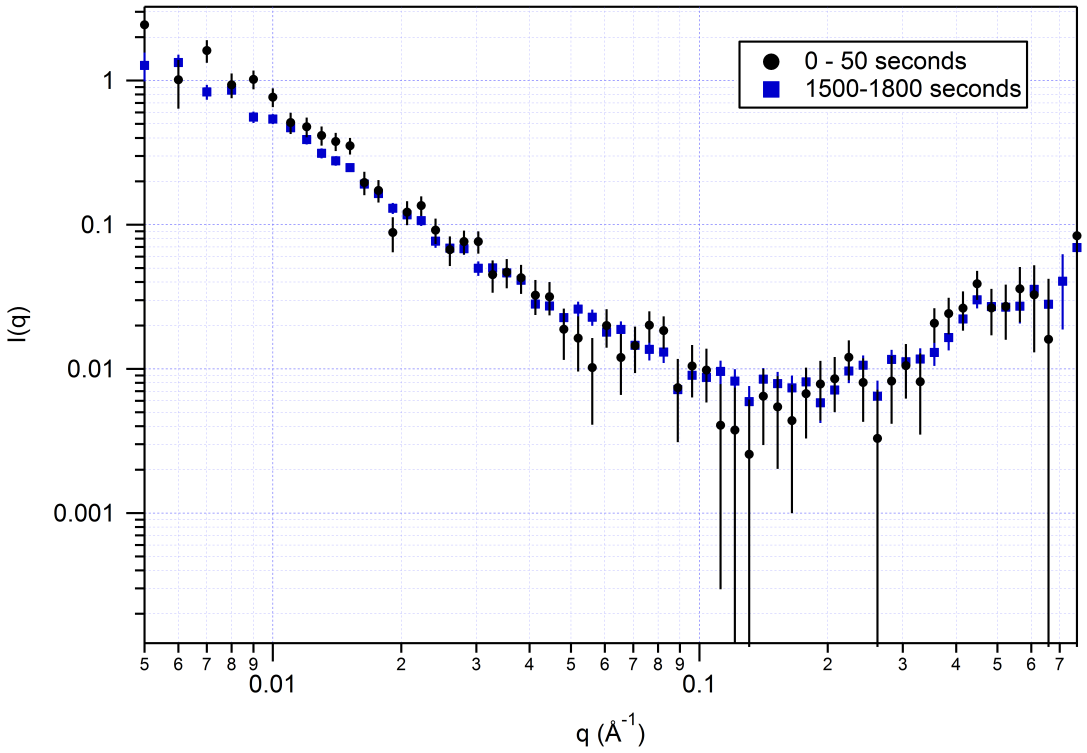

(b) 25 kDa BPEI 20:1 Complex in 10 mM NaCl

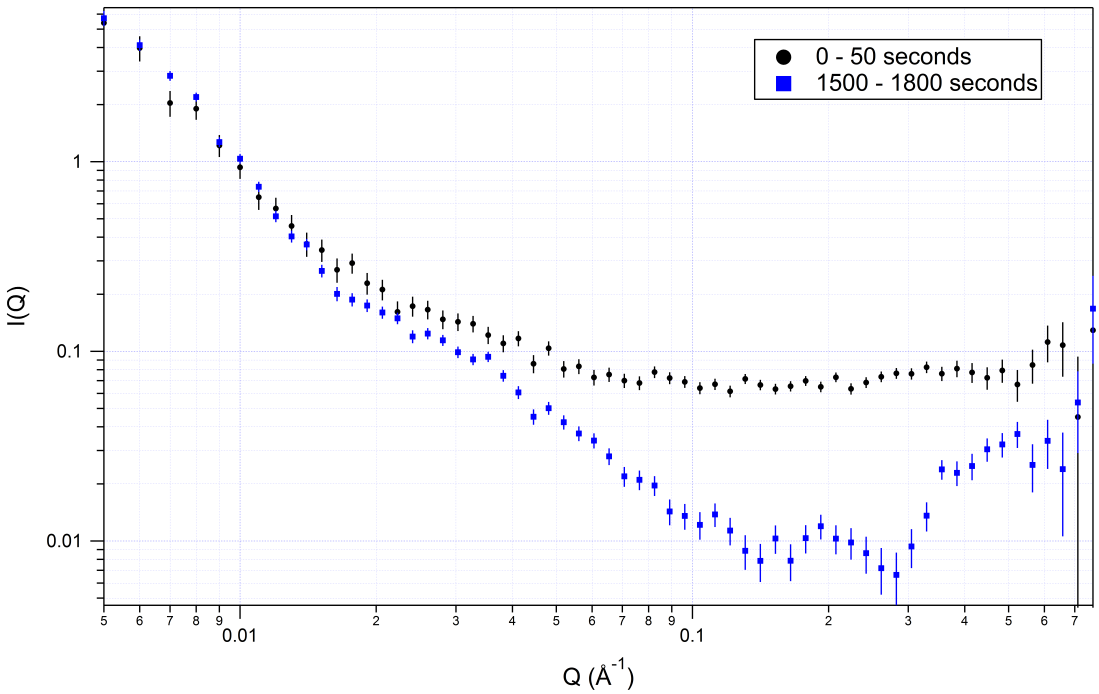

Figure 4.19: Porod plots of log(I) vs. log (Q) of time-sliced SANS data from complexes of large linear and branched PEI with DNA fragments in pH 7.4 10 mM NaCl in D_2O with DNA concentration of 1.5 mg/ml at charge ratios of N\P = 20:1 and 10:1 ; Legends indicate charge ratio and polymer type.Continued below.

(c) 25 kDa LPEI 10:1 Complex in 10 mM NaCl

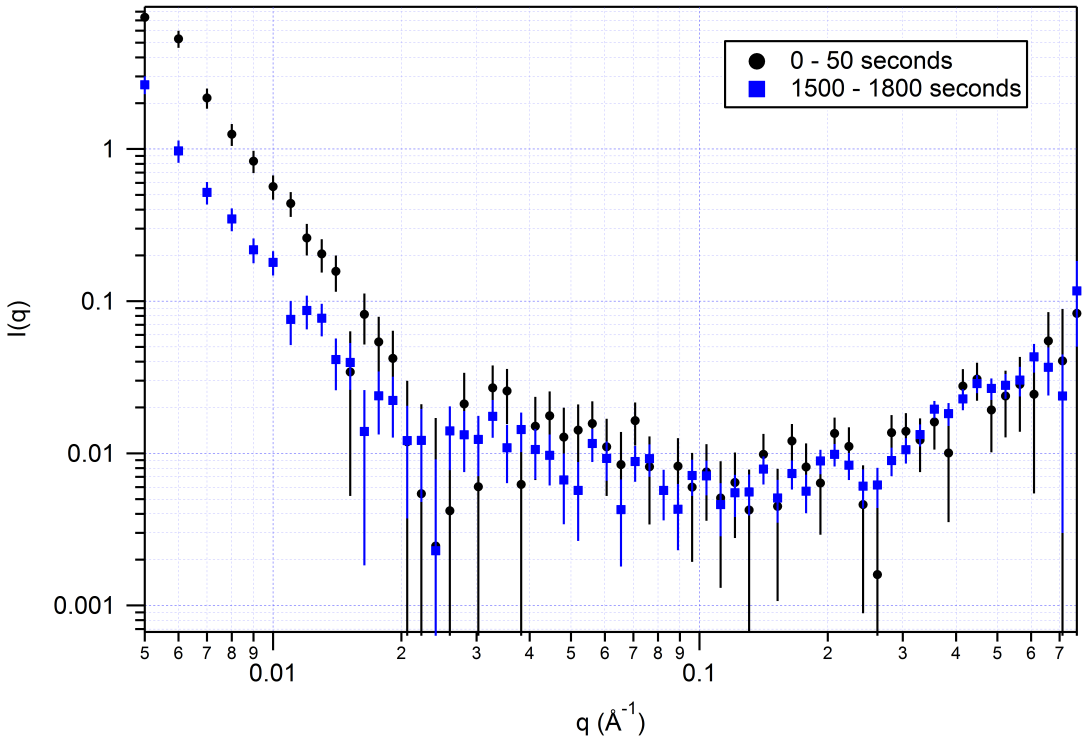

(d) 25 kDa LPEI 20:1 Complex in 10 mM NaCl

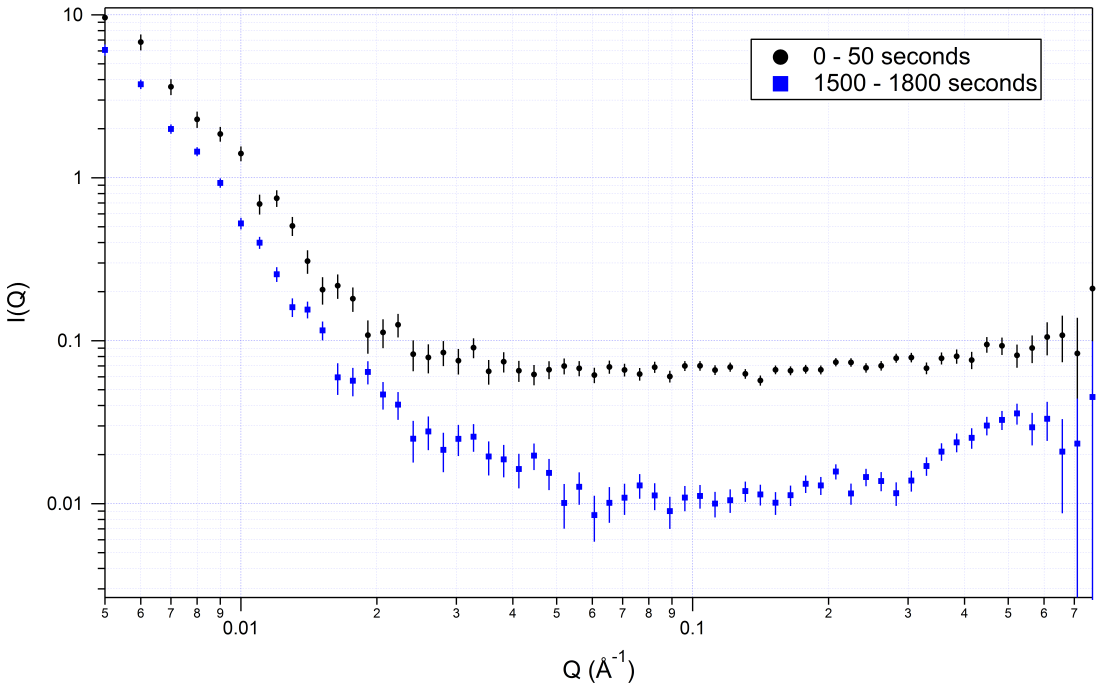

Figure 4.19: Continued:Porod plots of log(I) vs. log (Q) of time-sliced SANS data from complexes of large linear and branched PEI with DNA fragments in pH 7.4 10 mM NaCl in D_2O with DNA concentration of 1.5 mg/ml at charge ratios of N\P = 20:1 and 10:1 ; Legends indicate charge ratio and polymer type.

(a) 25 kDa BPEI 10:1 Complex in 10 mM NaCl

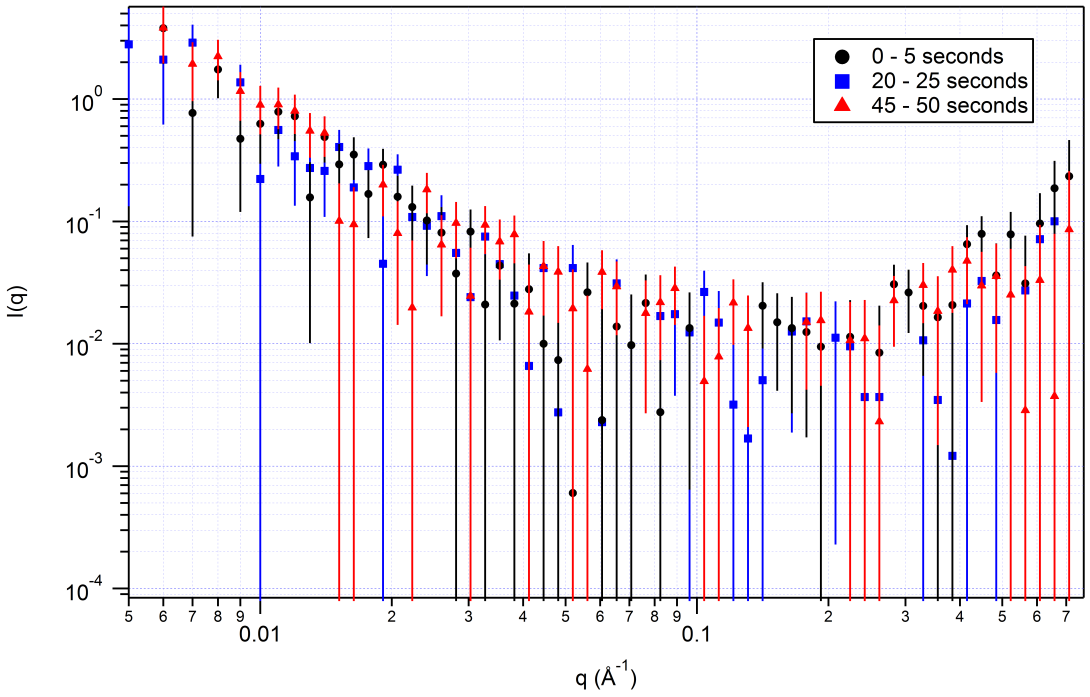

(b) 25 kDa BPEI 20:1 Complex in 10 mM NaCl

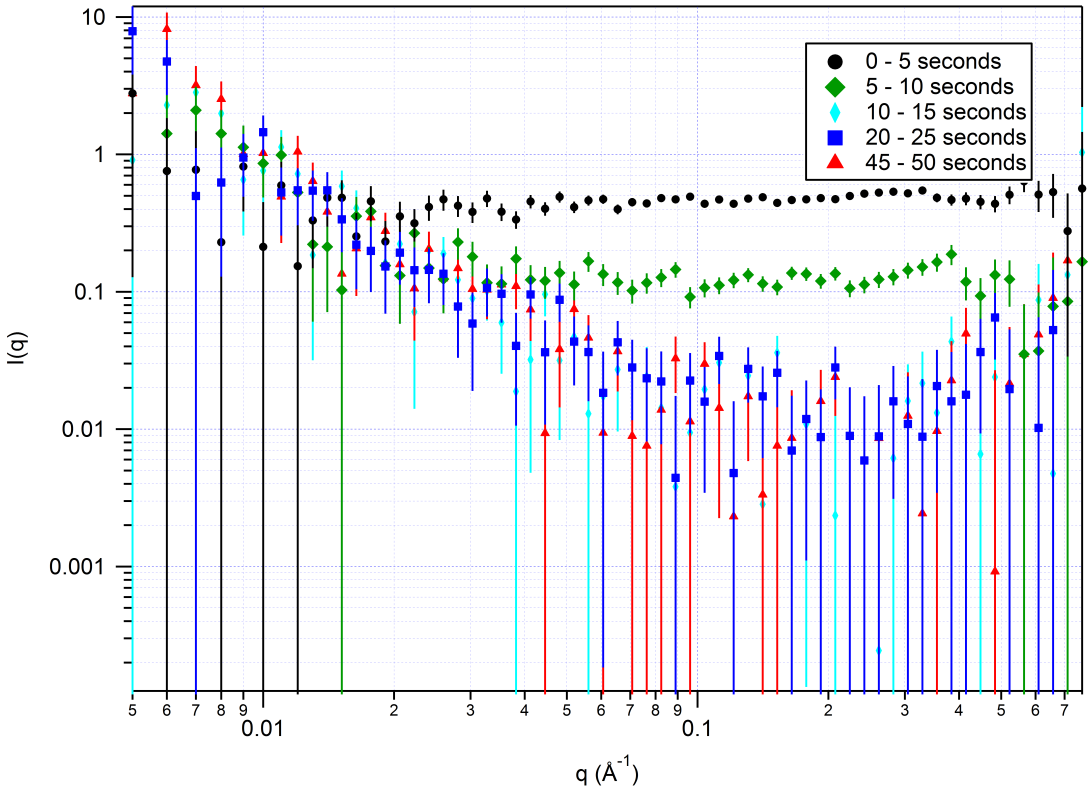

Figure 4.20: Porod plots of log(I) vs. log (Q) of time-sliced SANS data during the first 50 seconds after mixing for complexes of large linear and branched PEI with DNA fragments in pH 7.4 10 mM NaCl in D_2O with DNA concentration of 1.5 mg/ml at charge ratios of N\P = 20:1 and 10:1 ; Legends indicate age of complexes after mixing. Continued below.

(c) 25 kDa LPEI 10:1 Complex in 10 mM NaCl

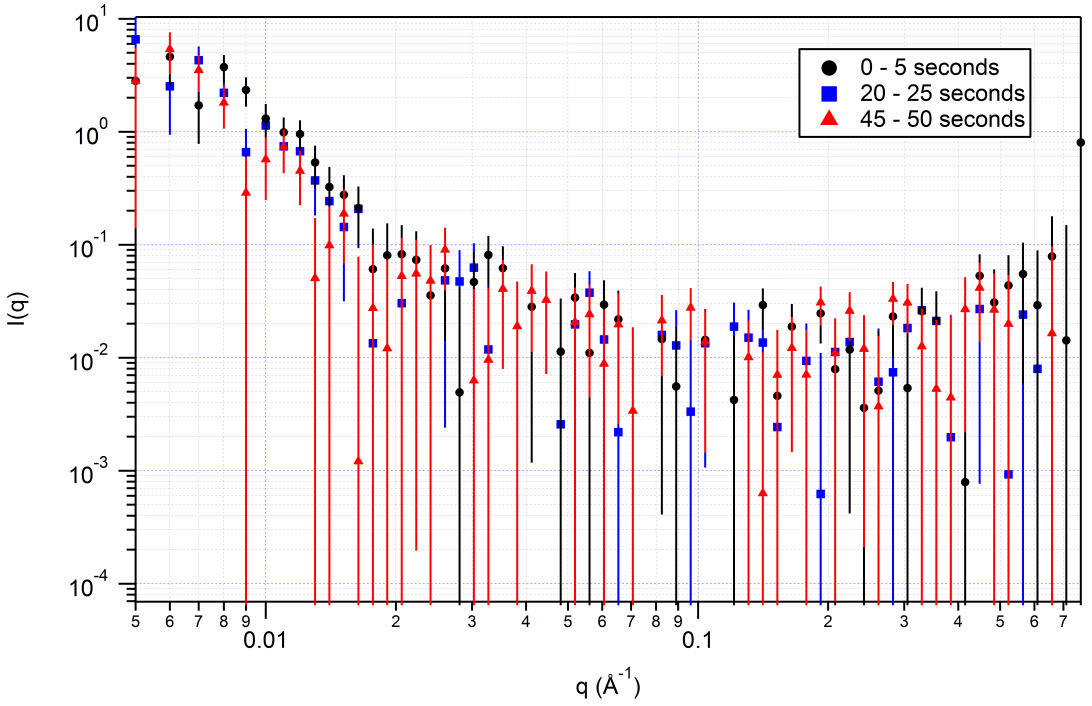

(d) 25 kDa LPEI 20:1 Complex in 10 mM NaCl

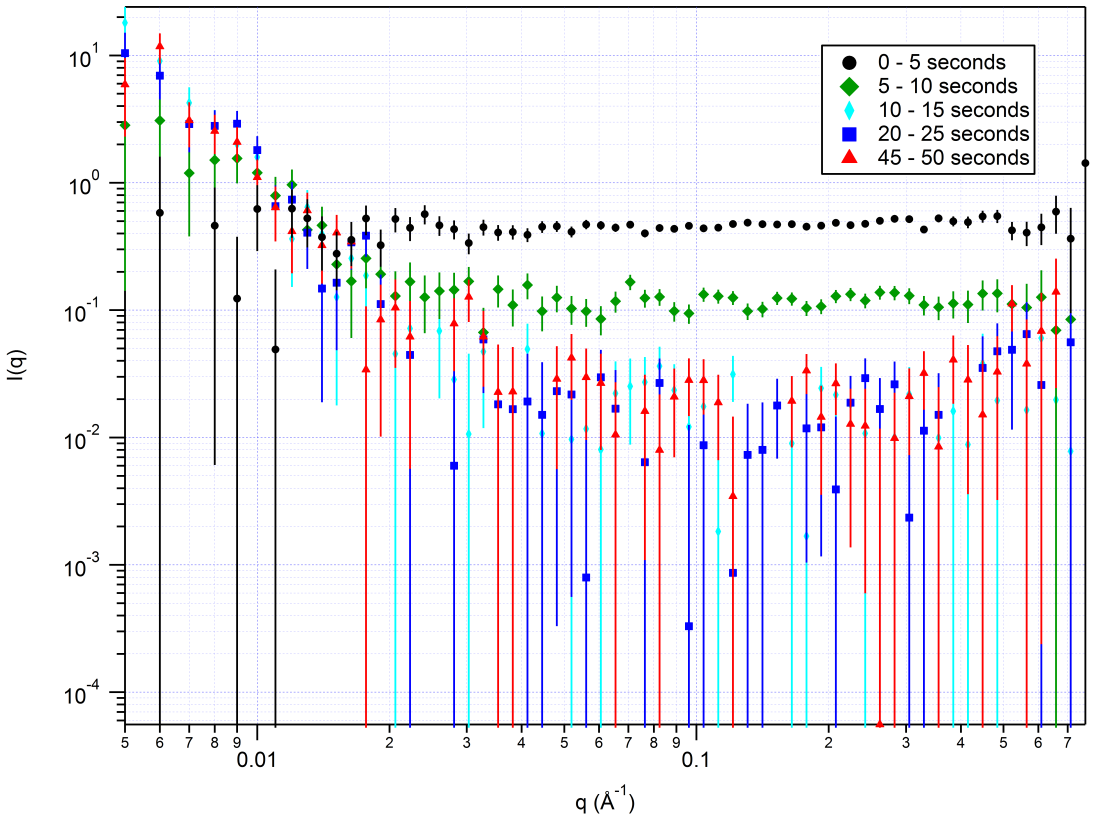

Figure 4.20: Continued: Porod plots of log(I) vs. log (Q) of time-sliced SANS data during the first 50 seconds after mixing for complexes of large linear and branched PEI with DNA fragments in pH 7.4 10 mM NaCl in D_2O with DNA concentration of 1.5 mg/ml at charge ratios of N\P = 20:1 and 10:1 ; Legends indicate age of complexes after mixing.

(a) Model parameters for the cylindrical structures fit to early time, time-resolved SANS data from complexes of 25 kDa LPEI with DNA fragments at a charge ratio of 20:1 in 10 mM NaCl in D_2O at pH 7.4

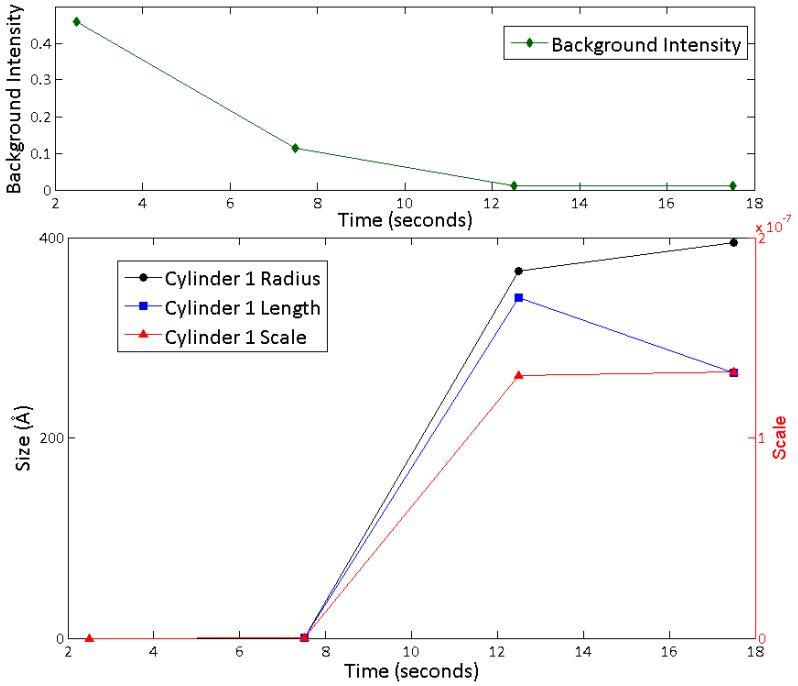

(b) Model parameters for the cylindrical structures fit to early time, time-resolved SANS data from complexes of 25 kDa LPEI with DNA fragments at a charge ratio of 20:1 in 10 mM NaCl in D_2O at pH 7.4

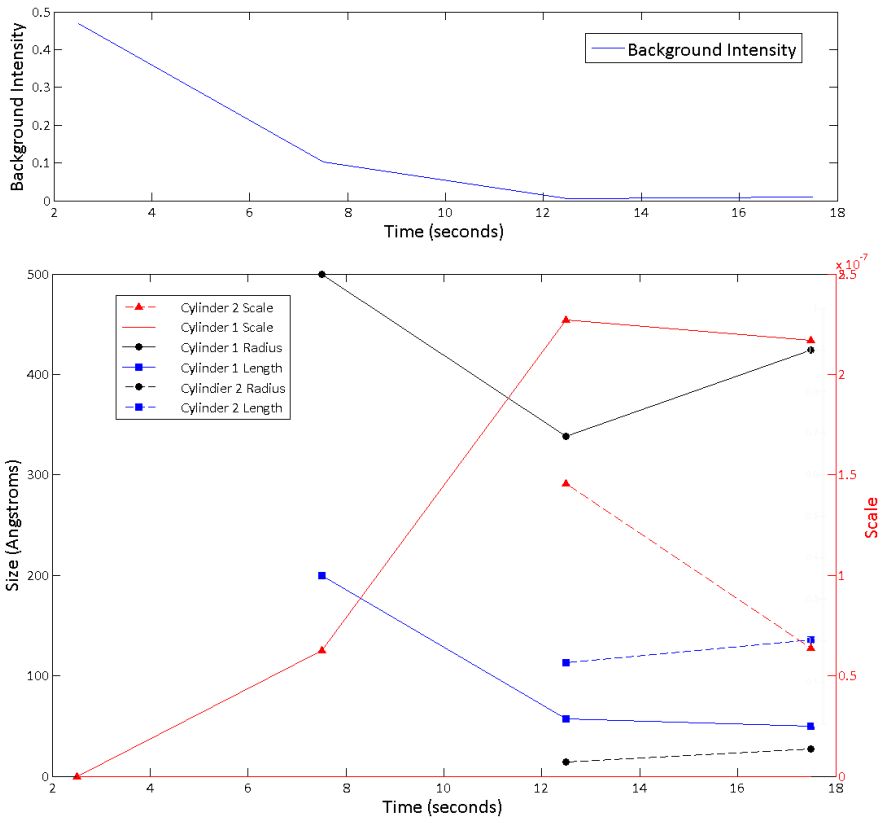

Figure 4.21: Time evolution of model parameters fit to time-sliced SANS data at early times for complexes of large, linear and branched PEI with DNA fragments at charge ratios of N\P = 20:1 in pH 7.4 10 mM NaCl in D_2O with a DNA concentration of 1.5 mg/ml; Legends indicate model fit parameter.

(a) Model parameters for the first of a mixture of twocylindrical structures fit to time-resolved SANS data from complexes of 25 kDa BPEI with DNA fragments at a charge ratio of 20:1 in 10 mM NaCl in D_2O at pH 7.4

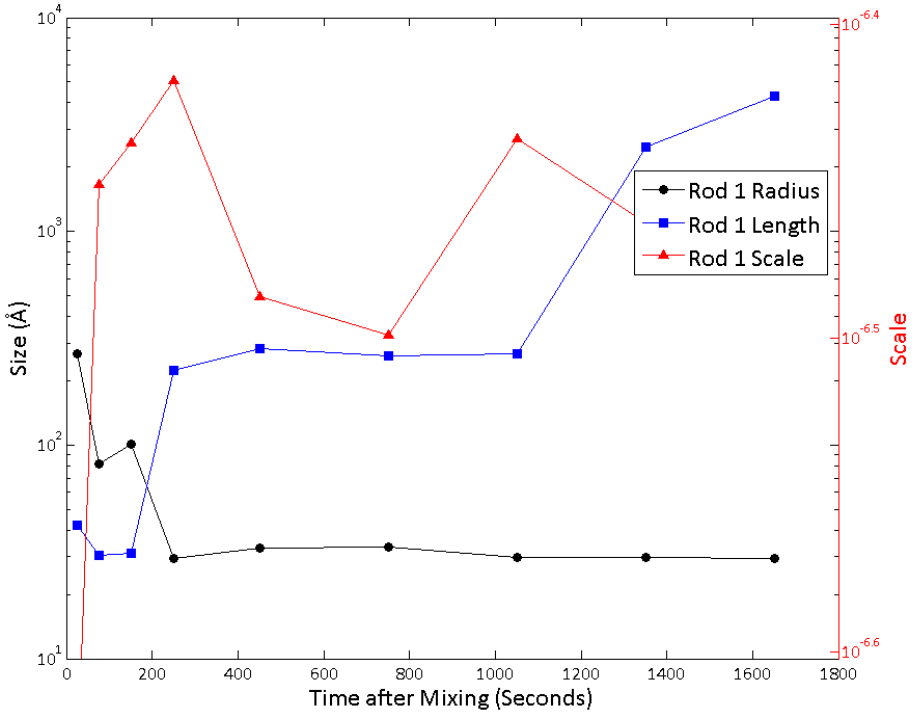

(b) Model parameters for the second of a mixture of two cylindrical structures fit to time-resolved SANS data from complexes of 25 kDa BPEI with DNA fragments at a charge ratio of 20:1 in 10 mM NaClin D_2O at pH 7.4

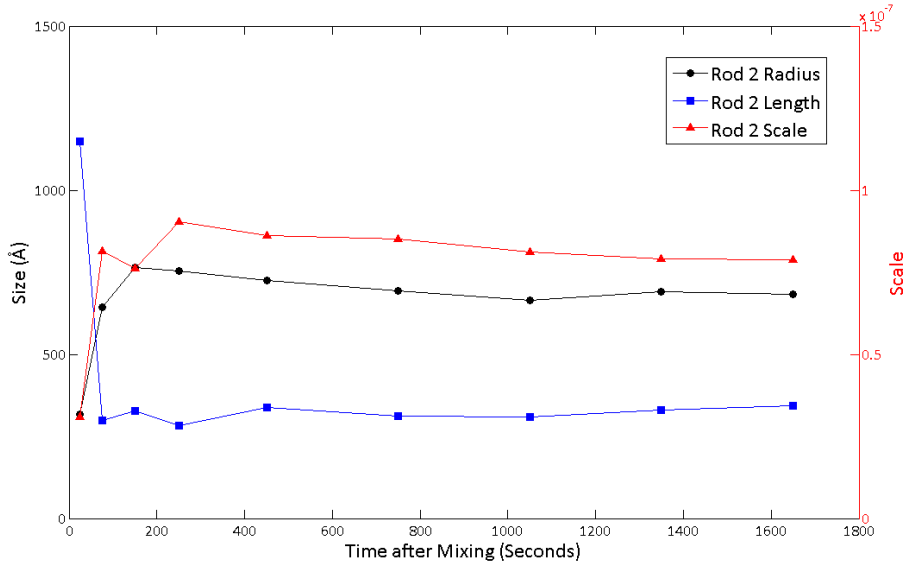

Figure 4.22: Variation of model parameters fit to time-sliced SANS data with time for complexes of large, linear and branched PEI with DNA fragments at charge ratios of N\P = 20:1 and 10:1 in pH 7.4 10 mM NaCl in D_2O with a DNA concentration of 1.5 mg/ml; Legends indicate model fit parameter; Continued below.

(c) Model parameters for the cylindrical structure fit to time-resolved SANS data from complexes of 25 kDa LPEI with DNA fragments at a charge ratio of 10:1 in 10 mM NaCl in D_2O at pH 7.4

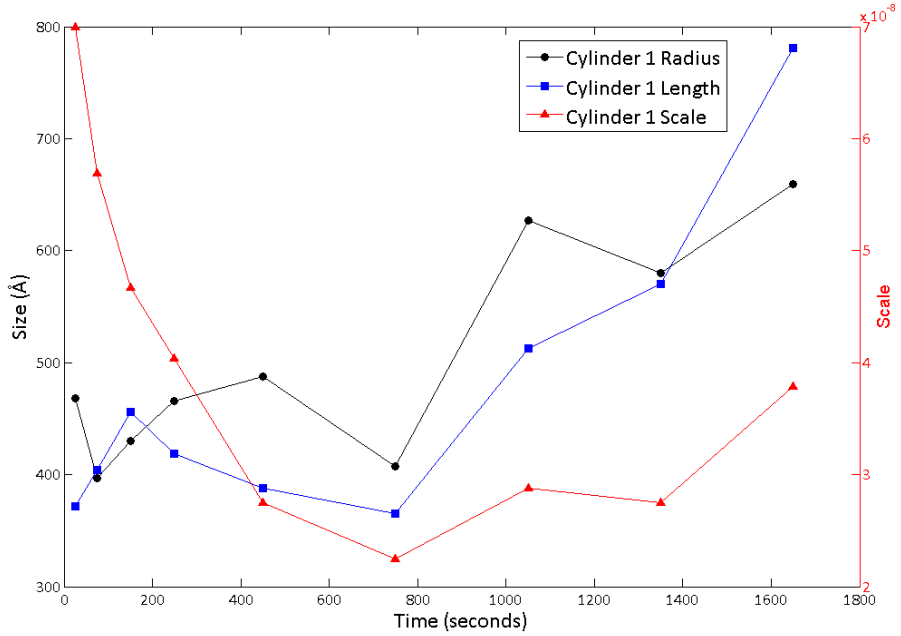

(d) Model parameters for the cylindrical structure fit to time-resolved SANS data from complexes of 25 kDa LPEI with DNA fragments at a charge ratio of 20:1 in 10 mM NaCl in D_2O at pH 7.4

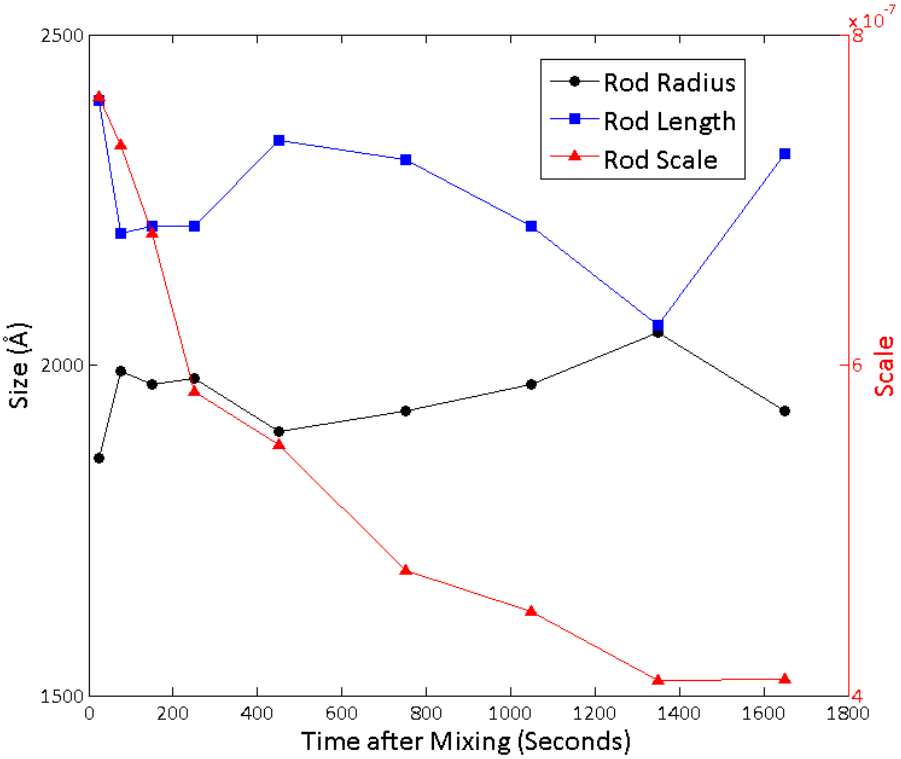

Figure 4.22: Continued: Variation of model parameters fit to time-sliced SANS data with time for complexes of large, linear and branched PEI with DNA fragments at charge ratios of N\P = 20:1 and 10:1 in pH 7.4 10 mM NaCl in D_2O with a DNA concentration of 1.5 mg/ml; Legends indicate model fit parameter.

Table 4.17: Time-evolution of model parameters fit to time-sliced SANS data at early times for complexes of large, linear and branched PEI at a charge ratio of N\P = 20:1 with DNA fragments in pH 7.4 10 mM NaCl in D_2O with DNA concentration of 1.5 mg/ml.

			Cylinder 1			Background Intensity	Cylinder 2		
Polymer Type	Charge Ratio (NnP)	Time After Mixing (Seconds)	$Scale_1$	$Radius_1$ (Å)	$Length_1$ (Å)	Background Intensity	$Scale_2$	$Radius_2$ (Å)	$Length_2$ (Å)
LPEI 25 kDa	20:1	0 - 5	0.00E+00	n/a	n/a	4.60E-01	—	—	—
		5 - 10	1.34E-10	3.93E-01	6.28E-01	1.14E-01	—	—	—
		10 - 15	1.31E-07	3.67E+02	3.40E+02	1.03E-02	—	—	—
		15 - 20	1.33E-07	3.95E+02	2.65E+02	1.14E-02	—	—	—
BPEI 25 kDa	10:1	0 - 5	0.00E+00	n/a	n/a	4.69E-01	—	—	—
		5 - 10	6.27E-08	5.00E+02	2.00E+02	1.03E-01	—	—	—
		10 - 15	2.27E-07	3.38E+02	5.75E+01	5.91E-03	2.91E-07	1.44E+01	1.13E+02
		15 - 20	2.17E-07	4.24E+02	4.99E+01	9.22E-03	1.28E-07	2.73E+01	1.36E+02

Table 4.18: Variation of model parameters fit to time-sliced SANS data with time for complexes of large, linear and branched PEI at charge ratios of N\P = 10:1 and 20:1 with DNA fragments in pH 7.4 10 mM NaCl in D_2O with DNA concentration of 1.5 mg/ml.

			Cylinder 1			Cylinder 2			Kholodenko Worm-like Chain			
Polymer Type	Charge Ratio (N\P)	Time After Mixing (Seconds)	$Scale_1$	$Radius_1$ (Å)	$Length_1$ (Å)	$Scale_2$	$Radius_2$ (Å)	$Length_2$ (Å)	$Scale_K$	n*	L (Å)	$R_a x$ (Å)
BPEI 25 kDa	10:1	0 - 50	—	—	—	—	—	—	6.96E-08	3.56E+03	6.57E+01	3.99E+01
		1500 - 1800	—	—	—	—	—	—	6.49E-08	5.25E+03	3.20E+01	2.65E+01
BPEI 25 kDa	20:1	0 - 50	2.32E-07	2.67E+02	4.22E+01	3.09E-08	3.17E+02	1.15E+03	—	—	—	—
		1500 - 1800	3.50E-07	2.96E+01	4.30E+03	7.87E-08	6.84E+02	3.43E+02	—	—	—	—
LPEI 25 kDa	10:1	0 - 50	7.00E-08	4.68E+02	3.72E+02	—	—	—	—	—	—	—
		1500 - 1800	3.79E-08	6.59E+02	7.81E+02	—	—	—	—	—	—	—
LPEI 25 kDa	20:1	0 - 50	7.62E-07	1.86E+03	2.40E+03	—	—	—	—	—	—	—
		1500 - 1800	4.10E-07	1.93E+03	2.32E+03	—	—	—	—	—	—	—

After observing this difference, it was thought necessary to investigate this substantial change further by taking new, shorter time-slices of the scattering data for these four polymer complex compositions, which are presented in Figure 4.20. Here, the data is sliced in 5 second intervals from 0 to 50 seconds after mixing. This is clearly too short an interval to produce good statistics and signal to noise ratio in normal circumstances, but for the purposes of investigating this particular effect, some clear trends can be seen, despite the large error bars.

As expected, at 10:1, both BPEI and LPEI complexes change relatively little over the first 50 seconds. However, it can be seen that at 20:1, the intermediate to high Q scattering is elevated with relatively little defined scattering structure at low Q in the first five-second

interval. From 5 to 10 seconds, the high Q scattering has fallen off and some upturn is starting to emerge at low Q and by the 10 to 15 second period, the low Q upturn feature observed at later times has appeared, with the high Q scattering having fallen completely to its late-time level.

This interesting phenomenon suggests that, as PEI-DNA complex aggregation is driven hydrophobically, with the surface charge of the complexes counteracting the tendency to aggregate, the increased presence of cationic polymer by doubling of the N\P ratio from 10:1 to 20:1, while maintaining the same, lower DNA mixing concentration of 1.5 mg/ml, slows the aggregation sufficiently to enable observation of the emergence of the large aggregates at low Q.

The question remains, however, as to why a lack of structure, but uniform, elevated background is observed at high Q. The stage of complexation which sees the DNA and polymer molecules initially bound may result in relatively flat scattering at high Q, in the same way as observed in the static, averaged scattering. The elevated background means that features which might be observed in a significant way on a logarithmic plot when the background level was low, would be masked at this higher level, but would still be likely to exist.

Solvent Media

The variation of kinetics between complexes of high MW BPEI and LPEI in a variety of solvent media was investigated. As SANS was undertaken on complexes in D_2O mainly for the purposes of a a static structural reference, time-sliced data are included but suffer from a much lower signal-to-noise ratio as the repetition and summation conducted for samples intended primarily for kinetic study was not undertaken for these. Consequently, the overall scattering form and Porod behaviour is still observable, but the error bars for time-sliced data are prohibitively large to elucidate nuanced structural evolutions with time in these complexes.

Overall, very little difference is evident for high MW PEI complexes of either type at a charge ratio of 10:1 in the different solvent media. In glucose, BPEI complexes exhibit a steeper low-Q Porod region with a more pronounced dip and smaller secondary peak at lower Q, at both early and late times, which appears to resemble the early time structure visible in the scattering curve in BPEI complexes in 10 mM NaCl, but which becomes

(a) 25 kDa BPEI 10:1 Complex in D_2O

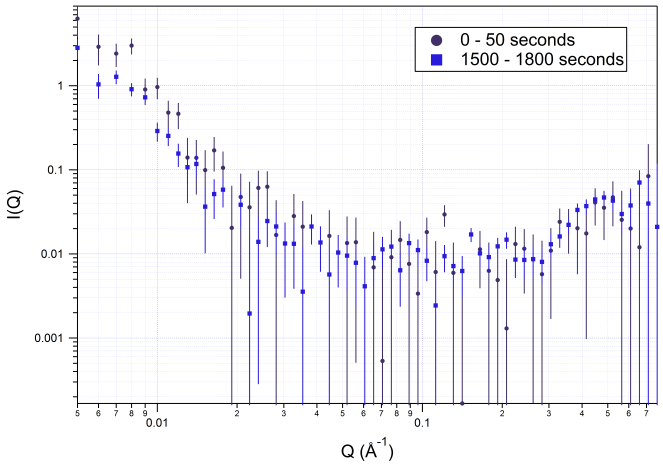

(b) 25 kDa BPEI 10:1 Complex in D_2O

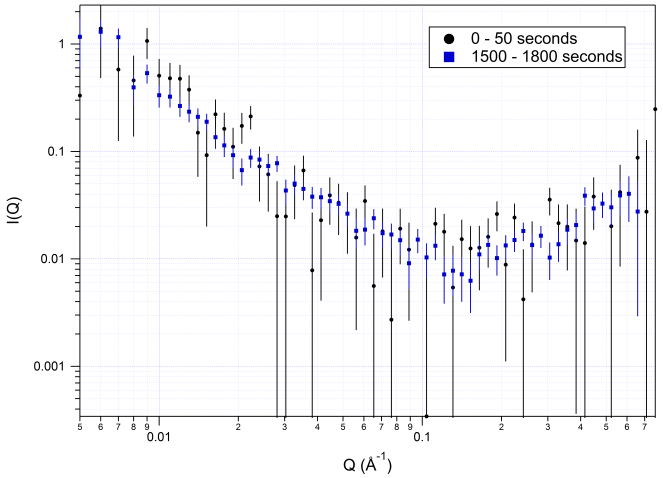

(c) 25 kDa LPEI 10:1 Complex in 10 mM NaCl in D_2O

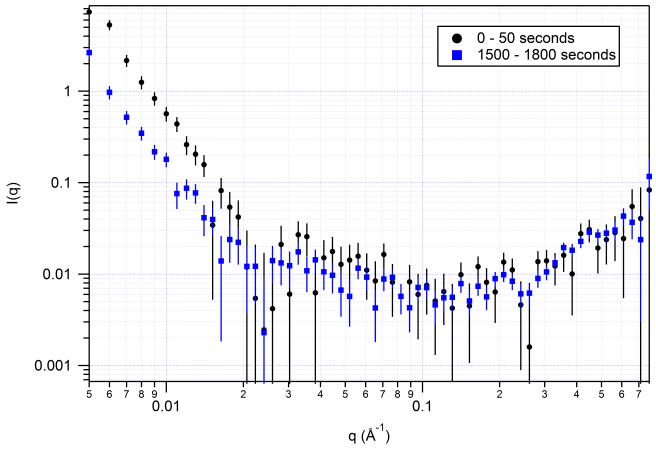

Figure 4.23: Porod plots of log(I) vs. log (Q) of time-sliced SANS data from complexes of large linear and branched PEI with DNA fragments in a range of solvent media at pH 7.4 with a DNA concentration of 1.5 mg/ml at a charge ratios of N\P = 10:1 ; Legends indicate solvent and polymer type. Continued below.

(d) 25 kDa BPEI 10:1 Complex in 10 mM NaCl in D_2O

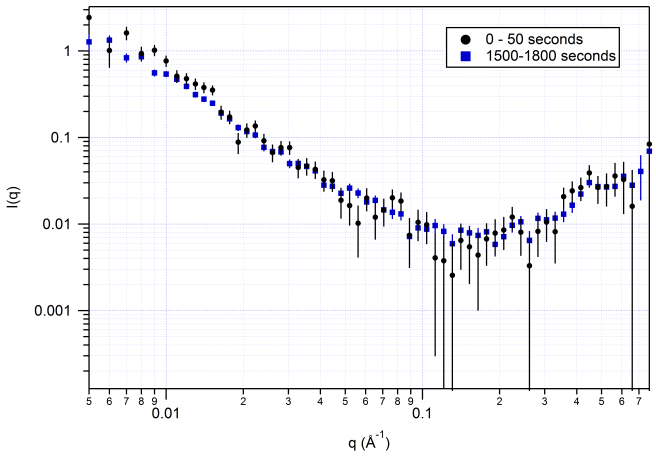

(e) 25 kDa LPEI 10:1 Complex in 5%w\v Glucose in D_2O

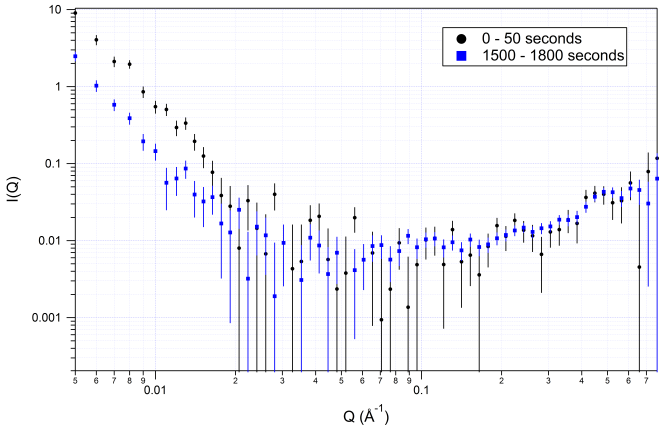

(f) 25 kDa LPEI 10:1 Complex in 5%w\v Glucose in D_2O

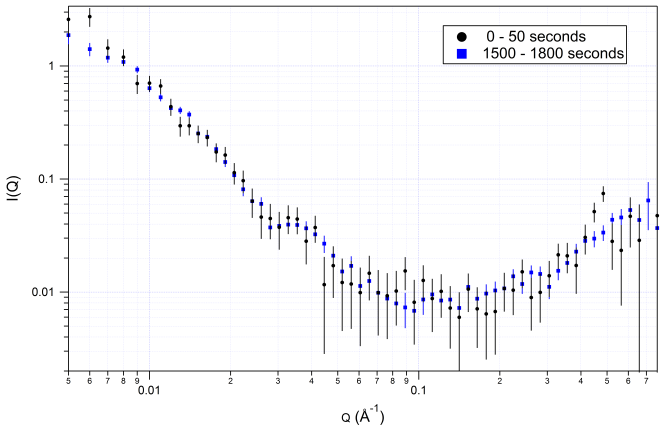

Figure 4.23: Continued:Porod plots of log(I) vs. log (Q) of time-sliced SANS data from complexes of large linear and branched PEI with DNA fragments in a range of solvent media at pH 7.4 with a DNA concentration of 1.5 mg/ml at a charge ratios of N\P = 10:1 ; Legends indicate solvent and polymer type.

(a) Model parameters for the cylindrical structures fit to time-resolved SANS data from complexes of 25 kDa LPEI with DNA fragments at a charge ratio of 10:1 in 10 mM NaCl in D_2O at pH 7.4

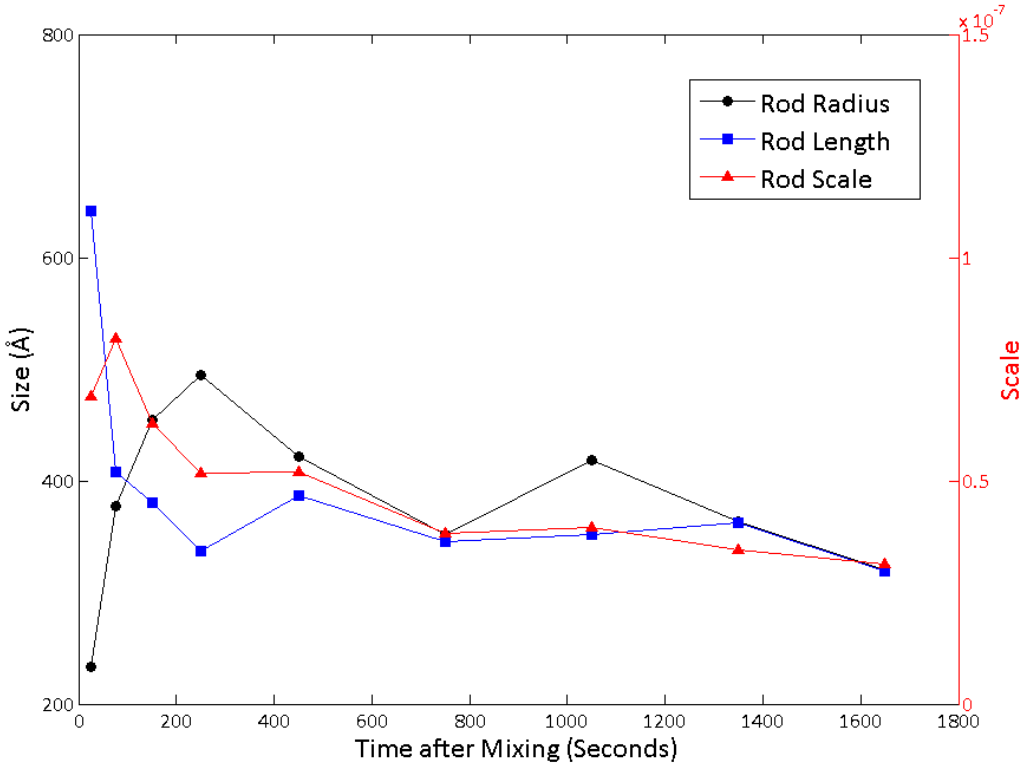

(b) Model parameters for the cylindrical structures fit to time-resolved SANS data from complexes of 25 kDa BPEI with DNA fragments at a charge ratio of 10:1 in 10 mM NaCl in D_2O at pH 7.4

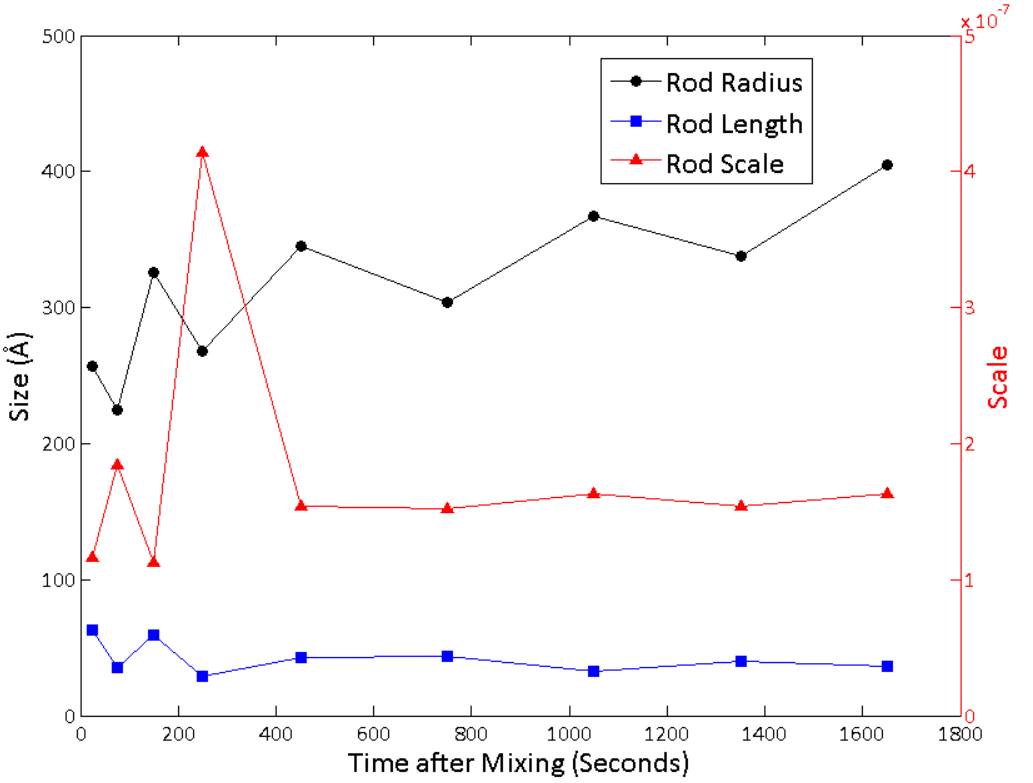

Figure 4.24: Variation of model parameters fit to time-sliced SANS data with time for complexes of large, linear and branched PEI with DNA fragments at charge ratios of N\P = 10:1 in various solvent media at pH 7.4 with a DNA concentration of 1.5 mg/ml; Legends indicate model fit parameter; Continued below.

(c) Model parameters for the cylindrical structure fit to time-resolved SANS data from complexes of 25 kDa LPEI with DNA fragments at a charge ratio of 10:1 in 10 mM NaCl in D_2O at pH 7.4

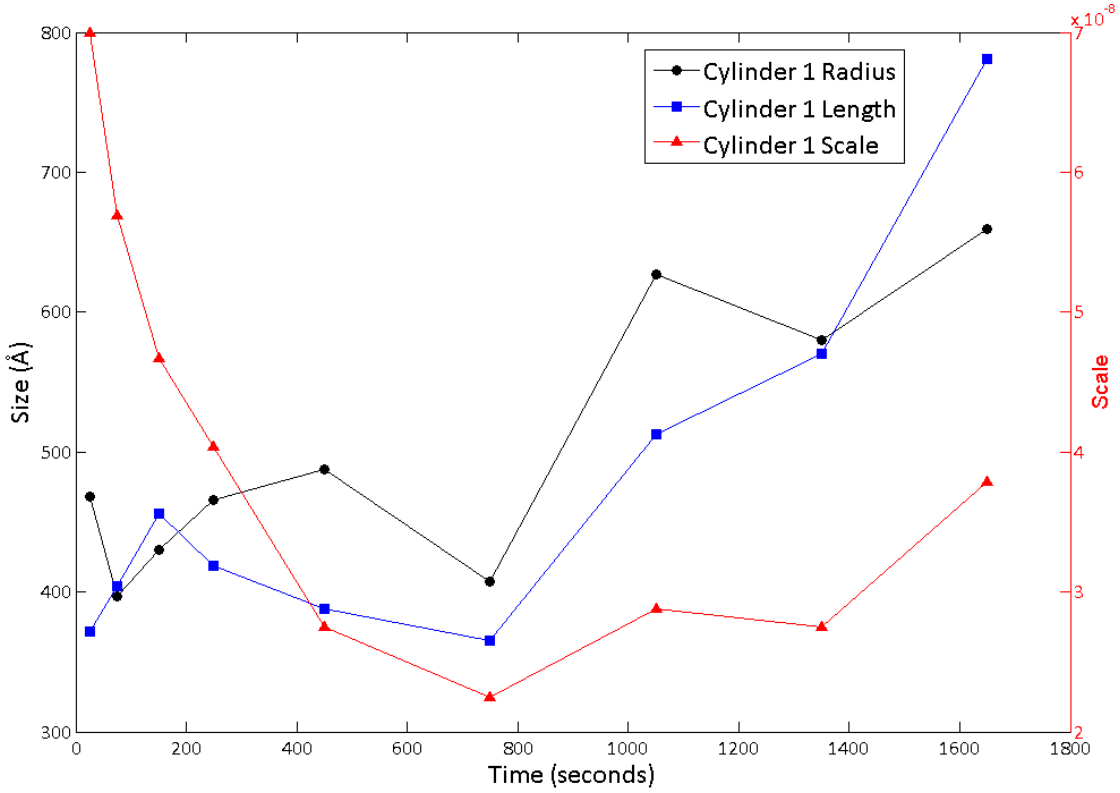

(d) Model parameters for the cylindrical structures fit to time-resolved SANS data from complexes of 25 kDa LPEI with DNA fragments at a charge ratio of 10:1 in 5%w\ Glucose in D_2O at pH 7.4

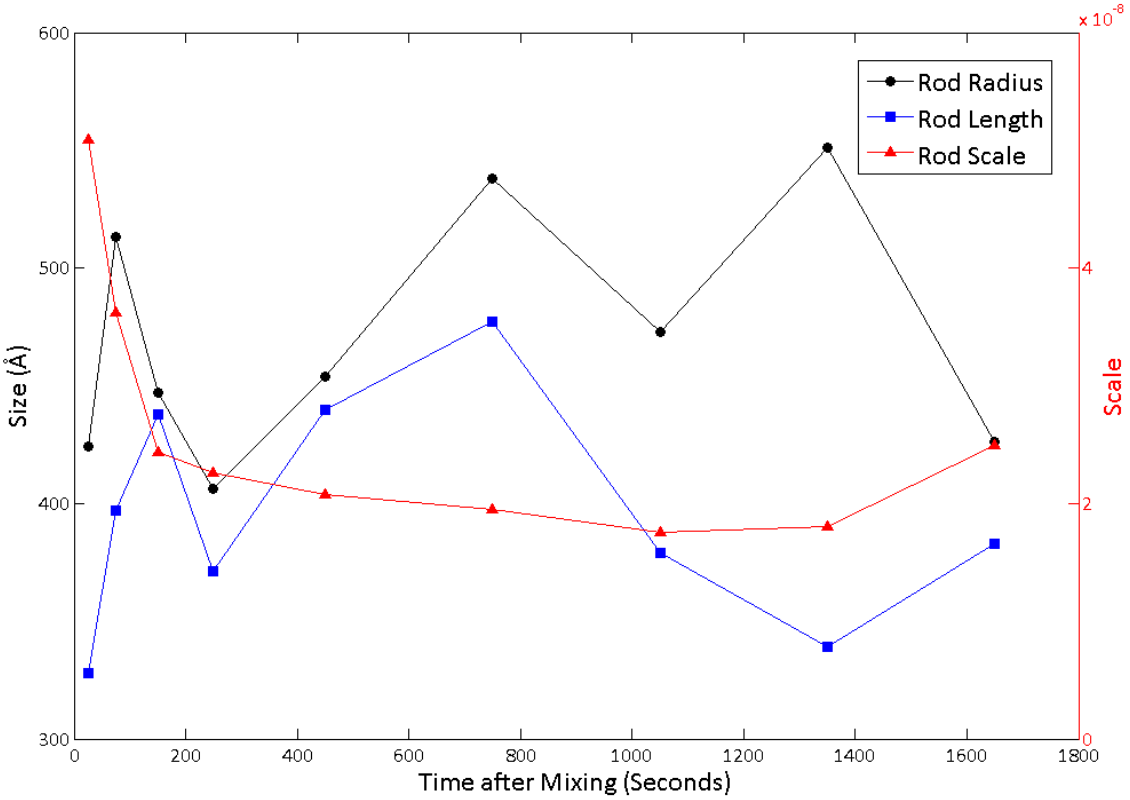

Figure 4.24: Continued: Variation of model parameters fit to time-sliced SANS data with time for complexes of large, linear and branched PEI with DNA fragments at charge ratios of N\P = 10:1 in various solvent media at pH 7.4 with a DNA concentration of 1.5 mg/ml; Legends indicate model fit parameter.

Table 4.19: Variation of model parameters fit to time-sliced SANS data with time for complexes of large, linear and branched PEI at a charge ratios of N\P = 10:1 with DNA fragments in various solvent media at pH 7.4 with DNA concentration of 1.5 mg/ml.

			Cylinder 1			Cylinder 2			Kholodenko Worm-like Chain			
Polymer Type	Solvent Type (N\P)	Time After Mixing (Seconds)	$Scale_1$	$Radius_1$ (Å)	$Length_1$ (Å)	$Scale_2$	$Radius_2$ (Å)	$Length_2$ (Å)	$Scale_K$	n*	L (Å)	R_ax (Å)
BPEI 25 kDa	D_2O	0 - 50	1.16E-07	257	63	—	—	—	—	—	—	—
		1500 - 1800	1.63E-07	405	37	—	—	—	—	—	—	—
LPEI 25 kDa	D_2O	0 - 50	6.89E-08	233	642	—	—	—	—	—	—	—
		1500 - 1800	3.14E-08	320	319	—	—	—	—	—	—	—
BPEI 25 kDa	10 mM NaCl in D_2O	0 - 50	—	—	—	—	—	—	6.96E-08	3556	66	40
		1500 - 1800	—	—	—	—	—	—	6.49E-08	5250	32	26
LPEI 25 kDa	10 mM NaCl in D_2O	0 - 50	7.00E-08	468	372	—	—	—	—	—	—	—
		1500 - 1800	3.79E-08	659	781	—	—	—	—	—	—	—
BPEI 25 kDa	5% w/v Glucose in D_2O	0 - 50	—	—	—	—	—	—	5.81E-08	1700	85	54
		1500 - 1800	—	—	—	—	—	—	5.39E-08	204	81	50
LPEI 25 kDa	5% w/v Glucose in D_2O	0 - 50	7.11E-08	424	328	—	—	—	—	—	—	—
		1500 - 1800	1.54E-08	426	383	—	—	—	—	—	—	—

smoothed out at later times under those solution conditions, indicating that some degree of structural change may occur in the presence of 5% glucose. Additionally, the low-Q Porod region continues fairly linearly to meet the flat background at a higher Q value in 10 mM NaCl than in 5% glucose, where a more curved structure gives way to flat background sooner, below 0.1 $\mathring{A}^{-1}$. Whether the glucose molecules themselves contribute directly through participation in complex formation with a change in structure and scattering pattern, or indirectly through stabilisation of the complexes, is uncertain, however it seems likely that glucose is involved to some degree in complexation directly.

For LPEI complexes at 10:1 in glucose, they again appear to exhibit a slight bump at low to mid Q at early times in 5% glucose compared to late times or complexes formed in 10mM NaCl. This is very slight in comparison to the errors, however, and overall the shape of scattering remains similar. Complexes formed in pure D_2O appear, despite their lower signal-to-noise level, to change less than those in 10 mM NaCl, or indeed in glucose over the measured time, indicating perhaps the absence of salt or other factors altogether leads to greater complex stability but also perhaps, as suggested previously, reduced capacity for polyelectrolyte binding. Ankerfors [6] describes how reversibility of binding and rearrangement is suppressed in polyelectrolyte complexes in the absence of any salt. They also imply that some degree of salt provides sufficient screening to enable the polyelectrolytes to aquire a higher degree of flexibility and bending. This may, hence, provide potentially greater binding capacity, which may result in complexes with lower net charge and more prone to agggregation, while progression to media of greater

ionic strength strongly promotes aggregation. It should also be noted that increasing ionic strength of the media screens intermolecular repulsion between polyelectrolyte chains within an aggregate.

However, it could be that under conditions of physiological ionic strength experienced during transfection, the presence of glucose provides some protection against catastrophic aggregation, as occurs with complexes in 150 mM NaCl, so this does not necessarily mean this would lead to the greatest stability overall of complexes when applied in transfection.

FISH modelling of complexes in the three media studied indicates that BPEI complexes' chains become slightly less rigid with time after mixing, possibly indicating progressively greater compaction of the complexes following binding, and associated bending of the polymer, as reversibility of binding and two stage rearrangement has been shown to occur in polyelectrolyte - nucleic acid complexes, dependent to an extent on the presence of some degree of salt [6] . However, the stability of the complexes with time is reinforced, as no significant change in scale factor was found. In glucose, however, the persistence lengths remain constant, and, although the number of segments appears to increase, this corresponds to large end-to-end length scales which are not accurately measured in the available Q-range so are, as discussed above 4.3.1, presented as fit although it is accepted that a considerable degree of uncertainty is associated with large lengths.

As expected, the change in scale factors for LPEI complexes in all media far exceeded the change in those of BPEI complexes, indicating the loss of scattering material from solution. The evolution of parameters fit to LPEI complexes is shown in Figure 4.24. While radius and scale factor for LPEI in D_2O decrease gradually, radius is seen to initially increase and then gradually fall again. In pure D_2O, kinetic BPEI complex data were fit as a single, ellipsoidal cylinder. Scale factor for BPEI complexes in D_2O are shown to remain relatively constant, as expected,but the radius of the complexes gradually increases over time, while the length gradually falls. The proportions of this rod make it oblate, close to lamellar, rather than cylindrical or prolate and it may be viewed more as a globular ellipsoid of chains, as BPEI complexes adopt this structure, but the resolution of the unrepeated data in pure D_2O was not sufficient to distinguish greater detail in the structure.

Time-sliced SANS data from 25 kDa LPEI complexes in 10 mM NaCl were fit by a single cylinder model, as the penalty for increasing temporal resolution in the time-sliced data is the loss of signal-to-noise strength, hence a slightly less nuanced structure than the combined, mixture of cylinders fit to static data was used, but which nonetheless enabled

study of evolution and comparison with similar complexes in other solvent media.

4.4.3 Conclusion - Principal Findings and Their Relevance

PEI is a commonly and successfully used transfection agent. In the literature, DLS, AFM or other sizing techniques have been frequently used to characterise the complexes formed between PEI and DNA or RNA. However, these tend to be limited to an overall size. AFM measurements can provide some further insight to the overal morphology, but interaction with the substrate can influence the outcome and it is, again, more suited to broad overall size measurements than detailed structure.

In this study, PEI complexes formed with DNA under various conditions were investigated on both a static and kinetic basis to explore the time evolution of the structure.

The use of multiple complementary analytical techniques to investigate the combination of static and kinetic data allowed a detailed picture of the system under study to be built.

Broadly, the conclusions from this study highlight the relative stability of high MW BPEI complexes with DNA, forming loose networks of chains, in contrast to low MW PEI or high MW LPEI complexes, which form large aggregates, in the case of LPEI, composed of rod-like constituent parts.

The DNA fragments used in this work are similar structurally to siRNA molecules, which have wide application for transfection, which enables these findings to be related to useful siRNA transfection systems.

The main findings from this study of the structural evolution of complexes formed between PEI and DNA are outlined and discussed below, with reference to their relevance in the broader field of understanding and application of these transfection complexes to the field of gene delivery.

Static structure

Static SANS studies on the complexes of linear and branched, high and low MW PEI cationic polymers with DNA fragments highlighted the broad difference that high MW BPEI forms large complexes which appear to be made of a network of gaussian chains, while LPEI of both sizes, and indeed low MW BPEI forms large, smooth aggregated complexes under the low ionic strength conditions around neutral pH used here, at a charge ratio of 10:1. The most severe cases of aggregation concerned low MW PEIs of

both architectures, which tended to form aggregates so large the SANS scattering signal was substantially reduced, thought to be due to the aggregation of the samples beyond the size limit accessible in the SANS setup. s

The effect of mixing N/P charge ratio was investigated for high MW BPEI and LPEI at 10:1 and 20:1 on SANS2D, which afforded an extended Q range, and high MW BPEI only on LOQ with N/P ranging from 2:1 to 20:1. At the higher charge ratio of 20:1 on SANS2D, an increasingly pronounced peak at mid-Q can be seen, which is suspected to be due to excess free polymer, particularly in the case of high MW BPEI, which is present above N\P = 2 according to some studies discussed earlier, (see Section 4.1.4), but becomes more clearly visible at high charge ratios for high MW BPEI, as can be seen by comparison with the region of predominant scattering from pure PEIs scattering. There are questions, however, as to the extent to which some DNA is bound to these excess polymers, particularly in the case of SANS2D mixing. It also appears that aggregation, as indicated by strong scattering at the lowest Q values, is suppressed as charge ratio increases, while increasing the charge ratio for high MW LPEI increased scattering intensity evenly across the Q range, suggesting little structural difference, except for perhaps the strength of binding and tightness of the complexes, but rather an effective increase in complexes similar to those existing at lower charge ratios.

LOQ studies extended the N/P ratio study to lower charge ratios of 2:1 and 5:1 for high MW BPEI, and the transition from 20:1 down to 2:1 resulted in progressive enlarging and aggregating of the complex structure, with a transition from losse swollen or Gaussian chains at 20:1, to a network of chains at 10:1 as electrostatic repulsion decreases, with the appearance of large, albeit rough aggregates or dense Gaussian chain networks at 5:1 and only dense networks with substantially reduced scattering intensity by 2:1, the expected point of overall neutrality, due to aggregation beyond the accessible size range.

The effect of doubling of component concentrations was not to increase the scattering intensity proportionately, as might be expected, but rather only to produce a slight increase in intensity. This may partly be due to the increased aggregation potential at higher concentrations, leading to a reduced density of particles scattering within the required Q-regime. Additionally, differences in the mixing methods between the two concentration levels studied which were conducted on SANS2D with stopped-flow turbulent injection mixing and LOQ beamlines, where samples were mixed in bulk by pipette addition of DNA solutions to polymer, which uneven mixing could lead to greater instability in the

case of LOQ, again contributing to the scattered intensity being lower than expected.

The effects of different solvent conditions were investigated, comparing samples prepared in pure D_2O, 10 mM NaCl in D_2O and 5% glucose in D_2O at pH 7.4 for high MW BPEI and LPEI complexes at a charge ratio of 10:1. Broadly, the scattering from samples in the different solvents appeared very similar, although some slight differences in the data fitting were noted. Some indication was found that a low level of salt in solutions is important for flexibility and strength of binding, in agreement with the literature. Suggestions were also noted that glucose may be involved directly in the binding, due to the more rounded, globular nature of the component particles in glucos-containing media, when compared to pure D_2O, and less clear fine structure at high Q. It should also be noted that glucose may have an impact on increasing the viscosity of the solution.

The range of physiological pHs likely to be encountered by gene delivery complexes on their journey from the cytosol to early and late endosomes and, potentially, lysosomes, was investigated with respect to its effect on the structure of the complexes. No significant structural effect was observable with this technique, while some slight tightening or loosening of the binding strength may occur, no broad structural changes were identified for complexes of high MW BPEI with DNA fragments, suggesting their likely stability during intra-cellular trafficking.

Kinetics and stability

The time-slicing of stopped-flow, time-resolved SANS data from complexes of PEI of different types and MWs and DNA fragments gave some insight into the change in complex structure with time after mixing. High MW BPEI complexes formed at N/P = 10:1 clearly showed superior stability in solution, wiht little noticeable change in the scattering pattern over the 30 minute period examined. High MW LPEI was less stable than high MW BPEI complexes, with low MW PEIs of either type forming the least stable complexes in 10 mM NaCl in D_2O, pH 7.4.

An interesting phenomenon of raised background level at mid- to high- Q, as well as decrease in visible structure was observed at charge ratios of 20:1, so the scattering was investigated further at shorter timescales. As can be seen from these data, the evolution took place over approximately the first 15 to 20 seconds, after which point the scattering remained stable, closely resembling 10:1 scattering. It was thought that the increase in positive charges in the complexes afforded by the excess cationic polymer available at

N/P = 20:1 causes the aggregation process to slow due to increased electrostatic repulsion. Thus, this enables visualisation of the aggregation process in a slowed format.

Complexes were also studied in different solvent media, which resulted in largely similar overall scattering. However, while glucose is thought to protect against agggregation, some degree of structural change was noted for samples prepared in 5% glucose. This could still be consistent with the ability of glucose to protect against significant aggreagtion in physiologicla media with increased ionic strength, as is likely to be encountered in transfection applications. For high MW LPEI complexes, complexes formed in D_2O appeared to be marginally less stable than those formed with a low (10 mM) concentration of NaCl. FISH modelling of all high MW BPEI identified a fall in peresistence length, consistence with gradual rearrangement and tightening of binding, leading to greater curvature of the compledxes.

SANS can provide a lot of detailed data, which must be interpreted with care and application of prior understanding of the system under investigation to ensure the most physically relevant and realistic picture possible is generated. Some features of the scattering are very clear, while others may have to be viewed in the context of other analytical techniques or prior knowledge from the literature to confirm the validity of their interpretation. In some cases, the best fitting model may not provide the most likely physical representation of the system under consideration, however, the best or one of the best fitting model options was selected wherever possible. In a time series, a consistent choice of model was preferred where more than one option existed for all time points in the series, to enable consistent comparison, unless it was found to be incompatible with a good fit to the data. However, this does require some initial understanding of the system and interpretation to be applied. However, it is possible that the best model for the system was not chosen in all cases.

It is also important to consider any potential areas of concern in the methodology or outcomes of this study and the extent of their potential impact on the interpretation of the findings. Identified areas of potential concern are described and addressed below.

4.4.4 Discussion and Citical Evaluation

It is important to explicitly consider factors which may have an impact on the results obtained and their potential to confound the identified causes of observed outcomes.

Repeatability

All kinetic studies conducted on SANS2D were repeated 5 times to enable time-slicing of the data without loss of statistical power. The separately repeated mixtures are presented in the figures below. for static and/or dynamic and refer to pH effect. The repeated mixtures give broadly similar, repeatable, scattering, although in some instances, a slight shift in scattering can be seen between the first and subsequent repeats. The variation is very small and so was not thought to be significant.

pH Stability and Impact

PEI is known for its strong buffering effect on pH changes, hencen pH drift or variation was a concern in these experiments, as solutions were typically freshly prepared from stock solutions and adjusted to the desired pH relatively shortly before kinetic experiments (static experiments took place subsequently, based on identified sample of interest identified through the kinetic studies, thus samples could be prepared further in advance and pH drift was less of a concern. It was suspected that the slight change in scattering between repeats, displayed in Section 4.4.4 above, could be due to a drift in polymer solution pH, as PEI is a strong buffer and final pH adjustments were carried out shortly prior to experiments. Limited checks on test samples following the experiment indicated that pH was thought to vary by less than +- 1 during experiments in the most extreme potential case. To ascertain whether this would be expected to have an effect, as well as to elucidate the effect of pH changes which complexes would likely experience intracellularly, a limited range of pHs were studied explicitly in the subsequent static SANS experiments conducted on LOQ, which showed over the range examined that minimal structural variation with pH could be observed . As polymers may have drifted up in pH as well as down, this may be higher than the pH range explicitly examined in static SANS, although there is little reason to suspect substantial state / phase change would occur so close to neutrality. In any case, unlike the cationic copolymers which contain a zwitterionic block, PEI are chemically uniform polymers, whether branched or linear, and do not undergo significant structural changes like micelle formation dependent on pH, so this is unlikely to be the cause of any observed effects. Even linear PEI, which undergoes recrystallisation at a certain pH point, does not undergo this transition, according to titration studies [188], as measured by a pH drop upon addition of excess NaOH at a critical point (see section

(a) 25 kDa BPEI Complexes

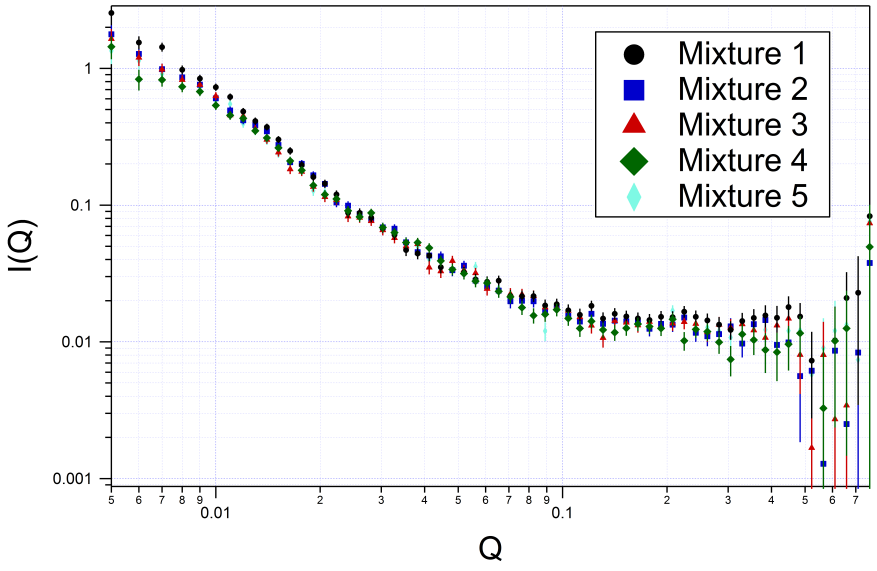

(b) 1.8 kDa BPEI Complexes

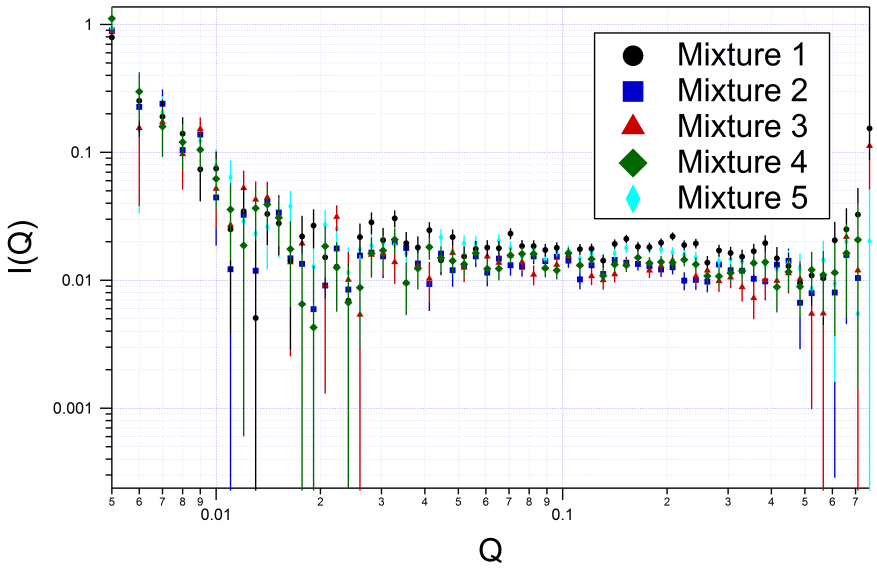

Figure 4.25: Variation of scattering from repeated mixing of DNA fragments with PEI at a charge ratio of N\P = 10:1 in 10mM NaCl in D_2O by polymer type; Legend indicates order of repeated mixing results. Continued below.

(c) 25 kDa LPEI Complexes

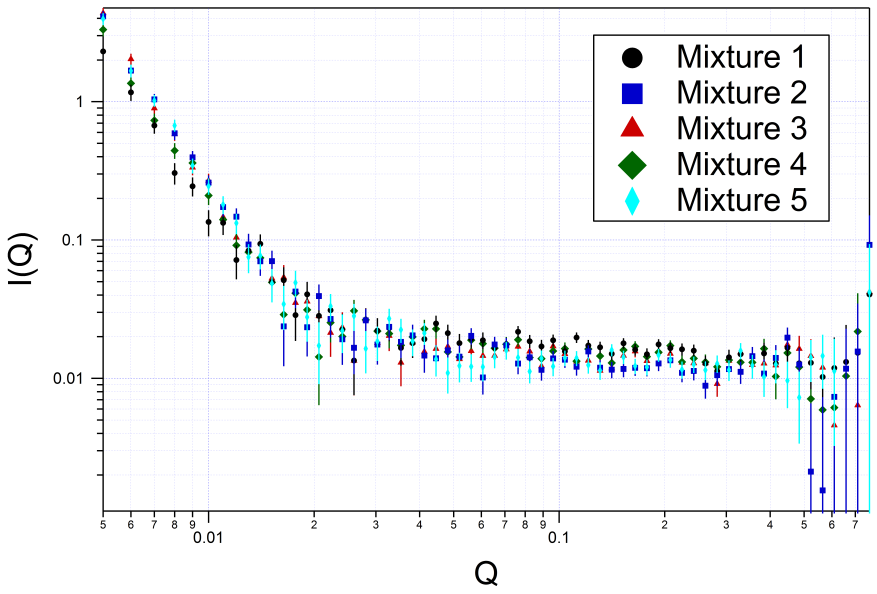

(d) 2.5 kDa LPEI Complexes

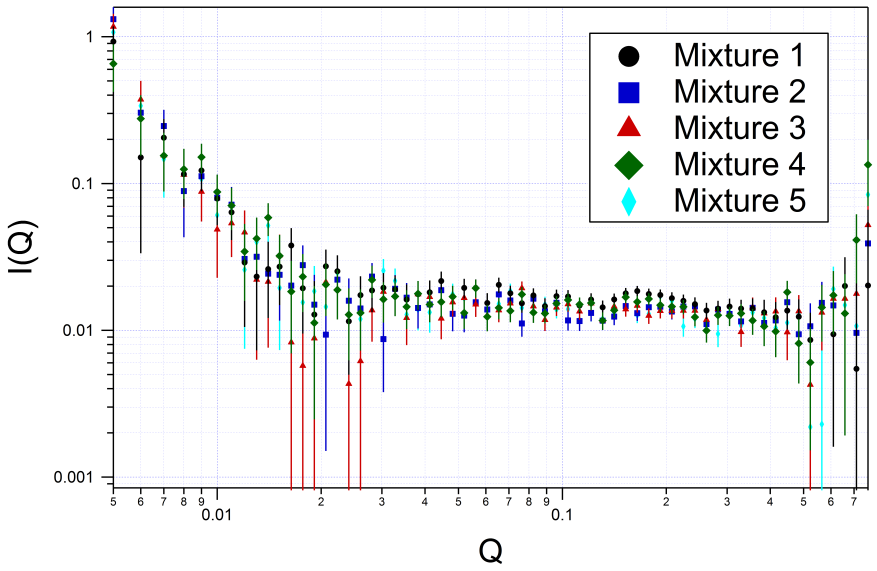

Figure 4.25: Continued: Variation of scattering from repeated mixing of DNA fragments with PEI at a charge ratio of N\P = 10:1 in 10mM NaCl in D_2O by polymer type; Legend indicates order of repeated mixing results

(a) 25 kDa BPEI Complexes, N\P = 20:1

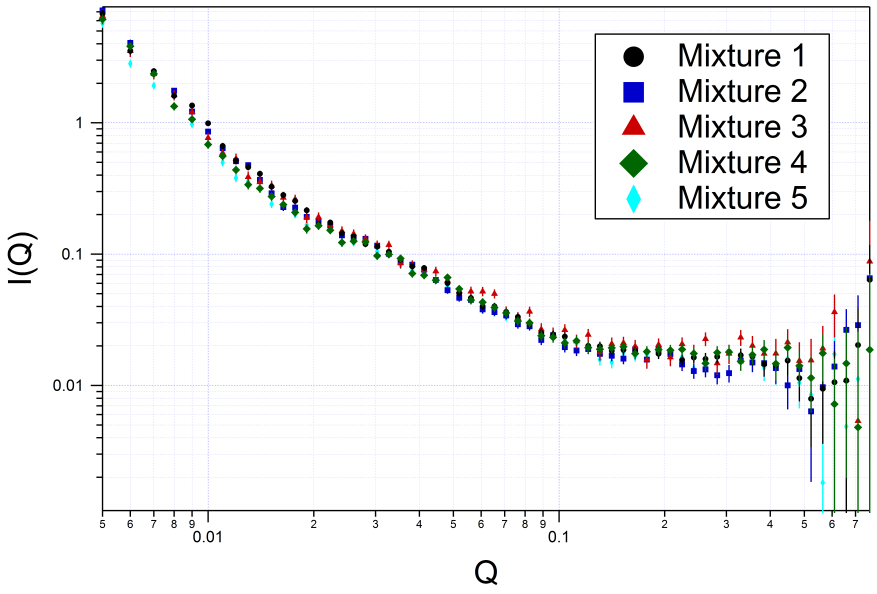

(b) 25 kDa LPEI Complexes, N\P = 20:1

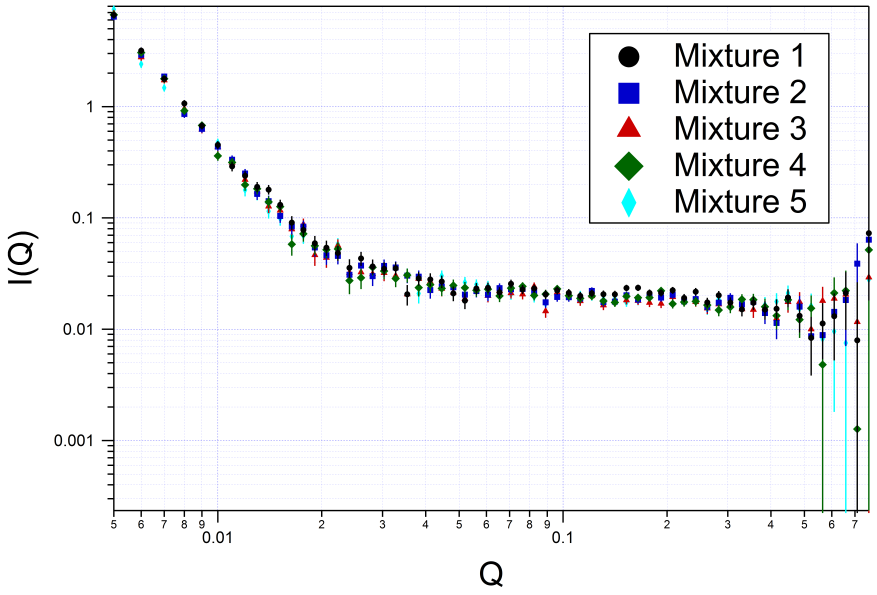

Figure 4.26: Variation of scattering from repeated mixing of DNA fragments with PEI at a charge Ratio of (N\P) = 20:1 in 10 mM NaCl in D_2O; Legend indicates order of repeated mixing results

4.2.3), until around pH 9.5, which was thought to be far beyond the range of variation. The slight differences in the scattering profile of the first repeat of some sets (ie. with freshly loaded polymers) which were sometimes present, indicated perhaps the minimal effect of pH drift in the initial minutes of experimentation or, alternatively, miscellaneous interaction with residual solution present from previous data (despite thorough flushing in all cases), or perhaps with salt adsorbed with polymer to charged surface of cell, for

(a) 25 kDa BPEI Complexes in 5% Glucose in D_2O

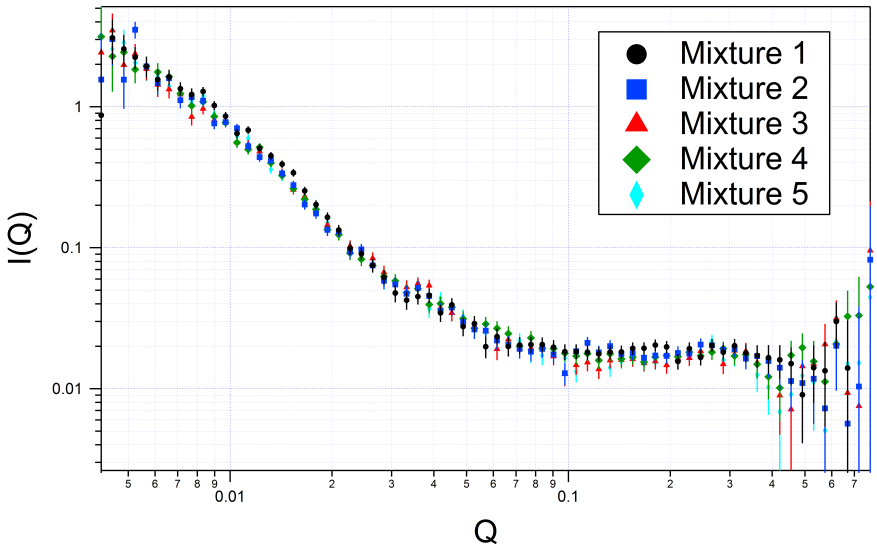

(b) 25 kDa LPEI Complexes in 5% Glucose in D_2O

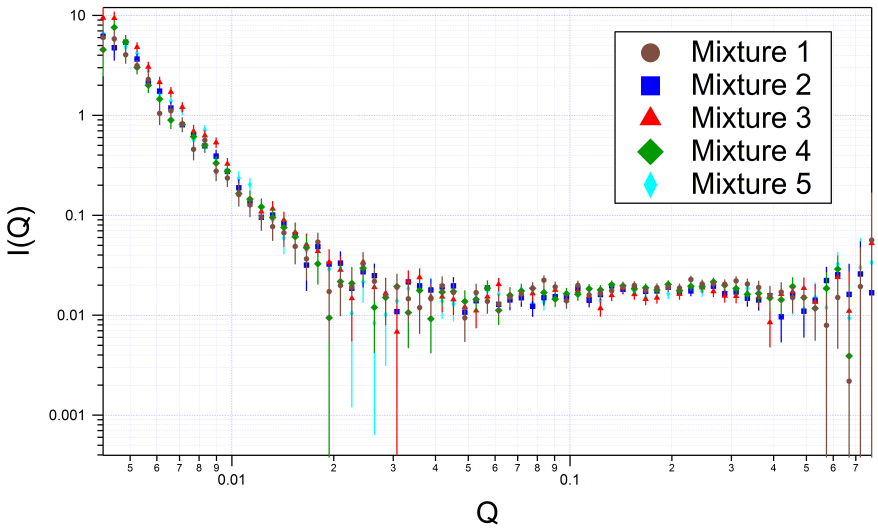

Figure 4.27: Variation of scattering from repeated mixing of DNA fragments and PEI at a charge ratio of N\P = 10:1 in 5% Glucose in D_2O; Legend indicates order of repeated mixing results

instance. Testing of the cleaning solutions in quartz DLS cell resulted in no visible precipitate, however, by the end of stopped flow experiments, some residual adsorbed material could be observed, indicating where long periods of adsorption (typically up to half an hour) were allowed back-to-back, some material resisted the cleaning procedures employed. Indeed, static SANS experiments were allowed to run for an hour, and cells were invariably clean following this, however it could be that the access to the cell allowed in these experiments facilitated more thorough physical cleaning than within the stopped-flow setup, which could not be dismantled for thorough cleaning between runs, which could also account for a difference. These differences were not large enough to be treated as significant and were treated as negligible effects in data analysis.

The only other possible identified differences which could confound potential effects were in age of the stock solutions, as the linear PEI solution was believed to be relatively less stable, due to its lower solutiblity in cold, aqueous solution, particularly at the elevated concentrations used in this work, and potential to recrystalise, which meant that it was prepared freshly (within several days) prior to experiments, whereas branched PEI was easily soluble and stored at 4^oC for longer periods. However, the most significant observed behaviour differences did not differentiate principally between linear or branched PEI samples as a set of all MWs, so much as between high and low molecular weight polymers of either architecture, with low MW polymers leading to weaker scattering hypothesised to be due to greater aggregation, so this was not thought to interfere significantly with conclusions.

Glucose-Containing Background Anomaly and Correction

An anomaly was identified for samples formed in 5% glucose solution, whereby the pure solvent background to be subtracted in initial data reduction had a higher intensity than the sample solutions themselves, which would lead to oversubtraction from the sample scattering.

Samples made in 5% glucose in D_2O solvent are likely to have an elevated incoherent background scattering level in comparison to pure D_2O, due to the increased amount of larger scattering hydrogen-containing molecules, so a stock solution of glucose was run for background subtraction. This solution gave rise to a higher level of background scattering when compared to the samples run in 5% glucose, suggesting the interaction of polymer

samples with the glucose into larger structures reduced their contribution to incoherent scattering.

As incoherent neutron scattering is dependent on both to the quantity of strong incoherent scatterers, such as Hydrogen atoms, and their self-correlation time, one possible explanation is that, when the incoherent scattering due to glucose molecules in D_2O is measured, it will be reduced if the glucose is bound to larger molecules or aggregates, which are relatively immobile compared to small molecules, free to diffuse, thus altering the self-correlation. Work by Fabo et al [48] shows evidence of an interaction between glucose and PEI,which is intuitively likely, as PEI-DNA complexes in glucose are found to have distinct properties from those in pure water. Hence, the background scattering from pure glucose may not be assumed identical to that of complexes in glucose.

As this effect was not foreseen, however, and background subtraction was planned by subtraction of the pure glucose solution scattering, rather than the scaled version ultimately used, from that of the samples, the possibility of an error in the background solution concentration must be considered, either due to incorrect dilution or incomplete dissolution of glucose. A detailed treatment of this observation to evaluate the extent to which complex effects or experimental error may have contributed to the apparent discrepancy is outside the scope of this study. It is not clear whether this anomalous effect is due to a legimitate phenomenon, experimental error or a combination of the two. Importantly, however, the main comparisons of interest relate to the stability of an individual sample, between the different kinetic stages of each PEI complex sample in 5% glucose, rather than directly between individual time-points of samples in glucose with those in other media. Thus, the comparison of different samples in glucose will not be affected, provided they all undergo the same background correction treatment, and self-comparison of a sample in glucose at different time points and the magnitude or of any differences may be compared in the same way as for other solvent media, despite any uncertainty in background correction, as changes are relative to other time points or samples, rather than absolute and hence dependent on an absolute background subtraction.

Various methods for background subtraction were compared in order to inform the most appropriate choice of data reduction and these are shown in the figures below. It was concluded that subtraction of the pure glucose background scaled by a factor of approximately 0.45 gave the most likely fit to the observed scattering, with the resultant signal portraying very similar features to similar samples in different media, and this method

was applied to all glucose samples.

(a) Comparison of different methods for glucose background subtraction and treatment for complexes of 25 kDa BPEI with DNA fragments at a charge ratio of N\P = 10:1

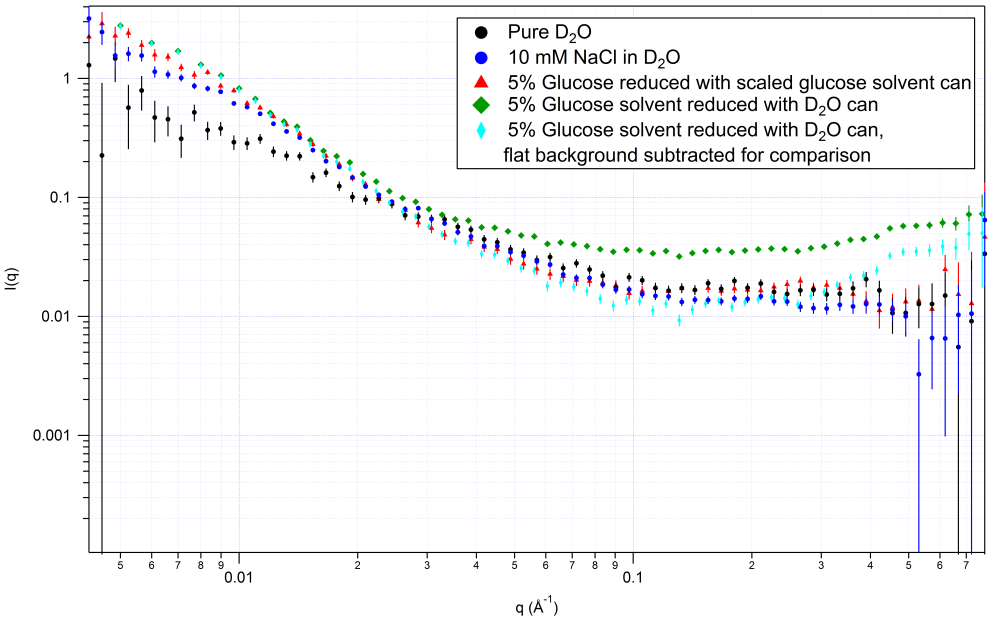

(b) Comparison of different methods for glucose background subtraction and treatment for complexes of 25 kDa LPEI with DNA fragments at a charge ratio of N\P = 10:1

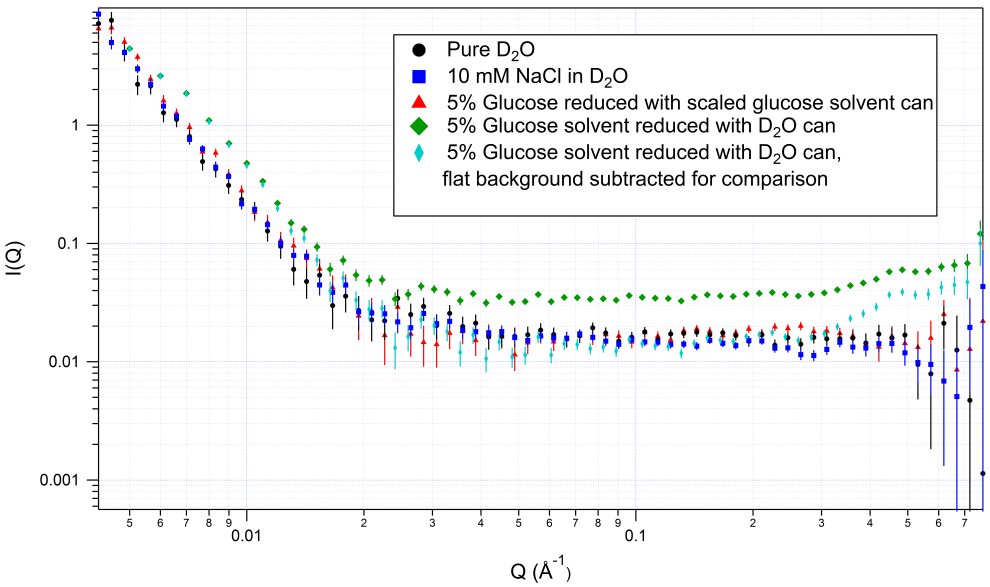

Figure 4.28: [Comparison of different methods for glucose background subtraction and treatment for complexes of 25 kDa linear and branched PEI with DNA fragments at a charge ratio of N\P = 10:1, pH 7.5; Legend indicates solvent and background correction treatment

Polydispersity and Aggregation and Their Impact on Analysis

Aggregation and polydispersity in complexes is evident from the low Q Porod and, particularly, Guinier plots. Polydispersity can affect interpretation of the Porod plot gradient and, particularly, the derived Guinier radius, which is in any case potentially uncertain for large particles where QR_g goes beyond the standard range, as is the case for much of these data. Hence, Guinier analysis in particular was taken as a broadly informative measure, rather than an absolute parameter.

The fact that static data was averaged over the initial 30 minutes following complex mixing, where structural evolution was anticipated (although it is not known that no further structural evolution would have taken place after this time period), was also an inevitable contributor to polydispersity. However, again, as aggregation proceeded, the averaged static data over this time would contain stronger contributions from the larger aggregates, and the apparent composition of the mixture would likely be weighted towards the steady state end of progression, therefore this was not considered to be a severe influence.

As was discussed above, although FISH model of multiple particles may take into account larger aggregates to an extent and provide good model fits to the data, even without an explicit polydispersity term, literature sources[84] caution against using data with aggregation and Primus's AutoRg program deems the data poor quality, apparently on this basis. However, some authors undertake analysis of aggregates, eg[157] [39]. Draget et al, in particular, model aggregated gel junctions during formation as two component systems, deriving the cross-sectional Guinier radius for early and late stages, hence the approximate aggregation number, and use the Debye-Bueche phase-separated random aggregates model to estimate aggregates' size.

The use of the same stopped-flow data over the initial 30 minutes following mixing for static as well as time-slicing analysis means that inevitably some changes in structure will be observed over the time period, leading to some blurring.

Although the Debye-Bueche model was well suited to the size range and presence of aggregation in the sample, ideally the effects would have been mitigated through the recording of scattering profiles from solutions at a wider range of concentrations, which would enable observation of the change in deviation from Guinier plot linearity with concentration indicating concentration-dependent aggregation and interparticle interaction potential, which

can not easily be modelled, except for spherical particles. This is something which could be beneficially explored in further work, however extending the concentration too far in the direction of excess dilution is likely have negative implications for the signal to noise ratio, due to the weak overall scattering intensity of these particular complexes.

4.4.5 Further Work

This study utilised advances in available neutron beam flux and stopped-flow apparatus on the SANS2D beamline at ISIS Neutron Facility, Harwell Oxford, to study cationic PEI-DNA complex structural evolution over short time periods after mixing, enabling detailed determination of the likely structure of complexes in a time-regime relevant to biological applications of transfection using this family of gene delivery vectors.

Several promising areas were identified over the course of this study for useful future work to expand the investigation, building on the foundations of this structural study.

Further investigation of the impact of pH on complex structure, both at higher pH values and for different sized PEIs would be informative as smaller PEIs were found by Mady et al [119] as described in Section 4.4.1 to have different pKas to larger PEI and they also found a greater instability against coagulation for small PEIs than for large, as was also observed here. Investigation of this connection could provide further explanation as to the greater colloidal instability of complexes formed with low molecular weight PEI.

AFM observations would help to verify some of the observations in this work, particularly concerning the broad size, conformation and compactness of the complexes. However, one of the main advantages of SANS is the ability to study particles' conformation in their native, solution environments, so comparison of structures observed with AFM would not necessarily be straightforward on an equivalent basis, as interaction with negatively-charged mica traps the particles in either a 2D or 3D conformation, depending on surface treatment, however the interaction with the highly charged surface is still likely to interfere in the observed structure. However, imaging such as this would provide beneficial indications of the likely structure and help to inform and give validation to the modelled structures. Imaging, such as with AFM or would be a helpful extension to this work.

As the DNA fragments used in this work were chosen to be similar in fragment length (less than 50 bp) and structure (double-stranded) to siRNA molecules, which have physiological relevance for gene delivery, their complexation efficiency after various incubation times

could be related to the structural changes observed here. A ubiquitous 'house-keeping' gene, such as GAPDH could be selected as a reporter and, following transfection with GAPDH siRNA for 48 hours, a commonly used time for observation of knockdown effects in expressed protein levels, the activity could be measured by a standard procedure, such as that available with KDalert kit, which measures the production of chromophores produced as a result of the reaction catalysed by GAPDH colorimetrically in a plate-reader UV absorption assay.

The findings presented in this work provide some structural insight into the changes which occur in complexes between DNA and PEI of various types. In some cases, confirmation of literature findings was observed, such as that the stability of small nucleic acid complexes (in this case, siRNA) with high MW BPEI is greater than with LPEI[103], while elsewhere a connection was not so clear cut.

Several promising areas for further exploration based on the SANS technique were also identified during the course of this analysis, incorporating either extended analysis of the existing data, or the extension of the range of samples already studied to support and further interpret the findings.

Due to the extent of aggregation present, it would be advisable to undertake studies of the system at multiple concentrations, to better enable elucidation of the radius of gyration and structure factors at low Q, where scattering contains a strong component from aggregation, which can lead to the superposition of an attractive interaction structure factor on the particle form factors, limiting the potential for drawing firm conclusions, particularly from the Guinier analysis, although good fitting to models was achieved in this case without the need for an explicit structure factor or interaction potential. [12]

Different solvent media contrasts for neutron scattering would also enable a more detailed investigation of the complex structures. Increasingly higher ionic strength by the addition of salt, and a wider range of charge ratios would give the opportunity for a more detailed examination of the kinetics factors affecting the kinetics of aggregation.

An extension of the study to investigate different types and sizes of nucleic acid would expand the area of application of the study. However, preliminary attempts at complexation with a large DNA fragment led to extreme flocculation at the concentrations required for SANS, so another nucleic acid sample would have to be chosen carefully. Further work could also be conducted to identify the true cause of discrepancy in the glucose background and whether it was due to the incorporation of glucose molecules into the complexes them-

selves, thus restricting their motion and reducing their correlation function, upon which incoherent scattering depends, or to another artefact or experimental error.

Chapter 5

Zeta Potential Study of Polyethylenimine Complexes with short interfering RNA

5.1 Introduction

5.1.1 Relation to SANS and relevant questions

In Chapter 4, the aggregation kinetics and structural evolution of complexes between branched and linear PEI molecules of varying molecular weights were studied using small angle neutron scattering. It was shown that low molecular weight PEIs of both architectures were relatively unstable in solution, quickly forming large, globular aggregates, while the most stable polymeric complex was formed with high MW BPEI, which adopted a chain-like network conformation in low ionic strength medium (10 mM NaCl).

An important physical property which is related to a colloid's stability in solution is the zeta potential, a measure of the particle's surface charge and double-layer properties, determined by its electrophoretic mobility. As mentioned in Chapter3, the repulsive potential contribution to the particles' total potential, which determines their stability in solution or tendency to aggregate, depends on the square of the particles' zeta potential as

$$V_R = 2\pi\epsilon a\zeta^2 e^{-\kappa D} \tag{5.1}$$

, where V_R is the repulsive potential contribution, ϵ the dielectric constant, a, the particle's radius, κ is related to the ionic composition, D is the particle separation and ζ the zeta potential.

5.1.2 Zeta potential and surface charge

DNA fragment sizes for the SANS study of complexation with PEI, presented in Chapter 4 were selected in part for their structural similarity, for the purposes of biophysical study, to commonly use siRNA molecules, although it was necessary for the SANS study to obtain a sample in far greater quantities than would have been feasible with siRNA.
Zeta potential studies were thus conducted on complexes of PEI and siRNA molecules, formulated to be complementary to the sequence for glyceraldehyde 3-phosphate dehydrogenase (GAPDH), a ubiquitous housekeeping gene in mammalian cells, which produces the GAPDH enzyme.

5.2 Theory

5.2.1 SiRNA Mechanism and Applications

siRNA is typically used to investigate the effect of knockdown of a particular gene by downregulating the production of the expressed protein from the corresponding mRNA in biological models. It is synthesised with a sequence which is complementary to that of the mRNA of interest, which then binds to the molecule and prevents translation into protein.
GAPDH is a useful target for evaluation of gene knockdown efficiency as it is a ubiquitous, house-keeping gene, found in mammalian cell types. Its use as a model siRNA for the study of zeta potential of complexes makes it relevant and straightforward to relate findings to transfection studies, or considering potential future extension of this work using the same siRNA as a marker for transfection.

5.2.2 Cationic Polymers

PEI are highly charged cationic polymers, available in both linear and branched architectures and at various molecular weights, as described in Chapter 4. Polymer solutions were

prepared as described previously in Section 3.1.5. Briefly, BPEIs have a high solubility in water at room temperature, so they were dissolved in UHQ with the subsequent addition of 10 mM Nacl with gentle rocking for $\geq$ 1 hour, before pH adjustment to the desired value, in this work, pH 7.4.

Linear PEIs, on the other hand, exhibit very low solubility in water at neutral pH and at room temperature, and thus were dissolved by addition of a small quantity of concentrated HCl (37%) until no visible polymer remained in solution. Subsequent incubation at room temperature with rocking served to ensure the polymer was thoroughly and completely dissolved, following which the pH was back-titrated to the desired value of pH 7.4.

PEI solution pHs were checked frequently, and always shortly prior to the experiment due to their high buffering capacity and tendency to drift. To account for the volumes of solid polymers in the solution concentration, the solution volume was measured following sample dissolution to readjust the determined stock solution value, and stock solutions were then used to make further dilutions for experiments at a typical concentration of around 0.1 mg/ml in 10 mM NaCl at pH 7.4. Each type of PEI solution was then diluted to a concentration equivalent to a charge ratio of N/P = 10 when mixed with siRNA solution in equal volume.

5.2.3 Biophysical Similarity to DNA fragments

SiRNA molecules of the type used here have diverse applications in vitro and in vivo for knockdown of overexpressed genes.

SiRNAs have a very similar structure from a biophysical perspective to the DNA fragments studied in complexation with PEI in the kinetic SANS work presented in Chapter 4. Their molecular length is typically around 20 - 25 base-pairs of double-stranded nucleic acid, while the model DNA fragments used in the previous chapter have a length around 50 bp. The average nucleotide mass is very similar in both molecules, differing only slightly due to the difference between the Uracil RNA base and Thymine DNA base. Finally,their persistence lengths are similar. However these are still of the order of magnitude which means the fragment sizes used for experiments are in both cases within one persistence length, meaning the fragments behave like rigid rods in both cases.

The similarity in size and structure of the kinetic aggregation study of DNA fragments complexed with PEI using SANS to siRNA fragments enables parallels to be drawn be-

tween the observed structure and stability of complexes of short, double-stranded nucleic acids with various forms and sizes of PEI.

5.2.4 Importance of Complexation and Optimal Conditions for Successful siRNA Delivery

RNA faces the same problem of electrostatic repulsion from the cell's membrane as DNA, hence complexation with cationic vectors is frequently used. Large, branched PEI molecular complexes have been found to have particularly high stability in 10 mM NaCl solution, which could be due to steric stabilisation, especially at high N/P ratios, by polymer side-chains uninvolved in complexation. This relationship between molecular weight of PEI and transfection efficacy is a question of interest when examining the zeta potential of the complexes and its evolution with time.

5.2.5 Zeta Potential

Zeta potential is related to surface charge, as described above, as well as to the double-layer of the particle. The zeta potential of colloidal complexes between PEI and siRNA has importance for several significant elements of gene delivery:

Electric Double Layer - The Importance of Zeta Potential for Stability

When particle possess a surface charge, a layer of counterions from the solution condense on the surface in a thin layer of solvent with a dense concentration of ions, known as the Stern layer, beyond which is a more diffuse layer, which together comprise the electric double layer. At a boundary within the diffuse layer, is a threshold of hydrodynamic shear, between the region of the double layer which associates strongly enough with the particle to move with it and the remainder which is static with the bulk solvent. The potential at this boundary point is known as the Zeta potential[123] and depends on the surface charge of the particle, ionic strength, pH and other properties such as viscosity of the media. It is an important factor in determining the repulsive potential between particles, which relates to their overall stability, as discussed in Section 5.4.1 , where further theoretical detail is also given. In general, a zeta potential of between + and -30 mV [80] [195] indicates significant aggregation, decreasing as the magnitude increases

up to stable values more strongly positive or negative than these thresholds, and with greatest likelihood of aggregation at the isoelectric point at which zeta potential is zero. While this is only an indicative value and will depend on the system in question, notably the steric effects between particles' surfaces and the solution's concentration of ions, it gives an idea of the likely stability level of the particles. The threshold is determined by the relative strengths of the electrostatic, repulsive inter-particle forces and the attractive, Van der Waals forces which tend to drive aggregation[195] The equilibrium point when these forces balance each other determines the treshold between stability and tendency to aggregate.

The fact that the particles' zeta potentials ultimately plateau in the region commonly assumed to indicate instability suggests they remain unstable or potentially an anomalous effect due to the particles' size comes is a factor in the interpretation, such as the model validity breaking down near the bounds of application, or the size or precipitation of particles out of solution could mean the results are skewed towards the remaining, solubilised particles, which may indeed be more unstable. A combination of factors is possible.

The Importance of Surface Charge for Transfection

Independent of the effect on particle stability, the value of the effective surface charge of a complex for gene delivery has significance for its attraction to or repulsion from cell membranes. Approach and interaction with a cell's external, negatively charged lipid bilayer is a necessary step in cellular entry and association with the membrane is likely to promote cellular uptake by specific or non-specific entry pathways.

The Impact of Colloidal Stability or Aggregation on Transfection Efficiency

There is much discussion in the literature of the implications of colloidal stability, or lack thereof, of transfection complexes and, while stability and a compact size has been shown to be beneficial for transfection in vivo, where pulmonary administration by inhalationor via injection into the bloodstream may trap severely aggregated particles , there is evidence to suggest that, at least in vitro, larger, aggregated complexes may have an advantage in cellular entry of increased rate of uptake, due perhaps to settling onto the cultured cell monolayer, or uptake through endocytic pathways which are more likely to result in active

transfection with biological impact, than others, such as clathrin-mediated entry, which has a size limit of around 150 nm, but has been shown not to lead to biological impact of the transfected nucleic acid. Thus the question of colloidal stability has many potential impacts and a predisposition towards aggregation related to the particles' zeta potential, and its evolution over time, is of interest to investigate.

Determination of Zeta Potential using Phase Analysis Light Scattering (PALS)

Zeta potential is related to electrophoretic mobility as shown in Equation 5.1. In the Zetasizer Nano, measurement takes place in a disposable folded capillary cell, which incorporates electrodes to apply an electric field across the sample. The applied field oscillates, such that the motion of charged particles also oscillates with a phase lag related to their electrophoretic mobility. The comparison of a split, reference laser beam from the beam which has passed through the sample enables this phase lag and, hence, the electrophoretic mobility to be determined, which , combined with knowledge of solution parameters, such as viscosity and dielectric constant, enables determination of the zeta potential in a given medium. This value is, however, extremely sensitive to fluctuations in ionic strength or pH, so care must be taken to establish these precisely, shortly prior to measurement.

5.2.6 Principle research questions

To complement and enable comparison with the structural studies of the process of aggregation in PEI-DNA complexes, the time-evolution of zeta potential over the course of 30 minutes or longer was of interest to examine with siRNA-PEI complexes in this chapter. It is of particular interest to relate the initial zeta potentials of complexes to their relative stabilities in low ionic strength media (10 mM NaCl in UHQ) and observe the change in the zeta potential as aggregation progresses over time.

5.3 Materials and Methods

5.3.1 Polymer Preparation

Small volumes of concentrated buffer or salt solutions were added as required to produce the desired pH and ionic strength, and the final solution pH was adjusted with minimal quantities of HCl or NaOH dissolved in UHQ. Stock solutions were then used to make up stock concentrations of a more relevant range, typically 1 mg/ml. PEI solutions were prepared similarly by addition of UHQ to an approximate concentration of 10 mg/ml. Concentrated HCl was then added to LPEI solutions, which are insoluble in water at neutral pH at room temperature, and solutions were then incubated with gentle rocking overnight at room temperature. The pH was subsequently adjusted to 7.4 with minimal quantities of HCl and NaOH, and the final volume measured to determine accurately the w\v% concentration of the stock solution. Stock solutions were subsequently diluted to a working stock of 1 mg/ml with the addition of the appropriate quantities of NaCl or glucose to the solvent as required and final pH adjustment. To account for the volume contributed by the polymer itself at this relatively high concentration, the total, final solution volume was measured the following day, and the stock solution concentration calculated from this value. Polymer solutions were stored at 4^oC when not in use for prolonged periods.

5.3.2 siRNA preparation

siRNA fragments were prepared as described in Section 3.1.2. Silencer GAPDH siRNA (Ambion) was obtained from Invitrogen as a concentrated stock solution in a storage buffer of 20 mM potassium acetate, 6 mM HEPES-KOH pH 7.4, 0.4 mM magnesium acetate. siRNA was diluted with a factor of approximately 150 times for zeta potential studies, so the low concentration original buffer was considered to be negligible.

All solutions were filtered with a 0.2μm pore size filter.

5.3.3 Zeta Potential measurement

Zeta potential measurements were conducted using the Malvern Zetasizer Nano with zeta potential ability and data collection was managed using the manufacturer's proprietary

software, DTS Nano. As the studies were time-dependent, complexes were mixed by addition of siRNA solution to an equal volume of PEI solution at the relevant concentration to give an N/P ratio of 10:1 and added, within 1-2 minutes, to a disposable capillary cell, which had been rinsed with ethanol followed by 10 mM NaCl solution, which was the dispersant used for all experiments. No equilibration time was given as samples were conducted at room temperature and it was important to commence measurement as soon as possible after mixing. The average measurement time per run was subtracted from the recorded time of the first measurement plus 1 minute to allow for mixing to attain the estimated age of the complexes and the measured zeta potential was plotted against this age for each polymer type. All samples were studied at pH 7.4 to enable comparison with SANS studies, also conducted at this pH equivalent in D_2O, and at a N/P ratio of 10:1, with a mixing concentration of siRNA of 0.3 μM, corresponding to a final concentration of 0.15 μM. Measurements were not repeated and hence no error bars can be included.

5.4 Results and Discussion

The zeta potential results for complexes between branched and linear PEI cationic polymers of different molecular weights with the siRNA for the house-keeping gene, GAPDH, plotted as function of time after complex mixing (estimated to be accurate to within $\pm$ 1 min) are displayed in Figures 5.1 to 5.4, below.

5.4.1 Interpretation and relevance

Complexes of all PEI types and MWs studied have an positive zeta potential at the earliest times studied, which rises for varying amounts of time before dropping off in all cases. Zeta potentials with a magnitude greater than around $\pm$ 30mV are taken to be very stable, while those between $\pm$ 30mV are highly unstable and likely to be strongly aggregating, with a continuous scale for values in between, according to Malvern Instruments' Zeta Potential guidance and Xu et al [80] [195].

All freshly-mixed complexes started off with zeta potential values of around 15 - 20. Although the exact interpretation of precise threshold zeta potential values with regard to colloidal stability must depend on the sample and solution conditions, a commonly accepted threshold in colloidal systems, according to Xu et al [195] is 30 mV. This indicates

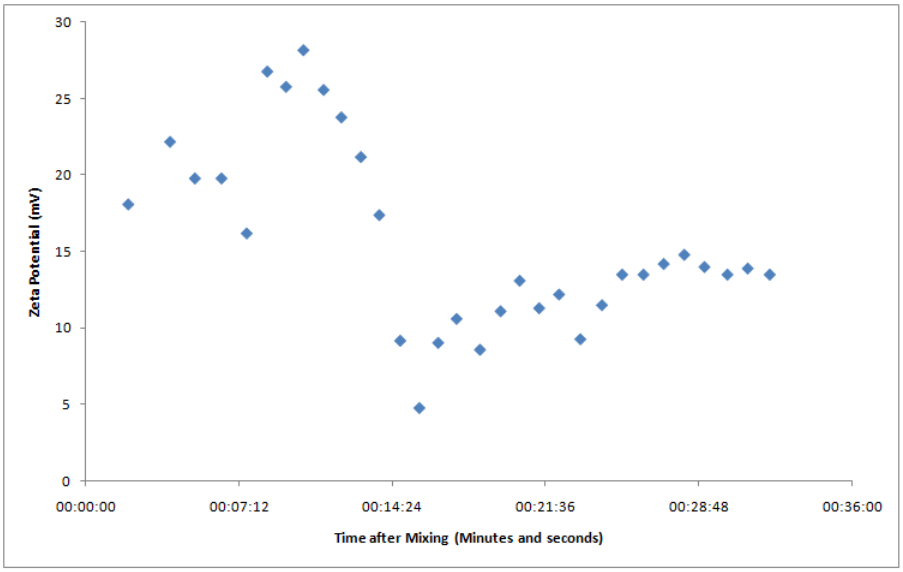

Figure 5.1: Zeta potential of complexes between 25 kDa BPEI and GAPDH siRNA with N/P = 10:1 in 10mM NaCl solution in UHQ, pH 7.4 as a function of time after mixing

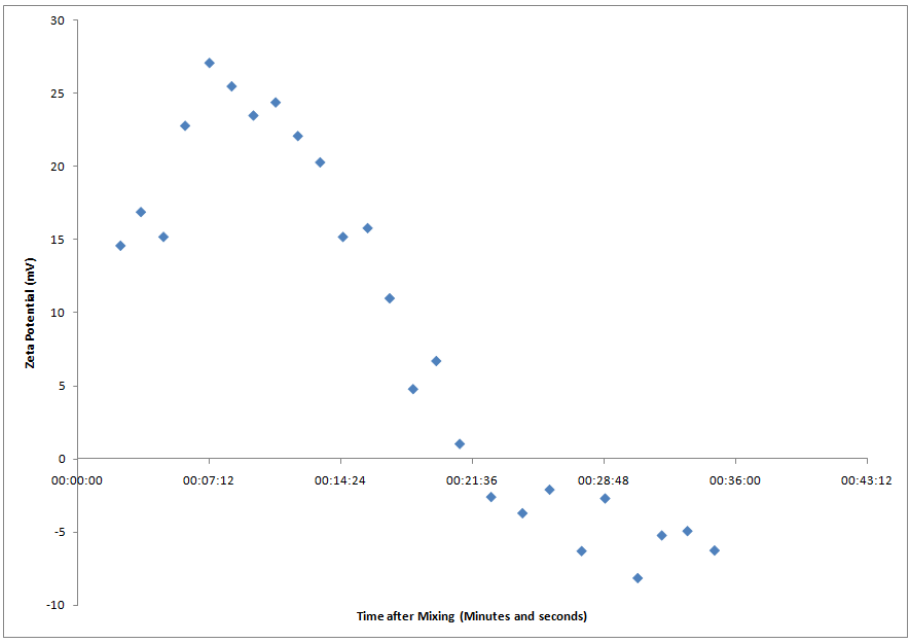

Figure 5.2: Zeta potential of complexes between 1.8 kDa BPEI and GAPDH siRNA with N/P = 10:1 in 10mM NaCl solution in UHQ, pH 7.4 as a function of time after mixing

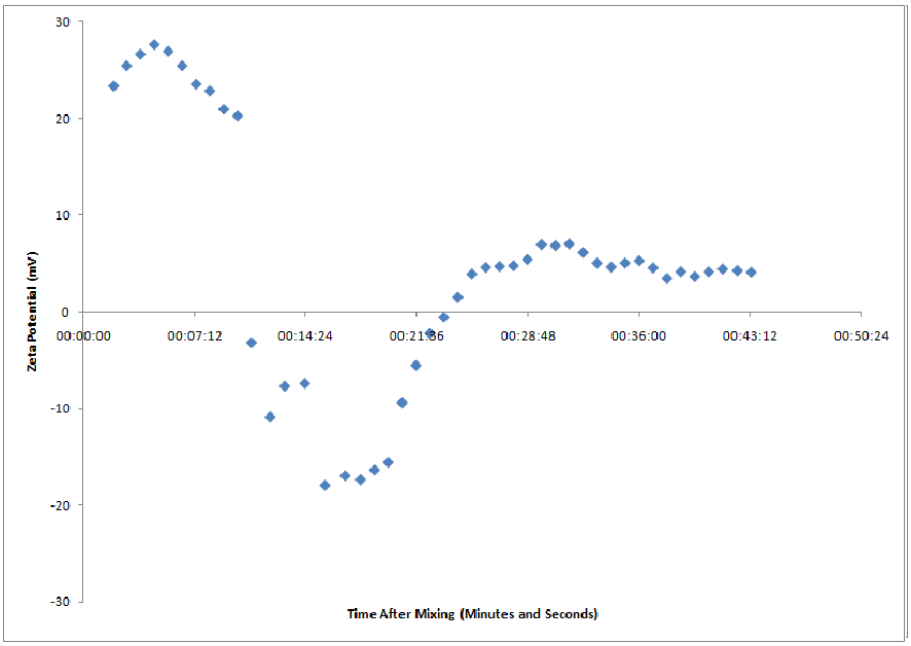

Figure 5.3: Zeta potential of complexes between 25 kDa LPEI and GAPDH siRNA with N/P = 10:1 in 10mM NaCl solution in UHQ, pH 7.4 as a function of time after mixing

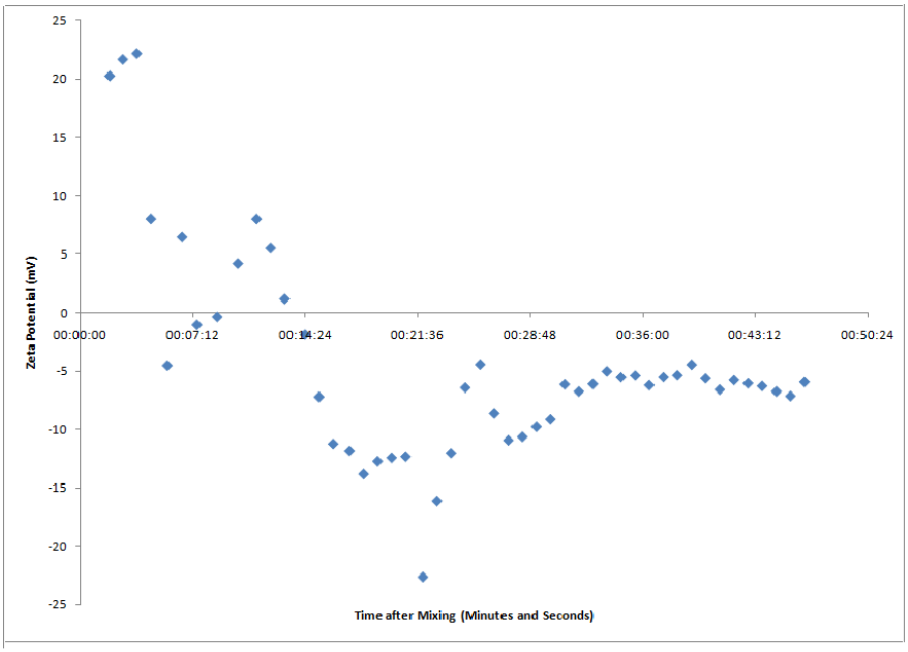

Figure 5.4: Zeta potential of complexes between 2.5 kDa LPEI and GAPDH siRNA with N/P = 10:1 in 10mM NaCl solution in UHQ, pH 7.4 as a function of time after mixing

the complexes are unlikely to be stable, as is already suspected, although the high MW branched and, especially, linear PEIs increase to reach values very close to 30 mV during the first few minutes following mixing.

All complexes' zeta potentials then begin to drop off, around 7 - 8 minutes after mixing for both high and low MW BPEI complexes, but earlier at around 4 minutes for LPEI complexes. Therefore, despite the high zeta potential, briefly seeming to approach the stable region for high MW LPEI, the rapid subsequent decline in zeta potential indicates a lack of stability commensurate with the severity of aggregation observed in the SANS data presented in Chapter 4.

The most distinguishable features of the zeta potential evolution curves with time are the steepness and extent of the initial drop, whether any rebound occurs, and the zeta potential value at and time after which the zeta potential value ultimately plateaus. Notably, the two high MW PEI complexes, both branched and linear, plateau at positive zeta potential values. While the zeta potential of 25 kDa BPEI complexes, expected to be the most stable based on SANS results, levels off soon after around 15 minutes and, indeed begins to increase again gradually, ultimately seeming to stabilise around 13 mV, while never having turned negative, thus appearing to confirm its relative stability, the 25 kDa LPEI complexes, on the other hand, drop steeply to almost -20 mV from its peak approaching +30 mV, before rebounding sharply and ultimately plateauing at a slightly positive value, around 5 mV, after approximately half an hour. This behaviour might suggest high instability following initial complexation and complex association, which is likely to be slowed at the lower concentrations used here with respect to SANS, followed by a gradual equilibration of the newly formed aggregates. Low MW LPEI behaves similarly to high MW LPEI, as its zeta potential also falls away sharply initially to a negative value, and subsequently rebounds, albeit more gradually than the high MW LPEI complexes. Furthermore, its zeta potential then plateaus at a negative value, thus appearing to be more unstable than its high MW analog. This is likely due to the lack of steric stabilisation available for small molecules.

The behaviour of low MW BPEI complexes is distinct from the others, as its zeta potential gradually falls away, initially sharply and later with a shallower slope, indicating perhaps that its aggregation continues to progress over extended periods of time, albeit less catastrophically than the linear polymers' complexes.

The reason for the initial increase observed in complexes of all four polymer types could

be an artefact, such as initial adsorption to the electrodes or solvent effects. However, it should also be considered that initial binding, rearrangement and association of complexes will occur on a significantly longer timescale than in the SANS studies conducted, due to the much higher sample concentrations required for SANS. It is therefore also likely that the average zeta potential of the complexes is increased during the initial stages of association and binding, due to overcharging of the siRNA molecules, which could potentially be resolved on observed timescales at these greater dilution levels, but progressed too rapidly to record at the concentrations used in SANS.

As direct measurements are of electrophoretic mobility, and the indicated zeta potential is inferred by estimation, the possibility should be considered that, if aggregation progresses, the effective viscosity of the solution may change additionally. However, in this instance the samples were so dilute that this was unlikely to be a significant factor. Another possible factor could be the increased size following aggregation, which may also contribute to reducing their electrophoretic mobility. In fact, the scattered intensity increased considerably for all complexes as time progressed, indicating that the particle size was increasing as scattered intensity is strongly dependent on particle size.

5.5 Future Work

It would be of interest to expand the zeta potential study to other charge ratios and, potentially, different forms of DNA, in order to uncover in more detail the driving forces behind the aggregation behaviour of these complexes.

Additionally, however, there is an opportunity to utilise the biological function of the GAPDH siRNA used in this investigation to probe the change in transfection efficiency with time following complexation of the various PEI types used here. The GAPDH siRNA comprises a complementary sequence for that of the GAPDH enzyme, which catalyses a reaction which generates a fluorophore, and whose rate of progress can be measured fluorescently or colorimetrically to derive an activity coefficient, directly related to the quantity of GAPDH present in the cells, provided no other necessary factors become limiting. In this assay, cell lysate is added to a mixture of reagents, and its UV absorption is measured after 15 minutes and compared to a control activity level of cells without knockdown, with the use of commercially available scrambled siRNA as negative controls.

As GAPDH is a house-keeping gene, which produces relatively large, constant quantities of enzyme, any reduction in measured activity in the negative control well results from toxicity of the transfection agent, hence a measure of the toxic effects of the PEI types used in such a study could also be derived from these controls. This would enable direct relation of the structural and zeta potential evolution to the efficacy of complexes to transfect in vitro.

Chapter 6

SANS Study of DNA Complexation with Cationic Diblock Copolymers

6.1 Introduction

6.1.1 Nucleic Acids Complexation and Vector Design

In previous chapters, a well-characterised and frequently used cationic polymer transfection agent, PEI, has been examined to evaluate the relatively little-studied questions surrounding structural evolution of the complexes during aggregation post-complexation, as well as the zeta potential values of these complexes and their accompanying evolution during the aggregation process.

However, many advantages, particularly surrounding storage of complexes and in vivo administration, are related to the colloidal stability of complexes and the progress of vector design and conjugation of ligands to non-viral gene delivery vectors is a promising area of work, and intuitively, seems a likely precursor to ultimate widespread commercial availability of genetic therapies for a range of potentially treatable conditions, as discussed in Chapter 1.

In this chapter, the structure of DNA complexes formed with a family of synthetic but biocompatible diblock copolymers, of which some have been found to have high transfection efficiencies in vitro [202], designed to simultaneously provide high cationic charge

density with, additionally, hydrophilic stability is investigated with preliminary screening by dynamic light scattering (DLS) and detailed structural investigation using small angle neutron scattering (SANS).

6.1.2 Polymer Structure

The synthesis of this family of biocompatible, diblock MPC-DEA copolymers by ATRP, described by Ma et al[118] resulted in well-defined polymers with low polydispersity ($M_w/M_n = 1.2 - 1.3$[202]) and well-defined degrees of polymerisation of 30 monomer units for the MPC block and 30, 70 or 100 for the DEA block, as shown in Figure 2.2. The zwitterionic phosphorylcholine (MPC) block was designed as a stabilising moiety to maintain hydrophilicity of the overall complex once charge neutralisation upon DNA binding has occurred, while the DEA block is highly charged, with one protonatable amine group per monomer unit, and is thought to be approximately 50% protonated at neutral pH [202] as the DEA block possesses a pka of around pH 7 - 7.5 [202][118]

6.1.3 DNA Types

Complexation was studied with two types of DNA, both of great relevance for therapeutic and biological gene delivery.

Short, single-stranded antisense oligodeoxynucleotides (ODNs) for the C-Myc gene formed the main focus of the study. C-Myc is a proto-oncogene, whose overexpression has been implicated in various cancer types and the ODN has a role in down-regulation of this gene. Plasmid DNA, such as luciferase, was also investigated. These large, circular double-stranded molecules of DNA pose a different problem. As plasmids are such large molecules (approximately 5 kBP)[202], condensation and compaction is desirable to attain cellular uptake. Hence, the diblock copolymers were investigated for their ability to compact plasmid DNA.

6.1.4 Preliminary DLS Screening

To inform the analysis of SANS data on the various complexes, preliminary dynamic light scattering was undertaken to explore the approximate size trends of the complexes. DLS data can be used to derive an estimate of the hydrodynamic radius of particles in

solution by evaluation of their auto-correlation function from a speckle pattern formed from scattered laser light, which depends on their speed of diffusion, and is closely related to their hydrodynamic or Stokes radius, which is the radius of an equivalent spherical particle with the same speed of diffusion. The DLS measurements presented here were just conducted as preliminary scoping of the sample systems giving indicative, likely size ranges, in preparation for SANS studies.

The theory of dynamic light scattering is described in further detail in Section 3.2.1. It can hence be seen that there are significant advantages to SANS over DLS as conducted here with the Zetasizer Nano, particularly in the estimation of likely structural features rather than merely broad size, but DLS nonetheless provides useful complementary size estimates.

6.1.5 SANS and structural investigation

Small angle neutron scattering (SANS) was used to determine the size and structural composition of the complexes in solution with nanometre resolution. SANS was carried out on the LOQ diffractometer instrument at the ISIS Spallation Neutron Source, Rutherford Appleton Laboratory (RAL), Oxfordshire. The experimental procedure is described in more depth in Section 3.2.1, and the brief protocol is provided again in Section 6.3.1 of this account.

6.1.6 Requirements of Complexation for Different Types of DNA

The question of the purpose of vector complexation is highlighted in the comparison of binding of two very diverse DNA molecules examined in this chapter: ODN and plasmid DNA. The many hurdles to successful gene delivery are discussed in detail in Chapter 1 and include cellular uptake, endocytic trafficking and endosomal escape, timely complex dissociation and nuclear entry. However, for successful transfection with ODN molecules, nuclear entry is not necessary as the functional binding to mRNA can take place throughout the cytoplasm. As the molecules are very small and flexible (see Section 2.1.1), compaction is not the primary concern, but rather the neutralisation of charge to facilitate cellular entry and tightness of binding to give protection from enzyme degradation, but

yet not hinder dissociation from the complex when necessary for biological efficacy of the transfected DNA.

Plasmid DNA, on the other hand, presents a very different challenge. It is inherently less flexible, due to its double-stranded structure, and is a much longer molecule, in the case of luciferase, used here, around 5 kBP and hence is likely to require significant condensation and compaction to facilitate cellular entry. In addition, nuclear entry is also required in order for significant transcription and translation of the transgene to take place, so the compacting vector must either enable early endosomal escape or afford protection against the pH drop and increased enzyme activity which occur in late endosomes and lysosomes. Additionally, a balance must be achieved between facilitating nuclear entry by compaction of the plasmid, and dissociation from the complex in order to allow transcription to take place.

6.1.7 Factors of Importance and Principle Research Questions

There are several key factors which are thought to influence structural features, shape and size of the complex, and tightness of binding, which are investigated in this work:

N/P Ratio

The degree of excess cationic polymer charge present is a key factor determining the binding of DNA. The DEA cationic polymer blocks used in this study are expected to be half protonated around neutral pH, so full neutralisation of the DNA's charge and hence efficient condensation (found to occur from around 90% charge neutralisation of DNA - see Section 2.1.2) and complex neutrality would be anticipated at an N/P of 2. However, this may not necessarily lead to a compact particle or efficient transfection. Indeed, an excess of free polymer has been shown in the case of the commonly used cationic polymer, PEI, to be necessary for efficient transfection[17], although it is not clear whether the excess is required to remain entirely free from complexation to take effect. This work will investigate the structural impact of varying charge ratios of mixing on complexes between MPC-DEA diblock copolymers and ODNs and plasmid DNA.

Diblock Copolymer Degrees of Polymerisation

The proportion of stabilising MPC blocks to the cationic DEA block which is involved in binding and complexing with DNA is a factor which can be tailored to achieve the optimum structure for stability and high DNA binding capacity. The effect of greater or lesser degrees of stabilising vs. cationic block polymers on complex structures with ODN or plasmid DNA are investigated here with SANS.

Elucidation of Binding Mechanism

Where the principle binding force is electrostatic, as is thought to be the case with the cationic polymers and anionic DNA molecules studied here, increasing salt concentration in solution should screen some of the charge interaction and lead to weaker binding, corresponding to swelling of the complexes. This is relevant, beyond for a purely fundamental understanding of the interaction, to determine likely structural changes which may occur when complexes enter the relatively high ionic strength medium within and surrounding cells, either in vitro or in vivo. SANS was therefore undertaken for complexes between ODN and MPC-DEA copolymers under increasing concentrations of salt. Complexes were formed as normal, as described in Section 6.3.1, at slightly elevated concentration, and the necessary, small quantity of concentrated NaCl solution was subsequently added to bring the ionic strength to the required level.

6.2 SANS Theory

Small angle neutron scattering (SANS) is a powerful technique for probing the structure of biological macromolecules, at relatively low energies without damaging the sample, and which enables study of samples in their native solution conditions. A detailed description of relevant theory is given in Section 3.2.1, but briefly, scattering bodies scatter incident neutrons through a scattering vector, Q, proportional to the inverse of the relevant length scale of the scatterer. By examination of the variation of scattering intensity with Q, therefore, information can be gleaned about likely structural features on various length scales in the sample of interest.

In this study, samples were dissolved in deuterated solvents to increase scattering contrast and reduce incoherent background scattering, which manifests itself as isotropic

background noise and must be subtracted prior to data analysis. Various model-free and model-based techniques may be usefully applied to small angle scattering data. Porod analysis, involving the plotting of a double-logarithmic graph of the intensity, I, against Q can provide information on the likely interfacial or internal structure, whether rough or smooth, globular, rod-, chain- or network-like, and on which length scale the features are present. A Guinier analysis allows the radius of gyration of the scattering body to be deduced from the gradient of a plot of ln(I) against Q^2 at the lowest Q values and is additionally a useful preliminary tool for detection of aggregtion in the sample, which manifests itself as an upturn or curved region superimposed on the linear region. However, the accuracy of the Guinier plots was not believed to be as high as for model-based data fitting, described below, where clear fits were visible, so while Guinier analyses were conducted for the samples, they were not used to determine the specific parameters presented here.

As mentioned, where a good idea of likely form factor structures is available, model-based least-squares data fitting based on the Levenburg-Marquardt algorithm can be undertaken using the FISH software written by R.K. Heenan at ISIS Neutron Source, RAL [71]. This enables specific structural parameters associated with a given structural model, or combination of models, to be fit to scattering data, giving detailed insight into the likely structure of the particle.

6.3 Materials and Methods

The polymer to DNA, N/P charge ratio is calculated based on the mass per nucleotide, as a single nucleotide contains a single P group. The mass of a DNA nucleotide is typically thought to be 330 Da, based on the extinction coefficient of DNA sodium salt. This represents an average, for large molecular weights, over the different molar masses of the different nucleotide bases, which differ considerably. Hence, for small nucleic acids, such as oligonucleotides, an accurate molecular mass must be calculated using the known composition and sequence to calculate the specific extinction coefficient. The extinction coefficient and associated molar mass and oligonucleotide concentration was quoted by the manufacturers for this specific sample, based on the guidance provided by Eurogentec[47]. The average nucleotide mass per phosphate was calculated to be 308, approximately the

same as the value of 311 calculated by Zhao et al for solutions provided , which was taken to be the same, within error, as the mass per unit Nitrogen on the MPC_{30}-DEA_{70} copolymers, calculated to be 311,[202] used in that study. The charge ratios for the related diblock copolymers used in this work, MPC_{30}-DEA_{30} and MPC_{30}-DEA_{100}, in addition to MPC_{30}-DEA_{70}, were calculated on the same basis. Some sample stock solutions were provided by Dr. XiuBo Zhao, who kindly also provided significant assistance in preparing for and performing the SANS experiments described in this chapter, in addition to Dr. Fang Pan. Otherwise, polymer solutions were dissolved in PBD overnight with gentle stirring. Where necessary for dissolution, a minimal quantity of concentrated HCl was added, and the pH subsequently re-adjusted to the required level once solubility had been achieved.

The 15 base antisense oligonucleotides for C-myc used in this study, with the sequence 5'-AAC-GTT-GAG-GGG-CAT-3', were originally purchased from Eurogentec Ltd. (UK) and dissolved in D_2O for preparation of a stock solution.

Luciferase plasmid DNA was cultivated in E-coli host cultures and extracted using a commercially available kit (Qiagen) with subsequent concentration and purity determination by UV absorption at 260 nm and 280 nm, respectively. The procedure is described in detail elsewhere (See Section 3.1.2).

6.3.1 Sample Preparation

Complexes were typically mixed in low ionic strength PBD at pH 7.4, closely following the procedure by Zhao et al [202]. DNA solutions were added to equal volumes of polymer solutions and mixed briefly followed by incubation at room temperature for at least 30 minutes before measurement.

For samples in varying NaCl concentrations, DNA and polymer solutions were mixed and allowed to incubate at room temperature for more than 30 minutes, and then a small volume of NaCl solution at the relevant concentration was added and mixed, and again allowed to incubate before measurement.

0.6 ml of complex samples were loaded into quartz measurement cuvettes with a 2 mm path length and loaded in an automated sample changing rack in preparation for their measurement. Each sample typically took approximately 1 hour to achieve sufficiently good measurement statistics.

6.3.2 Guinier Analysis

A Guinier analysis for rods was attempted on the complexes to deduce size parameters, but it was felt more accurate parameters could be achieved with model-based fitting with the FISH program, described below.

6.3.3 FISH Model Fitting

Model-based fitting was conducted with the FISH program by R.K. Heenan, ISIS Neutron Source, Rutherford Appleton Lab (RAL), which seeks to fit a mathematical model corresponding to a given form factor or combination of form factors using a least-squares Levenburg-Marquardt algorithm[71].
Once a suitable model was identified, several iterations of fitting were performed until the modelled data appeared to converge to the experimental data. The best model for fitting a range of samples studied here, as well as their best-fit parameters are presented in Section 6.4.

6.4 Results

6.4.1 DLS

ODN

It can be seen from the dynamic light scattering results (Figures 6.1 and 6.2) that the complexes with the smallest radius of gyration resulted from complex formation at the 10:1 N/P ratio with polymer greatly in excess. The peak size of these particles appears to be only slightly greater than that of the pure polymers (see Figure 6.5), demonstrating that no significant level of end to end binding or aggregation of polymer molecules by ODN occurs at high N/P ratios. As this ratio is reduced and more ODN is available for binding, the radii of gyration begin to increase, suggesting association of multiple polymer molecules, linked by the ODN. At N/P ratios of 2:1 and 1:1, near the point of charge neutrality, much larger aggregates are observed, and the sample solutions did indeed appear cloudy, suggesting large precipitates had formed. The mutual repulsion of complexes is neutralised here, allowing the particles to associate and form large aggregates in suspension. With ODN in excess, the complex sizes appear to be larger than at the

highest polymer:DNA ratios, but nonetheless have regained some net surface charge and thereby mutual repulsion of complexes avoids the formation of larger aggregates which are seen at 2:1 and 1:1.

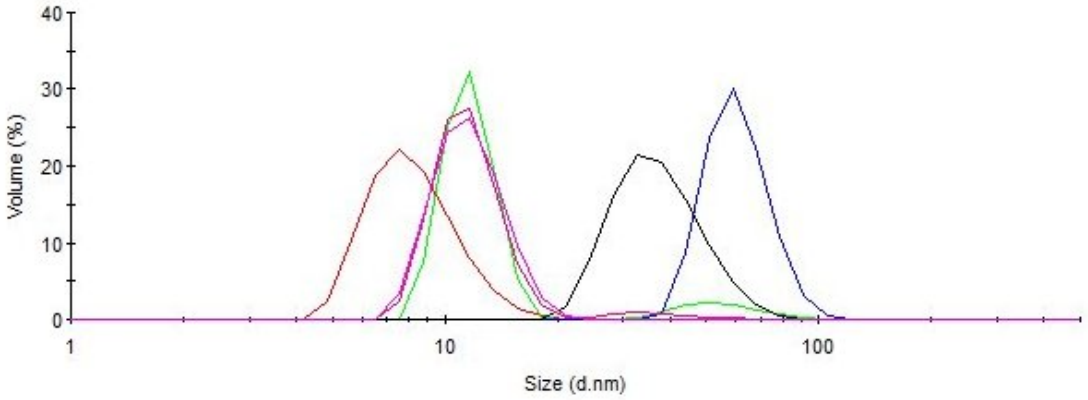

Figure 6.1: Size distribution by percentage volume of MPC_{30}–DEA_{30} complexes with ODN in phosphate buffer as measured by DLS at varying charge ratios: red = 10:1, green = 5:1, blue = 2:1, black = 1:1, magenta = 0.8:1, pink = 0.6:1 (image produced with DTS Nano Software)

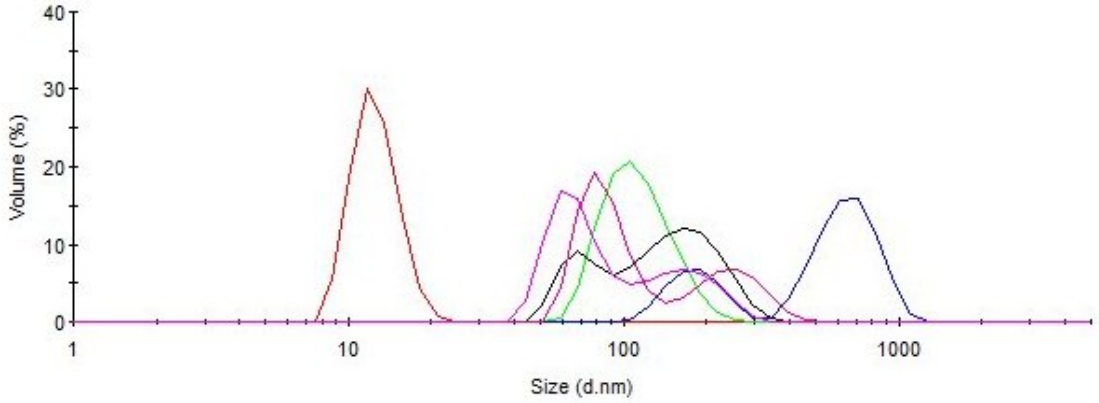

Figure 6.2: Size distribution by percentage volume of MPC_{30}–DEA_{100} complexes with ODN in phosphate buffer as measured by DLS at varying charge ratios: red = 10:1, green = 5:1, blue = 2:1, black = 1:1, magenta = 0.8:1, pink = 0.6:1 (image produced with DTS Nano Software)

Plasmid

The hydrodynamic radius of the complexes was evaluated by DLS and the initial results are shown in Figures 6.3 and 6.4 for charge ratios of N/P = 10:1, 5:1, 1:1 and 0.5:1. A greater degree of aggregation and polydispersity is evident in general here than for the small ODN complexes, which may be reasonable given the larger size of the plasmid. A similar trend is observed in general though, with the highest N/P ratio resulting in the

smallest complexes, condensing the DNA the most effectively, and larger aggregations tending to form at the ratio of 1:1 around the point of charge neutrality. It can, however, be seen that, unlike the ODN complexes, the radii of gyration are in general significantly larger than the pure copolymer, but rather on a similar order of magnitude to the pure plasmid DNA. (See Figure 6.5).

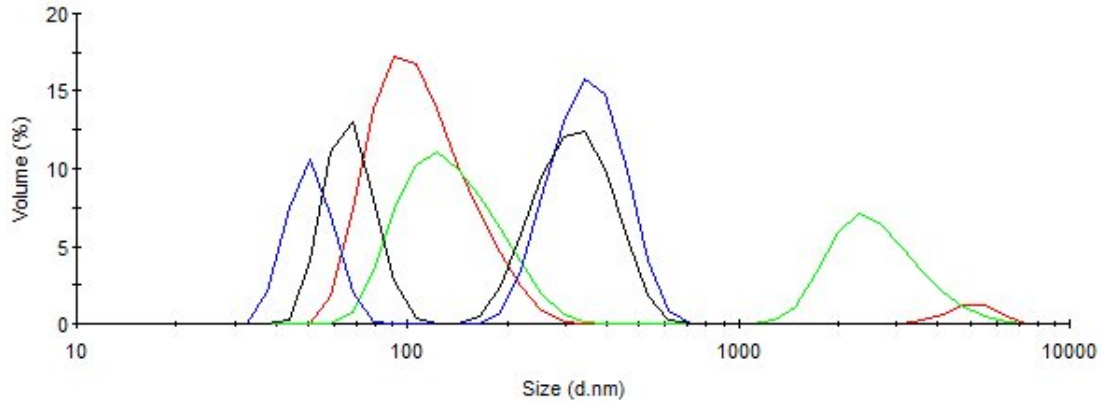

Figure 6.3: Size distribution by percentage volume of MPC_{30}–DEA_{30} complexes with Luciferase plasmid in phosphate buffer as measured by DLS at varying charge ratios, red 10:1, green 5:1, blue 1:1, black 0.5:1. Measurements obtained with DLS (image produced with DTS Nano Software)

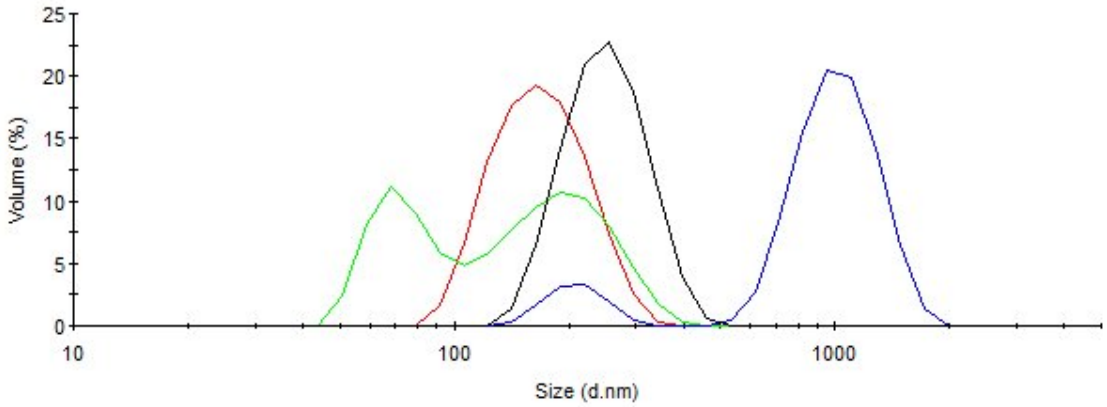

Figure 6.4: Size distribution by percentage volume of MPC_{30}–DEA_{-100} complexes with Luciferase plasmid in phosphate buffer, as measured by DLS at varying charge ratios, red 10:1, green 5:1, blue 1:1, black 0.5:1. Measurements obtained with DLS (image produced with DTS Nano Software)

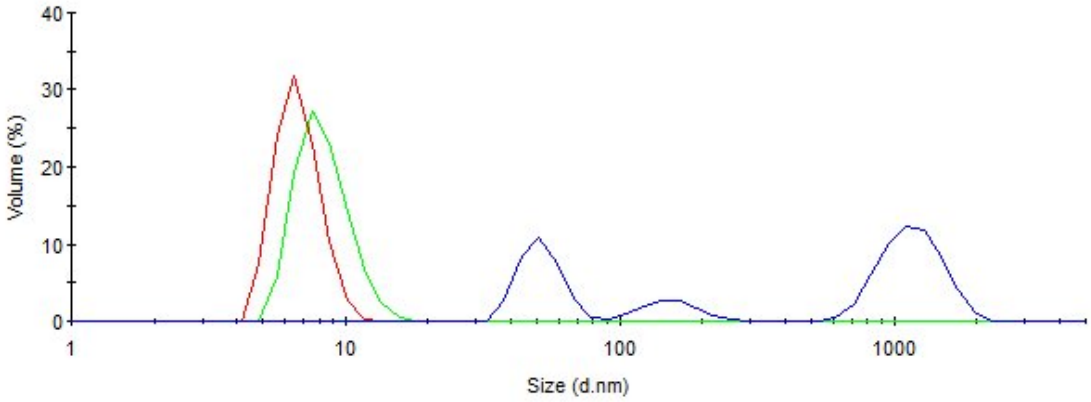

Figure 6.5: Size distribution by percentage volume of pure copolymers MPC_{30}–DEA_{30} at 7.8g/L (red) and MPC_{30}–DEA_{100} at 4.45 g/L (green) and pure Luciferase plasmid DNA at 0.5 g/L (black)Measurements obtained with DLS (image produced with DTS Nano Software)

6.4.2 SANS

ODN

Broad Porod Plot Features

Small angle neutron scattering was carried out on complexes of MPC_{30}–DEA_{30} and MPC_{30}–DEA_{100} with ODNs (See Figures 6.6 and 6.7). A fit to the data using a cylindrical rod model was attempted in the first instance, which has been found in the past to represent copolymer-DNA complexes [203], although it is possible that fitting with a semi-flexible chain model could also be suitable. It can be seen from the graphs of SANS data obtained that, as with DLS, the shape of the curve peak shifts to low Q at around the point of expected particle neutrality at N/P ratios of 2:1 and 1:1, with the simultaneous loss of high-Q structure, suggesting complexes are aggregating as they approach neutrality. The MPC_{30}–DEA_{30} results show slight deviations from this pattern, but precise physical interpretation of this data is only possible with successful fitting to a model. This suggests a broadly similar pattern of behaviour to that observed with DLS, with aggregation around the point of neutrality. Model fitting should offer further insight into the structures of the complexes.

Model-Based Data Fitting

The model types which showed the best fits to the MPC-DEA polymer complexes with ODN are presented in Table 6.1.

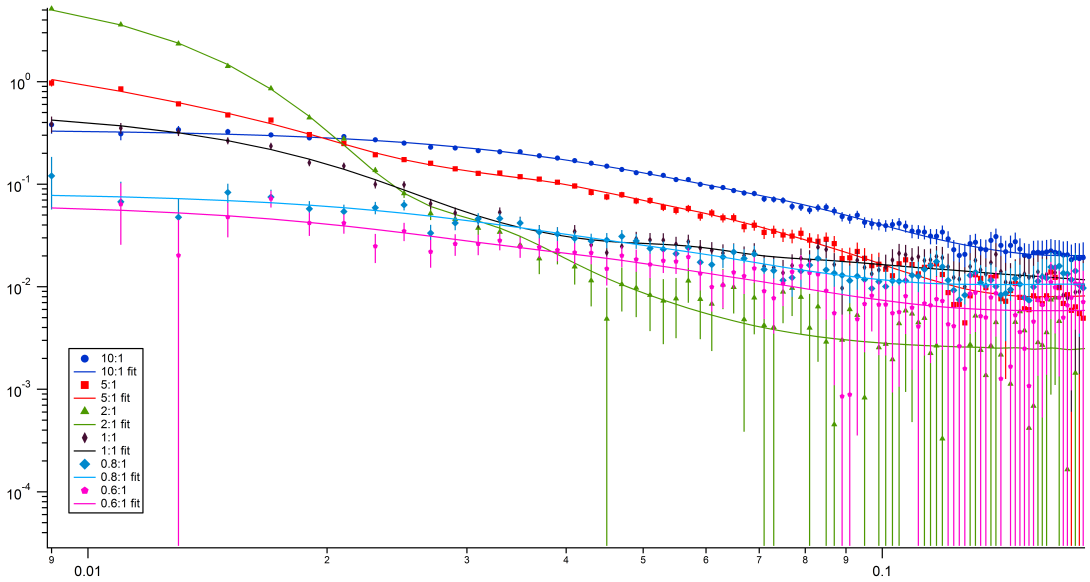

Figure 6.6: SANS scattering profile I(Q) vs. Q, for complexes of MPC_{30}-DEA_{30} with ODN with best fits from FISH software; Legend indicates charge ratio.

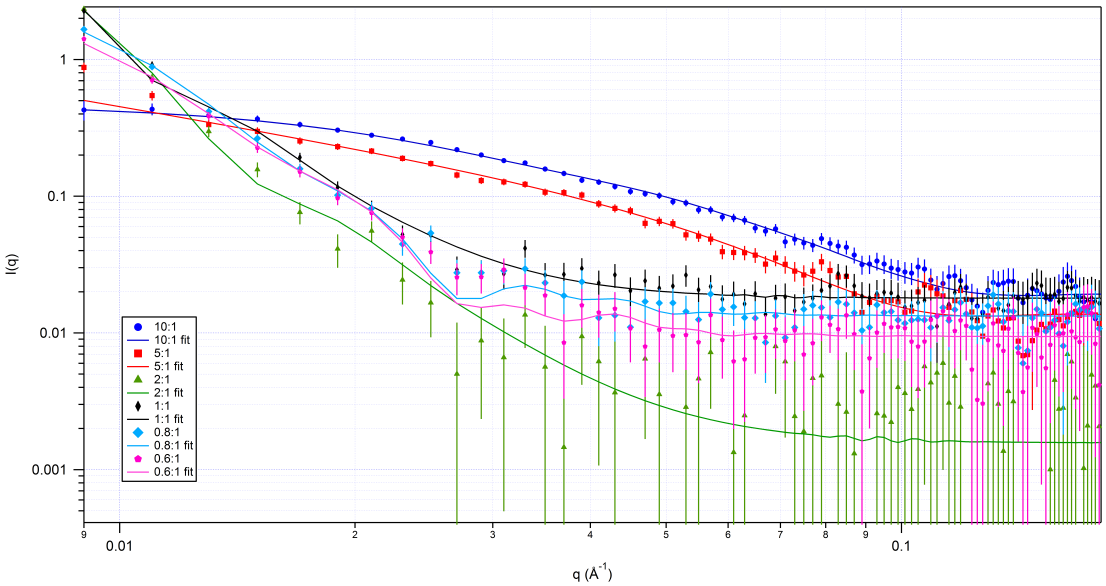

Figure 6.7: SANS scattering profile I(Q) vs. Q with best fits from FISH software, for complexes of MPC_{30}-DEA_{100} with ODN; Legend indicates charge ratio.

Polymer Type	N/P Ratio					
	10:1	5:1	2:1	1:1	0.8:1	0.6:1
MPC_{30}-DEA_{30}	1 rod	2 rods	sphere	2 rods	1 rod	1 rod
MPC_{30}-DEA_{100}	1 rod	1 rod	sphere	sphere	oblate rod	oblate rod

Table 6.1: Best model fits to SANS data from complexes of ODN and MPC_{30}-DEA_{30} and MPC_{30}-DEA_{100} at various N/P ratios from 10:1 to 0.6:1 in PBD at pH 7.4

Broadly, most particles adopted a rod-like conformation, with the exception of complexes formed around neutral charge ratios of 1:1 and 2:1, particularly for MPC_{30}-DEA_{100} complexes, where globular, spherical particles fit best to the scattering data, suggestive of aggregation. This would be a reasonable assumption, due to the relatively low amount of stabilising MPC polymer per molecule, compared with the MPC_{30}-DEA_{30} complexes, which do fit a spherical model at N/P = 2:1, but can be fit with rods at all other charge ratios, indicating potentially greater stability.

The fitting radii and lengths for the elongated cylindrical components fit to ODN - MPC_{30}-DEA_{30} and MPC_{30}-DEA_{100} complexes in the case where a mixture of cylinders are fit, rather than the aggregated globular large particle which was sometimes also present, at all charge ratios studied are shown in Figure 6.8 a) and b), respectively, with the exception of MPC_{30}-DEA_{100} polymer complexes at N/P = 2:1, which could not be fit with a rod-like structure, but only with a sphere, as discussed above.

SANS is very sensitive to the radius of cylindrical rods on the scale found to exist in these complex structures, which are largely cylindrical rods, most likely of flexible ODN wrapping around the polymer, as described by Zhao et al [202]. MPC_{30}-DEA_{100} showed greater tendency than MPC_{30}-DEA_{30} to aggregate when its net charge approaches neutrality, possibly due to the greater capacity for binding DNA due to its larger charge-mass ratio.

(a) FISH fit cylindrical model parameters for complexes of MPC_30-DEA_{30} with ODN

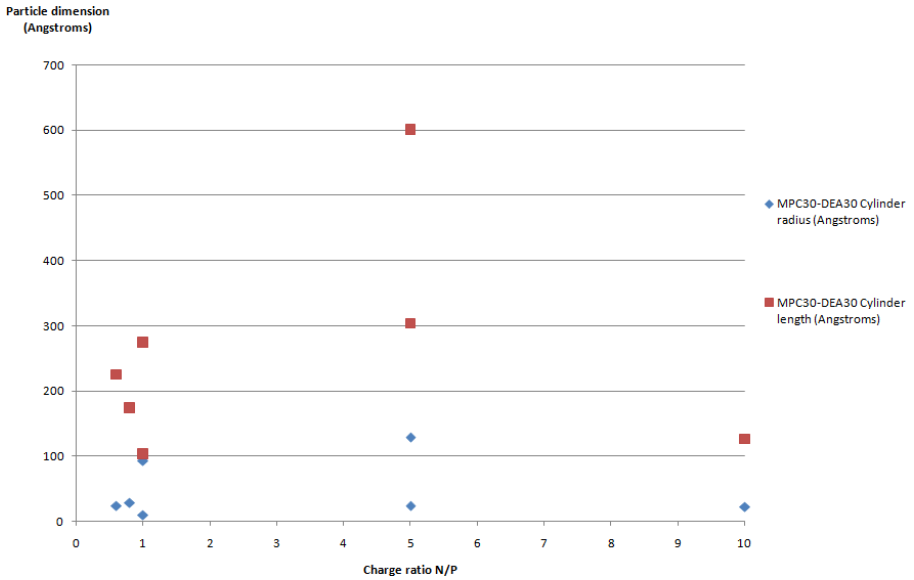

(b) FISH fit cylindrical model parameters for complexes of MPC_30-DEA_{100} with ODN

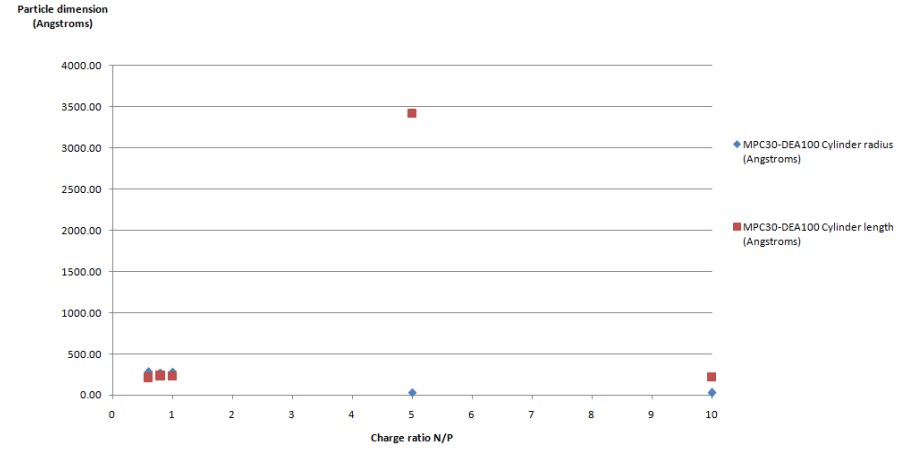

Figure 6.8: SANS cylindrical form factor model parameters radius and length ($\AA$), fit to scattering from complexes of MPC_{30}-DEA_{30} (a) and MPC_{30}-DEA_{100} (b) with ODN at various charge ratios ranging from 10:1 to 0.6:1; Data for charge ratios 2:1 has been omitted as it was consistent with spherical models, due to aggregation. While a spherical model fit marginally better to MPC30-DEA100 1:1 complexes, an oblate cylindrical model was almost equivalently good, so these parameters are shown here to enable comparison

Plasmid

Broad Porod Plot Features

The SANS data obtained for complexes of MPC30–DEA30 and MPC30–DEA100 with Luciferase plasmid are shown in Figures 6.9 and 6.10.

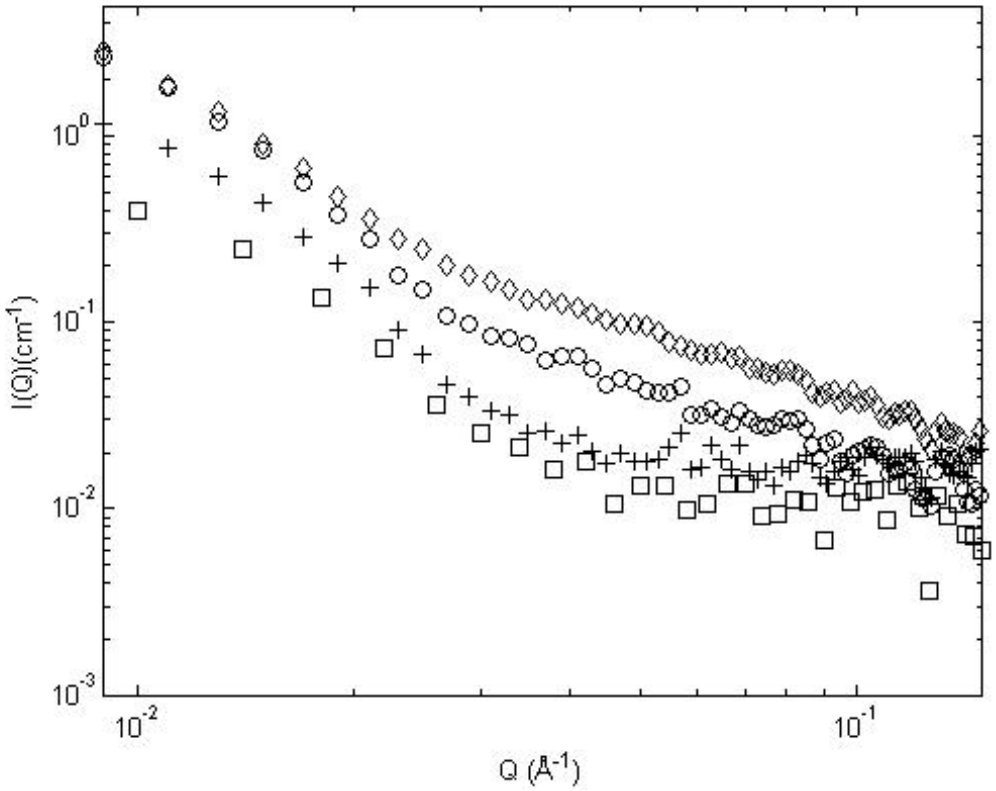

Figure 6.9: SANS scattering profile I(Q) vs. Q, for complexes of MPC_{30}–DEA_{30} with Luciferase plasmid; the diagram markers represent the following N/P charge ratios: diamond = 10:1, circle = 5:1, vertical cross = 1:1, square = 0.5:1

A similar dependence on charge ratio is observed in the trend of the curve shapes, with MPC_{30}–DEA_{100} again showing a shift at the point of expected charge neutrality compared to the other ratios to a steep low Q Porod gradint, suggestive of larger aggregates, with a loss of scattering intensity in the higher Q regimes which correspond to smaller structures. Again, these parameters will be determined precisely with fitting of the data to a model.

Model-Based Data Fitting

Luciferase plasmid complexes with copolymers at all charge ratios studied could be well fit with a model combining two cylindrical rods. Again, fitted radius and length parameters

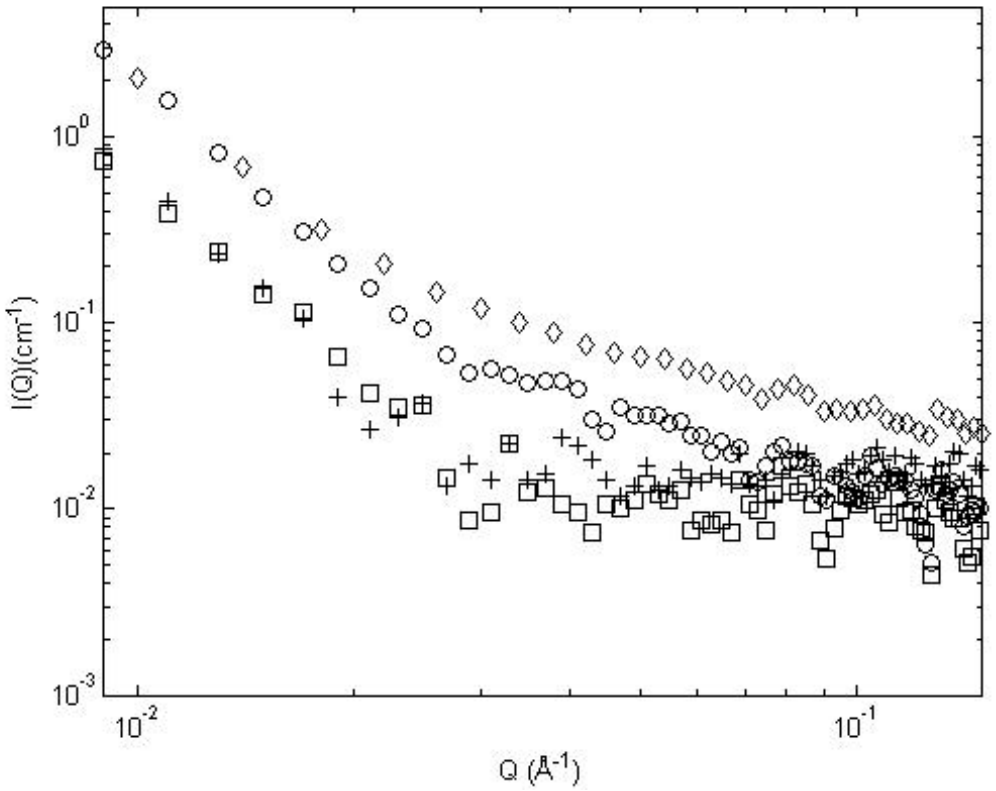

Figure 6.10: SANS scattering profile I(Q) vs. Q, for complexes of MPC_{30}–DEA_{100} with Luciferase plasmid; the diagram markers represent the following N/P charge ratios: diamond = 10:1, circle = 5:1, vertical cross = 1:1, square = 0.5:1

for the first cylinder which has a cylindrical structure, rather than the larger, globular structure often present also, are shown in Figure 6.11 a) for MPC_{30}-DEA_{30} complexes and Figure 6.11 b) for MPC_{30}-DEA_{100}.

6.4.3 The Effect of NaCl Concentration on Complex Structure

Small angle neutron scattering was conducted on complexes of ODN with MPC_{30}-DEA_{70} in perdeuterated phosphate buffer with a range of concentrations of added NaCl at a N/P ratio of 5 (see Figure 6.12). The scale factor, which was simultaneously fit to the data, and is proportional, among other factors, to the number density of the scattering particles in solution, is also shown in Figure 6.13 as a function of added NaCl concentration. The swelling of the particles with increasing monovalent salt concentration indicates their dependence on electrostatic interactions as the screening of the charges and compression

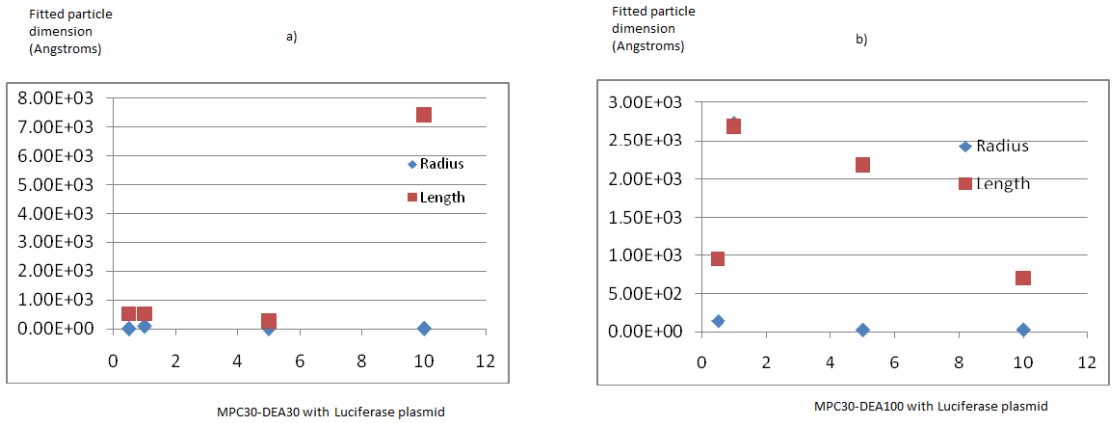

Figure 6.11: SANS cylindrical form factor model parameters radius and length ($\AA$), fit to scattering from complexes of MPC_{30}-DEA_{30} (a) and MPC_{30}-DEA_{100} (b) with Luciferase plasmid DNA at various charge ratios ranging from 10:1 to 0.6:1;

of the electric double-layers diminish the interaction potential and weaken the binding.

The radii shown are those of the predominant component of the solution, larger aggregates often also being present. The anomalous low radius at the highest salt concentration examined of 1250mM NaCl could be due to near-complete dissociation of the complexes under these conditions, or salting out of solution. The scale factor simultaneously fit within the rod-like model does not display a strong trend as salt concentration increases, but also falls off sharply at this highest concentration, indicating the sample could be precipitating out of the solution, or at least out of the size range accessible to SANS, limited by the lowest Q value accessible.

6.5 Discussion and Further Work

Complexes of block copolymers of MPC with DEA in ratios 30-30 and 30-100 with ODN were studied at various charge ratios. The particles largely adopted a rod-like conformation , with the exception of complexes around the point of neutrality, with charge ratios of 1:1 and 2:1, which exhibited more globular conformations.

There was some indication that MPC-30-DEA-100 showed a slightly greater tendency to form globular complexes with ODN near the point of neutrality, resulting perhaps from their proportionally lower stabilising MPC block. However, transfection studies would be necessary to understand whether this translated into a desirable effect.

The effect of increasing salt concentration on the complexes was also investigated. The

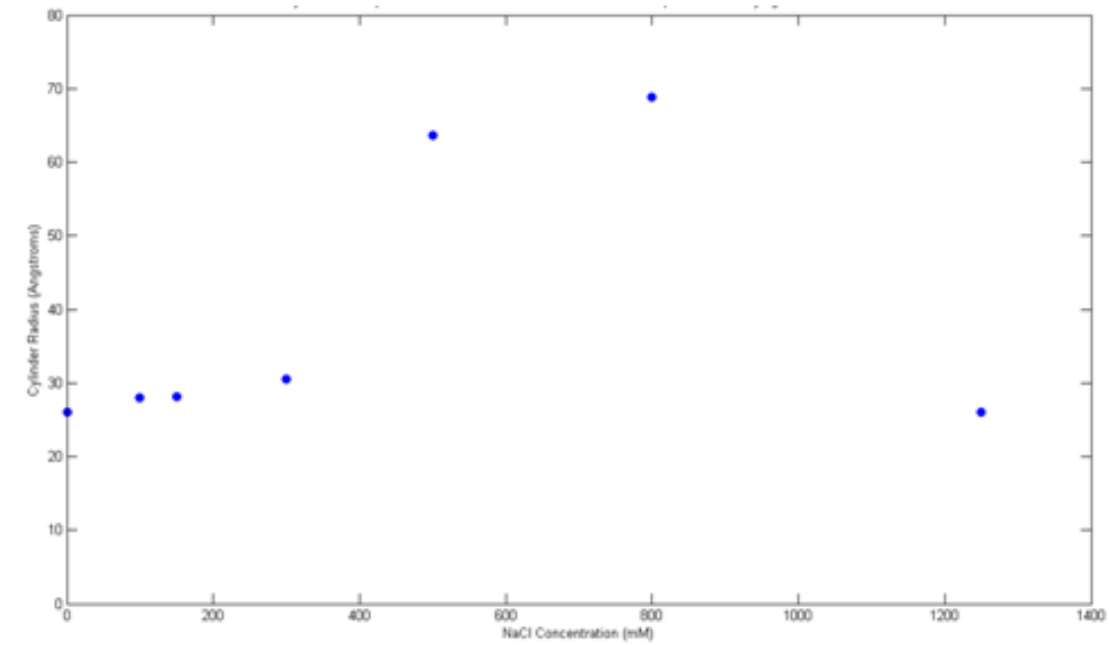

Figure 6.12: Radii of the predominant cylindrical component fit to SANS data for complexes of MPC_{30}–DEA_{70} with ODN at a charge ratio of N/P = 5:1 in varying concentrations of NaCl in PBD;

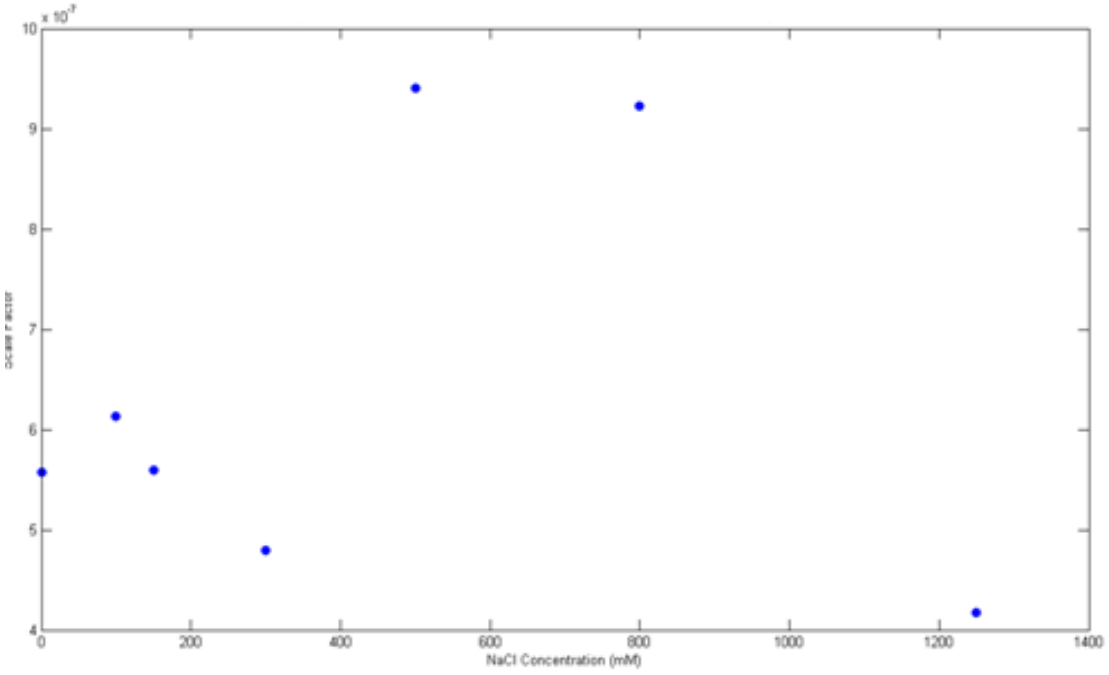

Figure 6.13: Scale factor of the predominant cylindrical component fit to SANS data for complexes of MPC_{30}–DEA_{70} with ODN at a charge ratio of N/P = 5:1 in varying concentrations of NaCl in PBD;

results here highlighted the electrostatic nature of the binding, although potential salting out effects may also play a role. This is interesting as for PEI complexes, Utsuno et al found that there are two modes of binding, one which does not require the PEI to be protonated, which may however be the case here also.

Overall, these complexes showed good stability in low salt media, except near the point of neutrality, indicating a likely positive candidate for transfection, which has been demonstrated for related polymers by Zhao et al.

6.6 Potential Future Work

Detailed transfection work in vitro would complement the structural observations made for these complexes' dependence on charge ratio and degree of polymerisation of the two polymer blocks. Literature reports vary as to the advantage or disadvantage of large, aggregated complexes for transfection, as discussed earlire, with several studies indicating an advantage for aggregated complexes, due either to sedimentation onto the cell monolayer, increasing association and uptake, or by restricting the accessible endocytic pathways for access to clathrin-independent ones which result, in the case of PEI, in higher transfection efficiency.

Assuming some degree of aggregation did not adversely affect transfection efficiency to a great degree, the advantages of increasing the cationic block of the polymer's degree of polymerisation with respect to the stabilising, DEA, block is that each complex is likely to bind a larger quantity of DNA and, hence, fewer discrete complexes are required to achieve cellular uptake to reach the same level of transfection.

Confocal studies on instruments such as the BD Pathway could enable a greater degree of quantitative analysis of fluorescently conjugated ODNs, as used in the work of Zhao et al [202], enabling identification of gene delivery to localised regions within cells and high resolution images to be taken to achieve counting of statistical numbers of transfected cells, while simultaneously observing their morphologies, an advantage with the solution-based technique of flow cytometry does not afford.

This could enable detailed, high content screening studies to be undertaken, varying many paramaters within one experiment. The application of drug treatments such as nocodazole or bafilomycin A1 to disrupt certain endocytic pathways in cells could be of interest to

explore whether the particles' cellular entry mechanism vary depending on the structural changes identified here.

Chapter 7

Discussion and Future work

7.1 Principal Findings

This work had as its principal aim to further understanding of the interaction between cationically charged polymers and nucleic acids to form complexes which are capable of transporting the nucleic acid into cells, overcoming the principle, fundamentally physical barrier of electrostatic repulsion between the anionic nucleic acid and the similarly charged cellular lipid bilayer membrane.

In order to achieve this, we took two fundamental approaches to contributing to expanding the existing body of knowledge: the application of an emerging technique to an existing cationic vector system of polyethylenimine, and the characterisation of a proprietary, designed gene delivery system, which has been relatively little studied.

7.1.1 Static and Dynamic Study of the Aggregation of PEI-DNA Complexes

PEI is generally well-characterised, as evidenced by the large body of literature on the applications and features of PEI as a gene delivery vector, a proportion of which is referenced in the initial review of the literature conducted, in Chapter 1. Much is known about the mechanisms of transfection of PEI, its routes of cellular entry, mechanisms of endosomal escape and efficiency in its various branched and linear forms, sizes and

modifications, such as pegylation. However, due to the inherent instability of this highly charged molecule when bound to an oppositely charged polyelectrolyte, the phenomenon of aggregation is well-documented and has been greatly studied by indirect observational techniques, such as isothermal titration calorimetry, which measure the binding energy of interaction between two particles, but do not as such build up a picture of the molecules involved. AFM is an alternative technique, which very directly produces a picture of the molecules of interest, however interactions between the complexes and the adsorbing surface, which is frequently highly charged, are likely to influence the conformation of the molecule away from its native state. It was therefore decided to undertake a small-angle neutron scattering study on the complexes, making use of the new, high flux SANS2D beamline at ISIS target station 2, combined with a stopped-flow apparatus to enable kinetic examination of the progression of aggregation in complexes of DNA fragments and PEI of both branched and linear architectures and of an order of magnitude's range in molecular weight.

The static and kinetic study of PEI-DNA complexes presented here was novel because, previously, to our knowledge, aggregation and precipitation had hampered most attempts to undertake SANS studies of PEI-DNA complexes, due to the requirement for them to remain solubilised for extended periods of time. Optimisation of the solution conditions was required to obtain a solvent media which did not entirely suppress aggregation, to enable its time-course to be studied, while not allowing it to escalate so far beyond the size range of SANS that complex structure was not observable. This system, combined with the stopped-flow apparatus coupled with the new, high-flux SANS2D beamline at ISIS, enabled time-slicing to follow the aggregation behaviour of complexes on the scale of seconds to minutes. Key differences in stability and structure between complexes formed from different polymer architectures and molecular weights were observed. Low MW PEI complexes of either branched or linear architecture appearing to have the greatest instability in solution, while high MW BPEI complexes were significantly more stable and could be modelled, using form factor based modelling, with a looser, network like structure. Large, smoother, apparently globular aggregates, meanwhile, were found to be characteristic of the less stable, low MW and linear polymer complexes.

As mentioned previously, it would be of great interest to compare the relative stability or instability of these various complexes with their ultimate transfection efficiency in vitro, to ascertain whether the aggregation helped or hindered gene delivery under various

circumstances. A model system of siRNAs, as used in the zeta potential studies from Chapter 5, described below, which are antisense RNAs to the GAPDH gene, a ubiquitous housekeeping gene which encodes the GAPDH enzyme, whose activity can be measured fluorometrically or colorimetrically in a bioassay, which should enable a clear indicator to be measured of the impact on enzyme activity, and hence efficiency of siRNA delivery of the various PEIs' complexes, which could also be studied at different time points after complexation to gain an idea of the impact of aggreation on transfection ability, and contribute to the optimisation of transfection protocols in the wider body of research on the subject.

PEI Complexation - Conclusions

The expected model described in Chapter 1 for binding of the PEI and DNA complexes expects that, as DNA comprises relatively short, stiff molecules, the PEI, where it is longer, may bind around the DNA, or where polymers are branched, these branches may afford greater flexibility in binding. The charged branches may also be expected to stabilise the complex in solution, particularly, again, for larger polymer molecules, where a greater proportion of the charges per molecule are likely to be free from direct binding to DNA, and therefore participate in stabilisation.

The key findings and implications of this research are set out below.

Static conclusions Polymer type:

Four types of PEI were investigated in this work - high and low molecular weights of branched and linear PEIs. Model fitting to the complexes indicated that the complexes formed were largely elongated, cylindrical, with high MW (25 kDa) BPEI complexes at N:P = 10:1 forming more flexible chains which could be well modelled by a Kholodenko wormlike chain model.

Small PEI of both branched and linear morphologies scattered weakly and appeared to form large aggregates, as indicated by Porod estimations, without flexibility or internal component structure detected.

Additionally, the high molecular weight branched PEI complex showed greater detailed structure than the linear, which would seem to support findings in the literature that linear PEI complexes are less colloidally stable than those formed with branched PEI. It is possible that the high molecular weight branched PEI complexes are binding with

multiple PEI molecules per complex, leading to these large structures. Alternative imaging methods, such as AFM, could provide insight into the physicality of these structures. It may be that, although the wormlike chain model provides the best fit to the data, another model would provide a more physical solution, which could be investigated further.

Even before examining the data on a time-sliced basis, however, the higher level of structure indicates the high molecular weight PEI experiences less of a tendency to aggregate, in contrast to the smaller, linear PEIs, which form large, globular aggregates, as indicated by the FISH model parameters. This supports the findings from the literature discussed in Chapter 1, that branched PEI tends to be more stable and have higher transfection efficiency, both for analagous siRNA and for larger DNA molecules, as discussed in Chapter 1.

Solvent media:

High MW BPEI DNA complexes were studied in 5% glucose, 10mM NaCl and D_2O. The indication from the modelling is that complexes formed in pure D_2O were marginally stiffer, resembling swollen chains rather than gaussian coils, in contrast to those formed in 10mM NaCl or D_2O, suggesting a mediating role in the binding for these other molecules.

Concentration and charge ratio:

Studies on LOQ at different concentrations showed differences in scattering profile which suggested a potential increase in aggregation at the higher concentration there. This was more notable for the seemingly more stable high MW BPEI complexes than for LPEI, which were already thought to be strongly aggregated and therefore may demonstrate less of a clear concentration-driven increase in aggregation in the accessible size range. The change in mixing mechanism from stopped-flow to manual mixing may have also had an impact on the structure. When the charge ratio was increased from 10:1 to 20:1 at the higher concentration, the deviation seen at 10:1 was no longer observed, suggesting the increase in net positive charge excess may have been sufficient to counteract the increase in binding pressure with concentration.

pH:

The effect of pH on the complex structure was investigated over the range pH 5.4 - 7.4, which is similar to the pH range which would be experienced through cellular internalisation via the endocytic pathway. Negligible structural differences were observed between

the different pHs, indicating that the complexes are likely to remain structurally stable in this range, although the ionic strength difference may mean outcomes are different intracellularly. Indeed, Utsuno et al found in their work that binding was likely to become tighter over this range.

Kinetic conclusions PEI type:

When the SANS data collected was time-sliced over the 30 minutes observed, key differences were confirmed between PEI types. Most notable, the high molecular weight branched PEI, hypothesised to form the most stable complexes, was found to undergo little structural change and the absence of large, smooth aggregates from the static scattering data was confirmed. A slight shortening of the statistical rod segment length was observed, suggesting possible increased curving and tightening of binding of the polymer in the DNA complex, however this was a relatively small effect.

Low molecular weight BPEI complexes, on the other hand, showed a much greater change, with fitted cylinders growing in radius, indicating growing aggregate sizes over the course of the 30 minutes studied.

For both high and low molecular weight LPEI complexes, cylindrical model fitting suggested a tendency to transition towards more globular-like aggregates over the course of the time period studied. However, low molecular weight LPEI complexes exhibited a more gradual structural transition than other polymer types.

When a higher charge ratio of 20:1 was studied for high MW LPEI and BPEI complexes, a significant change in the background level was observed during the early time frames, suggesting the possibility that this excess positive charge slowed the aggregation sufficiently to observe an earlier stage of complex formation. However, it could be that another effect was taking place.

7.1.2 Time Evolution of Zeta Potential of Complexes

Following on from the static and kinetic SANS study and given the observations which had been made concerning the tendencies to aggregate of different PEI complexes, it was of interest to further probe one of the driving force behind aggregation, or rather, perhaps, preventative forces which acts to suppress the aggregation, which is thought to be driven

by hydrophobic effects: surface charge and zeta potential in a time-resolved study.
To analyse the zeta-potential data from PEI-siRNA complexes of various PEI types in light of the SANS data, it was interesting to note the apparent similarities in findings concerning the most stable of the polymers, 25 kDa BPEI, which maintained a positive zeta-potential, although the magnitude was not high, suggesting that aggregation is still likely to proceed in this sample, even if not as aggressively as some others. Evolution of the smaller polymers' complexes was, perhaps more predictably, sharply dropping zeta potential towards zero and plateauing at negative values, indicative of a strongly aggregating sample, which was certainly found to be the case, based on the SANS data.
Overall, a clear picture was built up of the behaviour of these types of cationic polymers under complexation. ITC would be an interesting complementary technique to expand understanding of the aggregation process and driving forces, while the visual, measurable complex deposited and imaged with AFM would be very complementary to the modelled and fitted structures of the SANS analysis.
Zeta potential conclusions:

This led to the question of the driving force behind this aggregation behaviour, so it was decided to investigate the zeta potential of complexes between PEI and a structurally similar but physiologically active nucleic acid, the siRNA molecule for GAPDH.
This zeta potential study highlighted how unstable all four complex types were likely to be against aggregation in solution with nucleic acids, as none of their initial zeta potentials attained the commonly referenced stability threshold of 30 mV. However, it was still clear to see that a difference in zeta potential and stability behaviour was present in the high MW BPEI complex in comparison to the other PEI types, which supported the findings from the SANS studies, that high MW BPEI in 10 mM NaCl solution at pH 7.4 formed far more stable complexes than other PEI types. It was interesting to note here, however, that the 25 kDa BPEI complexes were still not entirely stable, according to the zeta potential results, and did change over the course of the time-frame observed, all remaining within the unstable range at the end of the measurement period. Additionally, from reference to the literature, it is not clear that the complex which is the most stable, delivers the greatest transfection efficiency, at least not in every circumstance, which intuitively might be thought to be so. In fact, it has been reported [103] that for the type of small nucleic acid molecules studied in this work, such as siRNA, relatively weak binding enables dissociation

of the nucleic acid from the complex, which is likely to be required at some stage, if the DNA is to have a chance of being biologically active within the cell. Low MW PEIs are therefore effective transfection agents for these types of DNA[187], also being optimally sized, according to the authors, for uptake through endocytosis.

The evolution of zeta potential with complexation time for all four PEI types, high and low molecular weight, linear and branched, with siRNA, analagous structurally to the systems studied in kinetic SANS, was investigated.

Both types of complex investigated remained in the likely aggregation zone, within the range of plus and minus 30 mV for the duration of the study, ultimately plateauing in all cases near neutrality, indicating they may be likely to continue to aggregate. However, 25 kDa BPEI complexes, as may be expected from the literature and the previous SANS study, appeared to tend towards the plateau of stability more quickly than other polymer types and plateaued at a more positive overall zeta potential, potentially indicating a lower driver for aggregation. This broadly supports the findings in the previous chapter on the stability of high MW BPEI complexes, and descriptions in the literature, as described in Chapter 1, Selection of the System.

A general further development to the study overall would be the extension and repetition of the work conducted here, which was frequently limited by availability of neutron beamtime or limited quantities of precious samples. While the observations presented contribute to forming a picture of the structural development of these systems, greater confidence could be obtained through independent repetition of the conditions investigated and exploration in greater detail of series of related conditions.

7.1.3 Sterically Stabilised Cationic Diblock Copolymer Complexes for Delivery of ODNs

Finally, the study's focus turned to the techniques which have been employed in novel vector design to overcome the hurdles associated with aggregation, which may indeed reduce transfection efficiency, particularly where in vivo delivery is required.

There is, necessarily, a strong electrostatic binding force underlying complexation between oppositely charged polyelectrolytes and, despite some degree of overcharging which is achievable, and serves to some extent to create electrostatic repulsion between complexes, this is not necessarily enough to prevent precipitation in the absence of some

other, stabilising force.

The family of cationic diblock copolymers, of which one particular member was widely explored in previous work by Zhao [202], was studied in the broader context of the variation of degrees of polymerisation between the highly cationic DEA block, designed to bind DNA, and the hydrophilic MPC block, which is conjugated to the cationic polymer in order to sterically stabilise the complex in solution, once the cationic charges are largely neutralised. Investigation with SANS in this case suggested the copolymer complexes were not necessarily always fully stable, in spite of their stabilising block, and do form larger, globular aggregates instead of the extended rod conformations which they adopt at high charge ratios where there is a great deal of free polymer excess.

In this case, cell culture transfection studies would be the most natural extension of the work, to investigate the relationship between the varying degrees of block polymerisation and the efficacy of this family of polymers as gene delivery vectors.

MPC-DEA conclusions

Block Ratio Complexes of block copolymers of MPC with DEA in ratios 30-30 and 30-100 with ODN were studied at various charge ratios. The particles largely adopted a rod-like conformation , with the exception of complexes around the point of neutrality, with charge ratios of 1:1 and 2:1, which exhibited more globular conformations.

There appeared to be some indication that MPC-30-DEA-100 showed a slightly greater tendency to form globular complexes with ODN near the point of neutrality, resulting perhaps from their proportionally lower stabilising MPC block. However, transfection studies would be necessary to understand whether this translated into a desirable effect.

The effect of increasing salt concentration on the complexes was also investigated. The results here highlighted the electrostatic nature of the binding, although potential salting out effects may also play a role. This is interesting as for PEI complexes, Utsuno et al has been found that there are two modes of binding, one which does not require the PEI to be protonated, which may however be the case here also.

Overall, these complexes appeared to show good stability in low salt media, except near the point of neutrality, indicating a likely positive candidate for transfection, which has been demonstrated for related polymers by Zhao et al. Further work would ideally expand the investigation of intracellular delivery mechanisms, hurdles and point of dissociation,

which could be undertaken using high resolution fluorescence microscopy and chemical assays, such as Bafilomycin A1 and nocodazole.

Bibliography

[1] J a Abels, F Moreno-Herrero, T van der Heijden, C Dekker, and N H Dekker. Single-molecule measurements of the persistence length of double-stranded RNA. *Biophysical journal*, 88(4):2737–44, April 2005. [cited at p. 27, 35]

[2] A. Akinc, M. Thomas, A. M. Klibanov, and R. Langer. Exploring polyethylenimine-mediated DNA transfection and the proton sponge hypothesis. *J. Gene Med.*, 7(5):657–663, 2005. [cited at p. 14, 16]

[3] Akin Akinc, Mini Thomas, Alexander M Klibanov, and Robert Langer. Exploring polyethylenimine-mediated DNA transfection and the proton sponge hypothesis. *J Gene Med*, 7:657663, 2005. [cited at p. 67]

[4] Bruce Alberts, editor. *Molecular Biology of the Cell.* Garland Publishing Inc, 2002. [cited at p. 20]

[5] Bruce Alberts, Dennis Bray, Julian Lewis, Martin Raff, Keith Roberts, and James D Watson. *Molecular Biology of the Cell, 3rd edn.* Elsevier, 1994. [cited at p. 11]

[6] Caroline Ankerfors. *Polyelectrolyte complexes: their preparation, adsorption behaviour and effect on paper properties.* PhD thesis, Royal Institute of Technology (KTH) Stockholm, 2008. [cited at p. 86, 160, 161]

[7] Suvi Asikainen, Liisa Heikkinen, Garry Wong, and Markus Storvik. Functional characterization of endogenous siRNA target genes in Caenorhabditis elegans. *BMC genomics*, 9:270, January 2008. [cited at p. 27, 35]

[8] K S Balaggan, Y Duran, a Georgiadis, C Thaung, S E Barker, P K Buch, a MacNeil, S Robbie, J W B Bainbridge, a J Smith, and R R Ali. Absence of ocular malignant transformation after sub-retinal delivery of rAAV2/2 or integrating lentiviral vectors in p53-deficient mice. *Gene therapy*, 19(2):182–8, February 2012. [cited at p. 17]

[9] Daniel a Balazs and Wt Godbey. Liposomes for use in gene delivery. *Journal of drug delivery*, 2011, January 2011. [cited at p. 24]

[10] Rikke V Benjaminsen, Maria a Mattebjerg, Jonas R Henriksen, S Moein Moghimi, and Thomas L Andresen. The possible "proton sponge " effect of polyethylenimine (PEI) does not include change in lysosomal pH. *Molecular therapy : the journal of the American Society of Gene Therapy*, 21(1):149–57, January 2013. [cited at p. 14, 69]

[11] J M Benns, J S Choi, R I Mahato, J S Park, and S W Kim. pH-sensitive cationic polymer gene delivery vehicle: N-Ac-poly(L-histidine)-graft-poly(L-lysine) comb shaped polymer. *Bioconjugate chemistry*, 11(5):637–45, 2000. [cited at p. 25]

[12] Aurélie Bertin, Amélie Leforestier, Dominique Durand, and Françoise Livolant. Role of histone tails in the conformation and interactions of nucleosome core particles. *Biochemistry*, 43(16):4773–80, April 2004. [cited at p. 176]

[13] Martin Bertschinger, Gaurav Backliwal, Arnaud Schertenleib, Martin Jordan, David L Hacker, and Florian M Wurm. Disassembly of polyethylenimine-DNA particles in vitro: implications for polyethylenimine-mediated DNA delivery. *Journal of controlled release : official journal of the Controlled Release Society*, 116(1):96–104, November 2006. [cited at p. 71, 75]

[14] R.J. Beynon and J.S. Easterby. *Buffer Solutions The Basics*. Oxford University Press, Taylor and Francis, 2005 edition, 1996. [cited at p. 47, 85]

[15] Bio-Logic. Bio-Logic Stopped-Flow Apparatus Description, 2012. [cited at p. 89]

[16] Ian S. Blagbrough, Abdekader A. Metwally, and Osama A. A. Ahmed. 9.2.4 Endosomal Escape. In Patrick Woster and Robert Casero, editors, *Polyamine Drug Discovery*, chapter 9. RSC Publishing. [cited at p. 14]

[17] Victor A Bloomfield. Condensation of DNA by multivalent cations: Considerations on mechanism. *Biopolymers*, 31(13):1471–1481, 1991. [cited at p. 36, 69]

[18] Sabine Boeckle, Katharina von Gersdorff, Silke van der Piepen, Carsten Culmsee, Ernst Wagner, and Manfred Ogris. Purification of polyethylenimine polyplexes highlights the role of free polycations in gene transfer. *The journal of gene medicine*, 6(10):1102–11, October 2004. [cited at p. 69, 74, 131, 196]

[19] O Boussif, F Lezoualc'h, M a Zanta, M D Mergny, D Scherman, B Demeneix, and J P Behr. A versatile vector for gene and oligonucleotide transfer into cells in culture and in vivo: polyethylenimine. *Proceedings of the National Academy of Sciences of the United States of America*, 92(16):7297–301, August 1995. [cited at p. 66, 69, 72]

[20] Andreas Brave, Andreas Boberg, Lindvi Gudmundsdotter, Erik Rollman, Kristian Hallermalm, Karl Ljungberg, Pontus Blomberg, Richard Stout, Staffan Paulie, Eric Sandstrm, Gunnel Biberfeld, Patricia Earl, Bernard Moss, Josephine H Cox, and Britta Wahren. A New Multi-clade DNA Prime/Recombinant MVA Boost Vaccine Induces Broad and High Levels of HIV-1-specific CD8+ T-cell and Humoral Responses in Mice. *The American Society of Gene Therapy*, 15(9):1724–1733, 2007. [cited at p. 9, 19]

[21] Blandine Brissault, Antoine Kichler, Christine Guis, Christian Leborgne, Olivier Danos, and Hervé Cheradame. Synthesis of linear polyethylenimine derivatives for DNA transfection. *Bioconjugate chemistry*, 14(3):581–7, 2003. [cited at p. 70]

[22] William H. Brown, Christopher S. Foote, Brent L. Iverson, Eric V. Anslyn, and Bruce M. Novak. 4.4 The Position of Equilibrium in Acid-Base Reactions. In *Organic Chemistry*, chapter 4. Acids a, page 164. Brooks/Cole, 6 edition, 2011. [cited at p. 11]

[23] Karen Butter, Armin Hoell, Albrecht Wiedenmann, Andrei V. Petukhov, and Gert-Jan Vroege. Small-angle neutron and X-ray scattering of dispersions of oleic-acid-coated magnetic iron particles. *Journal of Applied Crystallography*, 37(6):847–856, November 2004. [cited at p. 98]

[24] AL Chaves, CE Vergara, and JE Mayer. Dichloromethane as an economic alternative to chloroform in the extraction of DNA from plant tissues. *Plant Molecular Biology Reporter*, 13:18–25, 1995. [cited at p. 80]

[25] AM Chen, O Taratula, D Wei, and HI Yen. Labile catalytic packaging of DNA/siRNA: control of gold nanoparticles out of DNA/siRNA complexes. *ACS Nano*, 4(7):3679–3688, 2010. [cited at p. 25]

[26] Clive Chen and Junghae Suh. 9.4.2.2 Non-viral Vectors. In Volkmar Weissig and Gerard G. M. D'Souza, editors, *Organelle-Specific Pharmaceutical Nanotechnology*, chapter 9. Realti, page 171. Wiley, 2010. [cited at p. 15]

[27] Pierre Chodanowski and Serge Stoll. Polyelectrolyte Adsorption on Charged Particles in the Debye-Hckel Approximation. A Monte Carlo Approach. *Macromolecules*, 34(7):2320–2328, 2001. [cited at p. 37]

[28] Young Hun Choi, Feng Liu, Jin-Seok Kim, Young Kweon Choi, Jong Sang Park, and Sung Wan Kimb. Polyethylene glycol-grafted poly-L-lysine as polymeric gene carrier. *Journal of Controlled Release*, 54:39–48, 1998. [cited at p. 24]

[29] Sirirat Choosakoonkriang, Brian A. Lobo, Gary S. Koe, Janet G. Koe, and C. Russell Middaugh. Biophysical characterization of PEI/DNA complexes. *J. Pharm. Sci.*, 92(8):1710–1722, 2003. [cited at p. 26, 37, 67, 72]

[30] Feng Cong, Jianxuan Zhang, William Pao, Pengbo Zhou, and Harold Varmus. A protein knockdown strategy to study the function of beta-catenin in tumorigenesis. *BMC molecular biology*, 4(10), September 2003. [cited at p. 9]

[31] Nicolas Coquery, Nicolas Pannetier, Régine Farion, Aurélie Herbette, Leire Azurmendi, Didier Clarencon, Stéphane Bauge, Véronique Josserand, Claire Rome, Jean-Luc Coll, Jian-Sheng Sun, Emmanuel L. Barbier, Marie Dutreix, and Chantal C. Remy. Distribution and Radiosensitizing Effect of Cholesterol-Coupled Dbait Molecule in Rat Model of Glioblastoma. *PLoS ONE*, 7(7):e40567, July 2012. [cited at p. 27]

[32] L Cristofolini, T Berzina, V Erokhin, M Tenti, M Fontana, S Erokhina, and O Konovalov. The structure of DNA-containing complexes suggests the idea for a new adaptive sensor. *Colloids and Surfaces A: Physicochemical and Engineering Aspects*, 321(1-3):158–162, May 2008. [cited at p. 27, 44]

[33] Luigi Cristofolini, Tatiana Berzina, Svetlana Erokhina, Oleg Konovalov, and Victor Erokhin. Structural study of the DNA dipalmitoylphosphatidylcholine complex at the air-water interface. *Biomacromolecules*, 8(7):2270–5, July 2007. [cited at p. 27, 44, 80, 83]

[34] Stephen Cummings, Dazun Xing, Robert Enick, Sarah Rogers, Richard Heenan, Isabelle Grillo, and Julian Eastoe. Design principles for supercritical CO2 viscosifiers. *Soft Matter, The Royal Society of Chemistry*, 8(26), 2012. [cited at p. 104]

[35] Signe Danielsen. *Chitosan mediated DNA condensation as a basis for gene delivery: Influence of polyelectrolyte molecular parameters on the condensation behavior*. PhD thesis, Department of Physics, Norwegian University of Science and Technology, Trondheim, Norway, 2004. [cited at p. 35, 37]

[36] Rui Deng, Yanan Yue, Fan Jin, Yangchao Chen, Hsiang-Fu Kung, Marie C M Lin, and Chi Wu. Revisit the complexation of PEI and DNA - how to make low cytotoxic and highly efficient PEI gene transfection non-viral vectors with a controllable chain length and structure? *Journal of controlled release*, 140(1):40–46, November 2009. [cited at p. 72]

[37] Madiha Derouazi, Philippe Girard, Frédéric Van Tilborgh, Keyvan Iglesias, Natalie Muller, Martin Bertschinger, and Florian M Wurm. Serum-free large-scale transient transfection of CHO cells. *Biotechnology and bioengineering*, 87(4):537–45, August 2004. [cited at p. 67, 72, 88]

[38] J DeRouchey, R R Netz, and J O Rädler. Structural investigations of DNA-polycation complexes. *Eur. Phys. J. E*, 16:17–28, 2005. [cited at p. 36, 37, 38, 39]

[39] XQ Ding, RV Rao, and SM Kuntz. Impaired resensitization and recycling of the cholecystokinin receptor by co-expression of its second intracellular loop. *Molecular pharmacology*, 58(6):1424–1433, 2000. [cited at p. 14]

[40] Andrey V. Dobrynin and Michael Rubinstein. Theory of polyelectrolytes in solutions and at surfaces. *Progress in Polymer Science*, 30(11):1049–1118, November 2005. [cited at p. 39]

[41] Kurt Ingar Draget, Bjørn T Stokke, Yoshiaki Yuguchi, Hiroshi Urakawa, and Kanji Kajiwara. Small-angle X-ray scattering and rheological characterization of alginate gels. 3. Alginic acid gels. *Biomacromolecules*, 4(6):1661–8, 2003. [cited at p. 174]

[42] Gabriela R M Duarte, Wendell K T Coltro, Juliane C Borba, Carol W Price, James P Landers, and Emanuel Carrilho. Disposable polyester-toner electrophoresis microchips for DNA analysis. *The Analyst*, 137(11):2692–8, June 2012. [cited at p. 82]

[43] W. S. Dubner, J. M. Schultz, and G. D. Wignall. Estimation of incoherent backgrounds in SANS studies of polymers. *Journal of Applied Crystallography*, 23(6):469–475, December 1990. [cited at p. 58]

[44] S J Eastman, C Siegel, J Tousignant, a E Smith, S H Cheng, and R K Scheule. Biophysical characterization of cationic lipid: DNA complexes. *Biochimica et biophysica acta*, 1325(1):41–62, April 1997. [cited at p. 15]

[45] Michael L Edelstein, Mohammad R Abedi, Jo Wixon, and Richard M Edelstein. Gene therapy clinical trials worldwide 1989-2004 - an overview. *The Journal of Gene Medicine*, 6(6):597–602, 2004. [cited at p. 23]

[46] Pascal F Egea, Hiro Tsuruta, Gladys P de Leon, Johanna Napetschnig, Peter Walter, and Robert M Stroud. Structures of the signal recognition particle receptor from the archaeon Pyrococcus furiosus: implications for the targeting step at the membrane. *PloS one*, 3(11):e3619, January 2008. [cited at p. 97]

[47] EMA. European Medicines Agency Recommends First Gene Therapy for Approval. Technical report, European Medicines Agency - press office, press release, London, 2012. [cited at p. 17]

[48] Patrick Erbacher, Pascale Belguise, Jean-paul Behr, and Claire Weill. Polyplus transfection - in vivo-jetPEI : a potent vector for gene delivery in animals Feature article. *Manufacturer's Publication*, (01):1–8. [cited at p. 72, 76]

[49] Eurogentec. Eurogentec: Tips and Tricks: Quantification. [cited at p. 198]

[50] Alain Fabo. *Untersuchungen zur Wechselwirkung von Polyethylenimin (PEI) mit Holzkomponenten Dissertation.* PhD thesis, Universitaet Hamburg, 2004. [cited at p. 172]

[51] B Fahrenkrog and U Aebi. The Nuclear Pore Complex: Nucleocytoplasmic Transport And Beyond. *Nature Reviews: Molecular Cell Biology*, 2003. [cited at p. 16]

[52] Claudia Fallini, Gary J Bassell, and Wilfried Rossoll. High-efficiency transfection of cultured primary motor neurons to study protein localization, trafficking, and function. *Molecular neurodegeneration*, 5:17, January 2010. [cited at p. 9]

[53] Neftali Flores-Rodriguez, Salman S Rogers, David a Kenwright, Thomas a Waigh, Philip G Woodman, and Victoria J Allan. Roles of dynein and dynactin in early endosome dynamics revealed using automated tracking and global analysis. *PloS one*, 6(9):e24479, January 2011. [cited at p. 15]

[54] Barbara J Frisken. Revisiting the method of cumulants for the analysis of dynamic light-scattering data. *APPLIED OPTICS*, 40(24):4087–4091, 2001. [cited at p. 49]

[55] Arjen M Funhoff, Cornelus F van Nostrum, Gerben a Koning, Nancy M E Schuurmans-Nieuwenbroek, Daan J a Crommelin, and Wim E Hennink. Endosomal escape of polymeric gene delivery complexes is not always enhanced by polymers buffering at low pH. *Biomacromolecules*, 5(1):32–9, 2004. [cited at p. 14, 69]

[56] Shiroh Futaki, Yumi Masui, Ikuhiko Nakase, Yukio Sugiura, Takashi Nakamura, Kentaro Kogure, and Hideyoshi Harashima. Unique features of a pH-sensitive fusogenic peptide that improves the transfection efficiency of cationic liposomes. *J Gene Med*, 7:1450–1458, 2005. [cited at p. 24]

[57] M C Garnett and P Kallinteri. In Depth Review: Nanomedicines and nanotoxicology: some physiological principles. *Occupational medicine*, 56(5):307–11, August 2006. [cited at p. 21]

[58] W. T. Godbey, Michael A. Barry, Peter Saggau, Kenneth K. Wu, and Antonios G. Mikos. Poly(ethylenimine)-mediated transfection: a new paradigm for gene delivery. *Journal of biomedical materials research*, 51(3):321–8, September 2000. [cited at p. 15]

[59] D Goula, C Benoist, S Mantero, G Merlo, G Levi, and B A Demeneix. Polyethylenimine-based intravenous delivery of transgenes to mouse lung. *Gene therapy*, 5(9):1291–5, September 1998. [cited at p. 134]

[60] D Goula, J S Remy, P Erbacher, M Wasowicz, G Levi, B Abdallah, and B A Demeneix. Size, diffusibility and transfection performance of linear PEI/DNA complexes in the mouse central nervous system. *Gene therapy*, 5(5):712–7, May 1998. [cited at p. 66, 86]

[61] David Gould, Nasim Yousaf, Rewas Fatah, Maria Cristina Subang, and Yuti Chernajovsky. Gene therapy with an improved doxycycline-regulated plasmid encoding a tumour necrosis factor-alpha inhibitor in experimental arthritis. *Arthritis Research and Therapy*, 9(R7), 2007. [cited at p. 18, 19]

[62] Jordan J Green, Robert Langer, and Daniel G Anderson. A Combinatorial Polymer Library Approach Yields Insight into Nonviral Gene Delivery. *Acc. Chem. Res.*, 41(6):749–759, 2008. [cited at p. 24]

[63] Edward J Gunther, Susan E Moody, George K Belka, Kristina T Hahn, Nathalie Innocent, Katherine D Dugan, Robert D Cardiff, and Lewis A Chodosh. Impact of p53 loss on reversal and recurrence of conditional Wnt-induced tumorigenesis. *Genes & Development*, 17:488–501, 2003. [cited at p. 21]

[64] Boualem Hammouda. Chapter 23 - Empirical Models. *PROBING NANOSCALE STRUCTURES The Sans Toolbox*, 2008. [cited at p. 97]

[65] Boualem Hammouda. A new Guinier-Porod model. *Journal of Applied Crystallography*, 43:716–719, 2010. [cited at p. 95]

[66] Boualem Hammouda. Chapter 22 - Standard Plots. *PROBING NANOSCALE STRUCTURES The Sans Toolbox*, 2010. [cited at p. 60, 61]

[67] Boualem Hammouda. Probing Nanoscale Structures The SANS Toolbox. *NIST Center for Neutron Research*, 2010. [cited at p. 52, 53, 57, 58, 105, 106, 240]

[68] Boualem Hammouda. PROBING NANOSCALE STRUCTURESTHE SANS TOOLBOX. *NIST Center for Neutron Research*, page 224, 2010. [cited at p. 95]

[69] Boualem Hammouda and Derek L Ho. Insight Into Chain Dimensions in PEO / Water Solutions. *Journal of Polymer Science: Part B: Polymer Physics*, 45:2196–2200, 2007. [cited at p. 99]

[70] Jungho Han, SK Kim, TS Cho, JC Lee, and HS Joung. Polyplex formation of calf thymus DNA with branched and linear polyethyleneimine. *Macromolecular Research*, 12(5):501–506, 2004. [cited at p. 78, 131, 140]

[71] X Han, L Sun, Q Fang, D Li, X Gong, Y Wu, S Yang, and B Shen. Transient expression of osteopontin in HEK 293 cells in serum-free culture. *Enzyme and Microbial Technology*, 41(1-2):133–140, July 2007. [cited at p. 67, 72]

[72] Xiangzong Han, Qiangyi Fang, Feng Yao, Xiaoning Wang, Jufang Wang, Shengli Yang, and Bing Q Shen. The heterogeneous nature of polyethylenimine-DNA complex formation affects transient gene expression. *Cytotechnology*, 60:63–75, August 2009. [cited at p. 88]

[73] R K Heenan. The "FISH" reference manual. RAL REPORT 89-129 1989, revised Jan 2003; http://www.isis.rl.ac.uk/largescale/LOQ/FISH/instructions1.htm, 2005. [cited at p. 60, 61, 62, 94, 101, 104, 107, 110, 113, 123, 134, 135, 141, 198, 200, 246, 247]

[74] R K Heenan, S M King, D S Turner, and J R Treadgold. SANS2d at the ISIS Second Target Station. In *17 th Meeting of the International Collaboration on Advanced Neutron Sources*, 2005. [cited at p. 53, 93, 240]

[75] R. K. Heenan, J Penfold, and S M King. SANS at Pulsed Neutron Sources: Present and Future Prospects. *J. Appl. Cryst.*, 30:1140–1147, 1997. [cited at p. 53, 240]

[76] Roland W Herzog, J Nathan Hagstrom, Szu-Hoo Kung, Shing J Tai, James M Wilson, Krishna J Fisher, and Katherine A High. Stable gene transfer and expression of human blood coagulation factor IX after intramuscular injection of recombinant adeno-associated virus. *Proceedings of the National Academy of Sciences of the United States of America*, 94:5804–9, May 1997. [cited at p. 9]

[77] Sabrina Höbel, Robert Prinz, Anastasia Malek, Beata Urban-Klein, Johannes Sitterberg, Udo Bakowsky, Frank Czubayko, and Achim Aigner. Polyethylenimine PEI F25-LMW allows the long-term storage of frozen complexes as fully active reagents in siRNA-mediated gene targeting and DNA delivery. *European journal of pharmaceutics and biopharmaceutics*, 70:29–41, September 2008. [cited at p. 66, 67, 72, 88]

[78] U Hofmann, A Schreiber, D Haarer, S J Zilker, A Bacher, D D C Bradley, M Redecker, M Inbasekaran, W W Wu, and E P Woo. Investigations on the grating dynamics in a fast photorefractive guest-host polymer. *Chemical Physics Letters*, 311:41–46, 1999. [cited at p. 49]

[79] Isabelle Honoré, Stéphanie Grosse, Natacha Frison, Florence Favatier, Michel Monsigny, and Isabelle Fajac. Transcription of plasmid DNA: influence of plasmid DNA/polyethylenimine complex formation. *Journal of controlled release*, 107(3):537–46, October 2005. [cited at p. 66, 72]

[80] Craig Horbinski, Michal K Stachowiak, Dennis Higgins, and Sarah G Finnegan. Polyethyleneimine-mediated transfection of cultured postmitotic neurons from rat sympathetic ganglia and adult human retina. *BMC Neuroscience*, 2(2), 2001. [cited at p. 24]

[81] Marjukka Ikonen, Lasse Murtomäki, and Kyösti Kontturi. Controlled complexation of plasmid DNA with cationic polymers: effect of surfactant on the complexation and stability of the complexes. *Colloids and surfaces B: Biointerfaces*, 66(1):77–83, October 2008. [cited at p. 76, 134]

[82] Malvern Instruments. Zetasizer nano series user manual. 2004. [cited at p. 51, 182, 186]

[83] EPSRC ISIS. Accelerator Tour - ISIS. *Living in a Materials World, A-Level Physic*, S19-29. [cited at p. 52]

[84] ISIS Pulsed Neutron & Muon Source. Loq Technical Information - official ISIS webpage - isis.stfc.ac.uk/instruments/loq/technical/loq-technical-information7485.html. [cited at p. 53, 240]

[85] ISIS Pulsed Neutron & Muon Source. Sans2d Technical Information - official ISIS webpage isis.stfc.ac.uk/instruments/sans2d/technical/sans2d-technical-information7350.html. [cited at p. 53, 86, 240]

[86] David A. Jacques and Jill Trewhella. Small-angle scattering for structural biology–expanding the frontier while avoiding the pitfalls. *Protein science*, 19(4):642–57, April 2010. [cited at p. 174]

[87] Yuan Jiang and Laurie Gower. Hierarchical DL-Glutamic acid microspheres from polymer-induced liquid precursors. *Crystal Growth & Design*, 11:3243–3249, 2011. [cited at p. 140]

[88] María L Jiménez, Angel V Delgado, and Johannes Lyklema. Hydrolysis versus ion correlation models in electrokinetic charge inversion: establishing application ranges. *Langmuir*, 28(17):6786–93, May 2012. [cited at p. 37]

[89] Andreia F Jorge, Rita S Dias, Jorge C Pereira, and Alberto a C C Pais. DNA condensation by pH-responsive polycations. *Biomacromolecules*, 11(9):2399–406, September 2010. [cited at p. 75]

[90] Hiroyuki Kakuda, Tetsuo Okada, and Takeshi Hasegawa. Temperature-induced molecular structural changes of linear poly(ethylene imine) in water studied by mid-infrared and near-infrared spectroscopies. *The journal of physical chemistry. B*, 113(42):13910–6, October 2009. [cited at p. 114]

[91] H Kamiya, H Tsuchiya, J Yamazaki, and H Harashima. Intracellular trafficking and transgene expression of viral and non-viral gene vectors. *Advanced Drug Delivery Reviews*, 52(3):153–164, 2001. [cited at p. 14, 24]

[92] Michael G. Kaplitt, Andrew Feigin, Chengke Tang, Helen L. Fitzsimons, Paul Mattis, Patricia A. Lawlor, Ross J. Bland, Deborah Young, Kristin Strybing, David Eidelberg, and Matthew J. During. Safety and tolerability of gene therapy with an adeno-associated virus (AAV) borne GAD gene for Parkinson's disease: an open label, phase I trial. *The Lancet*, 369(9579):2097–2105, 2007. [cited at p. 9, 21]

[93] Gerald Karp. Gene Expression: From Transcription to Translation. In *Cell and Molecular Biology: Concepts and Experiments*, chapter 11, pages 419–474. John Wiley & Sons, Ltd., 2009. [cited at p. 18]

[94] Daniela Karra and Ralf Dahm. Transfection techniques for neuronal cells. *The Journal of neuroscience : the official journal of the Society for Neuroscience*, 30(18):6171–7, May 2010. [cited at p. 9]

[95] Tiia-Maaria Ketola, Martina Hanzlíková, Arto Urtti, Helge Lemmetyinen, Marjo Yliperttula, and Elina Vuorimaa. Role of polyplex intermediate species on gene transfer efficiency: polyethylenimine-DNA complexes and time-resolved fluorescence spectroscopy. *The journal of physical chemistry. B*, 115(8):1895–902, March 2011. [cited at p. 69]

[96] Zeena Khayat, Peter C Griffiths, Isabelle Grillo, Richard K Heenan, Stephen M King, and Ruth Duncan. Characterising the size and shape of polyamidoamines in solution as a function of pH using neutron scattering and pulsed-gradient spin-echo NMR. *International journal of pharmaceutics*, 317(2):175–86, July 2006. [cited at p. 94]

[97] Stephen M King. Small Angle Neutron Scattering, precursor to Chapter 7, Modern Techniques for Plymer Characterisation, R A Pethrick & J V Dawkins (editors), John Wiley 1999. http://www.isis.rl.ac.uk/largescale/loq/documents/sans.htm, 2003. [cited at p. 54, 58, 59]

[98] E Kleemann, M Neu, N Jekel, L Fink, T Schmehl, T Gessler, W Seeger, and T Kissel. Nanocarriers for DNA delivery to the lung based upon a TAT-derived peptide covalently coupled to PEG-PEI. *Journal of controlled release*, 109(1-3):299–316, December 2005. [cited at p. 76]

[99] Steven R. Kline. Reduction and analysis of SANS and USANS data using IGOR Pro. *Journal of Applied Crystallography*, 39(6):895–900, November 2006. [cited at p. 61, 97]

[100] Kazuto Kobayashi, Ching-i Huang, and Timothy P. Lodge. Thermoreversible Gelation of Aqueous Methylcellulose Solutions. *Macromolecules*, 32(21):7070–7077, October 1999. [cited at p. 97]

[101] Ilya Koltover, Kathrin Wagner, and Cyrus R Safinya. DNA Condensation in two Dimensions. *PNAS*, 97(26):14046–14051, 2000. [cited at p. 35, 36]

[102] Petr V Konarev, Vladimir V Volkov, Anna V Sokolova, Michel H J Koch, Dmitri I Svergun, and H J Koch. PRIMUS : a Windows PC-based system for small-angle scattering data analysis. 36:1277–1282, 2003. [cited at p. 87, 92]

[103] Idit Kopatz, Jean-Serge Remy, and Jean-Paul Behr. A model for non-viral gene delivery: through syndecan adhesion molecules and powered by actin. *The journal of gene medicine*, 6(7):769–76, July 2004. [cited at p. 13, 66]

[104] Stephen A. Krawetz and David D. Womble. Appendix 2 - A Collection of Useful Bioinformatic Tools and Molecular Tables. In Stephen A. Krawetz and David D. Womble, editors, *Introduction to Bioinformatics: A Theoretical and Practical Approach*, pages 719–722. Springer, 2003. [cited at p. 27, 35]

[105] Albert Kwok and Stephen L Hart. Comparative structural and functional studies of nanoparticle formulations for DNA and siRNA delivery. *Nanomedicine : nanotechnology, biology, and medicine*, 7(2):210–9, April 2011. [cited at p. 72, 78, 79, 88, 176, 218]

[106] Melike Lakadamyali, Michael J Rust, Hazen P Babcock, and Xiaowei Zhuang. Visualizing infection of individual influenza viruses. *Proceedings of the National Academy of Sciences of the United States of America*, 100(16):9280–5, August 2003. [cited at p. 70]

[107] GH Lander and AJ Diannoux. *Neutron Data Booklet, Second Edition*. ILL Neutrons for Science. Old City Publishing Group, 2003. [cited at p. 55, 57, 240]

[108] Irina Lebedeva, Robert Rando, Joshua Ojwang, Paul Cossum, and CA Stein. Bcl-xL in prostate cancer cells: effects of overexpression and down-regulation on chemosensitivity. *Cancer research*, 60:6052–6060, 2000. [cited at p. 19]

[109] Heidi Ledford. Cystic-fibrosis gene-therapy trial rescued. *Nature News Blog: Biology & Biotechnology, Health and medicine*, 2012. [cited at p. 9]

[110] ES Lee, Z Gao, and YH Bae. Recent progress in tumor pH targeting nanotechnology. *Journal of Controlled Release*, 132(3):164–170, 2008. [cited at p. 12]

[111] Kim Lefmann. Neutron Scattering : Theory , Instrumentation , and Simulation - Neutron Scattering Course notes. Technical report, Department of Materials Research, RisøNational Laboratory, Technical University of Denmark, 2007. [cited at p. 59]

[112] Weijun Li and Francis C Szoka Jr. Lipid-based Nanoparticles for Nucleic Acid Delivery. *Pharmaceutical Research*, 24(3):438–449, 2007. [cited at p. 24]

[113] Y Liu, LC Mounkes, HD Liggitt, Carolyn S. Brown, Igor Solodin, Timothy D. Heath, and Robert J. Debs. Factors influencing the efficiency of cationic liposome-mediated intravenous gene delivery. *Nature biotechnology*, 15:167 – 173, 1997. [cited at p. 66]

[114] Chun-Liang Lo, Chun-Kai Huang, Ko-Min Lin, and Ging-Ho Hsiue. Mixed micelles formed from graft and diblock copolymers for application in intracellular drug delivery. *Biomaterials*, 28(6):1225–35, February 2007. [cited at p. 25]

[115] Olga López, Mercedes Cócera, Ramón Pons, Nuria Azemar, Carmen López-Iglesias, Ernst Wehrli, Jose Luis Parra, and Alfonso de La Maza. Use of a Dynamic Light Scattering Technique To Study the Kinetics of Liposome Solubilization By Triton X-100. *Langmuir*, 15(13):4678–4681, 1999. [cited at p. 50]

[116] Yun Lu, Jing Yao, Jian-Ping Zhou, Wei Wang, Zu-Yuan Deng, and Li-Ye Guan. Formation and aggregation behavior of polyethyleneimine-DNA complexes, June 2009. [cited at p. 87]

[117] Dersy Lugo, Julian Oberdisse, Matthias Karg, Ralf Schweins, and Gerhard H. Findenegg. Electronic Supplementary Information: Surface aggregate structure of nonionic surfactants on silica nanoparticles. *Soft Matter*, 5(15):2928, 2009. [cited at p. 97]

[118] Kenneth Lundstrom. Latest development in viral vectors for gene therapy. *Trends in biotechnology*, 21(3):117–22, March 2003. [cited at p. 17, 19]

[119] Alexander V. Lyubimov. 17. Dosage formulation. In Shayne Cox Gad, editor, *Preclinical Development Handbook: ADME and Biopharmaceutical Properties*, page 583. Wiley, 2008. [cited at p. 69, 70, 74]

[120] Liang Ma, Zhe-Sheng Wen, Zi Liu, Zheng Hu, Jun Ma, Xiao-Qin Chen, Yong-Qiang Liu, Jian-Xin Pu, Wei-Lie Xiao, Han-Dong Sun, and Guang-Biao Zhou. Overexpression and small molecule-triggered downregulation of CIP2A in lung cancer. *PloS one*, 6(5):e20159, January 2011. [cited at p. 19]

[121] Yinghua Ma, Yiqing Tang, Norman C. Billingham, Steven P. Armes, Andrew L. Lewis, Andrew W. Lloyd, and Jonathan P. Salvage. Well-Defined Biocompatible Block Copolymers via Atom Transfer Radical Polymerization of 2-Methacryloyloxyethyl Phosphorylcholine in Protic Media. *Macromolecules*, 36(10):3475–3484, May 2003. [cited at p. 33, 194]

[122] MM MADY and WA MOHAMMED. Effect of polymer weight on the DNA/PEI polyplexes properties. *Rom. J. Biophys*, 21(2):151–165, 2011. [cited at p. 118, 175]

[123] Ram I. Mahato and Sung Wan Kim. Water-soluble Lipopolymers for Gene Delivery. In Mansoor Amiji, editor, *Polymeric Gene Delivery Principles and Applications*, page 182. CRC Press, 2005. [cited at p. 140]

[124] E Maltsev, JA Wattis, and HM Byrne. DNA charge neutralization by linear polymers. II. Reversible binding. *Physical review. E, Statistical, nonlinear, and soft matter physics*, 74(4 Pt 1), October 2006. [cited at p. 131]

[125] E Maltsev, JAD Wattis, and HM Byrne. DNA charge neutralization by linear polymers. I. Ireversible binding. *Physical Review E*, 74(4), 2006. [cited at p. 74, 119]

[126] Malvern. Zeta Potential An Introduction in 30 Minutes: Technical Note. Technical report, Malvern Instruments. [cited at p. 50, 182]

[127] Malvern Instruments Ltd., Enigma Business Park Grovewood Road Malvern Worcestershire UK WR14 1XZ. *TechNote: Dynamic Light Scattering MRK656-01.* [cited at p. 49]

[128] John F Marko. 3.2 Stretching single-stranded nucleic acids. In D Chatenay, S Cocco, R Monasson, D Thieffry, and J Dalibard, editors, *Course 7 - Multiple Aspects of DNA and RNA: from Biophysics to Bioinformatics: Lecture Notes of the Les Houches Summer School 2004 (Google eBook)*, page 236. Elsevier B.V., 2005. [cited at p. 34]

[129] R. May. Neutron Techniques: Particle Shape - 2.6 - Small angle techniques. In E. Prince, editor, *International Tables for Crystallography - Mathematical, Physical and Chemical Tables*, page 110. Springer, 3 edition, 2004. [cited at p. 97]

[130] Sumit Mehrotra, Ilsoon Lee, and Christina Chan. Multilayer mediated forward and patterned siRNA transfection using linear-PEI at extended N/P ratios. *Acta Biomater*, 5(5):1474–1488, 2009. [cited at p. 66, 78, 79, 131]

[131] Jerry R Mendell, Louise Rodino-Klapac, Zarife Sahenk, Vinod Malik, Brian K Kaspar, Christopher M Walker, and K Reed Clark. Gene therapy for muscular dystrophy: Lessons learned and path forward. *Neuroscience letters*, 527(2):90–99, May 2012. [cited at p. 9]

[132] Javier a Menendez, Luciano Vellon, Inderjit Mehmi, Bharvi P Oza, Santiago Ropero, Ramon Colomer, and Ruth Lupu. Inhibition of fatty acid synthase (FAS) suppresses HER2/neu (erbB-2) oncogene overexpression in cancer cells. *Proceedings of the National Academy of Sciences of the United States of America*, 101(29):10715–20, July 2004. [cited at p. 19]

[133] V Mengarelli, L Auvray, D Pastré, and M Zeghal. Charge inversion, condensation and decondensation of DNA and polystyrene sulfonate by polyethylenimine. *The European physical journal. E, Soft matter*, 34(11):127, November 2011. [cited at p. 26, 73, 77, 79]

[134] René Messina. Adsorption of oppositely charged polyelectrolytes onto a charged rod. *The Journal of Chemical Physics*, Vol. 119(No. 15):8133–8139, October 2003. [cited at p. 129]

[135] Joan W. Miller. Preliminary Results of Gene Therapy for Retinal Degeneration. *N. Engl. J. Med.*, 358(21):2282–2284, 2008. [cited at p. 9, 23]

[136] Meredith A Mintzer and Eric E Simanek. Nonviral vectors for gene delivery. *Chemical reviews*, 109(2):259–302, February 2009. [cited at p. 32]

[137] Lluis M Mir, Michel F Bureau, Julie Gehl, Ravi Rangara, Didier Rouy, Jean-Michel Caillaud, Pia Delaere, Didier Branellec, Bertrand Schwartz, and Daniel Scherman. High-efficiency gene transfer into skeletal muscle mediated by electric pulses. *Proc. Natl. Acad. Sci. USA*, 96:4262–4267, 1999. [cited at p. 18, 22]

[138] QS Mu, XB Zhao, and JR Lu. pH-responsive nanoaggregation of diblock phosphorylcholine copolymers. *The Journal of ...*, pages 9652–9659, 2008. [cited at p. 38]

[139] Nouri Nayerossadat, Talebi Maedeh, and Palizban Abas Ali. Viral and nonviral delivery systems for gene delivery. *Advanced biomedical research*, 1:27, January 2012. [cited at p. 23]

[140] Michael Neu. Modified Poly (ethylene imines) for plasmid delivery : Physico-chemical and in vitro / in vivo investigations. *Thesis, Philipps-Universitaet Marburg*, 2006. [cited at p. 66]

[141] Leila Nobs, Franz Buchegger, Robert Gurny, and Eric Allémann. Current methods for attaching targeting ligands to liposomes and nanoparticles. *Journal of pharmaceutical sciences*, 93(8):1980–92, August 2004. [cited at p. 13]

[142] Manfred Ogris. Gene Delivery using Polyethylenimine and Copolymers. In *Polymeric Gene Delivery: Principles and Applications*, chapter 7, page 106. Mansoor M.Amiji, CRC Press, 2005. [cited at p. 69, 70, 74, 76, 78, 119, 125, 129, 131, 133, 134, 138]

[143] N J Panaro, P K Yuen, T Sakazume, P Fortina, L J Kricka, and P Wilding. Evaluation of DNA fragment sizing and quantification by the agilent 2100 bioanalyzer. *Clinical chemistry*, 46(11):1851–3, November 2000. [cited at p. 44]

[144] William M Pardridge. Blood-brain barrier drug targeting: the future of brain drug development. *Molecular interventions*, 3(2):90–105, 51, March 2003. [cited at p. 10, 21]

[145] Fabio Pastorino, Davis R Mumbengegwi, Domenico Ribatti, Mirco Ponzoni, and Theresa M Allen. Increase of therapeutic effects by treating melanoma with targeted combinations of c-myc antisense and doxorubicin. *Journal of Controlled Release*, 126(1):85–94, 2008. [cited at p. 21]

[146] David Pastré, Olivier Piétrement, Fabrice Landousy, Loic Hamon, Isabelle Sorel, Marie-Odile David, Etienne Delain, Alain Zozime, and Eric Le Cam. A new approach to DNA bending by polyamines and its implication in DNA condensation. *Eur Biophys J*, 35:214–223, 2005. [cited at p. 35]

[147] Jan Skov Pedersen. Form and Structure Factors : Modeling and Interactions - lecture. *EMBO practical course on Solution Scattering from Biological Macromolecules, EMBL Hamburg*, 2012. [cited at p. 104]

[148] D Pelta and J Lairez. Diffusion de neutrons aux petits angles: application a l etude des macromolecules biologiques en solution. *J. Phys. IV France*, 1:12–13, 2004. [cited at p. 72]

[149] Justin Peters and J I M Maher. Investigating the electrostatic contribution to dna stiffness. *Conference Abstract - Coarse-Grain Mechanics of DNA: Part II From Electrons to Oligomers, CECAM*, 2011. [cited at p. 10]

[150] Holger Petersen, Klaus Kunath, Alison L Martin, Snjezana Stolnik, Clive J Roberts, Martyn C Davies, and Thomas Kissel. Star-shaped poly(ethylene glycol)-block-polyethylenimine copolymers enhance DNA condensation of low molecular weight polyethylenimines. *Biomacromolecules*, 3(5):926–36, 2002. [cited at p. 71]

[151] David L Porter, Bruce L Levine, Michael Kalos, Adam Bagg, and Carl H June. Chimeric antigen receptor-modified T cells in chronic lymphoid leukemia. *The New England journal of medicine*, 365(8):725–33, August 2011. [cited at p. 9, 21]

[152] Christopher D Putnam, Michal Hammel, Greg L Hura, and John a Tainer. X-ray solution scattering (SAXS) combined with crystallography and computation: defining accurate macromolecular structures, conformations and assemblies in solution. *Quarterly reviews of biophysics*, 40(3):191–285, August 2007. [cited at p. 98, 112, 136]

[153] Roger Pynn. Neutron Scattering - Lecture 1, Introduction and Neutron scattering "Theory". *NIST Summer School*, 2009. [cited at p. 56, 57, 58]

[154] Manuel Quesada-Pérez, Enrique González-Tovar, Alberto Martín-Molina, Marcelo Lozada-Cassou, and Roque Hidalgo-Alvarez. Overcharging in colloids: beyond the Poisson-Boltzmann approach. *Chemphyschem : a European journal of chemical physics and physical chemistry*, 4(3):234–48, March 2003. [cited at p. 37]

[155] J V Raja, M A Rachchh, and R H Gokani. Recent advances in gene therapy for thalassemia. *Journal of pharmacy & bioallied sciences*, 4(3):194–201, July 2012. [cited at p. 18]

[156] A Ramzi and M Sutter. Static light scattering and smallangle neutron scattering study on aggregated recombinant gelatin in aqueous solution. *Journal of pharmaceutical sciences*, 95(8):1703–1711, 2006. [cited at p. 99, 101, 102, 103]

[157] E Raspaud, M Olvera de la Cruz, J L Sikorav, and F Livolant. Precipitation of DNA by Polyamines: A Polyelectrolyte Behavior. *Biophysical Journal*, 74:381–393, 1998. [cited at p. 37]

[158] Sharon E Reed, Elizabeth M Staley, John P Mayginnes, David J Pintel, and Gregory E Tullis. Transfection of mammalian cells using linear polyethylenimine is a simple and effective means of producing recombinant adeno-associated virus vectors. *Journal of virological methods*, 138(1-2):85–98, December 2006. [cited at p. 72]

[159] Joanna Rejman, Alessandra Bragonzi, and Massimo Conese. Role of clathrin- and caveolae-mediated endocytosis in gene transfer mediated by lipo- and polyplexes. *Molecular therapy*, 12(3):468–74, September 2005. [cited at p. 66, 69]

[160] AT Robinson, NJ Rhodes, and EM Schooneveld. Development of scintillator arrangements and coding methods in neutron sensitive ZnS scintillation detectors. *SEPS Undergraduate Research Journal*, 2:22, 2007. [cited at p. 52]

[161] Sarah Rogers and Richard Heenan. A Rough Guide to FISH - software user guide. *ISIS Pulsed Neutron & Muon Source*, (August), 2008. [cited at p. 62]

[162] JN Roux, Daniel Broseta, and B Demé. SANS study of asphaltene aggregation: Concentration and solvent quality effects. *Langmuir*, 17(16):5085–5092, 2001. [cited at p. 174]

[163] Rutherford-Appleton. Accelerator and Target: The Accelerator Technical information - official ISIS webpage isis.stfc.ac.uk/groups/accelerator-science/accelerators-and-targets3389.html. http://www.isis.rl.ac.uk/accelerator, 2006. [cited at p. 52]

[164] Pelengaris S., Khan M., and Evan G. C-MYC: more than just a matter of life and death. *Nat. Rev. Cancer*, 2(10):764–776, 2002. [cited at p. 20]

[165] Ulrich Sigmar Schubert, Christine Weber, Krzysztof Babiuch, Igor Perevyazko, Richard Hoogenboom, and Sarah E. Rogers. Unexpected radical polymerization behavior of oligo(2-ethyl-2-oxazoline) macromonomers. *Polymer Chemistry*, 2012. [cited at p. 104]

[166] KS Schweizer and JG Curro. PRISM theory of the structure, thermodynamics, and phase transitions of polymer liquids and alloys. *Advances in Polymer Science*, 116:319 – 377, 1994. [cited at p. 104]

[167] Daniel T. Seaton, Stefan Schnabel, David P. Landau, and Michael Bachmann. From Flexible to Stiff: Systematic Analysis of Structural Phases for Single Semiflexible Polymers. *Physical Review Letters*, 110(2):028103, January 2013. [cited at p. 10]

[168] Vikas K Sharma, Mini Thomas, and Alexander M Klibanov. Mechanistic studies on aggregation of polyethylenimine-DNA complexes and its prevention. *Biotechnology and bioengineering*, 90(5):614–20, June 2005. [cited at p. 68, 73]

[169] L Shi, G P Tang, S J Gao, Y X Ma, B H Liu, Y Li, J M Zeng, Y K Ng, K W Leong, and S Wang. Repeated intrathecal administration of plasmid DNA complexed with polyethylene glycol-grafted polyethylenimine led to prolonged transgene expression in the spinal cord. *Gene therapy*, 10(14):1179–88, July 2003. [cited at p. 66, 72]

[170] Min Suk Shim, Xi Wang, Regina Ragan, and Young Jik Kwon. Dynamics of nucleic acid/cationic polymer complexation and disassembly under biologically simulated conditions using in situ atomic force microscopy. *Microscopy research Tech.*, 73(9):845–856, 2010. [cited at p. 66, 67]

[171] KR Spindler and TH Hsu. Viral disruption of the bloodbrain barrier. *Trends in microbiology*, 20(6):282–290, 2012. [cited at p. 10]

[172] Christopher B Stanley, Tatiana Perevozchikova, and Valerie Berthelier. Structural formation of huntingtin exon 1 aggregates probed by small-angle neutron scattering. *Biophysical journal*, 100(10):2504–12, May 2011. [cited at p. 101, 103, 108]

[173] E L Starostin. On the perfect hexagonal packing of rods. *J. Phys.: Condens. Matter*, 18:S187–S204, 2006. [cited at p. 39]

[174] J Suh. Ionization of Poly(ethylenimine) and Poly(allylamine) at Various pHs, September 1994. [cited at p. 71]

[175] Junghae Suh, Michelle Dawson, and Justin Hanes. Real-time multiple-particle tracking: applications to drug and gene delivery. *Advanced Drug Delivery Reviews*, 57:63–78, 2005. [cited at p. 15]

[176] Shi-Joon Sung, Sang Hyun Min, Kuk Young Cho, Seongnam Lee, Youn-Jin Min, Young Il Yeom, and Jung-Ki Park. Effect of polyethylene glycol on gene delivery of polyethylenimine. *Biological & pharmaceutical bulletin*, 26(4):492–500, April 2003. [cited at p. 73]

[177] Ryan J Taft, Michael Pheasant, and John S Mattick. The relationship between non-protein-coding DNA and eukaryotic complexity. *BioEssays : news and reviews in molecular, cellular and developmental biology*, 29(3):288–99, March 2007. [cited at p. 18]

[178] Bouna-Moussa Tandia, Michel Vandenbranden, Ruddy Wattiez, Zohir Lakhdar, Jean-Marie Ruysschaert, and Abdelatif Elouahabi. Identification of Human Plasma Proteins that Bind to Cationic Lipid/DNA Complex and Analysis of Their Effects on Transfection Efficiency: Implications for Intravenous Gene Transfer. *Molecular Therapy*, 8:264–273, 2003. [cited at p. 13]

[179] Mark Telling, Steve Cottrell, Anders Markvardsen, and Robert Whitley. Mantid 4 mu+ - Quick start guide for muon data processing. *The Mantid Project*, (1), 2012. [cited at p. 93]

[180] B Tinland, A Pluen, J Sturm, and G Weill. Persistence length of single-stranded DNA. *Macromolecules*, 30:5763–5765, 1997. [cited at p. 38]

[181] Conchita Tros de Ilarduya, Yan Sun, and Nejat Düzgüne. Gene delivery by lipoplexes and polyplexes. *European journal of pharmaceutical sciences*, 40(3):159–70, June 2010. [cited at p. 13, 36, 66, 73]

[182] CS Tsao, US Jeng, CY Chen, and TY Kuo. Small-angle X-ray scattering study of nanostructure evolution of β precipitates in AlMgSi alloy. *Scripta materialia*, pages 2–9, 2005. [cited at p. 101]

[183] Roman Tuma, Hiro Tsuruta, Kenneth H French, and Peter E Prevelige. Detection of intermediates and kinetic control during assembly of bacteriophage P22 procapsid. *Journal of molecular biology*, 381(5):1395–406, September 2008. [cited at p. 62]

[184] Masaki Uchida, Xiong Wei Li, Peter Mertens, and H Oya Alpar. Transfection by particle bombardment: delivery of plasmid DNA into mammalian cells using gene gun. *Biochimica et biophysica acta*, 1790(8):754–64, August 2009. [cited at p. 22]

[185] Karel Ulbrich and Vladimir Subr. Polymeric anticancer drugs with pH-controlled activation. *Advanced Drug Delivery Reviews*, 56:1023–1050, 2004. [cited at p. 12]

[186] Kuniharu Utsuno and Hasan Uluda. Thermodynamics of polyethylenimine-DNA binding and DNA condensation. *Biophysical journal*, 99(1):201–7, July 2010. [cited at p. 28, 71]

[187] Bloomfield VA, Wilson RW, and Rau DC. Polyelectrolyte effects in DNA condensation by polyamines. *Biophys Chem.*, 11(3):339–343, 1980. [cited at p. 35]

[188] Marieke a E M van der Aa, Enrico Mastrobattista, Ronald S Oosting, Wim E Hennink, Gerben a Koning, and Daan J a Crommelin. The nuclear pore complex: the gateway to successful nonviral gene delivery. *Pharmaceutical research*, 23(3):447–59, March 2006. [cited at p. 16]

[189] Amir K Varkouhi, Marije Scholte, Gert Storm, and Hidde J Haisma. Endosomal escape pathways for delivery of biologicals. *Journal of controlled release*, 151(3):220–8, May 2011. [cited at p. 14, 69]

[190] A von Harpe, H Petersen, Y Li, and T Kissel. Characterization of commercially available and synthesized polyethylenimines for gene delivery. *Journal of controlled release*, 69(2):309–22, November 2000. [cited at p. 70]

[191] Ernst Wagner. Review: Strategies to Improve DNA Polyplexes for in Vivo Gene Transfer: Will Artificial Viruses Be the Answer? *Pharmaceutical Research*, 21(1), 2004. [cited at p. 15, 22]

[192] Robert Wattiaux, Nathanael Laurent, Simone Wattiaux-De Coninck, and Michel Jadot. Endosomes, lysosomes: their implication in gene transfer. *Advanced Drug Delivery Reviews*, 41(2):201–208, 2000. [cited at p. 11, 14, 15]

[193] Stephanie Werth, Beata Urban-Klein, Lige Dai, Sabrina Höbel, Marius Grzelinski, Udo Bakowsky, Frank Czubayko, and Achim Aigner. A low molecular weight fraction of polyethylenimine (PEI) displays increased transfection efficiency of DNA and siRNA in fresh or lyophilized complexes. *Journal of controlled release*, 112(2):257–70, May 2006. [cited at p. 66, 72, 88, 219]

[194] KF Weyts and EJ Goethals. Back titration of linear polyethylenimine: Decrease of pH by addition of sodium hydroxide. *Die Makromolekulare Chemie, Rapid Communications*, 10:299–302, 1989. [cited at p. 85, 166]

[195] L Wightman, R Kircheis, V Rössler, S Carotta, R Ruzicka, M Kursa, and E Wagner. Different behavior of branched and linear polyethylenimine for gene delivery in vitro and in vivo. *The journal of gene medicine*, 3(4):362–72, 2001. [cited at p. 73, 88]

[196] RW Wilson and VA Bloomfield. Counterion-induced condensation of deoxyribonucleic acid. A light-scattering study. *Biochemistry*, 18(11):2192–2196, 1979. [cited at p. 74]

[197] J W Wiseman, C a Goddard, D McLelland, and W H Colledge. A comparison of linear and branched polyethylenimine (PEI) with DCChol/DOPE liposomes for gene delivery to epithelial cells in vitro and in vivo. *Gene therapy*, 10(19):1654–62, September 2003. [cited at p. 72]

[198] Zhao X, Pan F, Zhang Z, Grant C, Ma Y, Armes SP, Tang Y, Lewis AL, Waigh T, and Lu JR. Nanostructure of polyplexes formed between cationic diblock copolymer and antisense oligodeoxynucleotide and its influence on cell transfection efficiency. *Biomacromolecules*, 8(11):3493–3502, 2007. [cited at p. 38, 67]

[199] Xiao-Bing Xiong, Hasan Uluda, and Afsaneh Lavasanifar. III. Nanotechnology for the Delivery of Small Molecules, Proteins and Nucleic Acids. In Melgardt M. de Villiers, Pornanong Aramwit, and Glen S. Kwon, editors, *Nanotechnology in Drug Delivery*, chapter 13. Engine, page 404. Springer, 2008. [cited at p. 32, 66]

[200] Long Xu and Thomas J Anchordoquy. Cholesterol domains in cationic lipid/DNA complexes improve transfection. *Biochimica et biophysica acta*, 1778(10):2177–81, October 2008. [cited at p. 13]

[201] Renliang Xu. *Particle Characterization: Light Scattering Methods - Particle Technology Series*. Kluwer Academic Publishers, 2000. [cited at p. 182, 183, 186]

[202] Yunhe Xu, Annika Linde, Ola Larsson, Dorit Thormeyer, Joacim Elmen, Claes Wahlestedt, and Zicai Liang. Functional comparison of single- and double-stranded siRNAs in mammalian cells. *Biochemical and Biophysical Research Communications*, 316(3):680–687, 2004. [cited at p. 35]

[203] Jie Yan and JF Marko. Localized single-stranded bubble mechanism for cyclization of short double helix DNA. *Physical review letters*, 93(10):108108, 2004. [cited at p. 34]

[204] Jie Yan and John F Marko. Localized single-stranded bubble mechanism for cyclization of short double helix DNA. *Physical review letters*, 93(10):108108, September 2004. [cited at p. 34]

[205] Huijuan You, Ryota Iino, Rikiya Watanabe, and Hiroyuki Noji. Winding single-molecule double-stranded DNA on a nanometer-sized reel. *Nucleic acids research*, pages 1–6, July 2012. [cited at p. 34]

[206] Violeta Zaric, Denis Weltin, Patrick Erbacher, Jean-Serge Remy, Jean-Paul Behr, and Dominique Stephan. Effective polyethylenimine-mediated gene transfer into human endothelial cells. *The journal of gene medicine*, 6(2):176–84, February 2004. [cited at p. 66, 72]

[207] F Zhang, F Roosen-Runge, M W a Skoda, R M J Jacobs, M Wolf, Ph Callow, H Frielinghaus, V Pipich, S Prévost, and F Schreiber. Hydration and interactions in protein solutions containing concentrated electrolytes studied by small-angle scattering. *Physical chemistry chemical physics : PCCP*, 14(7):2483–93, February 2012. [cited at p. 96, 97]

[208] Xiubo Zhao. *Novel Biocompatible Diblock Copolymers as Gene Delivery Vehicle*. PhD thesis, University of Manchester, 2006. [cited at p. 10, 13, 29, 33, 34, 104, 108, 193, 194, 199, 205, 211, 220]

[209] XiuBo Zhao. *Novel Biocompatible Diblock Copolymers as Gene Delivery Vehicles*. PhD thesis, Faculty of Engineering and Physical Sciences, University of Manchester, 2006. [cited at p. 33, 203, 240]

[210] Jesse D Ziebarth and Yongmei Wang. Understanding the protonation behavior of linear polyethylenimine in solutions through Monte Carlo simulations. *Biomacromolecules*, 11(1):29, 2011. [cited at p. 32, 69, 71, 75, 76, 84]

[211] Arkadi Zintchenko, Alexander Philipp, Ali Dehshahri, and Ernst Wagner. Simple modifications of branched PEI lead to highly efficient siRNA carriers with low toxicity. *Bioconjugate chemistry*, 19(7):1448–55, July 2008. [cited at p. 67]

[212] Gabriella Zupi, Marco Scarsella, Sean C Semple, Marcella Mottolese, Pier G Natali, and Carlo Leonetti. Antitumor Efficacy of bcl-2 and c-myc Antisense Oligonucleotides in Combination with Cisplatin in Human Melanoma Xenografts: Relevance of the Administration Sequence. *Clinical Cancer Research*, 11:1990–1998, 2005. [cited at p. 9, 20, 21]

List of Symbols and Abbreviations

Abbreviation	Description
MPC	2-methacryloyloxyethyl phosphorylcholine
DEA	2-(diethylamino)ethyl methacrylate
MPC_30-DEA_70	Block copolymer consisting of 30 monomer units of 2-methacryloyloxyethyl phosphoryl-choline conjugated to 70 monomer units of 2-(diethylamino)ethyl methacrylate
PEI	Polyethylenimine
BPEI	Branched Polyethylenimine
LPEI	Linear Polyethylenimine
SLD	Scattering Length Density ODN
Antisense Deoxyoligonucleotide	
SVD	Singular Value Decomposition
MTT	(3-(4,5-Dimethylthiazol-2-yl)-2,5-diphenyltetrazolium bromide
DAPI	4',6-diamidino-2-phenylindole
PI	Propidium Iodide
SANS	Small Angle Neutron Scattering
DMSO	Dimethyl Sulfoxide, $(CH_3)_2SO$
FAM	6-Carboxyfluorescein
DMEM	Dulbecco's Modified Eagle Medium
FBS	Foetal Bovine Serum
PBS	Phosphate buffer
DLS	Dynamic Light Scattering
NLS	Nuclear Localisation Signals

List of Figures

List of Tables